Status of Progress Made Toward Safety Analysis and Technical Site Evaluations for DOE Managed HLW and SNF

Fuel Cycle Research & Development

Prepared for
U.S. Department of Energy
Used Fuel Disposition

S. David Sevougian
Emily R. Stein
Michael B. Gross
Glenn E. Hammond
Jennifer M. Frederick
Paul E. Mariner

Sandia National Laboratories

November 3, 2016

FCRD-UFD-2016-000082, Rev. 1
SAND2016-11232 R

Sandia National Laboratories is a multi-mission laboratory managed and operated by Sandia Corporation, a wholly owned subsidiary of Lockheed Martin Corporation, for the U.S. Department of Energy's National Nuclear Security Administration under contract DE-AC04-94AL85000.

APPENDIX E
FCT DOCUMENT COVER SHEET[1]

Name/Title of Deliverable/ Milestone/Revision No.	*Status of Progress Made Toward Safety Analysis and Technical Site Evaluations for DOE Managed HLW and SNF*, M2FT-16SN080504062, Rev. 1
Work Package Title & Number	Total system performance assessment - SNL, FT-16SN08050406
Work Package WBS Number	1.02.08.05.04
Responsible Work Package Manager	S. David Sevougian (Name/Signature)
Date Submitted	November 3, 2016

Quality Rigor Level for Deliverable/Milestone[2]	☐ QRL-1 ☐ Nuclear Data	☐ QRL-2	☐ QRL-3	☒ QRL-4 Lab- Specific

This deliverable was prepared in accordance with Sandia National Laboratories
(Participant/National Laboratory Name)

QA program which meets the requirements of

☒ DOE Order 414.1 ☐ NQA-1-2000 ☐ Other

This Deliverable was subjected to:

☐ Technical Review ☐ Peer Review

Technical Review (TR)
Review Documentation Provided

☐ Signed TR Report or,
☐ Signed TR Concurrence Sheet or,
☐ Signature of TR Reviewer(s) below

Peer Review (PR)
Review Documentation Provided

☐ Signed PR Report or,
☐ Signed PR Concurrence Sheet or,
☐ Signature of PR Reviewer(s) below

Name and Signature of Reviewers

NOTE 1: *Appendix E should be filled out and submitted with the deliverable. Or, if the PICS:NE system permits, completely enter all applicable information in the PICS:NE Deliverable Form. The requirement is to ensure that all applicable information is entered either in the PICS:NE system or by using the FCT Document Cover Sheet.*

- *In some cases there may be a milestone where an item is being fabricated, maintenance is being performed on a facility, or a document is being issued through a formal document control process where it specifically calls out a formal review of the document. In these cases, documentation (e.g., inspection report, maintenance request, work planning package documentation or the documented review of the issued document through the document control process) of the completion of the activity, along with the Document Cover Sheet, is sufficient to demonstrate achieving the milestone.*

NOTE 2: *If QRL 1, 2, or 3 is not assigned, then the QRL 4 box must be checked, and the work is understood to be performed using laboratory specific QA requirements. This includes any deliverable developed in conformance with the respective National Laboratory / Participant, DOE or NNSA-approved QA Program.*

ACKNOWLEDGEMENTS

This work was supported by the US Department of Energy Office of Nuclear Energy, through the Office of Spent Fuel and Waste Science and Technology, within the Office of Fuel Cycle Technologies.

The authors would like to thank Frank Perry (LANL), who gave important insights regarding potential crystalline host rock formations in the U.S., as well as members of the LANL DNFWorks Team, who helped with fracture mapping and representation of the natural system, including Hari Viswanathan (LANL), Satish Karra (LANL), Jeffrey Hyman (LANL), and Nataliia Makedonska (LANL). Teklu Hadgu (SNL) and Elena Kalinina (SNL) also contributed through discussions of the FCM representation for fractured granite. Kevin McMahon (SNL) and Bob MacKinnon (SNL) provided instrumental management input, while Dave Sassani (SNL) and Ed Matteo (SNL) provided important integration support through their separate DWR work packages. Ernie Hardin provided detailed knowledge regarding repository design and thermal constraints. FEPs analysis support was provided by Geoff Freeze (SNL). Peter Swift (SNL) and Gordon Appel (SNL) are also acknowledged for their integration support. We are particularly grateful to Mark Tynan (DOE NE-53), Bill Spezialetti (DOE NE-53), and Prasad Nair (DOE NE-53) for their integration suggestions and guidance. Special acknowledgement goes to Jens Wolf (GRS) and Dieter Buhmann (GRS), since they are the other half of the US/German collaboration that produced the new FEP matrix and list.

EXECUTIVE SUMMARY

The Spent Fuel and Waste Science and Technology (SFWST) Campaign of the U.S. Department of Energy (DOE) Office of Nuclear Energy (NE) is conducting research and development (R&D) on generic deep geologic disposal systems (i.e., repositories). This report describes specific activities in FY 2016 associated with the development of a Defense Waste Repository (DWR)[a] for the permanent disposal of a portion of the HLW and SNF derived from national defense and research and development (R&D) activities of the DOE.

One of the main components of a comprehensive DWR Safety Case will be a post-closure safety analysis or performance assessment (PA). This deliverable is a status update on R&D progress in this area during FY 2016 and addresses four major associated R&D areas:

- development of generic reference cases (i.e., knowledge or technical bases for "generic" or "non-site-specific" deep geologic repositories) for two primary host rocks under consideration for a DWR: crystalline (granite) and bedded salt;
- features, events, and processes (FEPs) analyses/screening to support the technical bases and PA;
- performance evaluation of alternative engineered concepts for the layout of a repository and the design of an engineered barrier system (EBS), corresponding to the given host rock; and
- post-closure safety assessment of the repository system under consideration.

A key aspect of the DWR post-closure safety evaluations is the development and application of an enhanced PA modeling capability. Development of an enhanced PA capability for geologic disposal of SNF and HLW has been ongoing for several years in the U.S. repository program, but has mainly been applied to evaluation of a repository for commercial SNF. This enhanced PA capability, called the Generic Disposal System Analysis (GDSA) modeling and software framework, can equally be applied to a much cooler defense waste repository, as described in this report.

Using the known inventory for defense-related SNF, as well as for defense-related HLW stored at the Savannah River and Hanford sites, a variety of single-realization (i.e., deterministic) and multi-realization (probabilistic) 3-D flow and transport simulations for the generic granite and bedded salt repositories are presented, over a post-closure performance period of one million years. Sensitivity analyses examine the effect of key uncertain parameters on repository performance, including the effects of fracture distribution, waste package degradation rate, buffer and disturbed rock zone (DRZ) properties, and sorption parameters. Two types of emplacement concepts are examined, including single-canister vertical-borehole emplacement for the hotter DSNF waste (KBS-3V concept) and multi-canister horizontal emplacement for DHLW (similar to Yucca Mountain co-disposal waste packages).

Important issues uncovered by this year's work on a granite reference case are related to the uncertainty and heterogeneity associated with the spatial distribution and connectivity of fracture networks. These issues include:

[a] Defense Waste Repository – a deep geologic repository developed by the DOE under the Atomic Energy Act for the disposal of HLW and SNF resulting from atomic energy defense activities, research and development (R&D) activities of the DOE, or both.

1) Degree of isolation. Isolation is one of three primary safety functions generally acknowledged and often used for the Safety Case for most international programs. Direct connectivity of large fractures with the surface (outcrops) may pose challenges for repository performance depending on the degree of *in situ* fracture/feature connectivity, as well as the degree of liquid saturation in the fracture network. Two possible modifications to the generic crystalline reference case are suggested in this regard: either a sedimentary overburden or a deep unsaturated zone.
2) Quantitative safety metrics used to establish conformance to regulations. For outcropping saturated fractures, concentration or dose at a single location may not be a stable measure of performance. A suggested improvement is to use an array of monitor wells for the case of saturated fractures outcropping at the surface.

These results also point to a greater reliance on engineered barrier performance for a DWR in fractured crystalline host rock, indicating that future modifications to the granite reference case may include a longer-lived waste package overpack composed of oxygen-free copper, rather than the current generic design of a stainless steel overpack. Also, the influence of hydrodynamic dispersion and numerical diffusion/dispersion in fractured media warrant further study.

The bedded salt reference case and simulation results are not dissimilar to earlier R&D for a commercial SNF repository in bedded salt, except the heat load is far lower for a Defense Waste Repository. Also, in the results presented here, a different emplacement concept is used than the previous commercial SNF repository. The DWR concept is on-floor emplacement of single waste canisters, which has operational advantages related to the much lower heat output of defense-related waste. The PA simulations show that because of the impermeable nature of the bedded salt host rock, radionuclide transport for this concept is greatly reduced compared to a generic crystalline concept, i.e., isolation from the surface is assured in bedded salt at all but extremely low radionuclide concentrations arising from the slow process of molecular diffusion.

This report fulfills the Safety Analysis and Technical Site Evaluation Work Package Level 2 Milestone – *Status of Progress Made Toward Safety Analysis and Technical Site Evaluations for DOE Managed HLW and SNF* (M2FT-16SN080504062).

CONTENTS

FIGURES

TABLES

ACRONYMS

CD	Critical Decision
CSNF	Commercial Spent Nuclear Fuel
Dakota	Design analysis toolkit for optimization and terascale applications
DFN	Discrete Fracture Network
DHLW	Defense High-Level Radioactive Waste
DOE	U.S. Department of Energy
DRZ	Disturbed Rock Zone
DSNF	Defense Spent Nuclear Fuel
DWR	Defense Waste Repository
EBS	Engineered Barrier System
ECPM	Equivalent Continuous Porous Medium
FEP	Feature, Event, and Process
FY	Fiscal Year
GDSA	Generic Disposal System Analysis
HLW	High-Level Radioactive Waste
HPC	High-Performance Computing
INL	Idaho National Laboratory
LHS	Latin hypercube sampling
MCO	Multicanister Overpack
MTHM	Metric Tons Heavy Metal
NBS	Natural Barrier System
NE	Office of Nuclear Energy
PETSc	Portable Extensible Toolkit for Scientific Computation
PWR	Pressurized Water Reactor
QA	Quality Assurance
THC	Thermal-Hydrologic-Chemical
THCM	Thermal-Hydrologic-Chemical-Mechanical
THCMBR	Thermal-Hydrologic-Chemical-Mechanical-Biological-Radiological
PA	Performance Assessment
R&D	Research and Development
RD&D	Research, Development, and Demonstration
SNF	Spent Nuclear Fuel
WIPP	Waste Isolation Pilot Plant
WF	Waste Form
WP	Waste Package

This page intentionally left blank

1. INTRODUCTION

This deliverable is the initial status report outlining progress toward developing key components of a Safety Case for the disposal of most high-level radioactive waste and spent fuel under the management of the U.S. DOE. In October 2014, the DOE issued a report (DOE 2014a) describing the potential advantages for "disposal of DOE-managed HLW from defense activities and some thermally cooler DOE-managed SNF, potentially including cooler naval SNF, separately from disposal of commercial SNF and HLW." In March 2015, the U.S. President directed that such a separate repository, hereafter called a Defense Waste Repository (DWR), is required for "defense HLW" (or HLW resulting from atomic energy defense activities), based on Section 8(b)(2) of the Nuclear Waste Policy Act of 1982 (NWPA 1987) and the analysis in DOE (2015).

The following pages describe R&D during FY2016 for several major components of a comprehensive Safety Case for a DWR: (1) development of generic reference cases (i.e., knowledge or technical bases for "generic" or "non-site-specific" deep geologic repositories); (2) features, events, and processes (FEPs) analyses and screening to support the technical bases and performance assessment (PA); (3) performance evaluation of alternative EBS design concepts; and (4) post-closure safety assessment of the repository system under consideration. As of this writing, funding has allowed investigations into two of the primary host rocks, granite (or other crystalline rock) and bedded salt, as well as two major EBS design concepts for granite (vertical and horizontal emplacement of waste packages) and one major EBS design concept for bedded salt (on-floor emplacement). Future R&D will include DWR design concepts and generic geologic investigations for argillite host rock, as well as refinement of the granite and salt reference cases and associated PA evaluations.

A key aspect of the DWR post-closure safety evaluations is the development and application of an enhanced PA modeling capability. Development of an enhanced PA capability for geologic disposal of SNF and HLW has been ongoing for several years in the U.S. repository program, but has mainly been applied to evaluation of a repository for commercial SNF—a waste which generates significant decay heat that might strongly influence porewater movement and associated transport of released radionuclides. This enhanced PA capability, called the Generic Disposal System Analysis (GDSA) modeling and software framework, can equally be applied to a much cooler defense waste repository, as described in this report. The intent is also to make the GDSA framework flexible enough to evolve through the various phases of repository activities (over several decades) and to be generally applicable to a variety of geologic system concepts and waste inventories (Mariner et al. 2016).

The GDSA Framework utilizes modern software and hardware capabilities by being based on open-source software architecture and being configured to run in a massively parallel, high-performance computing (HPC) environment. It consists of two main components, the open-source Dakota uncertainty sampling and analysis software and the PFLOTRAN reactive multi-phase flow and transport simulator (see Section 3.3.2). Generic repository PA evaluations based on the GDSA framework are a key subject of this report, described in Sections 3 and 4, for crystalline and bedded salt host rock, respectively. In addition to the results of PA simulations based on the GDSA framework, Sections 3 and 4 of this report give a full description of the parameterization and design concepts (including both engineered and natural barrier descriptions) for both the generic crystalline reference case and the generic bedded salt reference

case, as well as a preliminary FEPs screening for the crystalline reference case (Appendix A). Conclusions and recommendations in Section 5 indicate future R&D directions for improvements in the reference cases and simulations described herein.

This deliverable fulfills the Safety Analysis and Technical Site Evaluation Work Package Level 2 Milestone – *Status of Progress Made Toward Safety Analysis and Technical Site Evaluations for DOE Managed HLW and SNF* (M2FT-16SN080504062).

2. SAFETY CASE, FEP ANALYSIS, AND REFERENCE CASE METHODOLOGY

Figure 2-1 shows the major components of a Safety Case for establishing confidence in the technical feasibility, safety, and performance of a deep geologic repository. Such a case evolves during the decades-long siting and development process of a repository project, illustrated schematically in Figure 2-2. At each major milestone or stage in such a project, i.e., each Critical Decision (CD) point (DOE 2010; DOE 2011) shown in Figure 2-2, the major components of the project and its safety case are updated based on the most recent information available, through an iterative interplay between evolving knowledge/engineering bases and the latest Safety Assessment analyses, as illustrated in Figure 2-3. Figure 2-3 is based on Components 3.3 and 4.2 of the Safety Case shown in Figure 2-1, but in a relational or "flow-diagram/information-feed" fashion. The U.S. program, whether for commercial or defense waste, is currently at the indicated location on the timeline in Figure 2-2, which corresponds to generic (non site-specific) RD&D only.

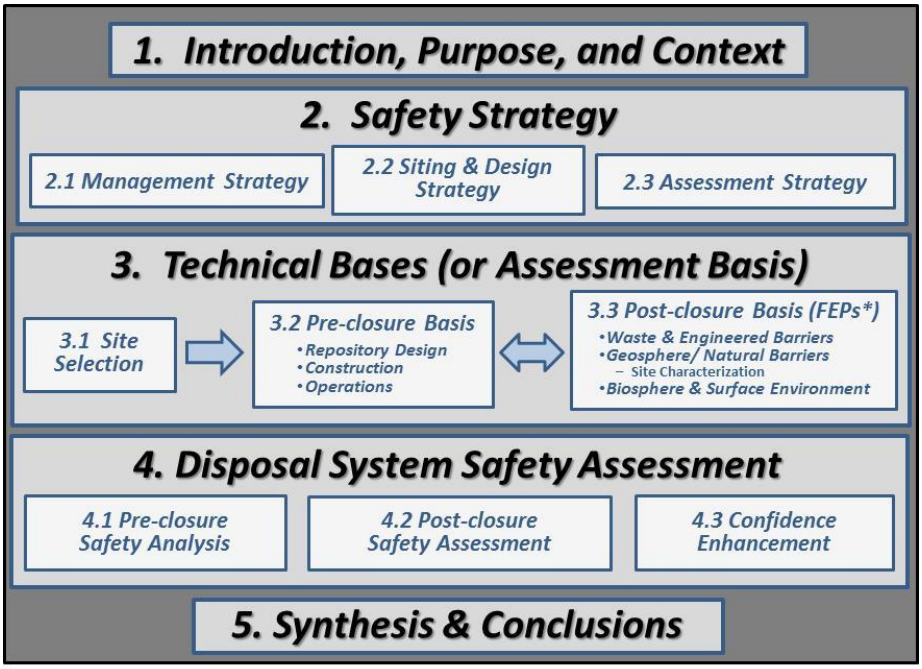

Figure 2-1. Major Components of the Safety Case [from Sevougian et al. 2016].

The generic Reference Cases for crystalline and salt host rocks address the key elements of Figure 2-3 outlined by the blue dotted lines. These major components of the granite and salt reference cases are described below in Sections 3 and 4. As noted by Vaughn et al. (2013), the development of conceptual models for *generic* disposal systems has challenges: "Normally, a safety case and associated safety assessment address a specific site, a well-defined inventory, waste form, and waste package, a specific repository design, specific concept of operations, and an established regulatory environment. This level of specificity does not exist for a "generic" repository, so it is important to establish a reference case, to act as a surrogate for site/design specific information upon which a safety case can be developed. (A reference case provides)

enough information to support the initial screening of FEPs and the design of models for preliminary safety assessments…"

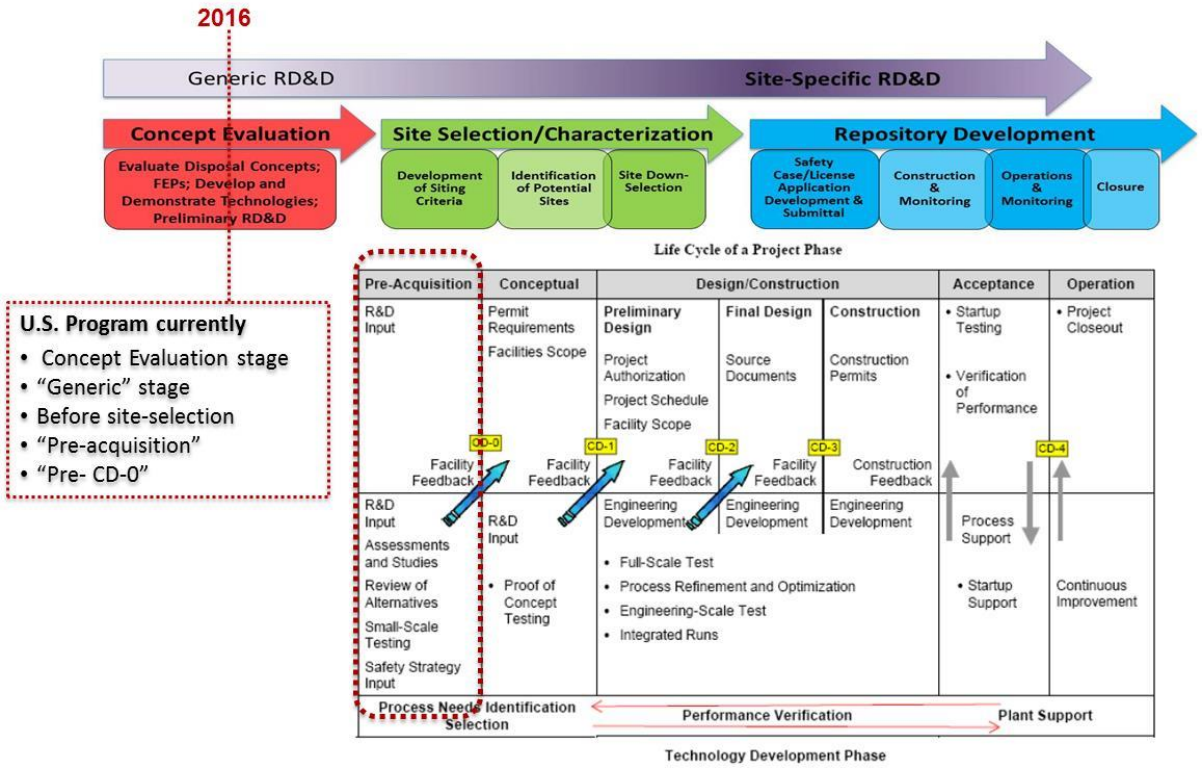

Figure 2-2. Illustrative timeline for a repository project and associated RD&D [from Sevougian 2016]. ["Life Cycle of a Project Phase" diagram illustrates the key Critical Decision (CD) points described in DOE (2011) and DOE (2010).]

This deliverable reports on generic RD&D related to the Performance Assessment box in Figure 2-3, as well as to the Reference Case components in Figure 2-3. Other closely related DWR deliverables and work packages are conducting additional RD&D related to key elements of the Reference Case, i.e., inventory and waste characterization (Sassani et al. 2016) and EBS design concepts (Matteo et al. 2016). Another closely related deliverable is *Advances in Geologic Disposal System Modeling and Application to Crystalline Rock* (Mariner et al. 2016), which describes in much greater detail the "Performance Assessment Model (GDSA Framework)" box shown in Figure 2-3, as well as its application to a generic repository for commercial SNF.

The FEP knowledge base and screening process, which is an important methodology for building the Performance Assessment conceptual model (among other things) is described here and in Appendix A of this report. As outlined in Sevougian et al. (2015) and Freeze et al. (2014), FEP analysis and scenario development are an integral part of the iterative PA process shown in Figure 2-3, and help inform the construction of repository post-closure PA models based on the most important FEPs, as well as ensuring completeness of the PA model. FEP screening is part of the iterative process, wherein uncertainty and sensitivity analyses of the results produced by those PA models indicate which FEPs are most important to post-closure repository performance. This information can then be used during the next stage to help refine the set of

FEPs and their representation in the PA model. FEPs and scenarios also provide a logical method for organizing and cataloging both existing knowledge and needed R&D within the context of the entire Safety Case, especially the remaining "issues" and uncertainties (DOE 2012).

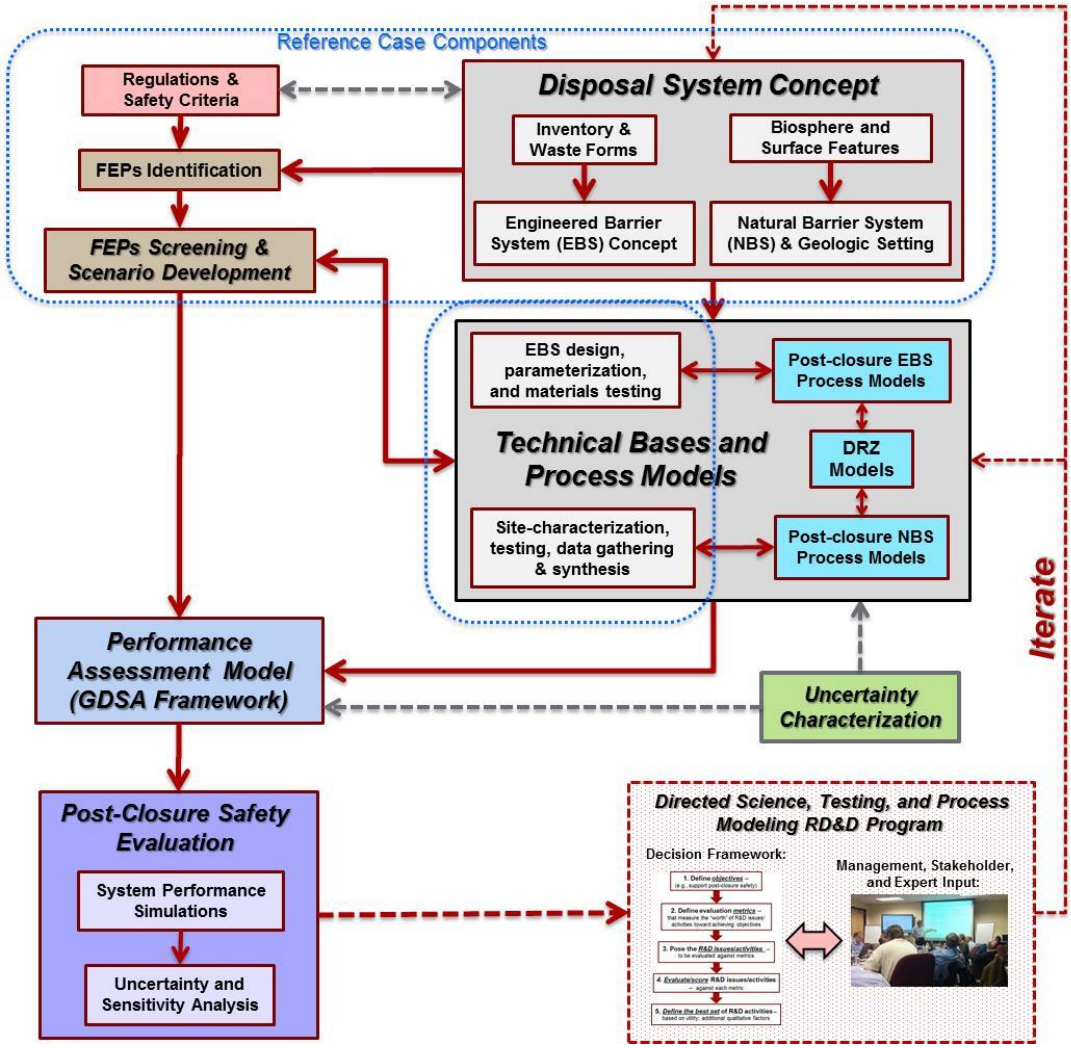

Figure 2-3. Evolution and Iteration of Technical Bases and Performance Assessment. [Reference Case elements enclosed by blue dotted boxes. GDSA = Generic Disposal System Analysis]

FEPs have traditionally been organized using the NEA-based classification scheme that is based on two overlapping sets of categories or headings: Features (e.g., waste form, waste package, backfill, and host rock) and multi-physics Processes (e.g., thermal, chemical, mechanical, and hydrologic). These NEA-based Heading categories overlap because an individual FEP, which is typically a process or event acting upon or within a feature (or several features), can often be mapped to more than one Heading (e.g., it can be mapped to both a feature-based Heading and to a process-based Heading). As a result, an NEA-based organizational structure may lead to ambiguity in finding a unique "home" for all FEPs—related FEPs are not always mapped under the same Heading category, making it difficult to group and/or find all related FEPs within a FEP list. In addition, the overlapping categories sometimes lead to the creation of the same or similar FEPs under different Headings.

During PA model construction and/or Safety Case development it is often necessary to analyze groups of FEPs related to specific topical areas (i.e., all FEPs relevant to the behavior of a specific repository feature, or all FEPs directly affecting or potentially coupled to a specific long-term process). The ability to efficiently search a FEP catalog or database to find the complete group of FEPs related to a topical area of interest greatly facilitates these types of evaluations. Searches within a FEP catalogue organized according to the NEA classification scheme can be difficult and produce incomplete results due to the overlapping categories and non-unique FEP mapping. Thus, to better inform PA modeling and safety case development, a new FEP organizational structure, the FEP classification matrix (Freeze et al. 2014), is under development that alleviates some of the foregoing issues. The FEP classification matrix is based on the concept that a FEP is typically a process or event acting upon or within a feature. The FEP matrix provides a two-dimensional organizational structure consisting of a Features axis that defines the "rows" and a Processes/Events axis that defines the "columns."

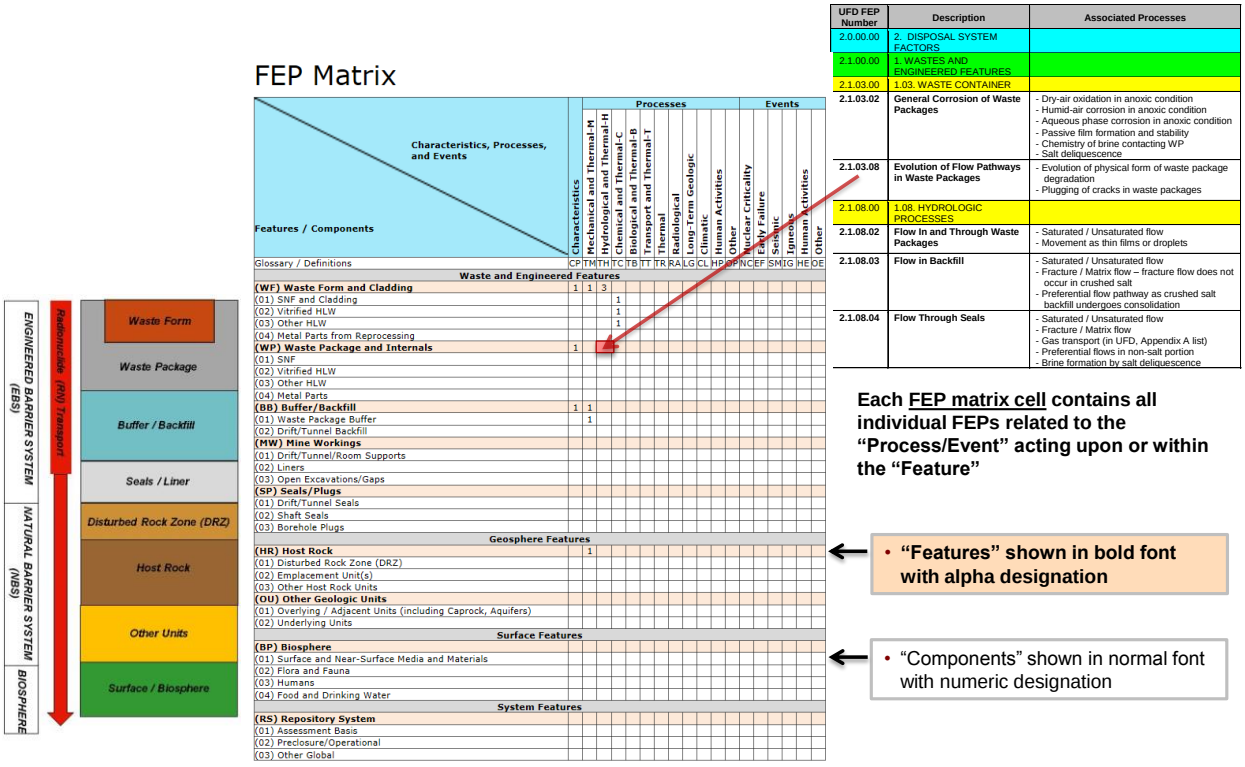

UFD FEP Number	Description	Associated Processes
2.0.00.00	2. DISPOSAL SYSTEM FACTORS	
2.1.00.00	1. WASTES AND ENGINEERED FEATURES	
2.1.03.00	1.03. WASTE CONTAINER	
2.1.03.02	General Corrosion of Waste Packages	- Dry-air oxidation in anoxic condition - Humid-air corrosion in anoxic condition - Aqueous phase corrosion in anoxic condition - Passive film formation and stability - Chemistry of brine contacting WP - Salt deliquescence
2.1.03.08	Evolution of Flow Pathways in Waste Packages	- Evolution of physical form of waste package degradation - Plugging of cracks in waste packages
2.1.08.00	1.08. HYDROLOGIC PROCESSES	
2.1.08.02	Flow In and Through Waste Packages	- Saturated / Unsaturated flow - Movement as thin films or droplets
2.1.08.03	Flow in Backfill	- Saturated / Unsaturated flow - Fracture / Matrix flow – fracture flow does not occur in crushed salt - Preferential flow pathway as crushed salt backfill undergoes consolidation
2.1.08.04	Flow Through Seals	- Saturated / Unsaturated flow - Fracture / Matrix flow - Gas transport (in UFD, Appendix A list) - Preferential flows in non-salt portion - Brine formation by salt deliquescence

Features / Components	Characteristics	Mechanical and Thermal-M	Hydrological and Thermal-H	Chemical and Thermal-C	Biological and Thermal-B	Transport and Thermal-T	Thermal	Radiological	Long-Term Geologic	Climatic	Human Activities	Other	Nuclear Criticality	Early Failure	Seismic	Igneous	Human Activities	Other
Glossary / Definitions	CP	TM	TH	TC	TB	TT	TR	RA	LG	CL	HP	OP	NC	EF	SM	IG	HE	OE
Waste and Engineered Features																		
(WF) Waste Form and Cladding	1	1	3															
(01) SNF and Cladding				1														
(02) Vitrified HLW				1														
(03) Other HLW				1														
(04) Metal Parts from Reprocessing																		
(WP) Waste Package and Internals	1																	
(01) SNF																		
(02) Vitrified HLW																		
(03) Other HLW																		
(04) Metal Parts																		
(BB) Buffer/Backfill	1	1																
(01) Waste Package Buffer		1																
(02) Drift/Tunnel Backfill																		
(MW) Mine Workings																		
(01) Drift/Tunnel/Room Supports																		
(02) Liners																		
(03) Open Excavations/Gaps																		
(SP) Seals/Plugs																		
(01) Drift/Tunnel Seals																		
(02) Shaft Seals																		
(03) Borehole Plugs																		
Geosphere Features																		
(HR) Host Rock		1																
(01) Disturbed Rock Zone (DRZ)																		
(02) Emplacement Unit(s)																		
(03) Other Host Rock Units																		
(OU) Other Geologic Units																		
(01) Overlying / Adjacent Units (including Caprock, Aquifers)																		
(02) Underlying Units																		
Surface Features																		
(BP) Biosphere																		
(01) Surface and Near-Surface Media and Materials																		
(02) Flora and Fauna																		
(03) Humans																		
(04) Food and Drinking Water																		
System Features																		
(RS) Repository System																		
(01) Assessment Basis																		
(02) Preclosure/Operational																		
(03) Other Global																		

Figure 2-4. Post-closure FEP matrix approach to FEP screening and analysis. [Note: The "thermal" processes column has since been changed from "TR" to "TL" as its alphanumeric designator.]

Figure 2-4 shows the complete FEP matrix (Sevougian 2016), with a portion of an old NEA-based FEP list in the upper right-hand corner (Freeze et al. 2013a)—the full FEP list may be hundreds to thousands of entries, each of which can be mapped to one or more FEP matrix cells. The Features axis (vertical) of the FEP matrix is organized to generally correspond to the direction of potential radionuclide migration, from the waste to the biosphere (i.e., from top to bottom in Figure 2-4). Features are organized in hierarchical categories. At the highest level are four Regions or "Feature Groups": Waste and Engineered Features (e.g., the EBS), Geosphere Features (e.g., the NBS), Surface Features (e.g., the Biosphere), and System Features. The

Surface Region is designed to capture FEPs that are relevant to the calculation of dose to the receptor, which may include radionuclide movement above the subsurface. The System Region is designed to include FEPs that are potentially relevant to the repository system as a whole. As shown in Figure 2-41, below each of the Regions are Features and Components categories. For example, in the Waste and Engineered Features Region are individual Features such as Waste Form and Cladding, Waste Package and Internals, Buffer/Backfill, Mine Workings, and Seals/Plugs. Below each of these Feature categories, a further level of detail is specified in the form of physical Components that comprise the repository system, such as Drift/Tunnel Seals and Shaft Seals. It should be noted that the hierarchical Region and Feature categories are fairly generic, but the Component category may become disposal-option specific.

As part of the work in developing the FEP matrix classification methodology (Freeze et al. 2014), a new organization and more transparent labeling of individual FEPs (corresponding to the rows and columns of the FEP matrix) has also been completed (Sevougian et al. 2016; Sevougian et al. 2015). This new FEP listing has been used as the basis for a preliminary FEP screening analysis for a generic crystalline host rock DWR, reproduced as Appendix A of this report. The preliminary FEP screening in Appendix A serves as an initial basis for the construction of the DWR PA model, as well as an initial basis for the completeness of an associated generic DWR safety case. Future process modeling and PA modeling can use this initial FEP screening as a starting point for refinement of the system model and for future justification as to the inclusion/exclusion of processes in the models.

3. CRYSTALLINE REPOSITORY REFERENCE CASE

The crystalline reference case for deep geologic disposal of defense-related HLW and SNF is similar to the crystalline reference case for disposal of commercial SNF developed in Mariner et al. (2016) because the natural barrier system (the far-field) is the same in both cases. The engineered system (the near field) is different for many repository features, including inventory, waste forms, and layout. The DWR assumes disposal of cooler (≤ 1 kW/canister) DOE-managed, research- and defense-related HLW and SNF in the year 2038. Potential inventory includes all existing and projected glass HLW from Savannah River and Hanford; the calcine waste at Idaho National Laboratory (INL)—either to be hot-isostatically pressed or vitrified; the cesium and strontium capsules at Hanford (either to be vitrified or directly disposed); research- and defense-related SNF (DSNF) with a heat output at the time of disposal of ≤ 1kW/canister; Naval SNF with a heat output at the time of disposal of ≤ 1kW/waste package; and other minor waste streams (Matteo et al. 2016). Specifically excluded from the DWR are waste forms of commercial origin including (but not limited to) glass HLW resulting from the West Valley Demonstration Project and DOE-managed SNF of commercial origin.

Excluding the hotter waste forms has little impact on the DSNF inventory eligible for disposal in the DWR, but significant impact on the Naval SNF inventory eligible for disposal. In particular, on the basis of canister wattages in 2010, 99.7% of DSNF is expected to have a thermal output of less than 1 kW/canister (Wilson 2016), and to be eligible for inclusion in a low-temperature DWR. Of the approximately 400 existing and projected Naval SNF waste packages, only 13 are expected to have a heat output ≤ 1 kW/canister (in 2025; SNL 2014, Section A-1.3). Thus, most would be excluded from a low-temperature DWR.

The DWR conceptual model consists of a mined repository approximately half a kilometer below the surface in sparsely fractured crystalline host rock, such as granite or metagranite in a stable cratonic terrain. Characteristics of the crystalline host rock that contribute to or impact post-closure safety include (Mariner et al. 2011; Freeze et al. 2013b; Mariner et al. 2016):

- The high structural strength of the host rock, which stabilizes engineered barriers;
- The depth of burial, which isolates the repository from surface processes (such as erosion and glaciation);
- The low permeability of the host rock, which isolates the repository from surface waters;
- The reducing chemical environment, which reduces waste package corrosion rates (contributing to waste containment), limits radionuclide solubility, and enhances radionuclide sorption (limiting and delaying radionuclide transport).
- The potential presence of a fracture network that creates a hydraulic connection between the repository and the biosphere, which if present could adversely impact the isolation of the repository while enhancing the transport of released radionuclides.

The remainder of this section includes a description of the engineered (Section 3.1) and natural (Section 3.2) barriers (including characterization of the fractured host rock), followed by a quantitative post-closure performance assessment (PA), including simulation of flow and transport coupled to the effects of decay heat (Sections 3.3 and 3.4). In addition to describing elements of the reference case that are unique to a DWR (including emplacement mode, inventory, and waste form), Section 3.2 and portions of Section 3.3 repeat descriptions of

elements that are identical in the commercial SNF and DWR crystalline reference cases, which were originally described in Mariner et al. (2016).

3.1 Waste and Engineered Barriers

Specific post-closure basis information related to the wastes and engineered barriers includes:

- Characteristics of the repository (Section 3.1.1),
- Inventory characterization (Section 3.1.2),
- Waste form characterization (Section 3.1.3),
- Waste package characterization (Section 3.1.4), and
- Characteristics of the engineered barriers (Section 3.1.5).

3.1.1 Characteristics of the Repository

This first iteration of the reference case considers disposal of existing and projected glass HLW from Savannah River and Hanford and of DSNF with a heat output at the time of disposal (2038) of less than 1 kW/canister. The reference case repository comprises a series of mined parallel disposal drifts connected by access halls. Repository access would be via vertical shafts and/or a ramp. HLW waste packages, each containing 5 glass logs, are axially emplaced in HLW disposal drifts on plinths of a low-permeability engineered material; drifts are buffered and backfilled with the same material, here assumed to be compacted bentonite. DSNF waste packages, each containing a single canister of DSNF, are emplaced in short vertical boreholes drilled beneath floors of DSNF disposal drifts. Each waste package sits on a plug of low permeability engineered material (assumed to be concrete) and is surrounded by low permeability engineered material (assumed to be compacted bentonite). DSNF drifts are also backfilled with low permeability engineered material, which is assumed to be compacted bentonite for the purposes of the post-closure PA reported herein. These two design concepts for vertical single-canister emplacement of hotter DSNF and horizontal in-drift multi-canister emplacement of cooler HLW are similar to those recommended by Matteo et al. (2016, Section 2.3). The former design concept has many of the characteristics of the Swedish KBS-3V concept (SKB 2011) and the latter has many of the characteristics of a Yucca Mountain co-disposal waste package (DOE 2008).

Assuming the canister counts listed in Wilson (2016), the current post-closure PA includes approximately 67% of the inventory of existing and projected glass HLW from Savannah River and Hanford and approximately 67% of the inventory of DSNF with a heat output of $\leq$ 1500 W/canister (calculated on the basis of 2010 wattages). The included inventory is accommodated in 42 disposal drifts, each 805 m in length, with drift centers separated by 20 m. This repository layout (Table 3-1) is the same as that simulated for the CSNF crystalline reference case (Mariner et al. 2016). However, waste package dimensions (described in Section 3.1.4) and emplacement modes (described in the previous paragraph) differ from the CSNF reference case, in which all waste packages were of uniform size and emplaced axially in-drift. Table 3-1 lists repository and waste package dimensions as derived from various sources under "Reference Value," with dimensions used in PA simulations listed under "Simulated Value"—simulated values reflect the smaller simulated inventory as well as adjustments needed to facilitate gridding. Further

description of the inventory, waste forms, and waste packages is given in the remainder of Section 3.1.

Table 3-1. Repository layout and EBS design for the DWR crystalline reference case.

Parameters	Reference Value	Simulated Value
HLW Waste Package (WP)		
WP length (m)	5.3 [a]	5.00
WP outer diameter (m)	2.1 [a]	1.67 (on a side) [h]
WP center-to-center spacing in-drift (m)	6.67	6.67
Inventory (glass logs per waste package)	5 [a]	5
Number of Hanford WPs/canisters	2216/11800 [b]	1485/7425
Number of Savannah River WPs/canisters	1512/7824 [b]	1014/5070
DSNF Waste Package (WP)		
WP length (m)	4.6 [c]	4.4
WP outer diameter (m)	0.61 [c]	0.56 (on a side) [h]
Emplacement borehole diameter (m)	1.5 [d]	1.67 (on a side) [h]
Emplacement borehole length (m)	8 [d]	7.8
Emplacement borehole spacing	≥6 [d]	10
Inventory (DSNF canisters per waste package)	1 [d]	1
Number of DSNF WPs (< 50 W bin)	1163 [b]	787
Number of DSNF WPs (50-100 W bin)	234 [b]	158
Number of DSNF WPs (100-200 W bin)	940 [b]	636
Number of DSNF WPs (200-300 W bin)	12 [b]	8
Number of DSNF WPs (300-500 W bin)	41 [b]	28
Number of DSNF WPs (500-1000 W bin)	88 [b]	60
Number of DSNF WPs (1000-1500 W bin)	4 [b]	3
HLW Emplacement Drift		
Number of HLW WPs per drift	119	119
Drift seal length (m)	10 [e]	5
Number of HLW drifts	~31	21
DSNF Emplacement Drift		
Number of DSNF WPs per drift	80	80
Drift seal length (m)	10 [e]	5
Number of HLW drifts	~31	21
Repository		
Drift diameter (m)	4.5 [e]	5.0 (on a side) [h]
Drift center-to-center spacing (m)	20 [e]	20
Drift length, including seals (m)	805 [e]	805
Total number of drifts	~62	42
Access hall/ramp height (m)	5 [e]	5
Access hall/ramp width (m)	8 [e]	8.35
Repository length (m)	1,618 [f]	821
Repository width (m)	605 [g]	825
Repository Depth (m)	600 [e]	585

[a] Yucca Mountain long co-disposal package (DOE 2008, Figure 1.5.2-5).
[b] On the basis of canister counts reported in Wilson (2016) and Carter et al. (2013).
[c] Large, long standardized canister (DOE 2008, Figure 1.5.1-9).
[d] Matteo et al. 2016, Section 2.3.
[e] Wang et al. (2014), Table 2-4; Mariner et al. (2016), Table 4-1.
[f] Length of 2 paired drifts, separated by median access hall, as assumed in Wang et al. (2014).
[g] On the basis of 31 drift pairs.
[h] PFLOTRAN simulations represent waste packages as rectangular cuboids instead of right circular cylinders, in order to simplify the gridding.

3.1.2 Inventory

The reference case inventory is based on glass HLW inventories reported in Carter et al. (2013) and DSNF inventories reported in Wilson (2016). It includes all projected glass HLW at Hanford, all existing and projected glass HLW at Savannah River, and all DSNF with a heat output of ≤ 1500 W/canister assuming 2010 wattages.

3.1.2.1 Glass HLW

Carter et al. (2013) provided canister counts for existing and projected glass HLW, as well as estimated radionuclide inventories for the bulk inventory of tank waste at Hanford (which is projected to become the Hanford inventory of glass HLW) and the bulk inventory of existing and projected glass HLW at Savannah River in the year 2017 (Carter et al. 2013, Table F-1). To calculate the radionuclide inventory per waste package for PA simulations, each bulk inventory was divided by the corresponding total number of canisters (11800 and 7824, respectively) and multiplied by the number of canisters per waste package (5). Radionuclide inventories were decayed as a function of time in order to calculate the heat of decay per waste package as a function of time. Resulting curves are plotted in Figure 3-1. Bulk and per canister inventories of selected radionuclides are listed in Table 3-2 and Table 3-3, respectively.

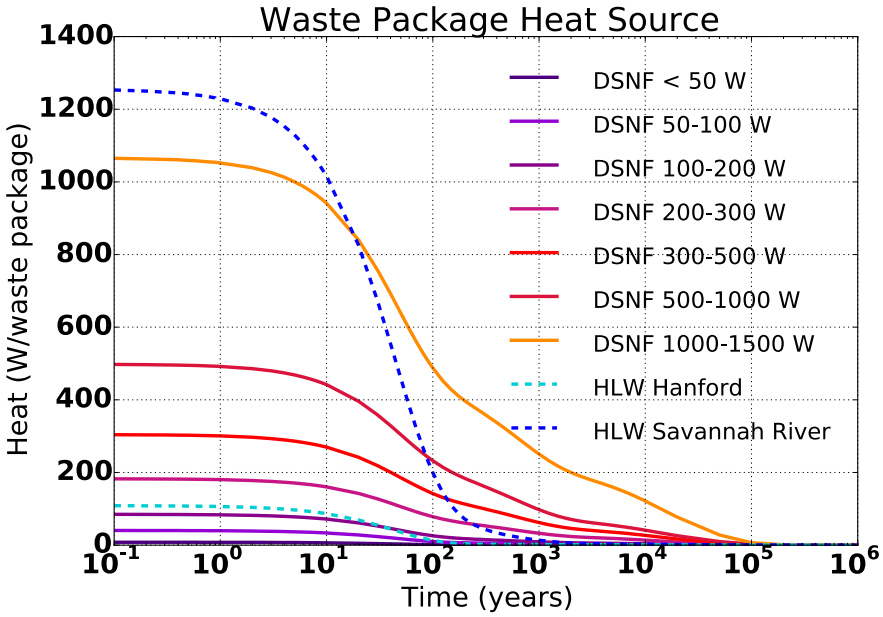

Figure 3-1. Heat of decay versus time per waste package for the glass HLW and DSNF bins included in DWR PA simulations. [Time zero is the year 2038.]

3.1.2.2 DSNF

Wilson (2016) provided canister counts (projected to the year 2035) and average radionuclide inventories for each of 8 thermal bins of DSNF. Bulk and average per canister inventories of the seven coolest bins, those included in PA simulations, are listed in Table 3-2 and Table 3-3, respectively; these bins account for all but 3 of 2485 canisters (viz., those with heat output > 1500 W/canister). Binning was based on canister heat output calculated from radionuclide inventories in 2010. On the basis of 2010 radionuclide inventories, almost half (47%) of the DSNF canisters have or are expected to have a heat output < 50 W, and most (94%) have or are

expected to have a heat output < 200 W (Wilson 2016). When the average inventories reported in Wilson (2016) are decayed to the year 2038, the hottest bin included in PA simulations (the 1000-1500 W bin), has an average heat output of approximately 1066 W/canister (Figure 3-1).

Table 3-2. Bulk radionuclide inventories for HLW and DSNF included in PA.

Isotope	Bulk inventory (g)									Decay Constant (1/s)[c]
	Hanford HLW[a]	Savannah HLW[a]	<50 W DSNF[b]	50-100 W DSNF[b]	100-200 W DSNF[b]	200-300 W DSNF[b]	300-500 W DSNF[b]	500-1000 W DSNF[b]	1000-1500 W DSNF[b]	
(canister count)	*(11800)*	*(7824)*	*(1163)*	*(234)*	*(940)*	*(12)*	*(41)*	*(88)*	*(4)*	
^{241}Am	4.1E+04	6.5E+05	3.0E+03	8.0E+03	1.0E+05	4.4E+03	2.7E+04	1.0E+05	7.6E+03	5.08E-11
^{243}Am	7.5E+01	4.6E+04	1.9E+02	1.0E+02	3.1E+03	1.5E+02	8.2E+02	3.5E+03	1.4E+01	2.98E-12
^{238}Pu	2.5E+02	3.6E+05	8.1E+02	3.8E+02	6.3E+03	2.2E+02	1.2E+03	4.9E+03	1.7E+02	2.56E-10
^{239}Pu	1.1E+06	1.9E+06	6.0E+04	1.9E+05	1.7E+06	7.9E+04	5.3E+05	1.7E+06	2.4E+05	9.01E-13
^{240}Pu	5.4E+04	2.6E+05	1.5E+04	4.2E+04	4.3E+05	2.1E+04	1.4E+05	4.4E+05	5.7E+04	3.34E-12
^{242}Pu	2.6E+02	3.8E+04	1.9E+03	8.2E+02	1.9E+04	8.3E+02	4.1E+03	1.2E+04	8.2E+01	5.80E-14
^{237}Np	2.0E+05	2.9E+05	3.9E+03	4.2E+03	4.9E+04	1.5E+03	7.8E+03	3.1E+04	1.5E+03	1.03E-14
^{233}U	5.3E+04	3.9E+04	4.8E+02	5.5E-01	2.0E+02	1.3E-01	7.7E-01	2.7E+00	1.5E-02	1.38E-13
^{234}U	3.5E+04	7.8E+04	1.1E+04	2.8E+03	1.9E+04	1.3E+02	7.0E+02	4.6E+04	9.1E+01	8.90E-14
^{236}U	9.3E+04	3.8E+05	1.9E+05	1.1E+05	8.5E+05	1.2E+04	6.9E+04	4.9E+05	2.2E+03	9.20E-16
^{238}U	5.9E+08	9.6E+08	1.2E+07	2.5E+07	1.7E+08	2.0E+06	9.2E+06	2.7E+07	2.9E+05	4.87E-18
^{229}Th	1.1E+01	4.4E+00	1.1E-01	8.6E-05	4.8E-02	3.0E-05	1.7E-04	5.3E-04	1.3E-06	2.78E-12
^{230}Th	7.0E-01	4.5E+00	1.1E+00	2.4E-01	1.8E+00	1.1E-02	6.1E-02	4.2E+00	7.8E-03	2.75E-13
^{129}I	2.7E+05	1.2E+04	2.8E+03	2.5E+03	2.0E+04	6.4E+02	2.5E+03	9.6E+03	1.3E+03	1.29E-15
^{135}Cs	1.3E+06	1.4E+05	1.1E+04	7.1E+03	3.9E+04	2.1E+03	4.8E+03	1.7E+04	7.8E+03	9.55E-15
^{99}Tc	1.8E+06	3.7E+06	1.5E+04	1.4E+04	1.0E+05	2.8E+03	1.1E+04	4.3E+04	5.4E+03	1.04E-13

[a] Bulk inventory in 2038 calculated on the basis of bulk inventory in 2017 as reported in Carter et al. (2013).
[b] Bulk inventory in 2038 calculated on the basis of average canister inventories in 2010 and canister counts reported in Wilson (2016).
[c] Decay constants from ORIGEN (Croff 1983).

Table 3-3. Per canister radionuclide inventories for HLW and DSNF included in PA.

Isotope	Canister inventory (g/canister)									Decay Heat (W/g)[c]
	Hanford HLW[a]	Savannah HLW[a]	<50 W DSNF[b]	50-100 W DSNF[b]	100-200 W DSNF[b]	200-300 W DSNF[b]	300-500 W DSNF[b]	500-1000 W DSNF[b]	1000-1500 W DSNF[b]	
(canister count)	*(11800)*	*(7824)*	*(1163)*	*(234)*	*(940)*	*(12)*	*(41)*	*(88)*	*(4)*	
^{241}Am	3.5E+00	8.3E+01	2.6E+00	3.4E+01	1.1E+02	3.6E+02	6.7E+02	1.1E+03	1.9E+03	1.140E-01
^{243}Am	6.4E-03	5.9E+00	1.7E-01	4.3E-01	3.3E+00	1.2E+01	2.0E+01	4.0E+01	3.5E+00	6.408E-03
^{238}Pu	2.1E-02	4.6E+01	7.0E-01	1.6E+00	6.7E+00	1.9E+01	3.0E+01	5.6E+01	4.2E+01	5.673E-01
^{239}Pu	9.4E+01	2.4E+02	5.2E+01	8.1E+02	1.8E+03	6.6E+03	1.3E+04	2.0E+04	6.0E+04	1.916E-03
^{240}Pu	4.6E+00	3.3E+01	1.3E+01	1.8E+02	4.6E+02	1.7E+03	3.3E+03	5.0E+03	1.4E+04	7.096E-03

Isotope	Canister inventory (g/canister)									Decay Heat (W/g)[c]
	Hanford HLW[a]	Savannah HLW[a]	<50 W DSNF[b]	50-100 W DSNF[b]	100-200 W DSNF[b]	200-300 W DSNF[b]	300-500 W DSNF[b]	500-1000 W DSNF[b]	1000-1500 W DSNF[b]	
^{242}Pu	2.2E-02	4.8E+00	1.7E+00	3.5E+00	2.0E+01	6.9E+01	1.0E+02	1.3E+02	2.0E+01	1.128E-04
^{237}Np	1.7E+01	3.6E+01	3.4E+00	1.8E+01	5.2E+01	1.2E+02	1.9E+02	3.5E+02	3.8E+02	2.154E-05
^{233}U	4.5E+00	5.0E+00	4.1E-01	2.3E-03	2.2E-01	1.1E-02	1.9E-02	3.0E-02	3.7E-03	2.815E-04
^{234}U	3.0E+00	1.0E+01	9.2E+00	1.2E+01	2.1E+01	1.1E+01	1.7E+01	5.2E+02	2.3E+01	1.800E-04
^{236}U	7.9E+00	4.9E+01	1.6E+02	4.7E+02	9.0E+02	1.0E+03	1.7E+03	5.5E+03	5.4E+02	1.753E-06
^{238}U	5.0E+04	1.2E+05	1.1E+04	1.1E+05	1.8E+05	1.7E+05	2.3E+05	3.0E+05	7.2E+04	8.528E-09
^{229}Th	9.2E-04	5.6E-04	9.7E-05	3.7E-07	5.1E-05	2.5E-06	4.0E-06	6.0E-06	3.2E-07	6.508E-03
^{230}Th	6.0E-05	5.8E-04	9.6E-04	1.0E-03	1.9E-03	9.5E-04	1.5E-03	4.8E-02	1.9E-03	5.712E-04
^{129}I	2.3E+01	1.6E+00	2.4E+00	1.1E+01	2.1E+01	5.3E+01	6.1E+01	1.1E+02	3.3E+02	8.166E-08
^{135}Cs	1.1E+02	1.8E+01	9.1E+00	3.0E+01	4.1E+01	1.7E+02	1.2E+02	1.9E+02	1.9E+03	3.843E-07
^{99}Tc	1.5E+02	4.7E+02	1.3E+01	5.9E+01	1.1E+02	2.3E+02	2.8E+02	4.8E+02	1.3E+03	8.501E-06

[a] Average canister inventory in 2038 calculated on the basis of bulk inventory in 2017 and canister counts as reported in Carter et al. (2013).
[b] Average canister inventory in 2038 calculated on the basis of average canister inventories in 2010 reported in Wilson (2016).
[c] Heat of decay from ORIGEN 2.2 database (Croff 1983). Additional radionuclides (e.g., ^{137}Cs, ^{90}Sr) contribute to the heat of decay plotted in Figure 3-1.

3.1.3 Waste Forms

3.1.3.1 Glass HLW

Existing and projected glass HLW from Savannah River and projected glass HLW from Hanford is/will be borosilicate glass (SNL 2014, Sections A-2.1.2, A-2.2.1, A-2.2.2). At Savannah River, eight macrobatches of glass production have resulted in 3339 canisters of glass, each containing approximately 1800 kg of glass (SNL 2014, Section A-2.1.2). Canisters are nominally 3 m in length and 0.61 m in diameter, and are constructed of 304L stainless steel. Future glass HLW canisters produced at Savannah River are expected to be consistent with those already in existence (SNL 2014, Section A-2.2.2). At Hanford, HLW will be vitrified in canisters nominally 4.5 m in length, 0.61 cm in diameter, and constructed of 304L stainless steel. Each canister is expected to hold 3020 kg of glass (SNL 2014, Section A-2.2.1).

Glass HLW is typically assumed to begin dissolving when exposed to water (Sassani et al. 2016, Section 3.2.2). Glass dissolution rates evolve over time as local pore fluids become saturated with silica and glass alteration products accumulate. PA simulations assume a rate law formulated by Kienzler et al. (2012, Equation 6) and summarized in Sassani et al. (2016, Table 3-4):

$$r = 560 \cdot exp\left(\frac{-7397}{T}\right) \quad (3\text{-}1)$$

where r is the rate of dissolution in kg m^{-2} d^{-1} and T is temperature in Kelvin. The rate law was derived from measurements in both water and salt solutions and is appropriate for the long-term dissolution of glass in the presence of silica-saturated pore fluids and glass alteration products.

See Section 3.3.2.5 for further discussion of the implementation in PA simulations.

3.1.3.2 DSNF

DSNF comprises multiple waste types, which may include (among others) metallic fuels such as those from N-Reactor, oxide fuels, and coated-particle fuels (SNL 2014, Section A-1.2.1). DSNF is packaged or projected to be packaged in multicanister overpacks (MCOs) and standardized canisters suitable for storage, transport, and disposal (SNL 2014, Section 1.2.2). MCOs are primarily in use to store N-Reactor fuel in configurations of 5 or 6 fuel assemblies per MCO; they are constructed of stainless steel and are approximately 4.2 m (166 inches) in length and 0.61 m (24 inches) in diameter. The projected inventory of MCOs is approximately 400 (DOE 2008, Section 1.5.1.3.1.2). Standardized canisters are planned to hold various wastes and will be manufactured of stainless steel in two lengths (3.0 m (10 feet) and 4.6 m (15 feet)) and two diameters (0.61 m (24 inches) and 0.46 m (18 inches)), for a total of 4 configurations (DOE 2008, Section 1.5.1.3.1.2).

The various DSNF waste types have various best-estimate models for waste form degradation (Sassani et al. 2016, Tables 3-6 to 3-8). Current PA simulations assume instantaneous degradation of DSNF at the time of exposure to water, as appropriate for metallic fuels.

3.1.4 Waste Packages

3.1.4.1 Glass HLW

The glass HLW waste package is stainless steel and assumed to be similar in dimensions to the Yucca Mountain co-disposal package (DOE 2008, Figure 1.5.2-5), which is 2.1 m in diameter and either 3.7 m (short co-disposal package) or 5.3 m (long co-disposal package) in length. Each HLW waste package contains five stainless steel pour canisters with vitrified borosilicate HLW in each canister. [Grid block size in the PFLOTRAN numerical grid resulted in a simulated waste package slightly smaller in volume than the long co-disposal package, viz., 5 m in length and 1.67 m in height and width (see Table 3-1).]

In PA simulations, each waste package is a single region containing a radionuclide source term and a heat source term (see Sections 3.3.2.4 and 3.3.2.5). Waste package material properties are set equal to those used in the CSNF reference case (Mariner et al. 2016): porosity is set to 0.5 to account for the void spaces between fuel assemblies and canister internals. Permeability is set several orders of magnitude higher than that of the surrounding materials (10^{-16} m^2), so that flow through waste packages is uninhibited. The waste package is given the thermal properties of stainless steel (Shelton 1934). Probabilistic simulations sample on waste package tortuosity (which scales the effective diffusion coefficient—see Appendix B) using a uniform distribution from 0.01 to 1.

The CSNF crystalline reference case was the first generic disposal system PA to take credit for waste package performance via calculation of "canister vitality" (Mariner et al 2016). The same model of waste package degradation via decreasing canister vitality is implemented here. See Section 3.3.2.5 for a description of the implementation of the waste-package degradation model in PA.

3.1.4.2 DSNF

DSNF waste packages are likely to consist of corrosion-resistant overpacks with a wall thickness of up to 10 cm, which would each hold a single MCO or standardized canister (Matteo et al.

2016). Current PA simulations assume waste package dimensions identical to those of the large, long, standardized canister: 4.6 m in length and 0.61 m in diameter (DOE 2008, Figure 1.5.1-9). As gridded, DSNF waste packages are 4.4 m in length and 0.55 m in height and width, resulting in a volume nearly identical to that of the large, long standardized canister.

In PA simulations, each waste package region is assigned material properties identical to those used for the glass HLW waste packages, and the same waste package degradation model is applied (see preceding section).

3.1.5 Bentonite Buffer (Emplacement Boreholes, Drifts, and Access Halls)

The crystalline reference case assumes horizontal, in-drift emplacement of glass HLW with waste packages elevated on plinths of compacted bentonite and drifts buffered and filled with compacted bentonite pellets and/or bricks in one or two layers, as shown in Figure 3-2(a) (Wang et al. 2014). Another option would be individual waste package vaults prefabricated of compacted bentonite arches (Matteo et al. 2016). PA simulations assume a single layer, single material buffer. DSNF waste packages in vertical emplacement boreholes are assumed to be emplaced within prefabricated rings of bentonite buffer as in the Swedish KBS-3V concept (Figure 3-2(b); Pettersson and Lonnerberg 2008); additionally, bentonite pellets may fill any remaining void space in the emplacement borehole (Matteo et al. 2016). Access halls may be filled with a mixture of crushed rock and bentonite or another geologic material rich in clay minerals (Mariner et al. 2011; Wang et al. 2014; Matteo et al. 2016), but the present simulations assume the halls and drifts are both filled with a compacted bentonite buffer.

Compacted bentonite has low permeability, high sorption capacity (see Section 3.2.2.8), and may be engineered to achieve desirable thermal properties; for instance, quartz sand or graphite can be added to increase thermal conductivity (Choi and Choi 2008; Jobmann and Buntebarth 2009; Wang et al. 2015). The current set of simulations employs material properties appropriate for a compacted mixture of 70% bentonite and 30% quartz sand. The buffer is assigned a porosity of 0.35 (Liu et al. 2016), a permeability of 10^{-20} m^2 (Liu et al. 2016), and a water-saturated thermal conductivity of 1.5 $Wm^{-1}K^{-1}$ (Wang et al. 2015). Probabilistic simulations sample on porosity using a uniform distribution over the range 0.3 to 0.5.

3.1.6 Cement slabs

Cement slabs (0.56 m in length) are assumed to sit at the base of each vertical emplacement borehole as in the KBS-3V disposal concept, which specifies a 0.5 m cement slab at the base of an 8.2 m borehole (Pettersson and Lonnerberg 2008). Properties of cement vary with water-to-cement ratio and degree of hydration; intact cement has low porosity of 0.15 (Jove Colon et al. 2014) and very low permeability on the order of 10^{-18} to 10^{-21} m^2 (Halamickova et al. 1995; Jove Colon et al. 2014). PA simulations assume a porosity of 0.15, a permeability of 10^{-19} m^2, and a thermal conductivity of 1.7 $Wm^{-1}K^{-1}$.

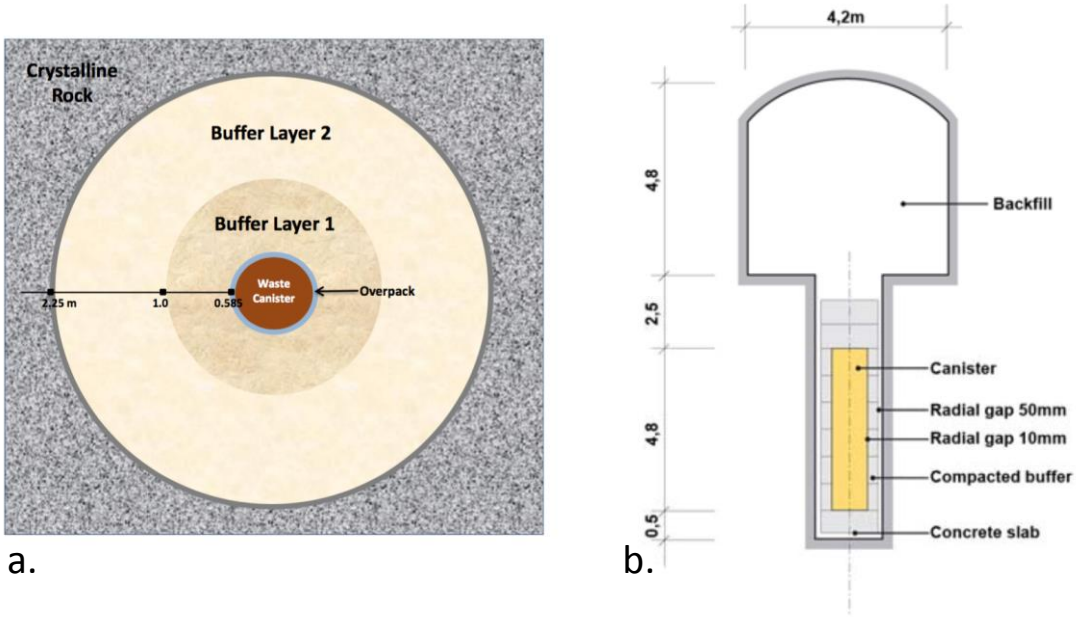

Figure 3-2. (a) Schematic cross-section of a double-layer buffer in a disposal drift of a CSNF crystalline repository (Wang et al. 2014). (b) Cross-section of a vertical emplacement borehole showing placement of compacted bentonite buffer in the KBS-3V concept (Pettersson and Lonnerberg 2008).

3.2 Geosphere/Natural Barriers

Specific post-closure basis information related to the geosphere and natural barriers include:

- Characteristics of the natural barriers (e.g., location, geologic setting) (Section 3.2.1),
- Host rock characterization (Section 3.2.2),
- Disturbed rock zone (DRZ) characterization (Section 3.2.3), and
- Overburden characterization (Section 3.2.3).

3.2.1 Natural Barrier Characteristics

The present concept for a mined repository in crystalline rock places the repository approximately half a kilometer below the land surface in a sparsely fractured crystalline rock (such as granite) that either outcrops or subcrops near surface. Regionally, the topographic slope is < 1°, and the water table is unconfined, a combination which would provide little driving force for deep fluid flow. The reference repository site has a stable cratonic terrain with low probabilities of seismicity, igneous activity, and human intrusion. The latter probability is reduced by avoiding regions with known geologic resources such as extensive fresh water aquifers, ore deposits, fossil fuels, or high geothermal heat flux (which offers the potential for geothermal development). This concept is consistent with international concepts of disposal in crystalline rock (e.g., SKB 2007).

Locations fitting this concept occur in the north-central and eastern United States as shown in Figure 3-3 (Perry et al. 2016), where outcropping/subcropping crystalline basement is Precambrian to Archean in age (e.g., Barton et al. 2003) and measured heat flow is generally between 35 and 65 mW/m^2 (Blackwell et al. 2011). At repository depth, the host rock is saturated, likely with brackish water (see Section 3.2.2.6). The driving force for regional flow at depth is assumed to be similar to that in deep sedimentary basins, on the order of 0.001 m/m (e.g., Downey and Dinwiddie 1988).

3.2.2 Crystalline Host Rock

The representation of fractured crystalline rock is based primarily on the well-characterized, sparsely fractured metagranite at Forsmark, Sweden (Follin et al. 2014; Joyce et al. 2014). The Forsmark site is in the Fennoscandian Shield and consists of crystalline bedrock (primarily granite with lesser amounts of granodiorite, tonalite, and amphibolite) that formed between 1.89 and 1.85 Ga (1 Ga = 1 billion years), experienced ductile deformation and metamorphism, and cooled to the limit of brittle deformation between 1.8 and 1.7 Ga (SKB 2007). Subsequent brittle deformation occurred associated with later tectonic events (1.7 to 1.6 Ga and 1.1 to 0.9 Ga), and recent glaciation (< 1 Ma) has resulted in crystalline basement outcrops and thin (< 25 m) Quaternary sedimentary deposits of variable thickness and extent (SKB 2008). Crystalline basement with similar history exists within the United States (for instance at the southern margin of the approximately 2-Ga-old Superior Craton in Minnesota (Perry et al. 2016), and can be reasonably expected to have similar hydraulic properties.

Conceptually, the crystalline host rock is comprised of two media: fractures and matrix. Numerically it is simulated with two types of grid cells: those containing a fracture or fractures and those without fractures (the matrix). Hydraulic parameters (permeability and porosity)

describing fracture grid cells are derived from fracture parameters developed for the Forsmark metagranite (Follin et al. 2014; Joyce et al. 2014; Wang et al. 2014). Hydraulic parameters describing matrix cells are derived from measurements made in tunnel walls of underground research laboratories (URLs) in crystalline rock at the Grimsel Test Site, Switzerland (Schild et al. 2001; Soler et al. 2015), Lac du Bonnet batholith, Canada (Martino and Chandler 2004), and the Korean Underground Research Tunnel (Cho et al. 2013). All other parameters are identical in fracture and matrix cells.

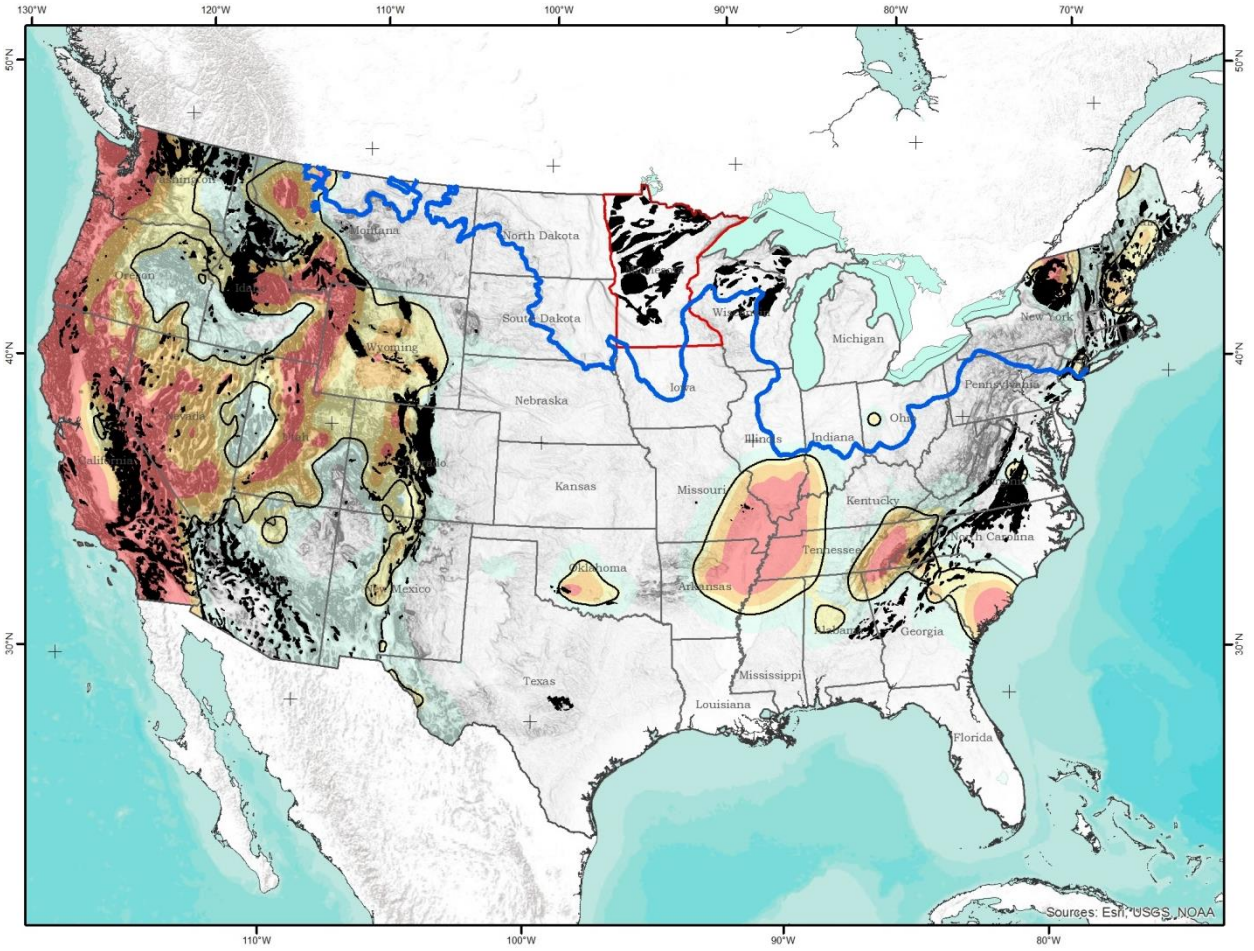

Figure 3-3. Locations of crystalline rock outcrop and near-surface subcrop in the US (black). Regions of high seismic hazard are shown in warm color shading. The blue line is the maximum extent of the last glacial maximum. [Figure from Perry et al. (2016, Fig. 2-2).]

3.2.2.1 Fracture Permeability and Porosity

Host rock permeability due to fractures depends upon the distribution, orientation, and transmissivity of open, conductive fractures. Fracture porosity additionally depends on fracture aperture. Statistical descriptions of these fracture properties are used to generate multiple realizations of fracture networks, which are mapped to an equivalent continuous porous medium (ECPM) domain (Mariner et al. 2016, Section 3.1.3.1) in order to calculate the permeability and porosity of each grid cell intersected by a fracture or fractures. PA simulations use fracture parameters derived from parameters applicable to the sparsely fractured granite at Forsmark, Sweden.

At Forsmark, large-scale mappable features of concentrated brittle and/or ductile deformation (termed "deformation zones") bound volumes of relatively undeformed rock (Follin et al. 2014; Joyce et al. 2014). Each volume of relatively undeformed rock (termed a "fracture domain") is sparsely fractured, and the fractures within each can be described in terms of a number of "fracture sets," distinguished from each other on the basis of fracture orientation. At Forsmark six fracture domains are defined, each containing five fracture sets. As appropriate, three depth zones are defined (< 200 m below sea level (mbsl), 200-400 mbsl, and > 400 mbsl) in order to account for the decrease in fracture density and fracture transmissivity with depth. Each fracture set within a particular fracture domain and depth zone is described using a 3-dimensional Fisher distribution to describe the orientation of fracture poles in space, a truncated power-law distribution for fracture radii, and a fracture density, P_{32}, which is defined as the surface area of fractures per volume of rock (m^2/m^3). For each depth zone within a fracture domain, a relationship is given between fracture radius and fracture transmissivity. A schematic of how fracture domains and depth zones might apply to a volume of crystalline rock containing a mined repository is shown in Figure 3-4.

Table 2 Hydrogeological DFN parameters for each fracture domain, fracture set and depth zone

Fracture domain/elevation (m.a.s.l)[a]	Fracture set name	Orientation set pole: (trend, plunge), conc.	Size model, power-law (r_0, k_r) (m, −)	Intensity, (P_{32}), valid size interval: r_0 to 564 m (m^2/m^3)	Parameter values for the transmissivity models: Semi-correlated (a,b,σ)	Correlated (a,b)	Uncorrelated (μ,σ)
FFM01 and FFM06>−200	NS	(292, 1) 17.8	(0.038, 2.50)	0.073	$6.3 \cdot 10^{-9}$, 1.3, 1.0	$6.7 \cdot 10^{-9}$, 1.4	−6.7, 1.2
	NE	(326, 2) 14.3	(0.038, 2.70)	0.319			
	NW	(60, 6) 12.9	(0.038, 3.10)	0.107			
	EW	(15, 2) 14.0	(0.038, 3.10)	0.088			
	HZ	(5, 86) 15.2	(0.038, 2.38)	0.543			
FFM01 and FFM06 −200 to −400	NS	(292, 1) 17.8	(0.038, 2.50)	0.142	$1.3 \cdot 10^{-9}$, 0.5, 1.0	$1.6 \cdot 10^{-9}$, 0.8	−7.5, 0.8
	NE	(326, 2) 14.3	(0.038, 2.70)	0.345			
	NW	(60, 6) 12.9	(0.038, 3.10)	0.133			
	EW	(15, 2) 14.0	(0.038, 3.10)	0.081			
	HZ	(5, 86) 15.2	(0.038, 2.38)	0.316			
FFM01 and FFM06<−400	NS	(292, 1) 17.8	(0.038, 2.50)	0.094	$5.3 \cdot 10^{-11}$, 0.5, 1.0	$1.8 \cdot 10^{-10}$, 1.0	−8.8, 1.0
	NE	(326, 2) 14.3	(0.038, 2.70)	0.163			
	NW	(60, 6) 12.9	(0.038, 3.10)	0.098			
	EW	(15, 2) 14.0	(0.038, 3.10)	0.039			
	HZ	(5, 86) 15.2	(0.038, 2.38)	0.141			
FFM02>−200	NS	(83, 10) 16.9	(0.038, 2.75)	0.342	$9.0 \cdot 10^{-9}$, 0.7, 1.0	$5.0 \cdot 10^{-9}$, 1.2	−7.1, 1.1
	NE	(143, 9) 11.7	(0.038, 2.62)	0.752			
	NW	(51, 15) 12.1	(0.038, 3.20)	0.335			
	EW	(12, 0) 13.3	(0.038, 3.40)	0.156			
	HZ	(71, 87) 20.4	(0.038, 2.58)	1.582			
FFM03, FFM04 and FFM05>−400	NS	(292, 1) 17.8	(0.038, 2.60)	0.091	$1.3 \cdot 10^{-8}$, 0.4, 0.8	$1.4 \cdot 10^{-8}$, 0.6	−7.2, 0.8
	NE	(326, 2) 14.3	(0.038, 2.50)	0.253			
	NW	(60, 6) 12.9	(0.038, 2.55)	0.258			
	EW	(15, 2) 14.0	(0.038, 2.40)	0.097			
	HZ	(5, 86) 15.2	(0.038, 2.55)	0.397			
FFM03, FFM04 and FFM05<−400	NS	(292, 1) 17.8	(0.038, 2.60)	0.102	$1.8 \cdot 10^{-8}$, 0.3, 0.5	$7.1 \cdot 10^{-9}$, 0.6	−7.2, 0.8
	NE	(326, 2) 14.3	(0.038, 2.50)	0.247			
	NW	(60, 6) 12.9	(0.038, 2.55)	0.103			
	EW	(15, 2) 14.0	(0.038, 2.40)	0.068			
	HZ	(5, 86) 15.2	(0.038, 2.55)	0.250			

[a] Meters above sea level

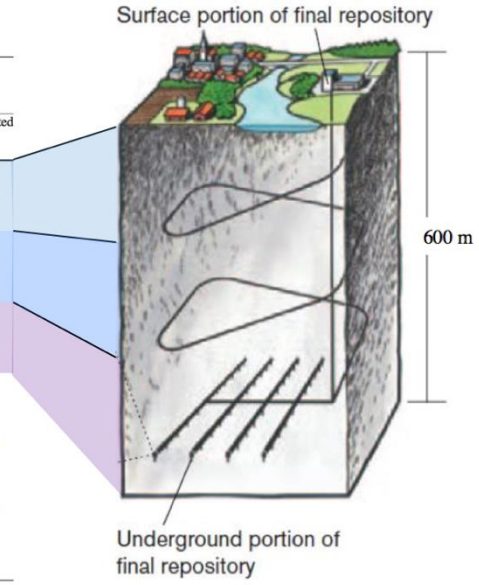

Figure 3-4. Schematic representation of how fracture domains and depth zones could be applied to a model domain containing a mined repository in crystalline rock. Highlighted fracture parameters apply to three depths below sea level (approximately coincident with the land surface at Forsmark). Fracture density decreases with depth and fracture transmissivity calculated from the given relationships decreases with depth. [Table from Joyce et al. (2014). Image from Wang et al. (2014).]

Parameters used to generate the fracture networks for use in PA simulations are listed in Table 3-4. Relative to the Forsmark fracture description, the current crystalline reference case makes several simplifying assumptions. These include:

- In the absence of a specific site with mapped features, the reference case domain contains a single deterministic deformation zone in order to acknowledge the need to map and model such features when a site is available.
- A single fracture domain (FFM01, 200-400 mbsl) is applied to the entire model domain.

- Only three fracture sets from the chosen domain are simulated, those with the largest number of open and flowing fractures (NS, NE, and HZ; Follin et al. 2014).
- For generality, the NE trending set is rotated to an EW orientation (joint sets tend to develop at right angles to each other; Twiss and Moores 1992).
- Although the Forsmark parameters are valid over the range of fracture radii from 0.038 m to 564 m (Follin et al. 2014; Joyce et al. 2014), the crystalline reference case uses a maximum fracture radius of 500 m and a minimum radius of 15 m (see discussion below).
- The fracture density is increased to ensure a percolating network.
- The crystalline reference case uses a direct correlation between fracture radius and fracture transmissivity.

Choices regarding fracture radii, density, and transmissivity are further discussed below.

Table 3-4. Parameters used to generate discrete fracture networks (modified from Wang et al. 2014).

	Orientation: Fisher Distribution for Poles			**Size: Truncated Power Law for Radii**			**Fracture density (Requested)**
Set	Mean Trend	Mean Plunge	κ	α	Min Radius r_0 (m)	Max Radius r_x (m)	Number of fractures in 1 km^3
NS	90°	0.0°	22	2.5	15	500	2100
EW	180°	0.0°	22	2.7	15	500	2000
HZ	360°	90.0°	10	2.4	15	500	2300

Fracture radii: Eliminating fractures with a radius smaller than 15 m is an acceptable simplification given the nature of the simulated fracture network, i.e., a sparse network with a large variation in fracture radius and direct correlation of fracture transmissivity to fracture radius. Hyman et al. (2015a) demonstrated that in this type of network, eliminating fractures with radii up to 25 m has essentially no effect on particle transport, because the largest fractures create a fracture backbone, through which the bulk of fluid flow occurs.

Fracture density: The fracture density necessary to ensure a percolating network (one that connects faces of a domain) is proportional to the length scale of the domain (Stauffer and Aharony 1994; Bour and Davy 1997). Forsmark fracture parameters (including density, P_{32}) were fit to borehole counts of open and flowing fractures assuming a percolation length scale of 200 m, the estimated distance between any given borehole and a deformation zone (Follin et al. 2014). Given P_{32} values, the number of fractures per unit volume ($n(r)$) associated with the radius interval 15 m to 500 m can be calculated according to (Hedin 2008):

$$n(r)dr = P_{32}\frac{(\alpha-2)r_0^{\alpha-2}}{\pi r^{\alpha+1}}dr \tag{3-2}$$

where α is the power law parameter, r_0 is the minimum fracture radius in the original distribution (0.038 m), and r is the minimum of the desired radius interval. Substituting 15 m for r, the appropriate values for α (Table 3-4), and the P_{32} values of 0.142, 0.345, and 0.316 (Follin et al. 2014), we find that the number of fractures per cubic kilometer for the NS, EW, and HZ fracture sets is 337, 346, and 1091, respectively. The crystalline reference case uses a higher number of fractures per cubic kilometer (Table 3-4) in order to ensure a percolating fracture network within the multi-kilometer PA model domain.

Fracture transmissivity: The Forsmark parameter set includes three relationships between fracture radii and fracture transmissivity: direct correlation, partial correlation, and no correlation. The crystalline reference case implements direct correlation between fracture transmissivity and fracture radius according to (Follin et al. 2014):

$$\log(T_f) = \log(ar^b) \tag{3-3}$$

where T_f is fracture transmissivity (m^2/s), r is fracture radius (m), and a and b are constants with values of 1.6×10^{-9} and 0.8, respectively, for fracture domain FFM01 at a depth of 200-400 mbsl.

The simplifications discussed above bias the fracture networks generated for the crystalline reference case toward greater connectivity than what is likely to exist in a potential host rock. However, creating a simple, percolating network enables development of the simulation tools required to represent a fractured medium.

3.2.2.2 Matrix Permeability

The matrix permeability of crystalline rock is low. *In situ* tests in the Lac du Bonnet URL and the Korean Underground Research Tunnel give matrix permeability values between 10^{-22} m^2 and 10^{-20} m^2 for granitic rock (Martino and Chandler 2004; Cho et al. 2013); laboratory tests on samples of the Grimsel granodiorite give values on the order of 10^{-20} m^2 to 10^{-19} m^2 (Schild et al. 2001). Laboratory permeability tests performed on gneisses and amphibolites from the KTB borehole indicate a decrease in matrix permeability with increasing effective stress, but *in situ* borehole tests demonstrate no dependence of matrix permeability on depth. Instead, mean values throughout the 9 km KTB borehole are 7×10^{-20} m^2 with a log standard deviation of 1.2 (Huenges et al. 1997).

DWR PA simulations use a matrix permeability of 10^{-20} m^2.

3.2.2.3 Matrix Porosity

Matrix porosity in deep crystalline rock is generally very small. Laboratory measurements of porosity in core samples of crystalline rock often give values of approximately 1% (Schild et al. 2001), but these values may be exaggerated due to formation and growth of microcracks during unloading and sample preparation. Using samples of the Grimsel (meta)granodiorite, Schild et al. (2001) found that when rock samples were impregnated with resin prior to being sampled from depth, the measured porosity was between 0.55% and 0.59%, while non-impregnated samples measured between 1% and 1.17% porosity. Schild et al. took the difference between values measured on impregnated and non-impregnated samples to be the *in situ* porosity, approximately 0.4%, but even this value may be high, since they were unable to avoid sampling within the DRZ. (Had the sampling process not created porosity, the impregnated samples would have had 0% porosity.)

DWR PA simulations use a matrix porosity of 0.5%.

3.2.2.4 Diffusion and Dispersion

Soler et al. (2015) modeled *in-situ* diffusion of ^{3}H, $^{22}Na^{+}$, $^{134}Cs^{+}$ and $^{137}Cs^{+}$ in granite matrix (unfractured but with an apparently thin borehole disturbed zone on the order of 1.5 mm) at a maximum length scale of 20 cm (i.e., "lab scale") and found diffusion coefficients in the range of 2×10^{-13} to 4×10^{-12} m^2/s. Zhou et al. (2007) reviewed "matrix diffusion" coefficients calculated from meter- to kilometer-scale tracer tests in fractured rock, based on an assumed dual continuum transport model with parallel fractures of identical spacing, constant fracture aperture, and constant matrix diffusion coefficient. In this conceptual model, the solute diffuses perpendicularly at the fracture-matrix interface between the fracture domain and the matrix domain (Bear et al. 1993). The observed effective matrix diffusion coefficient at the field scale, D_e^{md}, when computed with this model, is almost always found to be larger than the diffusion coefficient measured in the lab on a small unfractured sample. The scale dependency is attributed to a number of effects, including the heterogeneity of fracture sizes at the field scale (i.e., the fact that there are multiple spatial scales for fractures, such as global-flow fractures, small fractures, ultrasmall fractures, and bypassed fractures), the presence of fracture infill material and a degraded zone along fracture walls, variability of fracture aperture within a single fracture, and multi-rate diffusion processes caused by heterogeneity in matrix porosity and the rock matrix diffusion coefficient.

The field-scale matrix diffusion coefficients in crystalline rocks compiled by Zhou et al. ranged from 3×10^{-12} to 4×10^{-8} m^2/s and were (with two exceptions) larger than matrix diffusion coefficients calculated for core-scale samples of the same rocks, by a factor of 1.3 to 884. The largest of these values is even larger than values for diffusion in free water which, though solute-specific and dependent on fluid properties, tend to be on the order of 1×10^{-9} m^2/s (Li and Gregory 1974). These values for the effective, large-scale matrix diffusion coefficient, D_e^{md}, may be useful in future PA simulations, if the matrix diffusion formulation in PFLOTRAN is utilized. For the current DWR work, which adopts an ECPM formation (see Section 3.2.2.1), PA simulations use an effective diffusion coefficient of 10^{-12} m^2/s throughout the crystalline host rock (in both fractured cells and matrix cells)—see Table 3-10.

The other important dispersive or concentration spreading process in porous media flow is hydrodynamic dispersion, which is discussed at some length in Appendix B. As described there, it is usually split into two spreading processes: mechanical (or advective) dispersion caused by heterogeneities in the microscopic pore velocities and molecular diffusion by Brownian motion. At the field scale, it can be difficult to separate the two contributions to hydrodynamic dispersion, and usually mechanical dispersion dominates unless the diffusion Peclet number (ratio of interstitial velocity to molecular diffusion coefficient) is very low. Zhou et al. (2007) have also reported dispersivity coefficients (see Appendix B) for the same set of experiments for which they derived matrix diffusion coefficients. They compared their values (for fractured rock) with the values of longitudinal dispersivity, α_L, given in the classic study by Gelhar et al. (1992). A spatial scale dependence is evident in both studies, wherein longitudinal dispersivity increases with the length scale of the test or the distance of plume movement. Zhou et al.'s study is for tracer tests in fractured rock, while Gelhar et al.'s includes both fractured and unfractured media. Zhou et al. state: "Still, in spite of the differences in the two data sets, the behavior of the scale-dependent macrodispersivity at the field scale revealed from the two data sets is similar.

Macrodispersivity increases with observation scale for fractured rock shown in this study, at a slope close to that discovered by Gelhar et al. (1992) for both fractured rock and porous media." Zhou et al. also discuss the possible causes for dispersive spreading during advective flow through a fractured medium, the two most important of which are (1) spatial variability of velocities within a fracture, caused by wall roughness and heterogeneity in fracture aperture; and (2) mixing at fracture intersections. Their reported values of α_L are generally less than 10 m for all length scales, with just two outliers, one at 250 m; however, as strongly propounded by Gelhar et al., large measured values of α_L (e.g., greater than 50 m) are suspected to be unreliable. Their largest "high-reliability" value for α_L is 4 m. However, they do report a value of 47 m at a length scale of 538 m, in which they seem to have confidence. They indicate that horizontal transverse dispersivity values, α_{TH}, are about an order-of-magnitude less than α_L and vertical transverse dispersivity values, α_{TV}, are 1 to 2 orders of magnitude lower than α_{TH}—see Appendix B.1 (Eqs. B-9 and B-10) for further discussion regarding estimating dispersitivities for a given system length.

For the initial reference case for a crystalline DWR, longitudinal and transverse dispersivities (both in fracture and matrix cells) are set to zero in the PA simulations. This is conservative with respect to peak dose but will be re-examined in future work.

3.2.2.5 Thermal Properties and Thermal Environment

The thermal properties of rock depend strongly on temperature—thermal conductivity decreases and heat capacity increases with increasing temperature (Vosteen and Schellschmidt 2003). Vosteen and Schellschmidt (2003) measured thermal properties of a variety of igneous and metamorphic rocks at temperatures from 0°C to 500°C, and compared their results to previous results in the literature. Their review indicates that for felsic rocks at temperatures up to approximately 25°C, thermal conductivity is between approximately 2.4 and 3.3 $Wm^{-1}K^{-1}$. At temperatures between 100°C and 200°C, thermal conductivity is between approximately 2.3 and 2.7 $Wm^{-1}K^{-1}$. Between 0°C and 200°C, heat capacity increases from 750 to over 900 $Jkg^{-1}K^{-1}$ (Vosteen and Schellschmidt 2003).

DWR PA simulations assume a thermal conductivity of 2.5 $Wm^{-1}K^{-1}$ and a heat capacity of 830 $Jkg^{-1}K^{-1}$.

Temperature in the repository depends on the background geothermal heat flux and on the heat generated by radioactive decay of the waste. A geothermal heat flux of 60 mW/m^2, an annual mean surface temperature of 10°C, and a thermal conductivity of 2.5 $Wm^{-1}K^{-1}$ result in a geothermal temperature gradient of approximately 25°C/km, and an ambient temperature at the depth of the repository (600 m) of approximately 25°C. Peak repository temperatures are predicted to be just under 90°C (Section 3.4.1). Though such a change in temperature will affect diffusion rates and radionuclide solubility and sorption, at this time these processes are not modeled as a function of temperature.

3.2.2.6 Pore Fluid Chemistry

Pore fluid chemistry will influence waste package degradation rate, waste form dissolution rate, and solubility and transport (diffusion and sorption) of dissolved radionuclides. Pore fluid chemistry is site-dependent, but can be expected to be brackish, reducing, and of circumneutral pH, similar to pore fluids found in granite repository research sites in Finland, Sweden, and

Canada (Table 3-5). Waste-package degradation rate and waste-form dissolution rate have been discussed above (Sections 3.1.4 and 3.1.3). Solubility, sorption, and diffusion are discussed elsewhere (Sections 3.2.2.7, 3.2.2.8, and 3.2.2.4).

Table 3-5. Groundwater compositions in granite at depths from 360 to 708 m (Mariner et al. 2011).

Parameter	Olkiluoto, Finland	Olkiluoto, Finland	Olkiluoto, Finland	Laxemar, Sweden	Forsmark, Sweden	Pinawa, Canada	East Bull Lake, Canada
Borehole	OL-KR20	OL-KR10	OL-KR12	KLX03	KFM02A	WN-4	EBL-2
Depth (m)	360	487	708	380	512	513	538
TDS (g L^{-1})	10.5	22.1	49.5	2.8	9.3	7.5	2.3
Ionic strength (eq L^{-1})	0.22	0.48	1.18	0.05	0.19	0.16	0.05
pH	7.4	8.0	8.2	7.9	7.2	8.1	7.4
Na (mol L^{-1})	0.11	0.21	0.36	0.03	0.09	0.07	0.03
Ca (mol L^{-1})	0.03	0.09	0.25	0.01	0.02	0.03	0.01
K (mol L^{-1})	2.8×10^{-4}	3.6×10^{-4}	4.9×10^{-4}	1.4×10^{-4}	9.0×10^{-4}	5.3×10^{-4}	5.4×10^{-5}
Mg (mol L^{-1})	2.6×10^{-3}	1.6×10^{-3}	1.5×10^{-3}	4.4×10^{-4}	9.3×10^{-3}	1.1×10^{-3}	7.0×10^{-5}
Sr (mol L^{-1})	1.6×10^{-4}	3.7×10^{-4}	1.1×10^{-3}	nr	nr	nr	3.3×10^{-5}
Mn (mol L^{-1})	5.8×10^{-6}	7.3×10^{-6}	9.3×10^{-6}	nr	nr	nr	nr
Cl (mol L^{-1})	0.18	0.38	0.86	0.04	0.15	0.11	0.04
SO_4 (mol L^{-1})	2.1×10^{-4}	1.0×10^{-5}	5.0×10^{-5}	1.3×10^{-3}	5.2×10^{-3}	6.6×10^{-3}	1.4×10^{-4}
CO_3 (mol L^{-1})	5.5×10^{-4}	1.1×10^{-4}	4.0×10^{-5}	3.1×10^{-3}	2.2×10^{-3}	3.5×10^{-3}	5.0×10^{-4}
SiO_2 (mol L^{-1})	3.6×10^{-4}	2.8×10^{-4}	2.1×10^{-4}	nr	nr	nr	5.4×10^{-5}
Fe (mol L^{-1})	2.5×10^{-6}	2.0×10^{-6}	3.8×10^{-7}	8.0×10^{-6}	3.3×10^{-5}	nr	nr
S(-II) (mol L^{-1})	5.6×10^{-6}	$<3.1 \times 10^{-7}$	1.3×10^{-6}	3.0×10^{-7}	0.0E+00	nr	nr
Reference	Posiva (2010), Table 6-6	Posiva (2010), Table 6-6	Posiva (2010), Table 6-6	SKB (2006b), p. 382	SKB (2006b), p. 382	Gascoyne et al. (1987), Table 3	Gascoyne et al. (1987), Table 3

nr = not reported

3.2.2.7 Solubility

PA simulations use the element solubility limits calculated by Mariner et al. (2011) throughout the model domain. Mariner et al. (2011) assumed a solution of 0.3 M NaCl, 0.05 M $CaCl_2$, and 0.001 M Na_2SO_4, a fixed partial pressure of H_2 of 10^{-7} atm, a pH of 7.5, and a temperature of 25°C. Additionally, it was assumed that element solubility is limited by relatively soluble hydroxide and hydrated phases, except in the case of U, for which UO_2 was assumed to be the solubility-controlling phase because of its presence in the waste form. The resulting solubility limits are listed in Table 3-6.

Assuming that no fractionation of isotopes occurs between the liquid and solid phases, the solubility limit of a given isotope (e.g., ^{238}Pu, ^{239}Pu, ^{240}Pu, or ^{242}Pu) in the transport domain of a

cell can be calculated by multiplying the element solubility limit by the isotope's element mole fraction in the transport domain (e.g., $^{238}Pu/Pu_{TOTAL}$) (Mariner et al. 2016, Section 3.2.4).

Table 3-6. Element solubility calculated at T = 25°C, pH = 7.5 (Mariner et al. 2011).

Element	Solubility-Limiting Phase	Dissolved Concentration [a] (mol L^{-1})	Notes
Am (Ac, Cm)	$Am(OH)_3$	6×10^{-6}	Ac and Cm are assumed analogous to Am
Np (Pa)	$Np(OH)_4$	1×10^{-9}	Pa is assumed analogous to Np
Nb	$Nb(OH)_5$	4×10^{-5}	Posiva (2010, Table 1-9)
Pd	$Pd(OH)_2$	3×10^{-6}	Posiva (2010, Table 1-9)
Pu	$Pu(OH)_4$	2×10^{-7}	
Ra	$RaSO_4$	1×10^{-6}	(SO_4^{2-}) fixed at 10^{-3} mol L^{-1}
Sb	$Sb(OH)_3$	1×10^{-7}	
Se	$FeSe_2$	4×10^{-8}	
Sn	SnO_2	3×10^{-8}	
Tc	$TcO_2{:}2H_2O(am)$	3×10^{-8}	
Th	$Th(OH)_4$	4×10^{-7}	
U	UO_2	4×10^{-10}	
Zr	$Zr(OH)_4$	2×10^{-8}	Posiva (2010, Table 1-9)

[a] Calculated using the PHREEQC code version 2.14.2 and the thermo.com.V8.R6.230 database from Lawrence Livermore National Laboratories, except where noted. The solution assumed 0.3 M NaCl, 0.05 M $CaCl_2$, 10^{-3} M Na_2SO_4, and 10^{-7} atm H_2 (g).

3.2.2.8 Sorption

Many different models for surface adsorption have been developed with varying levels of sophistication. The crystalline reference case assumes the simplest model, which is linear sorption characterized by a distribution coefficient K_d for each element. K_d values are material specific and depend heavily on pore fluid characteristics, including temperature, pH, redox conditions, ionic strength, and concentrations of other solutes, but these latter dependencies are not represented explicitly.

DWR PA simulations assume no sorption within the waste packages. Within the bentonite buffer, K_d values are chosen appropriate for the brackish pore fluid compositions listed in Table 3-5, and reducing conditions. These elemental K_d values are given in Table 3-7 and are used for the deterministic simulations in Section 3.4.1. Within the natural barrier (host rock, DRZ, and sediments), deterministic K_d values are set equal to those used for modeling sorption in the far-field granite at Olkiluoto (Table 3-8).

Probabilistic PA simulations sample on Np K_d values in both the bentonite buffer and the natural barrier. Np K_d in the bentonite buffer is sampled between 0.1 m^3/kg (Mariner et al. 2011) and 702 m^3/kg, the upper limit recommended for "highly saline porewater" by SKB 2004. Np K_d in the natural barrier system is sampled between 0.047 m^3/kg and 20 m^3/kg, as recommended for granite with saline pore water by SKB (2006a). Both distributions are log uniform.

Table 3-7. Bentonite K_d values for the chemical conditions of a granite repository (Mariner et al. 2011).

Element	K_d (m^3 kg^{-1})	Source/Notes
Ac [a]	10	Baston et al. (1999), see Am
Am	10	Ikeda and Amaya (1998) (high μ,[b] pH 5-10, Eh -220 mV)
C, Cl	0	Adsorption low, assumed non-sorbing
Cm	10	Baston et al. (1999)
Cs	0.1	Mucciardi et al. (1979) (montmorillonite, high μ, high Ca, pH 7-9.3)
I	0	Mucciardi et al. (1979) (montmorillonite, high μ, high Ca, pH 7.4-8.4)
Nb	3	Ikeda and Amaya (1998); Erdal (1977); Taki and Hata (1991)
Np, Pa [a]	0.1	Kitamura et al. (2002); Ashida et al. (1999) (pH 8-9, Eh -550 to -400 mV, μ =1M)
Pb	10	Ulrich and Degueldre (1993); Ikeda and Amaya (1998) (high μ, pH 5-8.5)
Pd	3	Tachi et al. (1999b)
Pu	1	Mucciardi et al. (1979); Ames et al. (1981) (high μ, pH 7-9)
Ra	1	Tachi and Shibutani (1999) for solution/solid ratio > 100; Ames et al. (1983)
Sb	0.1	Ikeda and Amaya (1998) (low Eh, high μ, bentonite)
Se	0.03	Tachi et al. (1999a)
Sn	30	Oda et al. (1999) (depends on pH)
Sr	0.01	Mucciardi et al. (1979) (bentonite, high μ, high Ca)
Tc	10	Baston et al. (1999) (high μ, high Na, high Ca, Eh ~ -400 mV, pH 8-10)
Th	3	Baston et al. (1991); Ueta (1998) (high μ)
U	10	Baston et al. (1999) (high μ, high Na, high Ca, Eh ~ -400 mV, pH 8-10)
Zr	30	Rancon and Rochon (1979) (depends on pH)

[a] K_d values for Ac are set equal to those of chemically similar Am. K_d values for Pa are set equal to those of chemically similar Np. [b] μ = ionic strength.

Table 3-8. Granite matrix K_d values used in Posiva (2010) for dilute/brackish groundwater (Mariner et al. 2011).

Element	K_d (m^3 kg^{-1})
C, Cl, I	0
Se	0.0005
Pd, Sn	0.001
Sr	0.005
Nb	0.02
Am, Cm, Ac [a]	0.04
Pa, Tc, Cs	0.05
U	0.1
Np, Th, Ra, Zr	0.2
Pu	0.5

[a] K_d values for Ac are set equal to those of chemically similar Am.

3.2.3 Disturbed Rock Zone (DRZ)

The DRZ is defined as the portion of the host rock adjacent to the engineered barrier system that experiences durable (but not necessarily permanent) changes due to the presence of the repository (Freeze et al. 2013b). The DRZ is expected to have elevated permeability with respect to the permeability of the host rock matrix due to changes in *in situ* stress induced by mining.

In-situ DRZ permeability has been measured in URLs in crystalline rock in Korea (Cho et al. 2013) and Canada (Martino and Chandler 2004). In both locations permeability was variable but generally decreased from disturbed to undisturbed values over a discrete distance from the tunnel wall. In the Korean URL gas permeability was as high as 10^{-17} m^2 for a distance of 2 m from the tunnel wall; beyond that distance it was approximately 10^{-20} m^2 (fluid permeabilities are approximately an order of magnitude less than gas permeabilities—see Cho et al. 2013). In the Canadian Lac du Bonnet URL, fluid permeability was between 10^{-16} and 10^{-19} m^2 for a distance of 0.3 to 0.5 m from the tunnel wall, beyond which it was between 10^{-22} and 10^{-20} m^2 (Martino and Chandler 2004).

DWR PA simulations assume a 1.67-m-thick DRZ on all sides of emplacement drifts and access halls. DRZ porosity is assumed to be 0.01, twice that of the undisturbed matrix; the effective diffusion coefficient is assumed to be 10^{-11} m^2, one order of magnitude higher than in the undisturbed host rock; and DRZ permeability is assumed to be 10^{-16} m^2, the highest value measured in the Canadian Lac du Bonnet URL (Martino and Chandler 2004). In probabilistic DWR PA simulations, DRZ porosity is sampled using a uniform distribution over the range 0.005 to 0.05, which also affects the value of the effective diffusion coefficient (see Eq. B-14, Appendix B).

3.2.4 Sedimentary Overburden

The crystalline reference case assumes a 15-m-thick overburden of glacial sediments. Material properties, including porosity (0.2) and permeability (10^{-15} m^2), are appropriate for a silty glacial till (Freeze and Cherry 1979). Probabilistic simulations sample on sediment permeability using a log-uniform distribution over the range 10^{-16} m^2 to 10^{-13} m^2, effectively allowing the sedimentary overburden to represent anything from a clay-rich till to a silty sand (Freeze and Cherry 1979).

3.3 Post-Closure Performance Assessment

3.3.1 Conceptual Model

The conceptual framework for this preliminary generic post-closure PA focuses on the components of the engineered barrier (Section 3.1) and the natural barrier (Section 3.2) in the undisturbed scenario (e.g., no human intrusion, seismicity, or glacial fluid influx). Key characteristics of and processes occurring in each of the components of the engineered and natural barriers are summarized in Table 3-9. Because the PA does not consider the biosphere, the performance metric is maximum radionuclide concentration rather than dose.

Simulations assume: (1) a mined repository at 585 m depth in fractured crystalline rock; (2) 15 m of unconsolidated sedimentary overburden; (3) a head gradient of –0.0013 m/m from west to east (as in the CSNF crystalline reference cases—see Mariner et al. 2016); (4) a regional heat flux of 60 mW/m^2 and a mean annual surface temperature of 10°C; and (5) a saturated domain.

Table 3-9. Conceptual representation of the engineered and natural barriers in PA.

Region	Component	Key characteristics	Key processes included in PA
Engineered Barrier	HLW (source term)	Glass waste form	Radionuclide decay, waste form dissolution
	DSNF (source term)	Metallic fuel waste form	Radionuclide decay, instantaneous dissolution
	Waste Package (control on source terms)	Stainless steel	Degradation and breach
	Waste Package (region of domain)	Package plus contents	Radionuclide advection, diffusion, and decay
	Bentonite Buffer	Low permeability, high sorption capacity	Radionuclide advection, diffusion, sorption, decay
	Cement Slab	Low permeability	Radionuclide advection, diffusion, decay
Natural Barrier	Crystalline Basement	Sparsely fractured, low permeability	Radionuclide advection, diffusion, sorption, decay
	DRZ	Enhanced permeability	Radionuclide advection, diffusion, sorption, decay
	Sediments	Thin, unconsolidated	Radionuclide advection, diffusion, sorption, decay

3.3.2 Numerical Implementation

PA simulations, comprising 15 deterministic simulations and a suite of 50 probabilistic simulations for uncertainty and sensitivity analyses, were implemented within the Generic Disposal System Analysis (GDSA) framework (Mariner et al. 2015; Mariner et al. 2016), which is based on PFLOTRAN for numerically solving the energy, flow, and transport equations; and on Dakota for probabilistic sampling and analysis.

PFLOTRAN, a massively parallel multiphase flow and reactive transport code (Hammond et al. 2011; Hammond et al. 2014; Lichtner and Hammond 2012; Lichtner et al. 2015), was used to simulate flow and transport in the geologic disposal system. PFLOTRAN solves the non-linear partial differential equations describing non-isothermal multi-phase flow, reactive transport, and geomechanics in porous media. Parallelization is achieved through domain decomposition using

the Portable Extensible Toolkit for Scientific Computation (PETSc) (Balay et al. 2013). PETSc provides a flexible interface to data structures and solvers that facilitate the use of parallel computing. PFLOTRAN is written in Fortran 2003/2008 and leverages state-of-the-art Fortran programming (i.e. Fortran classes, pointers to procedures, etc.) to support its object-oriented design.

The suite of probabilistic simulations was run using the Dakota toolkit, an analysis package for uncertainty quantification, sensitivity analysis, optimization, and calibration in a parallel computing environment (Adams et al. 2016a; 2016b). Given parameter ranges and distributions, Dakota performs Latin Hypercube Sampling, inserts sampled values into the PFLOTRAN input deck, and calls PFLOTRAN. It also provides tools for quantifying uncertainty and parameter sensitivity after the suite of simulations is complete.

The unstructured mesh was gridded with Cubit (Blacker et al. 2016). DFNs were generated with DFNWorks (Hyman et al. 2015a; Hyman et al. 2015b) and mapped to an equivalent continuous porous medium domain with mapDFN.py (Mariner et al. 2016).

3.3.2.1 Model Domain and Discretization

The model domain (Figure 3-5) is 3015 m in length (*x*), 2025 m in width (*y*), and 1260 m in height (*z*). Most of the domain is discretized into cells 15 m on a side. The repository and adjacent cells are discretized into cells 1.67 m (5/3 m) on a side. Within the repository, vertical emplacement boreholes are discretized into cells 0.56 m (5/9 m) on a side. A narrow transitional zone of cells 5 m on a side exists between the repository cells and the remainder of the domain. Figure 3-6 shows an *x*-*z* slice through the repository at the *y*-midpoint of the repository. Figure 3-7 shows an *x*-*y* slice at the *z*-midpoint of the repository. The domain contains 8,593,944 cells; of these, approximately 6.2 million are the smaller cells in and around the repository.

The left half of the repository (21 drifts) contains DSNF emplaced in 80 vertical boreholes per drift. From left to right and front to back, DSNF is emplaced in the order: 787 of < 50 W waste packages, 158 50 to 100 W waste packages, 636 100 to 200 W waste packages, 8 200 to 300 W waste packages, 28 300 to 500 W waste packages, 60 500 to 1000 W waste packages, and 3 1000 to 1500 W waste packages. See Section 3.1.2 for an explanation of these bins, including radionuclide and thermal source terms. The right half of the repository (21 drifts) contains HLW glass emplaced in 119 waste packages per drift. These drifts are filled first with Hanford glass (7425 waste packages), followed by Savannah River glass (5070 waste packages).

3.3.2.2 Initial Conditions

Initial conditions specified are pressure, temperature, and radionuclide concentrations. Initial pressures and temperatures throughout the model domain are calculated by applying a liquid flux of 0 m/s and an energy flux of 60 mW/m^2 to the base of the domain and holding temperature (10°C) and pressure (approximately atmospheric) constant at the top of the domain, and allowing the simulation to run to 10^6 years. Pressure at the top of the domain decreases from west (left) to east (right), with a head gradient of –0.0013 (m/m). This technique results in initial conditions that represent a geothermal temperature gradient and hydrostatic pressure gradient in the vertical direction, and a horizontal pressure gradient that drives flow from west to east. Simulations include the 16 radionuclides listed in Table 3-2 and Table 3-3; initial concentrations of all radionuclides in all cells are 10^{-20} mol/L.

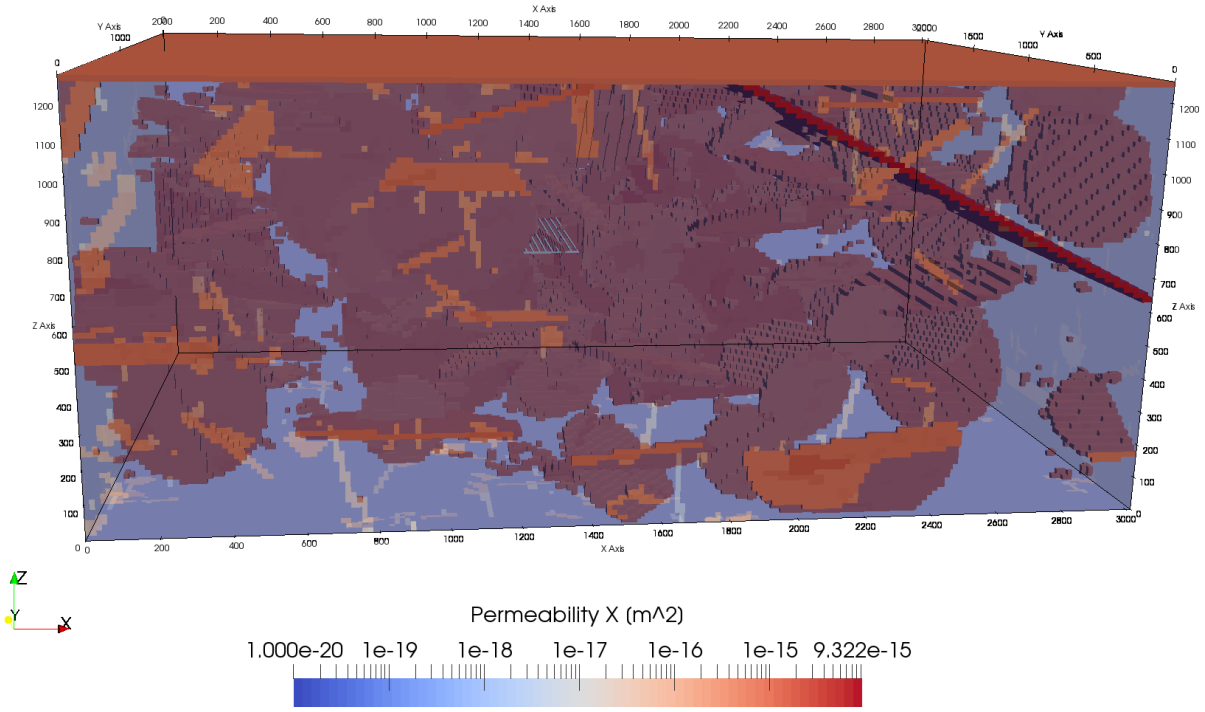

Figure 3-5. Transparent view of the model domain colored by permeability. The 3-dimensional structures inside the domain are the repository (colored gray rather than by permeability); the deterministic deformation zone, colored red due to its high permeability; and the largest fractures of a stochastically generated fracture network (Domain6 in Table 3-12). Small fractures do not appear in this image because grid cells with permeability less than 5×10^{-16} m^2 were not plotted.

3.3.2.3 Boundary Conditions

Boundary conditions must be set for the six faces of the model domain. At all faces, initial pressures and temperatures are held constant. Radionuclide concentrations are held such that any fluid entering the model domain contains 10^{-20} mol/L of each radionuclide, while fluid exiting the model domain is allowed to carry with it ambient concentrations. Diffusive flux across boundaries is disallowed by specifying a zero concentration gradient.

3.3.2.4 Waste Package Heat Sources

Each waste package is modeled as a transient heat source. The energy (watts per waste package) entering the model domain is updated periodically according to values in a lookup table. The initial value for each waste type is that in the year 2038 (plotted in Figure 3-1). Between times specified in the lookup table, the energy input is linearly interpolated.

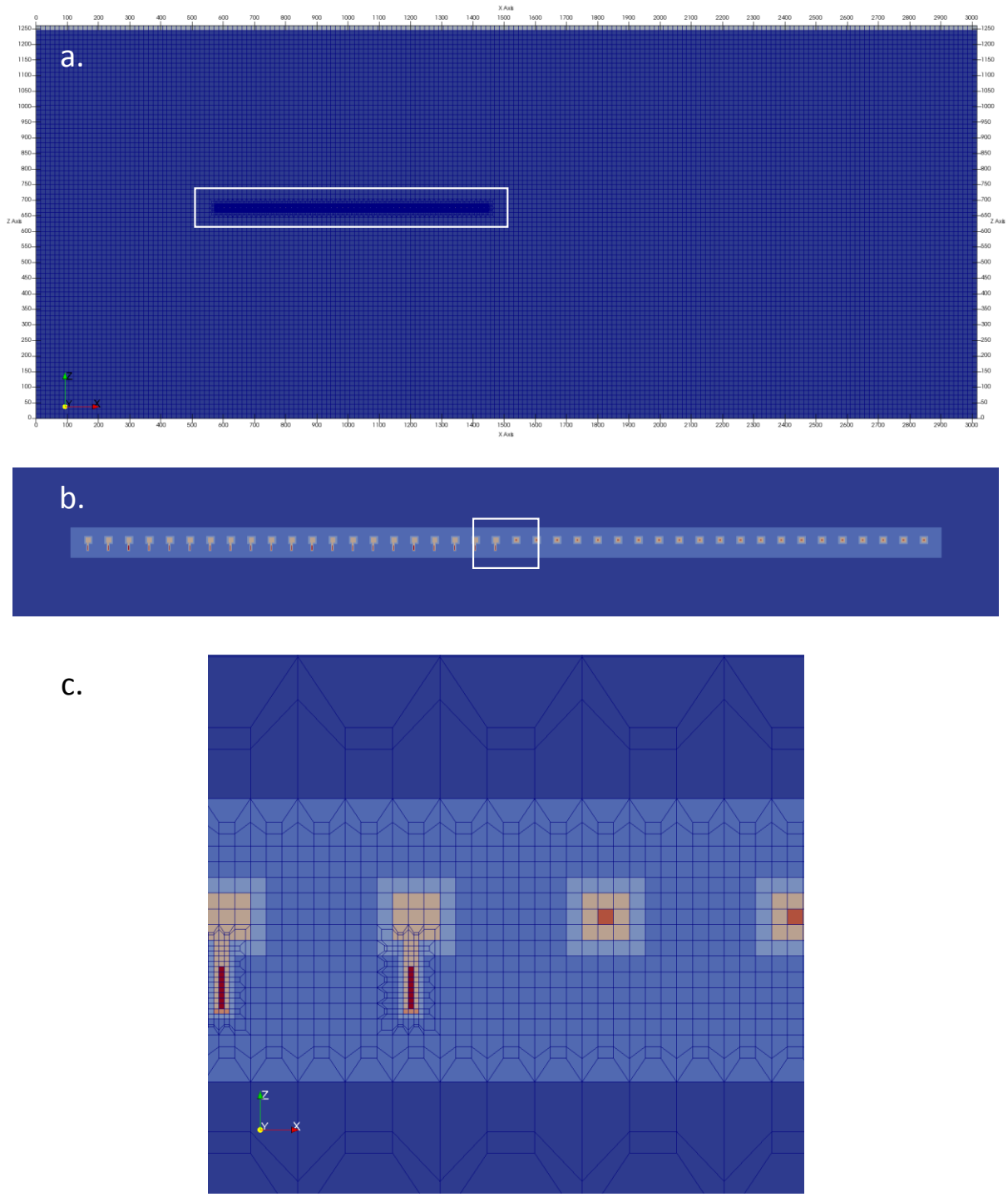

Figure 3-6. *X-Z* slice of model domain. (a) Most of the domain is discretized with cells 15-m on a side. White box in (a) shows area of (b), in which DSNF drifts (left) and HLW drifts (right) can be seen. White box in (b) shows area of (c), in which discretization of the repository (to 5/3 m (HLW) and 5/9 m (DSNF)) can be seen. Colors represent materials: dark blue and medium blue, undisturbed host rock; light blue, DRZ; tan, buffer; light orange, cement; dark orange, HLW; red, DSNF; grey, sediment.

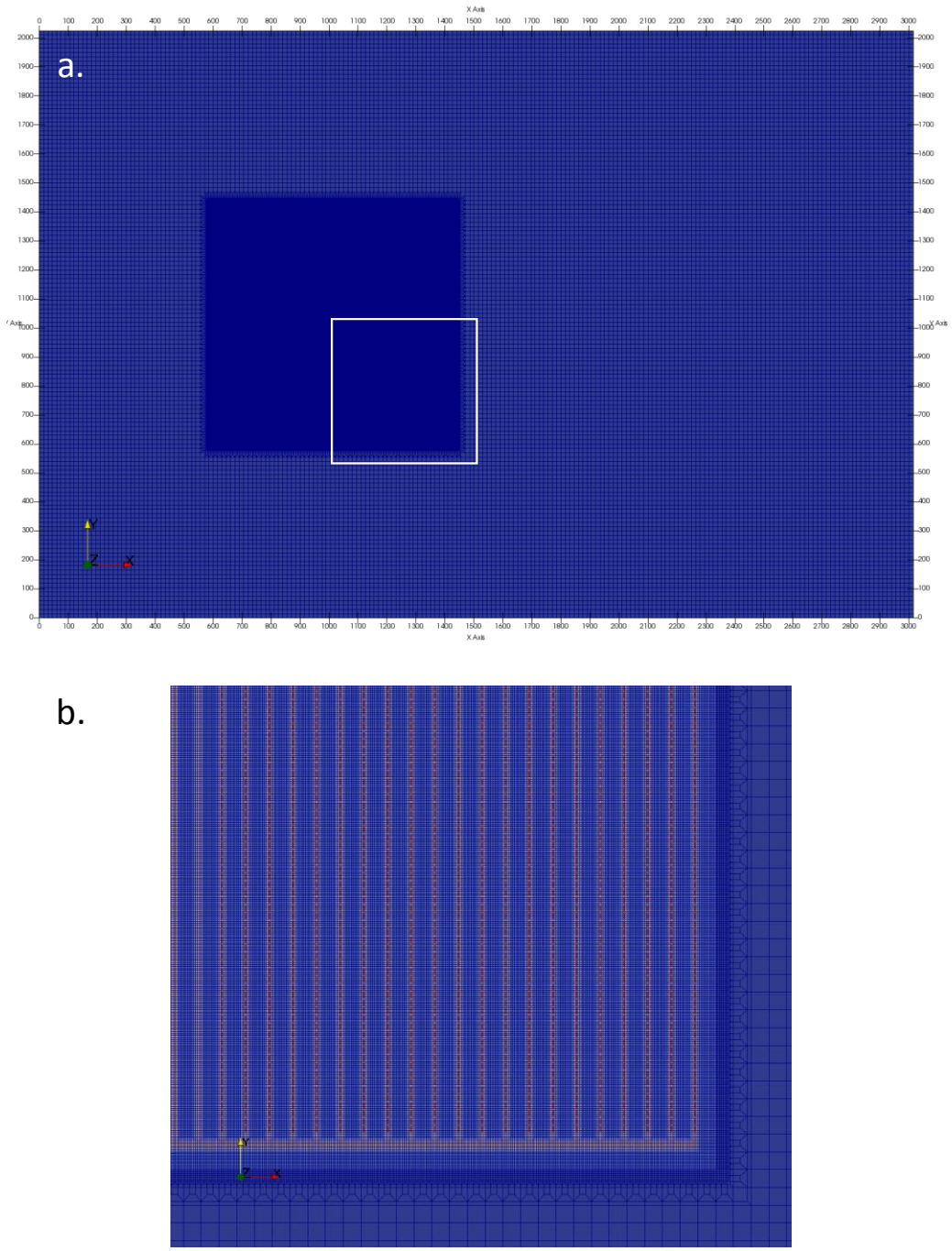

Figure 3-7. *X-Y* slice of model domain. (a) Most of the domain is discretized with cells 15 m on a side. Area of the repository is too finely-discretized to resolve at this scale. White box shows area of (b), in which discretization of the HLW drifts (with cells 5/3 m on a side) can be seen. Colors as in Figure 3-6.

3.3.2.5 Waste Package Breach and Radionuclide Source Term

The waste package degradation model implemented in PFLOTRAN (Mariner et al. 2016, Section 3.2.1) calculates canister *vitality* (fractional remaining waste-package wall thickness) at each time step as a function of a base canister degradation rate, a canister material constant, and

temperature. Waste package breach occurs when the canister vitality reaches zero. The canister vitality is initialized to 1, and is reduced at each time step by the effective canister vitality degradation rate R_{eff}, according to

$$R_{eff} = R \cdot e^{C\left(\frac{1}{333.15} - \frac{1}{T(\boldsymbol{x},t)}\right)} \tag{3-4}$$

where R is the base canister vitality degradation rate at 60ºC, $T(\boldsymbol{x}, t)$ is the local temperature (in Kelvin), and C is the canister material constant. This equation assumes that reaction rates are a function of temperature as described by the Arrhenius equation. For general corrosion, R represents the normalized general corrosion rate at 60ºC in units of 1/time (i.e., units of length/time normalized by the thickness of the canister wall), and the associated canister vitality is then a normalized measure of the remaining canister thickness before breach. Once canister vitality drops below zero, the canister is considered breached, and a Boolean flag is turned on for the waste form object inside of it.

The user may alternatively specify the canister breach time for each waste package. This functionality was included to allow for early breach times, or to guarantee a breach time if the effect of temperature cannot be estimated to calculate a degradation rate.

Deterministic simulations assign a base canister degradation rate for each waste package by sampling on a truncated log normal distribution with a mean of $10^{-4.5}$/yr, a standard deviation of 0.5 (log units) and an upper truncation of –3.5 (log units). Probabilistic simulations sample on the mean degradation rate using a log-uniform distribution from $10^{-5.5}$/yr to $10^{-4.5}$/yr.

PA simulations assume that exposure to water occurs (dissolution begins) at the time of waste package breach (Mariner et al. 2016, Section 3.2.2). DSNF waste forms are assumed to dissolve instantaneously: following the breach, the radionuclide inventory (updated to the current time) is released into the DSNF waste package region.

Following breach, a HLW waste form begins to dissolve congruently (radionuclides are released in proportion to their current concentration in the waste form) according to the temperature-dependent rate law (Eq. 3-1) presented in Section 3.1.3.1. The resulting rate in kg m^{-2} d^{-1} is multiplied by the exposed surface area (m^2/kg) in order to calculate the fractional rate of glass dissolution (1/d). Exposed surface area (S) is calculated according to (Strachan 2004, Section 6.5.4):

$$S = f_e A \tag{3-5}$$

where f_e is an exposure factor that accounts for the presence of cracks, and A is the specific surface area calculated on the basis of the cylindrical geometry of the glass waste forms—2.8×10^{-3} m^2/kg for Savannah River glass and 2.6×10^{-3} m^2/kg for Hanford glass (Strachan 2004, Section 6.5.4). Specific surface area, A, is updated with time as a function of the mass of glass remaining. Though it is possible to assign each glass waste form a unique value of f_e, in the current PA simulations all glass waste forms are assigned the same value of f_e (= 4 in deterministic simulations). Probabilistic simulations sample on f_e using a triangular distribution with a minimum and mode of 4 and a maximum of 17 (Strachan 2004).

3.3.2.6 Material Properties

Material properties are discussed in Sections 3.1 and 3.2; values used in PA simulations are summarized in Table 3-10 (deterministic parameter values) and Table 3-11 (sampled parameter ranges). Additional information regarding the calculation of tortuosity and effective diffusion coefficient is given in Appendix B. Longitudinal and transverse dispersivities (both in fracture and matrix cells) are set to zero in the PA simulations—see Appendix B.

Table 3-10. Parameter values used in deterministic simulations.

Model Region	Permeability (m^2)	Porosity, φ	Tortuosity[a], τ	Effective Diffusion Coefficient[b], D_e (m^2/s)	Saturated Thermal Conductivity (W/m/K)	Heat Capacity (J/kg/K)	Grain Density (kg/m^3)
Waste Package	1×10^{-16}	0.50	1	5×10^{-10}	16.7	466	5000
Bentonite Buffer	1×10^{-20}	0.35	0.35	1.225×10^{-10}	1.5	830	2700
Cement Slab	1×10^{-19}	0.15	0.15	2.25×10^{-11}	1.7	830	2700
Crystalline Matrix	1×10^{-20}	0.005	0.2	1×10^{-12}	2.5	830	2700
Fractures	Calc'd[c]	Calc'd[c]	Calc'd[c]	1×10^{-12}	2.5	830	2700
DRZ	1×10^{-16}	0.01	1	1×10^{-11}	2.5	830	2700
Sediments	1×10^{-15}	0.20	0.20	4×10^{-11}	1.7	830	2700

[a] Tortuosity as used in PFLOTRAN is defined in Appendix B.

[b] $D_e = D_w \varphi \tau s$, where s is the liquid saturation, assumed here to be = 1, and D_w is the free water diffusion coefficient $= 1 \times 10^{-9} m^2/s$ (Li and Gregory 1974).

[c] Calculated on a cell by cell basis for each fracture realization. Fracture cells have permeability on the order of 10^{-15} to 10^{-19} m^2; porosity on the order of 10^{-6} (Mariner et al. 2016, Section 3.1.3.1); and computed tortuosity, $\tau = D_e/(D_w \phi) = (1 \times 10^{-12})/(\varphi \cdot 1 \times 10^{-9}) = 0.001/\varphi$ in order to force $D_e = 1 \times 10^{-12}$ m^2/s (see Sec. 3.2.2.4), assuming a fully saturated medium, s =1, with D_w = 1 x 10^{-9} m^2/s (Li and Gregory 1974).

Table 3-11. Sampled parameters and their distributions.

Parameter	Range	Units	Distribution
Glass exposure factor (f_e)	4 – 17 (mode = 4)		triangular
Mean Waste Package Degradation Rate	$10^{-5.5} – 10^{-4.5}$	yr^{-1}	log uniform
Waste Package τ	0.01 – 1.0		log uniform
Bentonite φ	0.3 – 0.5		uniform
DRZ φ	0.005 – 0.05		uniform
Np K_d bentonite	0.1 – 702	m^3kg^{-1}	log uniform
Np K_d natural barrier	0.047 – 20	m^3kg^{-1}	log uniform

3.3.2.7 Fracture Realizations

Fifteen fracture realizations were generated for the crystalline reference case. Parameters used to generate the fracture realizations are listed in Table 3-4. Each realization contains a single deterministic deformation zone striking north-south with a dip of 30° and a transmissivity of 1.5×10^{-6} m^2/s. Bulk permeability of the model domain for each realization was calculated for the equivalent porous medium representation in the west to east direction (left to right) by applying a known pressure gradient to the domain, finding the steady state Darcy velocity, q [m/s], across the east end of the domain, and calculating permeability, k [m^2], from (Freeze and Cherry 1979):

$$q = -\frac{k}{\mu}\frac{dp}{dx} \tag{3-6}$$

where μ is dynamic fluid viscosity [kg/(s·m)], and dp/dx is the pressure gradient [kg/(s^2·m^2)] in the west to east direction. Characteristics of the fifteen realizations are listed in Table 3-12. Bulk permeabilities for the simulated fracture domains are on the order of those calculated from borehole packer tests at the Forsmark site (Follin et al. 2014).

Table 3-12. Characteristics of 15 DFN realizations.

Realization	Requested number of fractures	Connected number of fractures	P_{32} of connected fractures (m^2/m^3)	Bulk permeability (m^2)
Domain1	49234	9112	0.0082	1.1×10^{-17}
Domain2	49234	9028	0.0083	7.1×10^{-18}
Domain3	49234	8380	0.0076	8.8×10^{-18}
Domain4	49234	9086	0.0083	1.7×10^{-17}
Domain5	49234	8787	0.0080	1.3×10^{-17}
Domain6	49234	8425	0.0076	7.5×10^{-17}
Domain7	49234	8522	0.0079	1.1×10^{-17}
Domain8	49234	8807	0.0081	9.6×10^{-18}
Domain9	49234	8915	0.0080	9.4×10^{-18}
Domain10	49234	8838	0.0079	7.6×10^{-18}
Domain11	49234	8622	0.0079	1.5×10^{-17}
Domain12	49234	8903	0.0080	1.3×10^{-17}
Domain13	49234	8412	0.0077	1.9×10^{-17}
Domain14	49234	8739	0.0079	1.1×10^{-17}
Domain15	49234	8332	0.0076	7.4×10^{-18}

3.4 Simulation Results

Deterministic and probabilistic results are discussed in terms of concentrations of the long-lived radionuclides ^{129}I ($t_{½}$ = 1.57×10^{7} yr) and ^{237}Np ($t_{½}$ = 2.14×10^{6} yr). ^{129}I is assumed to have unlimited solubility and to be non-sorbing; it thus behaves nearly conservatively. ^{237}Np is solubility-limited and sorbing. Temperature fields, flux vectors, and waste package breach times for a single deterministic simulation are also presented.

The current PA simulations are limited by their generic nature as well as the bias toward fracture connectivity discussed in Section 3.2.2.1, and are therefore a conservative representation of repository performance in fractured crystalline host rock. Their main purpose is to demonstrate the capability of the GDSA Framework as a robust PA tool for representing the potential performance of a DWR in crystalline host rock, if such a location were selected during a consent-based siting process (BRC 2012, Sections 4.3 and 6).

3.4.1 Deterministic Results for Fracture Map "Domain6"

3.4.1.1 Temperature and Fluid Flow Fields

Figure 3-8 shows two waste package temperature histories for each of the two primary EBS design concepts under consideration here: vertical borehole emplacement of a waste package with a single canister of DSNF and horizontal emplacement of a much larger waste package containing five canisters of DHLW (see Sections 3.1.1 and 3.1.4). These two EBS designs for a crystalline DWR have been discussed at length by Matteo et al. (2016, Sec. 2). For each of the two designs, Figure 3-8 shows two temperature extremes for each type of waste: a relatively cool DSNF bin (100-200 W) and the hottest DSNF bin (1000-1500 W)—see Table 3-2, and the coolest DHLW (Hanford glass) and hottest DHLW (Savannah River glass).

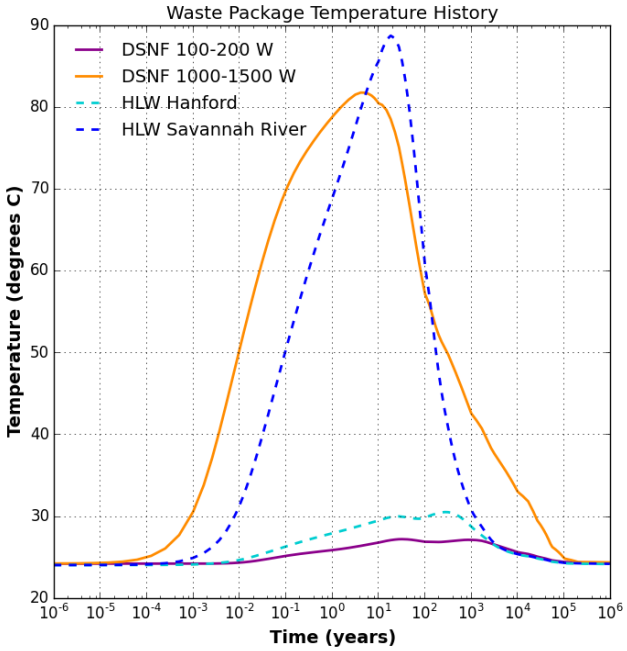

Figure 3-8. Waste package temperature histories for two DSNF thermal bins (a cooler bin and the hottest bin), and the hottest and coolest DHLW for the generic DWR in crystalline host rock.

3-D temperature and fluid flow fields at various times for the fracture realization "Domain6" are shown in Figure 3-9 through Figure 3-14. The background geothermal temperature gradient and regional flow field at the initial time are shown in Figure 3-9. At 1 year post-closure (or post-waste-emplacement—all waste is assumed to be instantaneously emplaced at time 0), increases in temperature associated with the Savannah River HLW and the warmer DSNF bins are apparent, and fluid fluxes associated with rising temperatures are established (Figure 3-10). Peak repository temperatures occur at approximately 20 years (Figure 3-11), with temperatures in the Savannah River HLW drifts being slightly less than 90°C (see also Figure 3-8). The repository remains warmer than background at 100 years (Figure 3-12), and fluid flow out of the repository is still occurring. By 10,000 years repository temperatures have returned to near background, and the thermal influence on the flow field is diminished (Figure 3-14).

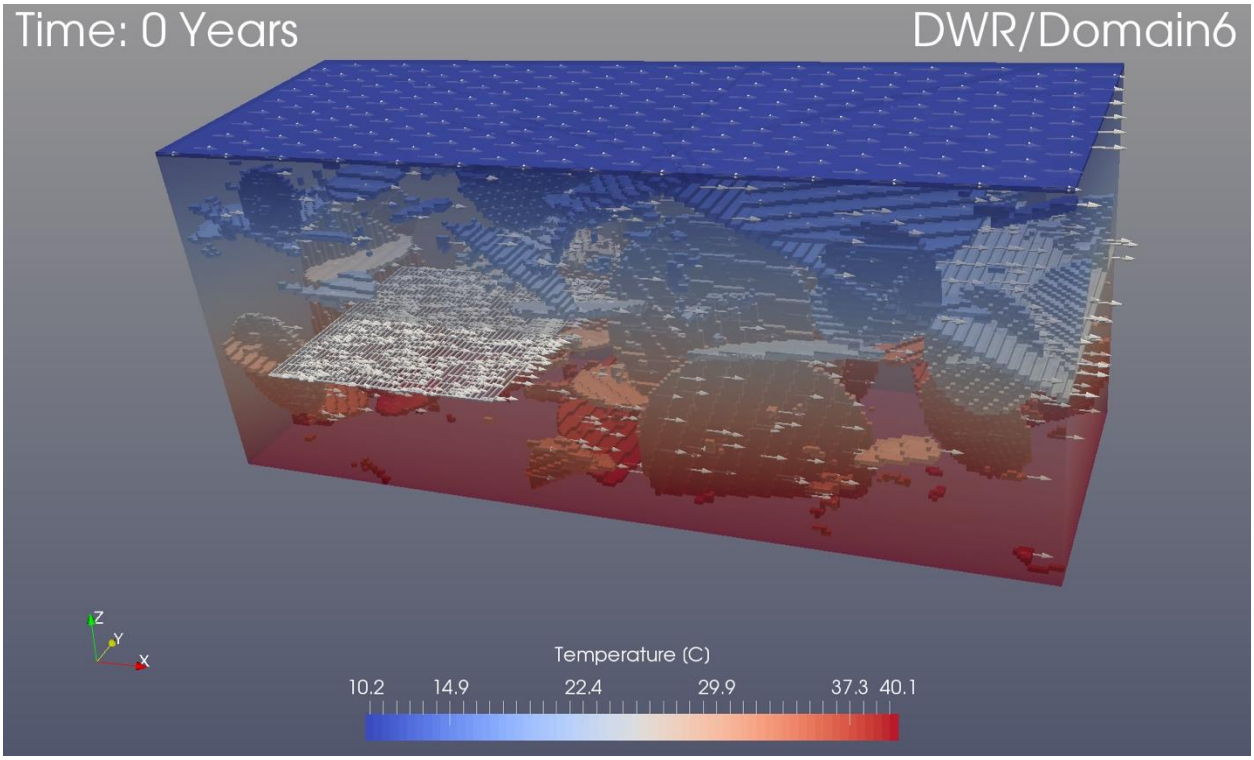

Figure 3-9. Background geothermal temperature gradient and regional flow field at 0 years (shown for the deterministic simulation of Domain6). The transparent model domain is truncated at y = 1012.5 m (the midpoint); the full repository and fractures with permeability greater than 5×10^{-16} m^2 (and y > 1012.5 m) are plotted. All elements are colored by temperature, except the flux vectors, which simply indicate the direction of flow. Notice that the maximum temperature on the color scale of 40 °C in this figure is less than the maximum of 90°C in the figures that follow.

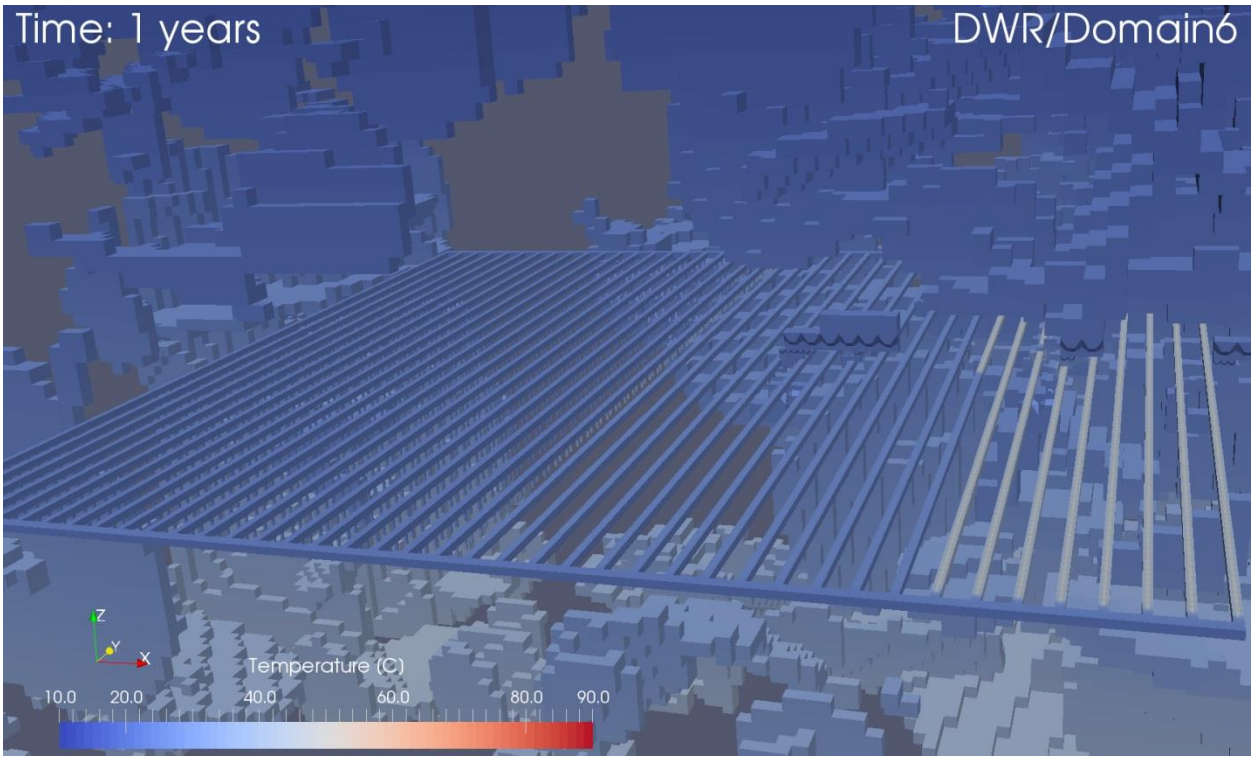

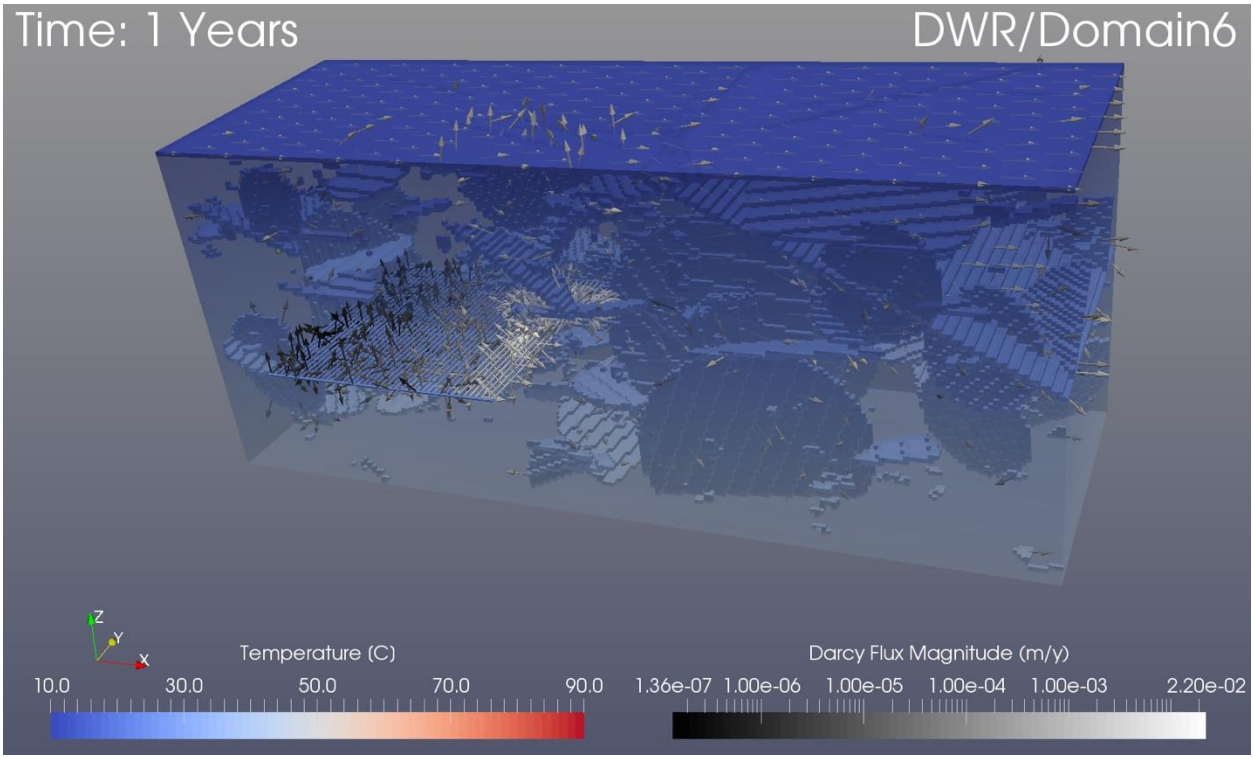

Figure 3-10. Repository temperature field at 1 year in the deterministic simulation of Domain6 (top)—plotted and colored as in Figure 3-9 except for difference in scale. Flux vectors at 1 year (bottom)—vectors are plotted for a subset of cells in fractures, sediments, and repository and colored by flux magnitude.

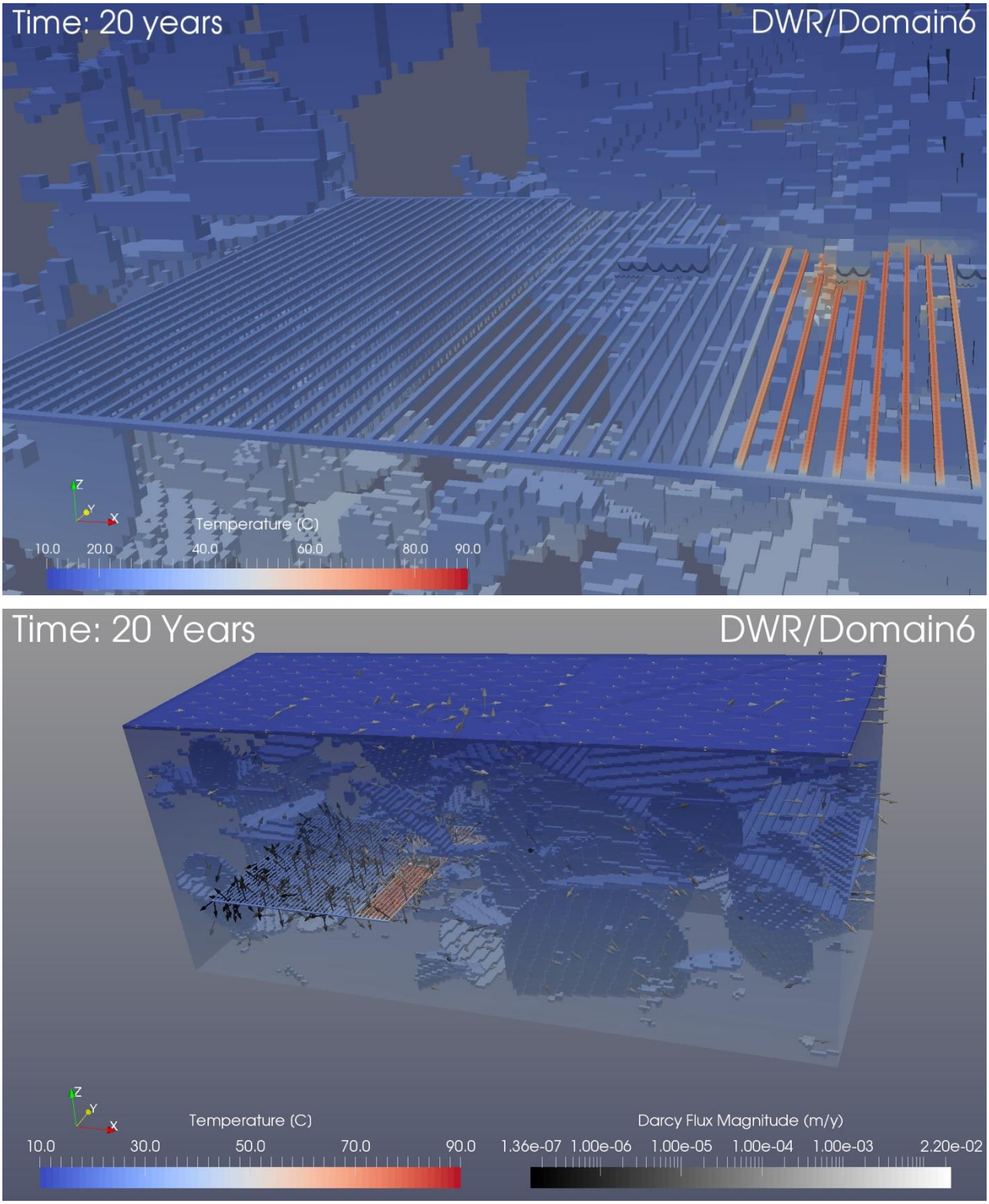

Figure 3-11. Repository temperature field (top) and Darcy flux vectors (bottom) at 20 years in the deterministic simulation of Domain6. Plotted and colored as in Figure 3-10.

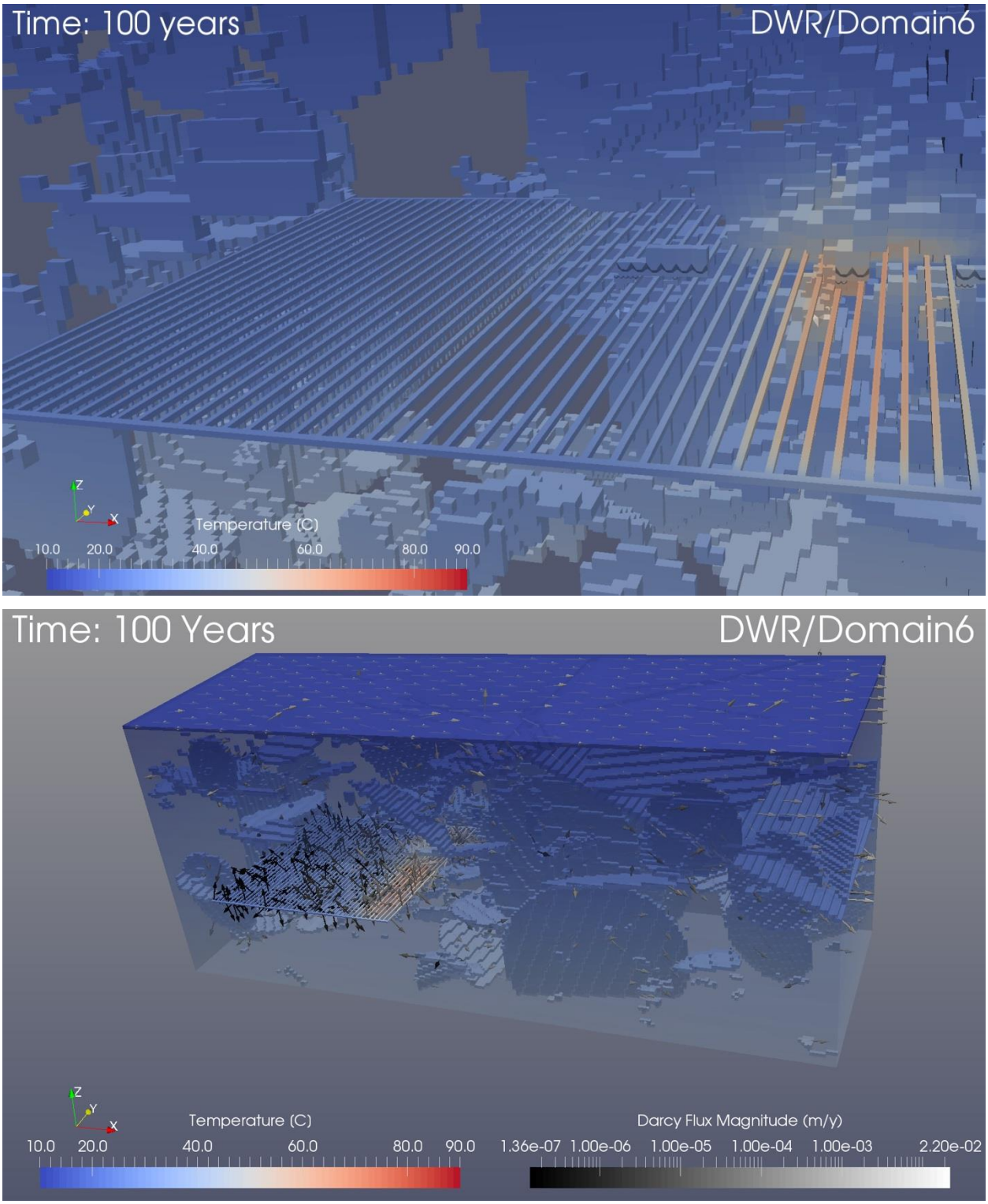

Figure 3-12. Repository temperature field (top) and Darcy flux vectors (bottom) at 100 years in the deterministic simulation of Domain6. Plotted and colored as in Figure 3-10.

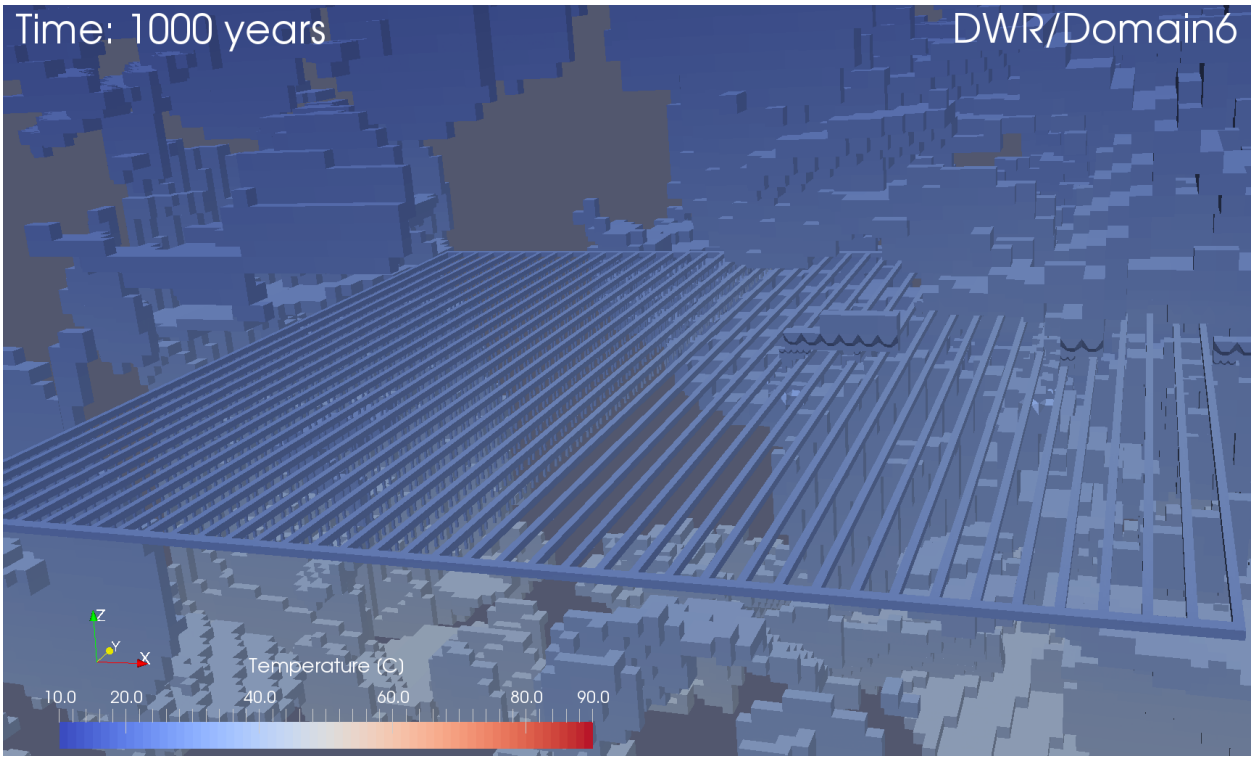

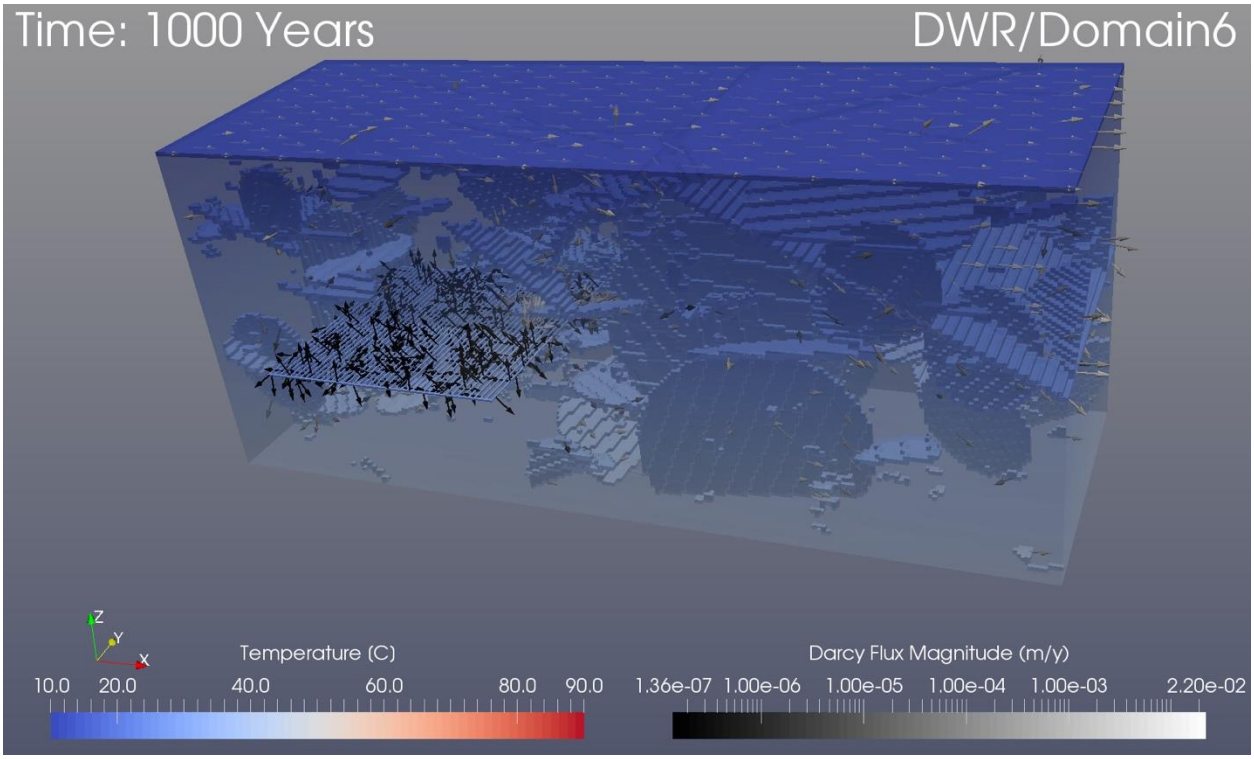

Figure 3-13. Repository temperature field (top) and Darcy flux vectors (bottom) at 1,000 years in the deterministic simulation of Domain6. Plotted and colored as in Figure 3-10.

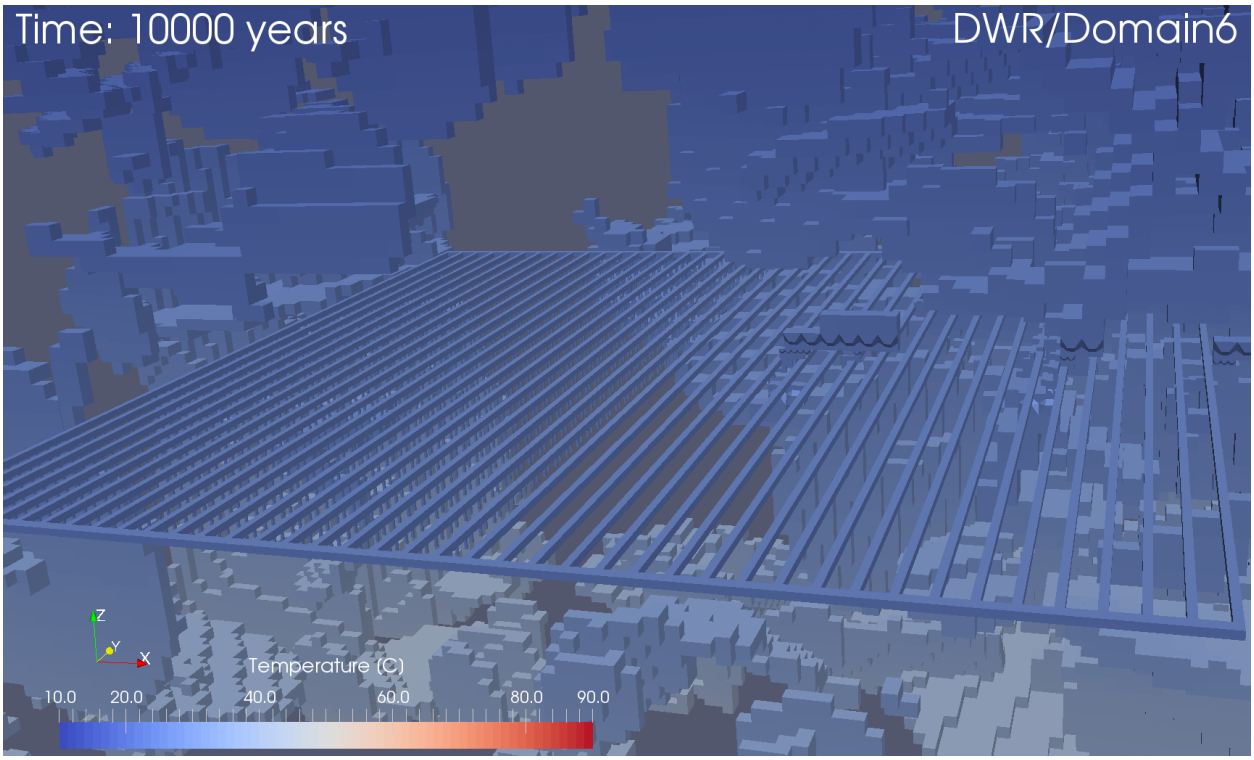

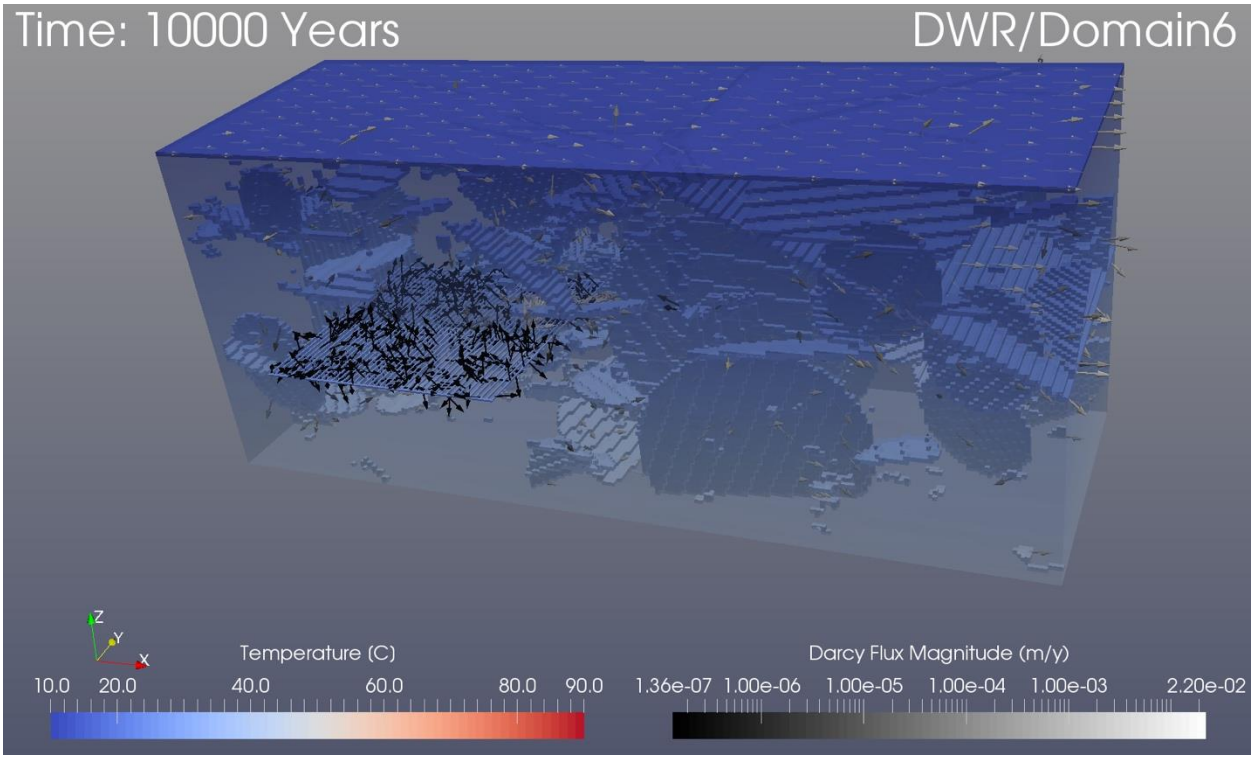

Figure 3-14. Repository temperature field (top) and Darcy flux vectors (bottom) at 10,000 years in the deterministic simulation of Domain6. Plotted and colored as in Figure 3-10.

3.4.1.2 Radionuclide Releases

Radionuclide releases depend not only on fluid fluxes, but on the timing of waste package breach and the resultant waste form degradation. The DSNF waste form is assumed to degrade instantaneously upon breach of the waste package (Section 3.1.3.2), i.e., when the waste package vitality—see Eq. 3-4 in Section 3.3.2.5—reaches zero, as shown in Figure 3-15. The DHLW waste form degrades exponentially—see Eq. 3-1 in Section 3.1.3.1, as shown in Figure 3-16.

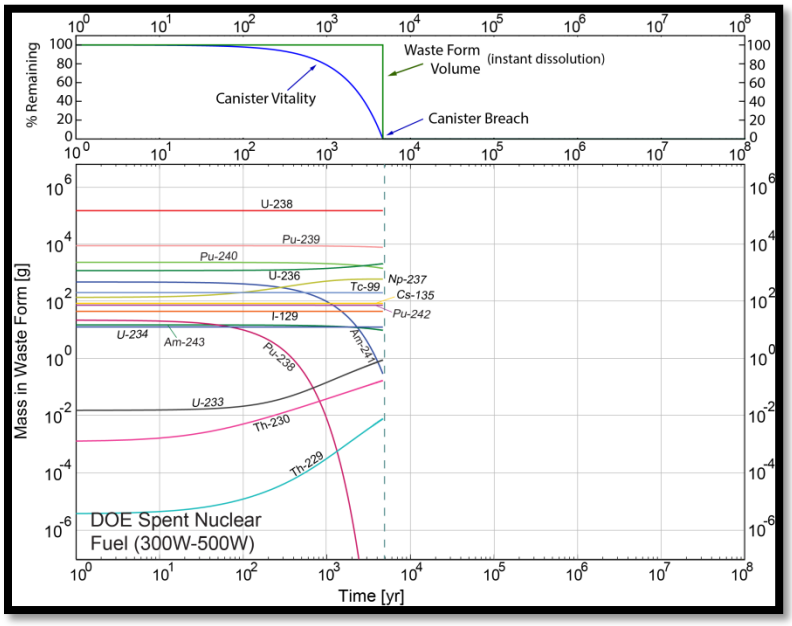

Figure 3-15. DSNF waste form degradation, waste package degradation, and radionuclide releases versus time for the 300-500 W DSNF bin, based on a relatively fast waste-package degradation rate.

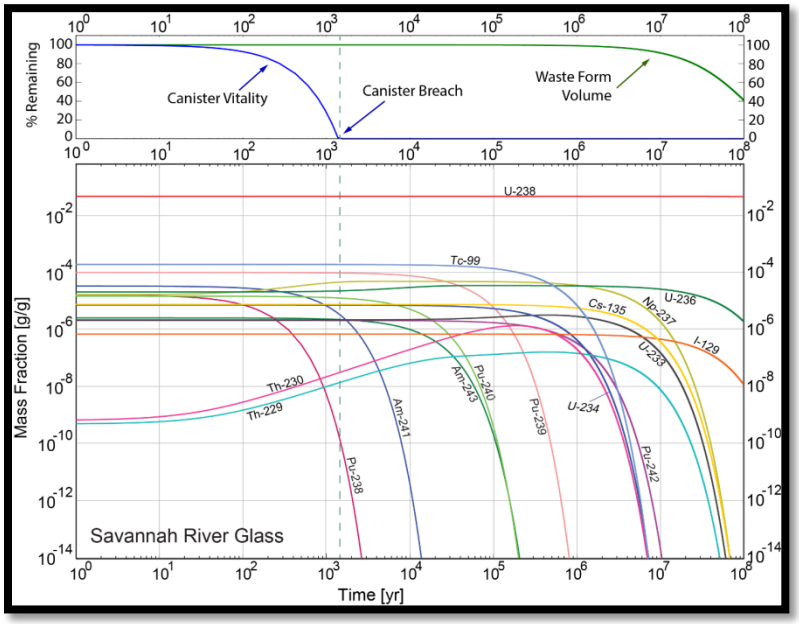

Figure 3-16. DHLW waste form degradation, waste package degradation, and radionuclide releases versus time for Savannah River glass, based on a relatively fast waste-package degradation rate.

In this generic PA model fewer than 1% of the waste packages have breached 1000 years into the simulation, while all waste packages have breached by 345,000 years (Figure 3-17). Most waste packages breach after the thermal driving force for fluid flow has dissipated. Breach times do not vary from one fracture realization to another because the same spatial heterogeneity of canister degradation rates (based on a mean rate of $10^{-4.5}$ yr^{-1}—see Section 3.3.2.5) was used in all deterministic realizations; and, although the waste package degradation function is temperature-dependent, heat conduction is not affected by fracture distribution.

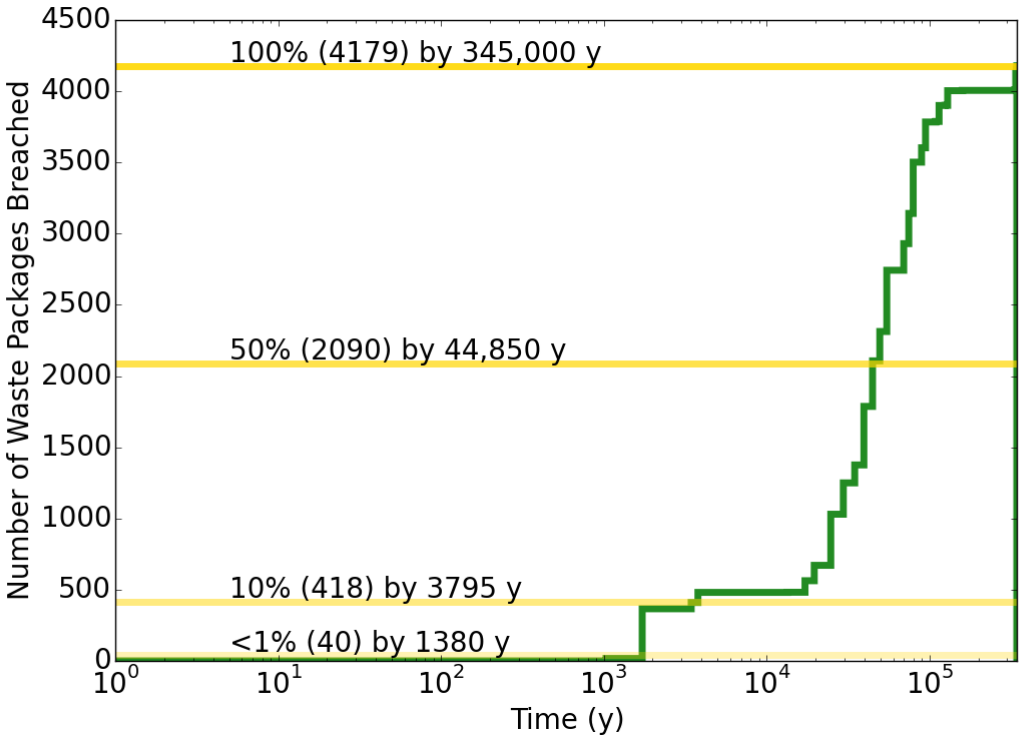

Figure 3-17. Cumulative number of waste packages breached versus time for the generic crystalline repository reference case.

The spatial distribution of ^{129}I at times up to 10^6 years is shown in Figure 3-18 through Figure 3-20. Between 1000 and 2000 years, transport in fractures carries ^{129}I at dilute (10^{-12} mol/L) concentrations to the east (right) face of the model domain over 1.5 km from the repository (Figure 3-18). With time, ^{129}I diffuses from the repository and from fractures into the crystalline rock matrix.

The spatial distribution of ^{237}Np, which can precipitate and/or sorb, is shown in Figure 3-20 (bottom). In 10^6 years, the 10^{-12} mol/L contour of ^{237}Np is only a few meters beyond the edge of the repository.

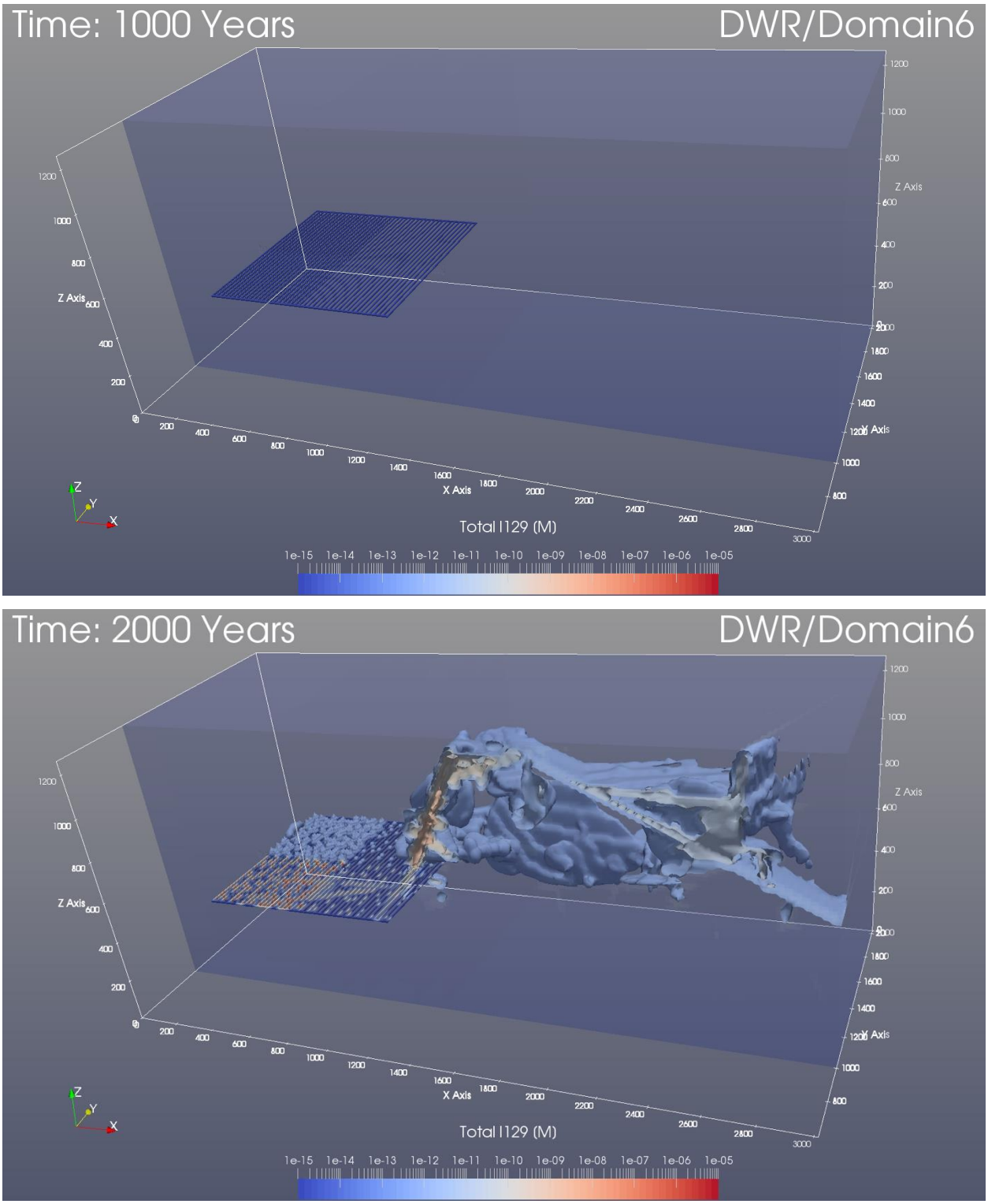

Figure 3-18. ^{129}I concentration at 1000 years (top) and 2000 years (bottom) in the deterministic simulation of Domain6. [Note: Concentration contours in the far-field plume are not displayed below 10^{-12} mol/L in order to show more definition in the plume movement.]

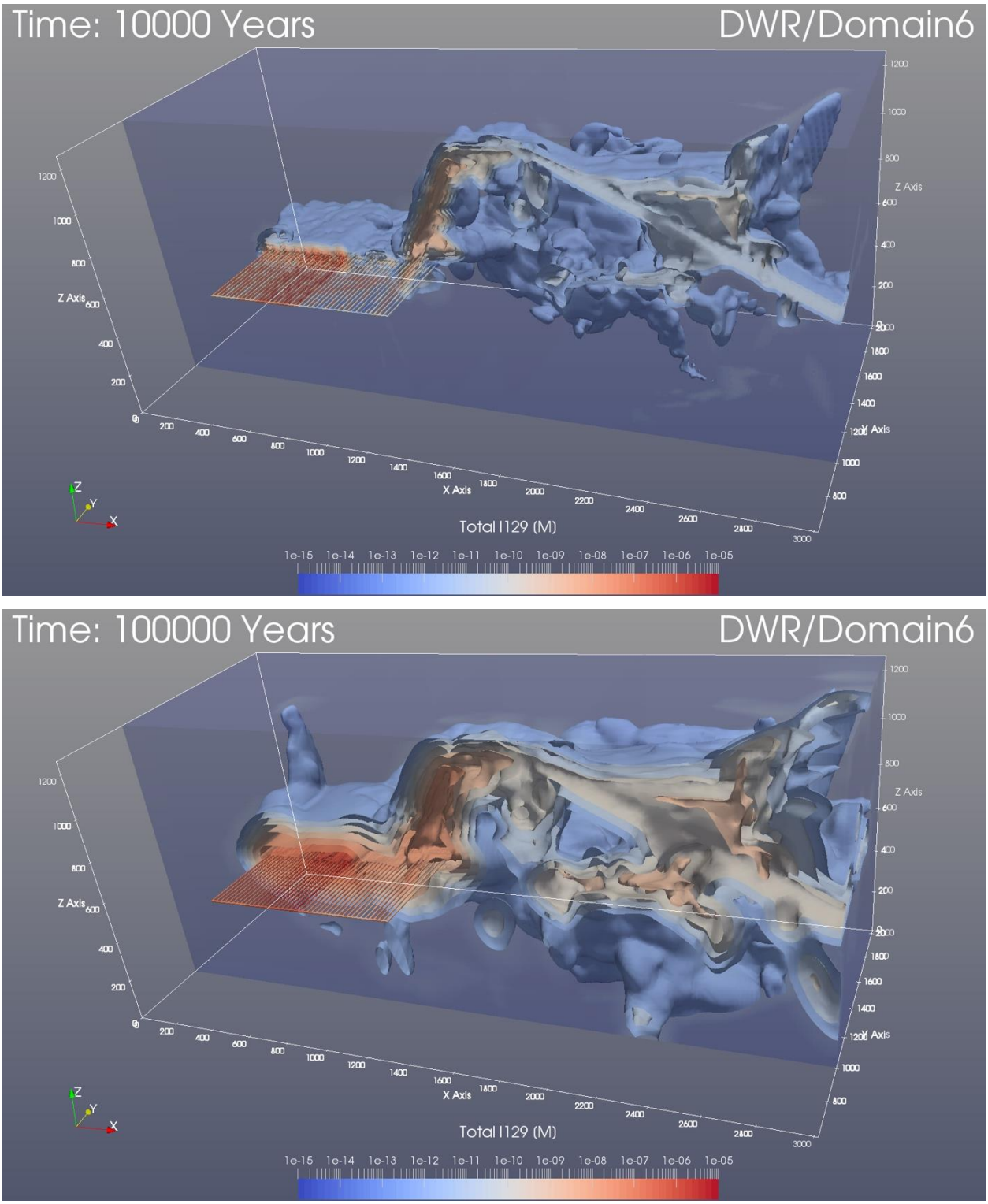

Figure 3-19. ^{129}I concentration at 10,000 years (top) and 100,000 years (bottom) in the deterministic simulation of Domain6. Contoured and colored as in Figure 3-18.

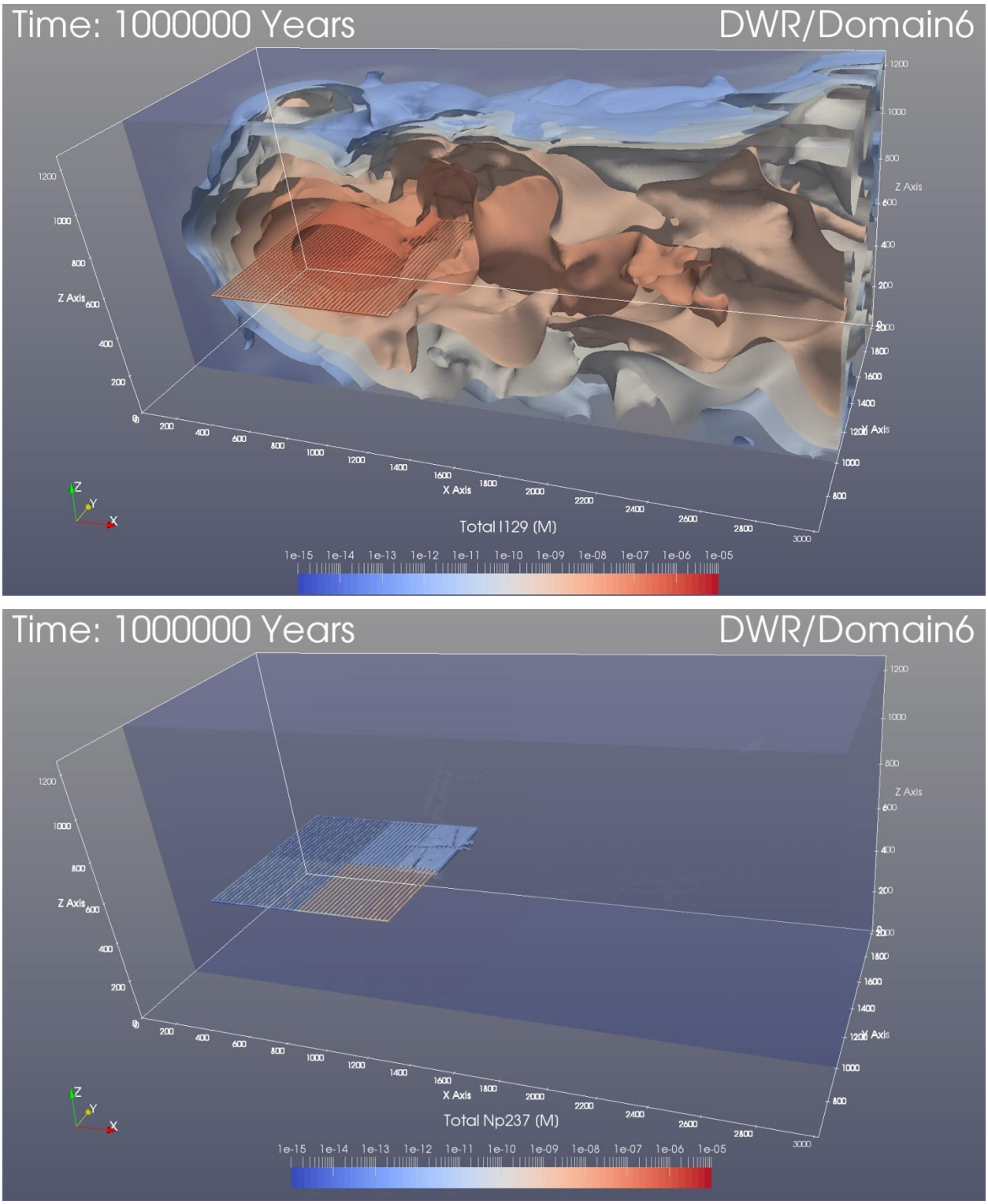

Figure 3-20. ^{129}I concentration (top) and ^{237}Np concentration (bottom) at 10^6 years in the deterministic simulation of Domain6. Concentration is contoured and colored on the same scale as in previous figures of ^{129}I.

3.4.2 Comparing Fracture Map Realizations

Breakthrough curves for ^{129}I at three observation points in the surficial sediment ("glacial1", "glacial2", and "glacial3") and three observation points in the deformation zone ("dz1", "dz2", and "dz3") (Figure 3-21) are compared in Figure 3-22 and Figure 3-23. Breakthrough curves for ^{237}Np are compared in Figure 3-24 and Figure 3-25. Neptunium concentration does not exceed 10^{-16} mol/L in any fracture realization at any observation point, and is not further discussed in the context of deterministic simulations.

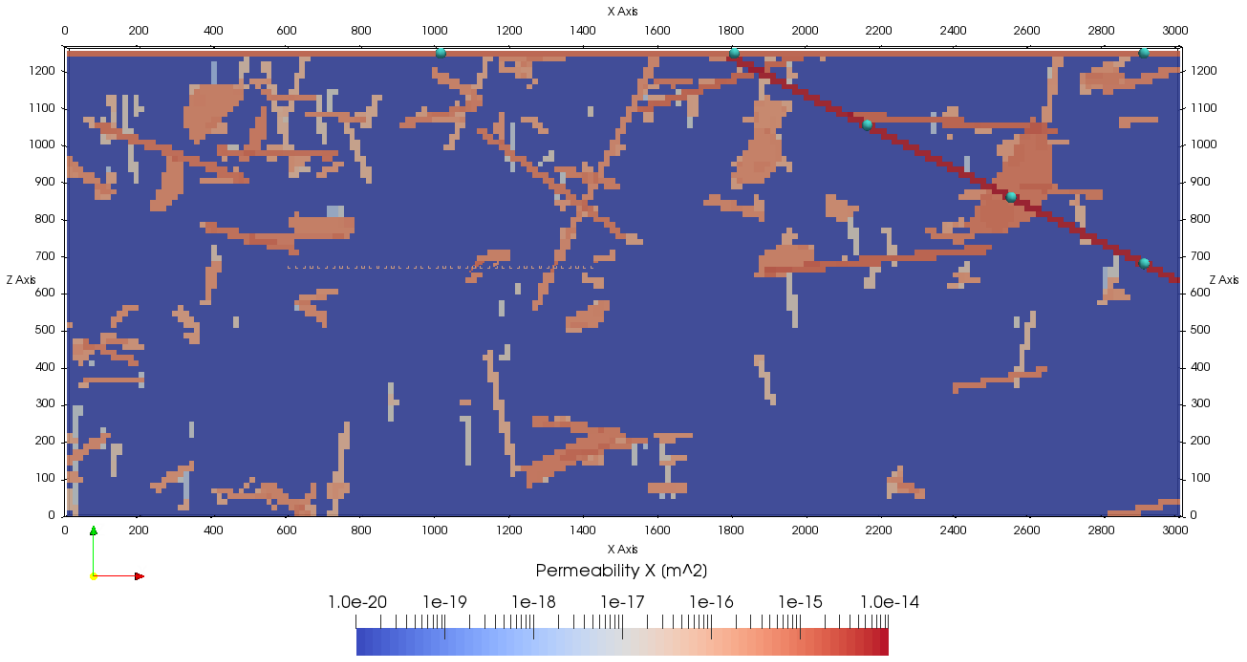

Figure 3-21. *X-Z* cross section at the *Y* midpoint of the domain showing the locations of observation points (teal spheres) used in comparison of fracture realizations and in uncertainty and sensitivity analysis (Section 3.4.3). From left to right in uppermost layer (sediments): "glacial1," "glacial2," and "glacial3." From top to bottom in deformation zone: "dz1," "dz2", "dz3."

Among the sediment observation points, the spread in time of earliest arrival (taken to be the time at which a concentration of 10^{-19} mol/L is reached) is approximately two orders of magnitude, between thousands and hundreds of thousands of years at each observation point. At which observation point ^{129}I first arrives depends on the fracture realization. In Figure 3-22, the dashed line indicates a simulation in which ^{129}I arrived at the two furthest points from the repository first (approximately 20,000 years into the simulation) and at the closest observation point over 100,000 years later. Among the deformation zone observation points, the time of earliest arrival occurs almost uniformly at "dz1" and "dz2" approximately 2000 years into the simulation. This timing is nearly coincident with early waste package breach times and indicative of rapid transport in fractures. At all observation points, the spread in maximum concentration of ^{129}I is approximately four orders of magnitude. The time of earliest arrival at any given point in the domain depends heavily on the connectivity (or lack thereof) between that point and the repository, while the magnitude of maximum concentration likely has an additional dependence on the transmissivity of flow paths in the direction away from the repository.

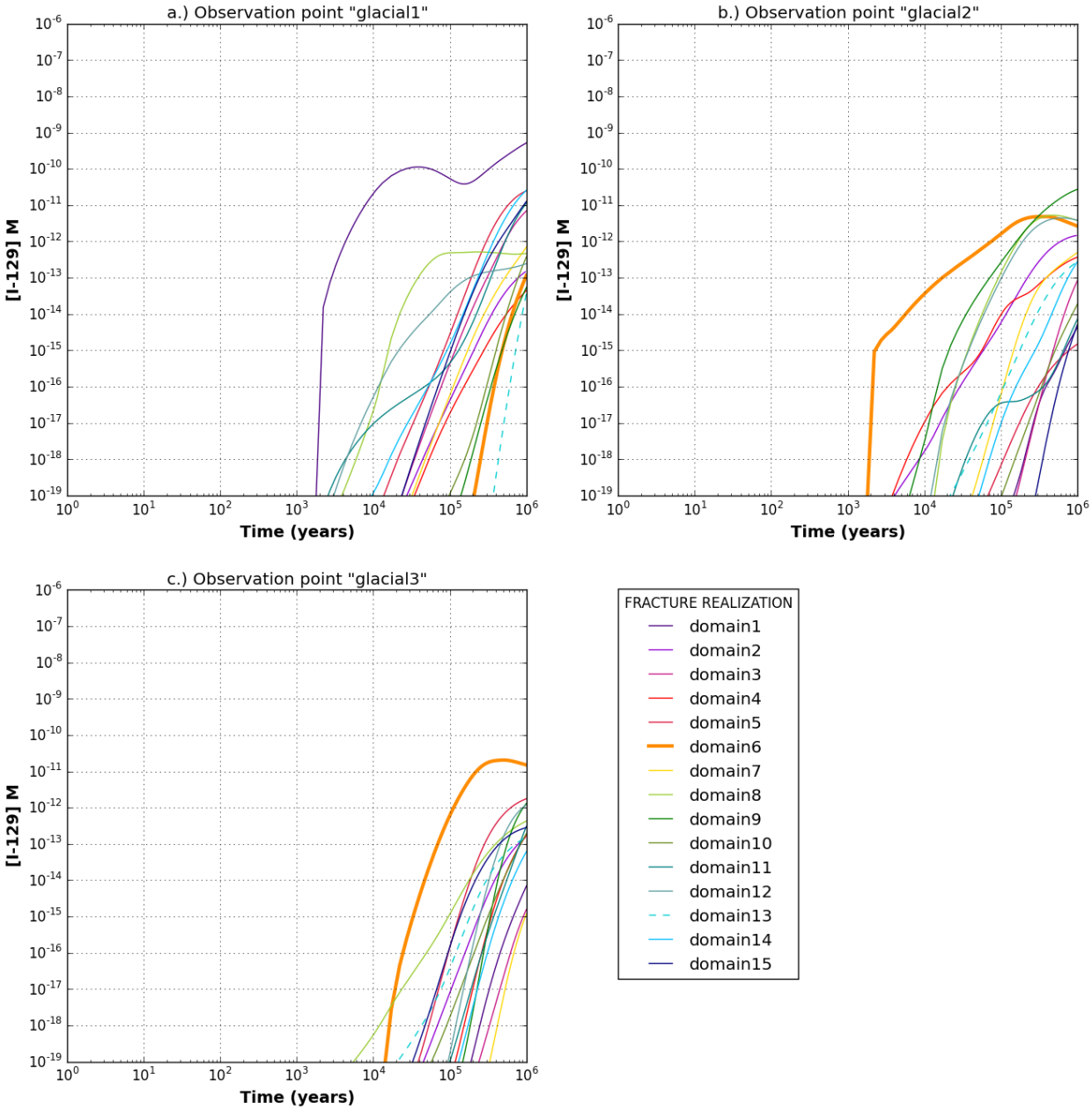

Figure 3-22. Predicted concentration of ^{129}I versus time for 15 fracture realizations at observation points a.) glacial1, b.) glacial2, and c.) glacial3. The heavy orange line is Domain6, the fracture realization used in probabilistic simulations.

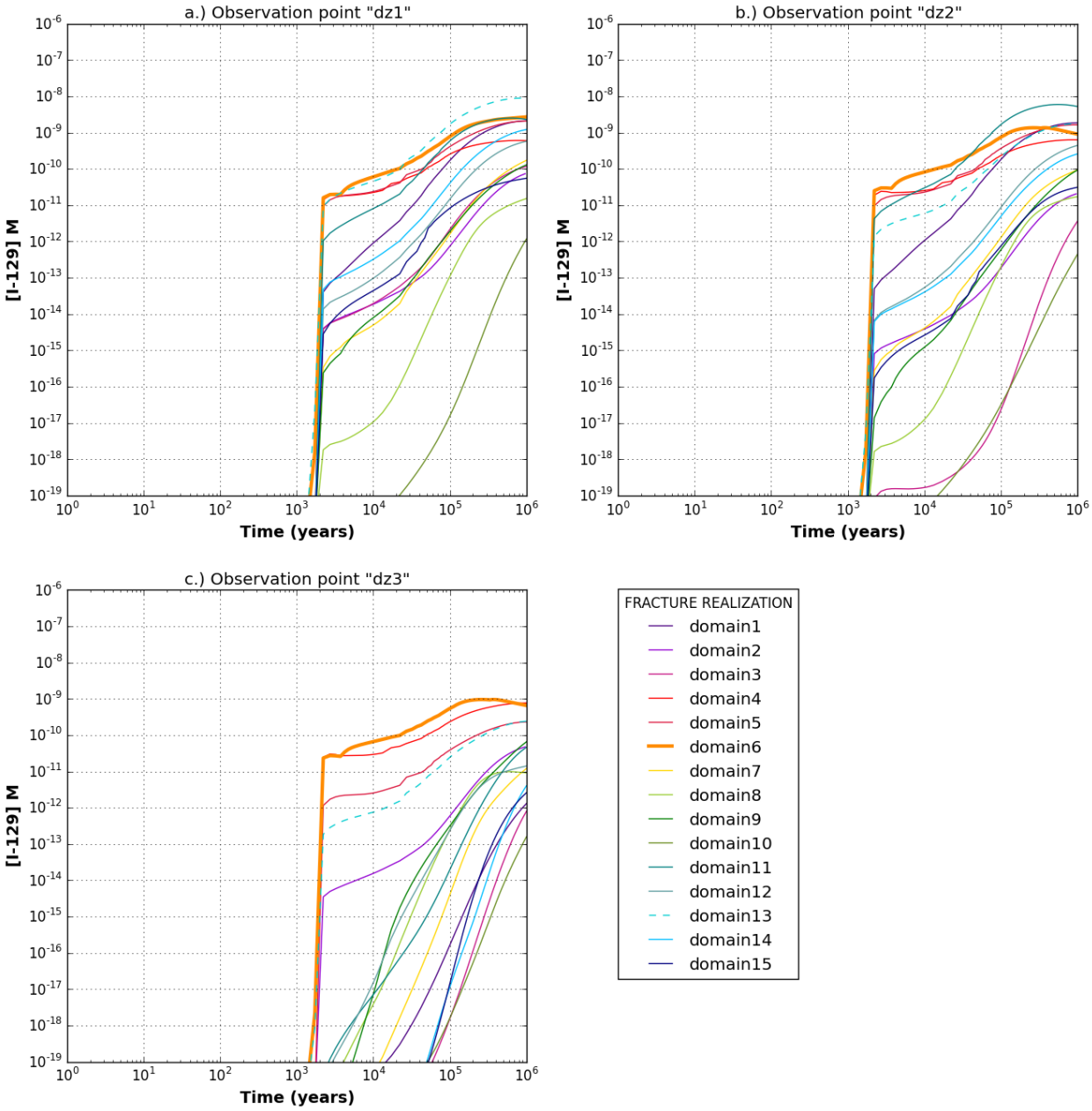

Figure 3-23. Predicted concentration of ^{129}I versus time for 15 fracture realizations at observation points a.) dz1, b.) dz2, and c.) dz3. The heavy orange line is Domain6, the fracture realization used in probabilistic simulations.

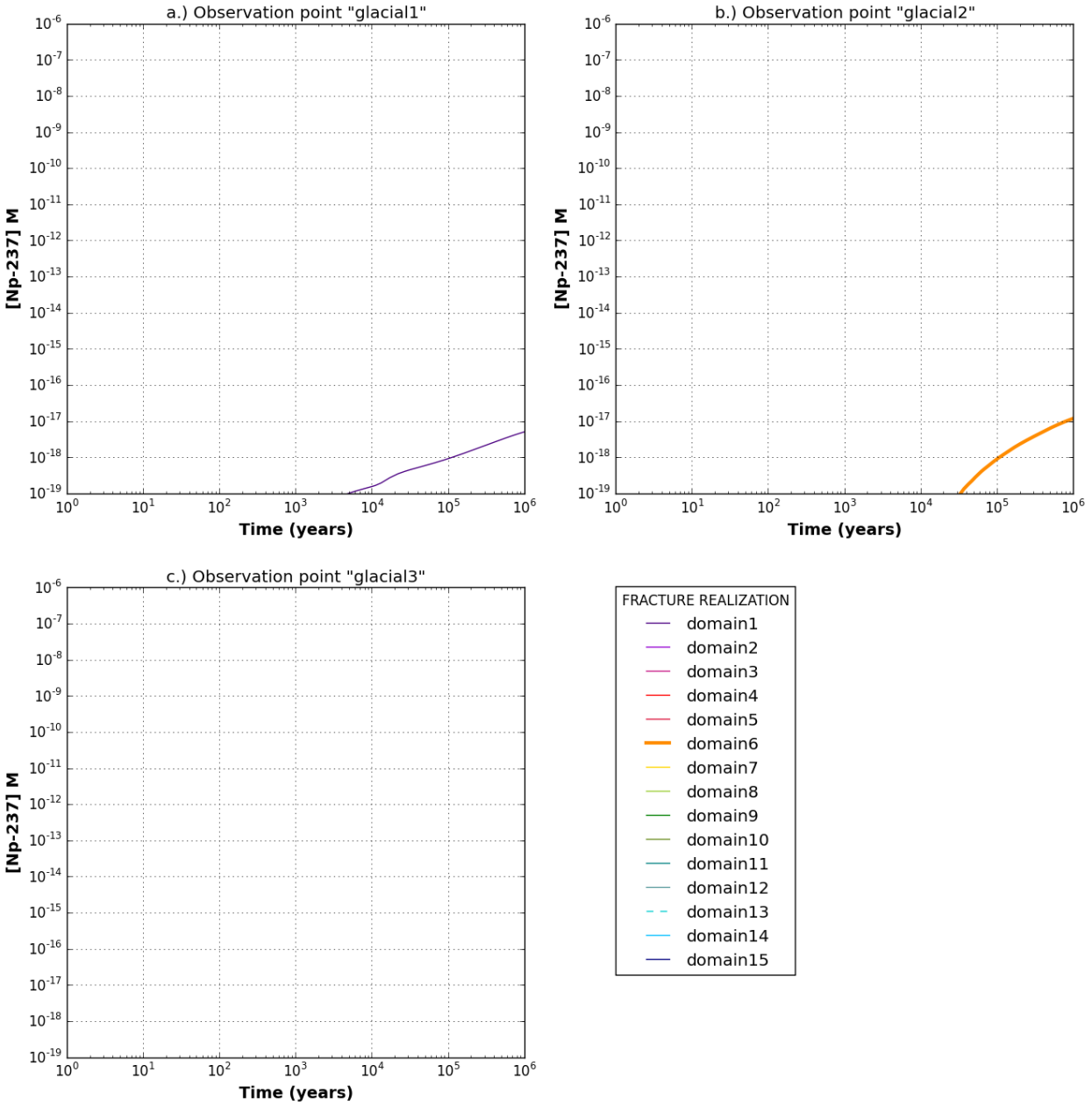

Figure 3-24. Predicted concentration of ^{237}Np versus time for 15 fracture realizations at observation points a.) glacial1, b.) glacial2, and c.) glacial3. The heavy orange line is Domain6, the fracture realization used in probabilistic simulations.

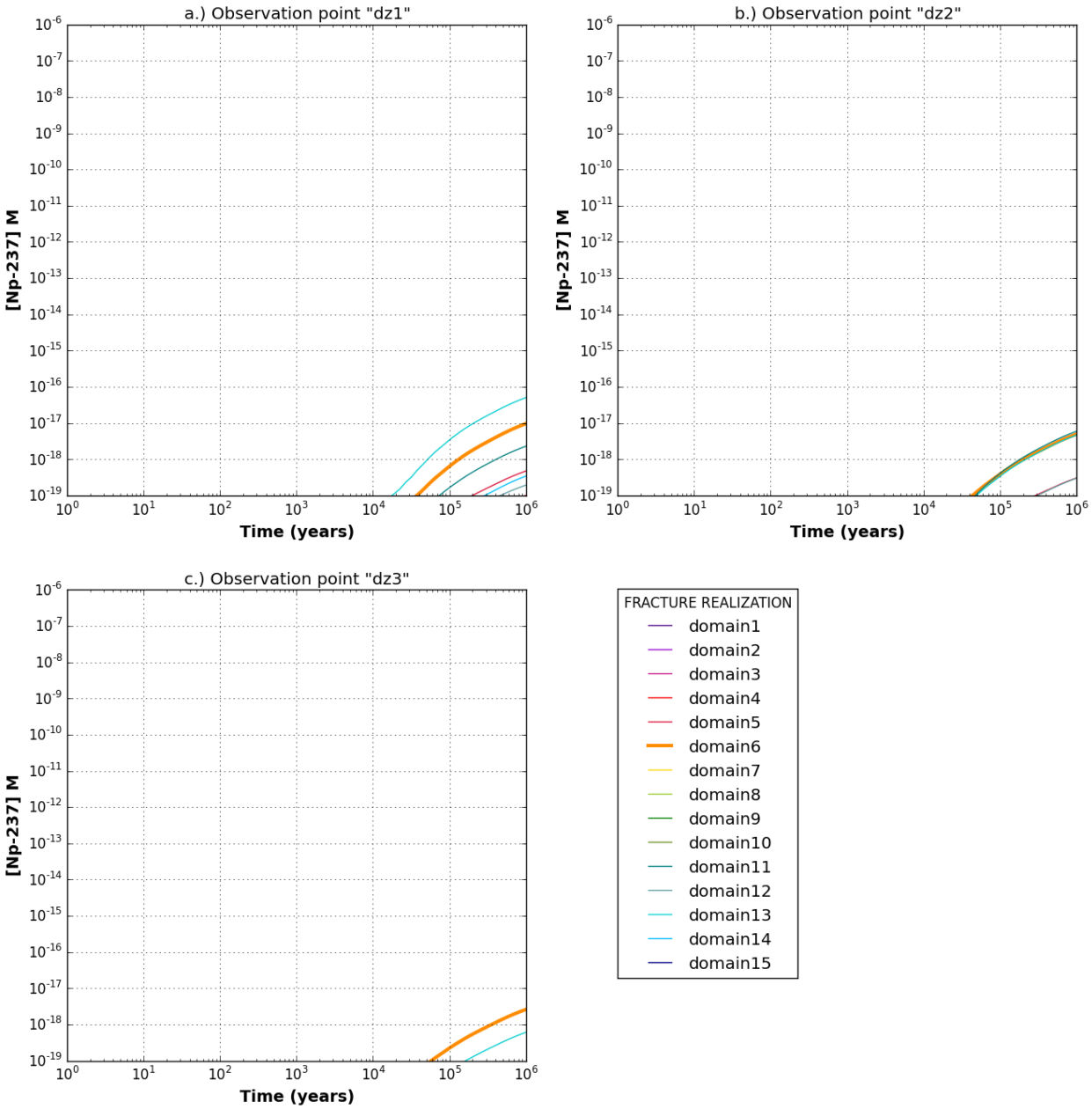

Figure 3-25. Predicted concentration of ^{237}Np versus time for 15 fracture realizations at observation points a.) dz1, b.) dz2, and c.) dz3. The heavy orange line is Domain6, the fracture realization used in probabilistic simulations.

3.4.3 Probabilistic Results

A suite of 50 probabilistic simulations was run using a single fracture realization (Domain6) and the parameter distributions listed in Table 3-11. Concentrations were observed at the same observation points used to compare fracture realizations (Figure 3-21). Mean breakthrough curves for all simulated radionuclides are plotted in Figure 3-26 (each point on a mean breakthrough curve is an average at that time of the 50 concentration values). Horsetail plots of breakthrough curves for ^{129}I are plotted in Figure 3-27 and Figure 3-28, and for ^{237}Np in Figure 3-29 and Figure 3-30.

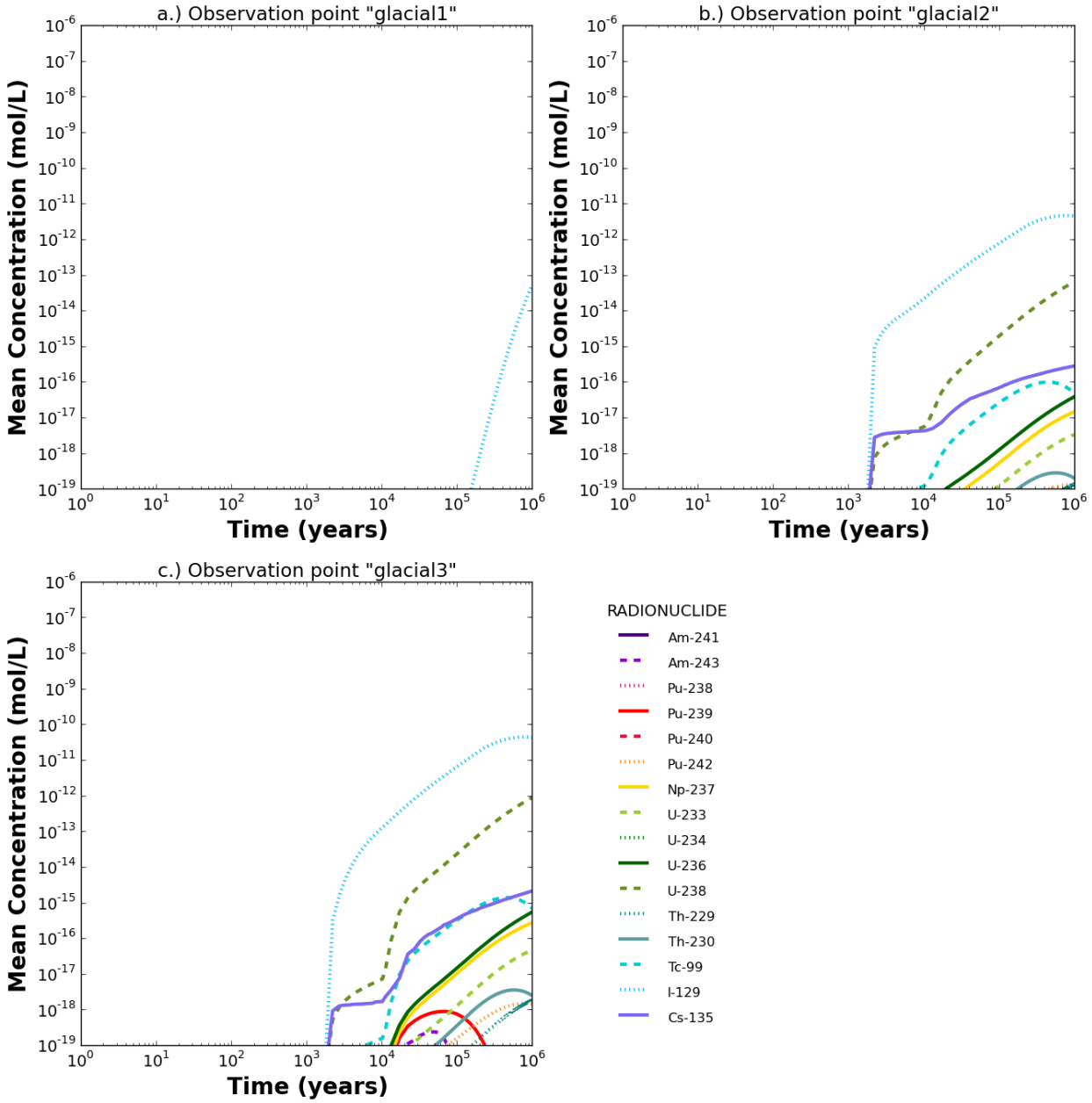

Figure 3-26. Mean concentrations of all simulated radionuclides, predicted on the basis of 50 sampled realizations.

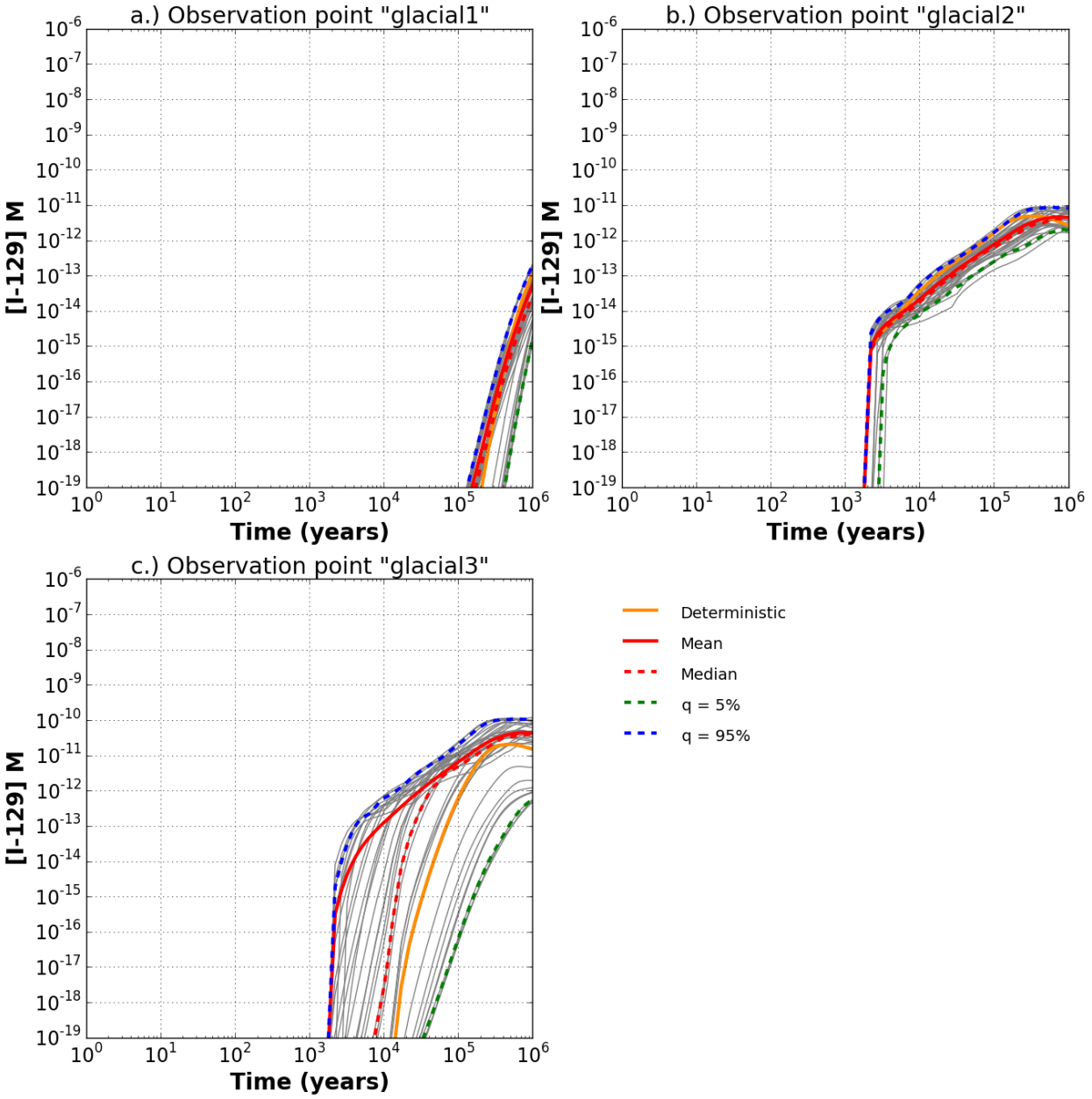

Figure 3-27. Predicted concentration of ^{129}I versus time for 50 sampled realizations at observation points a.) glacial1, b.) glacial2, and c.) glacial3. The heavy orange line is the deterministic simulation of Domain6.

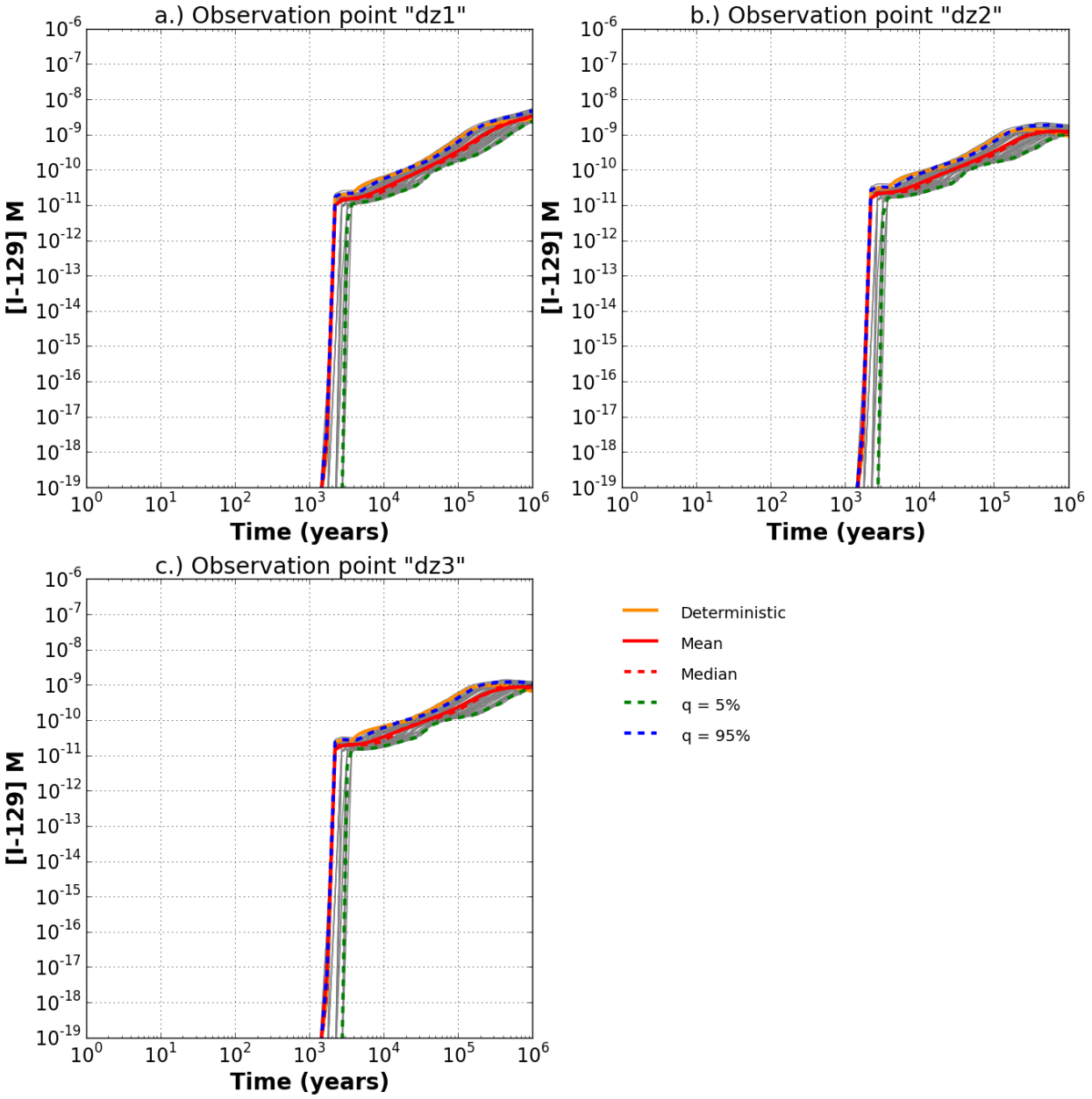

Figure 3-28. Predicted concentration of ^{129}I versus time for 50 sampled realizations at observation points a.) dz1, b.) dz2, and c.) dz3. The heavy orange line is the deterministic simulation of Domain6.

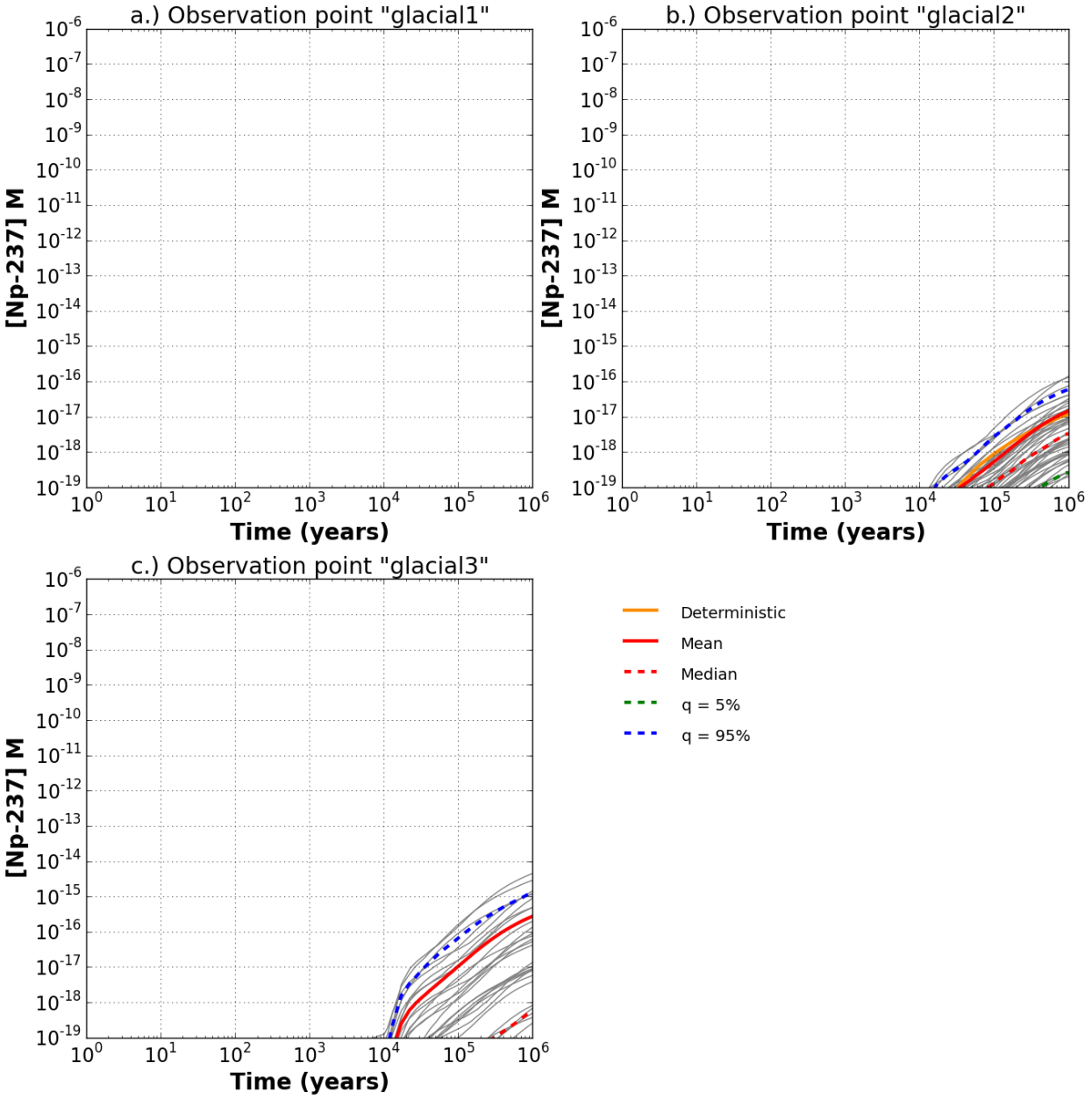

Figure 3-29. Predicted concentration of ^{237}Np versus time for 50 sampled realizations at observation points a.) glacial1, b.) glacial2, and c.) glacial3. The heavy orange line is the deterministic simulation of Domain6.

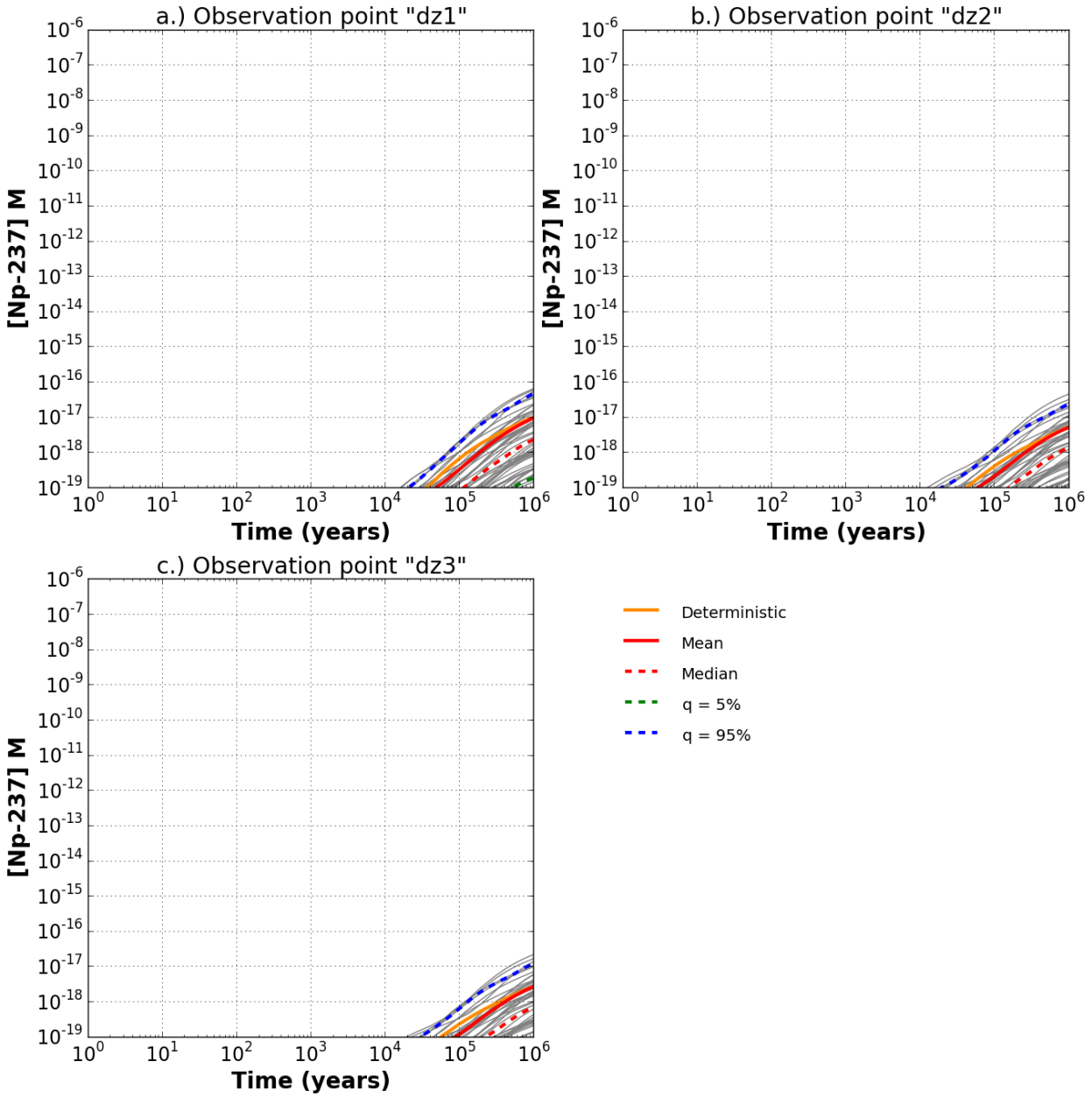

Figure 3-30. Predicted concentration of ^{237}Np versus time for 50 sampled realizations at observation points a.) dz1, b.) dz2, and c.) dz3. The heavy orange line is the deterministic simulation of Domain6.

Predicted concentrations of ^{129}I vary less due to the sampled parameters of Table 3-11 than due to variations in flow paths among fracture realizations (cf. Figure 3-22 to Figure 3-27; and Figure 3-23 to Figure 3-28). At all observation points except "glacial3," the time of earliest ^{129}I arrival varies by less than a factor of four (Figure 3-27a,b). At "glacial3," the furthest observation point from the repository (Figure 3-27c), the time of earliest arrival varies by approximately a factor of 10 (from 2000 to 30,000 years), compared with a nearly hundredfold variation due to fracture realization (Figure 3-22c). Similarly, the variation in maximum concentration of ^{129}I is much less over these probabilistic simulations for Domain6 than the variation across fracture realizations discussed in the previous section.

Domain6 was one of the few fracture realizations in which ^{237}Np arrived at any of the observation points (Figure 3-24 and Figure 3-25). Among the probabilistic simulations, the time of earliest arrival at all observation points other than "glacial1" (at which ^{237}Np does not arrive), varies from approximately 10,000 years to almost 10^6 years (Figure 3-29 and Figure 3-30). Maximum concentration varies over several orders of magnitude, but does not exceed 10^{-14} mol/L over the million-year duration of the simulation.

Spearman's rank correlation coefficients (SRCCs) (Helton et al. 2006) were calculated in order to assess the sensitivity of maximum concentration of ^{129}I and ^{237}Np to sampled parameters (Figure 3-31 through Figure 3-33). To calculate the ^{129}I or ^{237}Np SRCC for a given input parameter, entries in the input and output vectors for the 50 probabilistic simulations are ranked from smallest to largest and their ranks ("1" through "50") are substituted for the actual variable values. The SRCCs are then calculated as:

$$SRCC = \frac{cov(r_X, r_Y)}{\sigma_{r_X}\sigma_{r_Y}} \tag{3-7}$$

where $cov(r_X, r_Y)$ is the covariance of the ranked input (X) and output (Y) vectors, σ_{r_X} is the standard deviation of the ranked input vector and $\sigma_{r_Y}$is the standard deviation of the ranked output vector, where output is the maximum concentration at an observation point regardless of time. For a finite set of N sampled values (x_i, y_i), i =1, …, N, Eq. 3-7 becomes (Adams et al. 2016a, Sec. 5.2.1):

$$SRCC = \frac{\sum_{i=1}^{N}(x_i - \bar{x})(y_i - \bar{y})}{[\sum_{i=1}^{N}(x_i - \bar{x})^2 \sum_{i=1}^{N}(y_i - \bar{y})^2]^{\frac{1}{2}}} \tag{3-8}$$

where $\bar{x}$ is the mean of x_i and $\bar{y}$ is the mean of y_i.

Maximum concentration of ^{129}I at the sediment observation points exhibits a positive correlation with sediment permeability especially at observation point "glacial3" (Figure 3-31). Maximum concentration of ^{237}Np at the sediment observation points exhibits a strong negative correlation with the neptunium K_d in the natural barrier, and (at "glacial3") a positive correlation with sediment permeability (Figure 3-32).

At the deformation zone observation points (Figure 3-33 and Figure 3-34), maximum concentrations of both ^{129}I and ^{237}Np are positively correlated with glass exposure factor (f_e)—although weakly for ^{237}Np. Maximum concentration of ^{129}I is positively correlated with waste package degradation rate and negatively correlated with sediment permeability. Maximum

concentration of ^{237}Np is strongly negatively correlated with the neptunium K_d in the natural barrier.

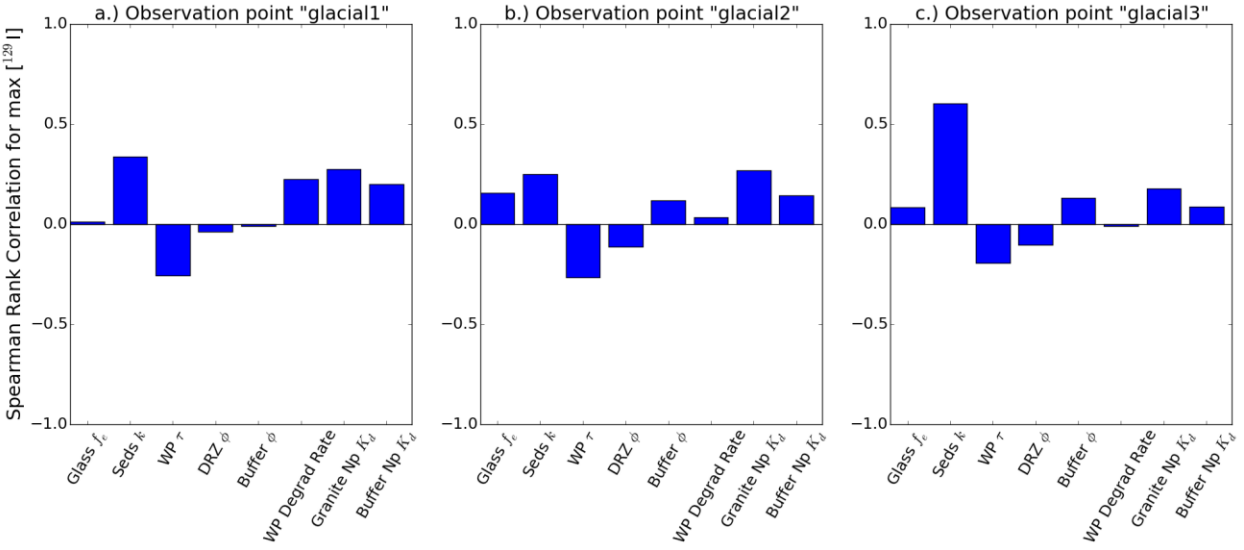

Figure 3-31. Spearman's rank correlation coefficients for maximum concentration of ^{129}I at sediment observation points.

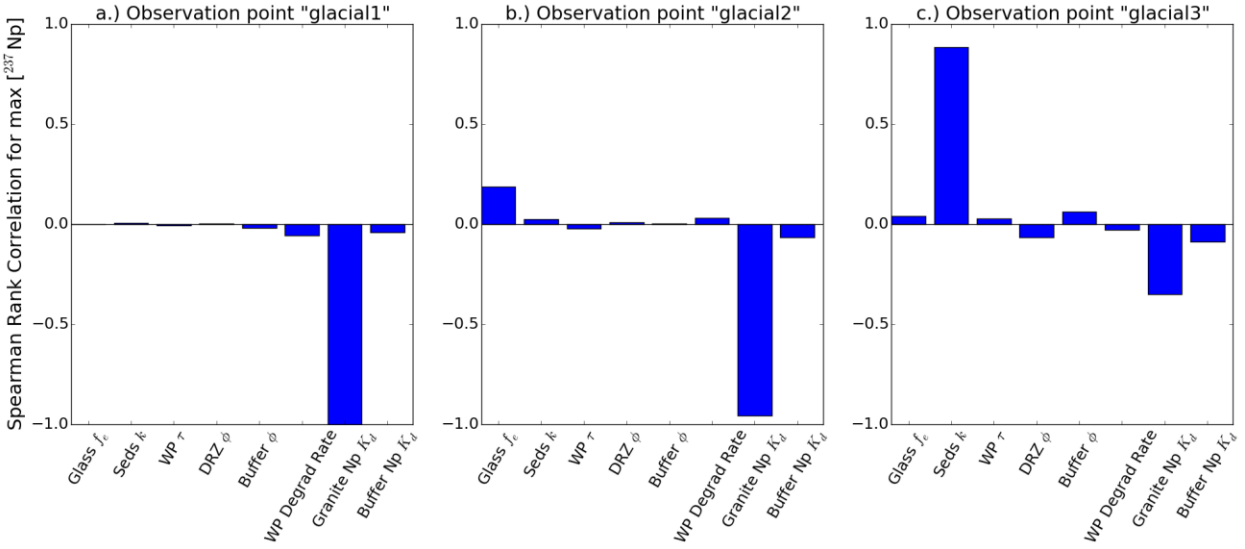

Figure 3-32. Spearman's rank correlation coefficients for maximum concentration of ^{237}Np at sediment observation points.

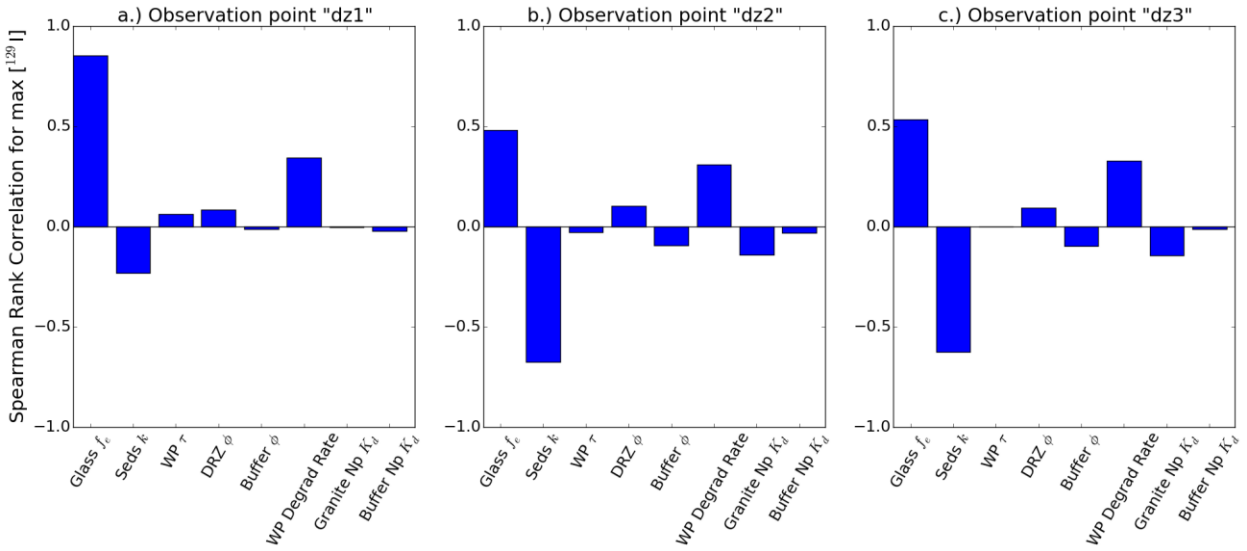

Figure 3-33. Spearman's rank correlation coefficients for maximum concentration of ^{129}I at deformation zone observation points.

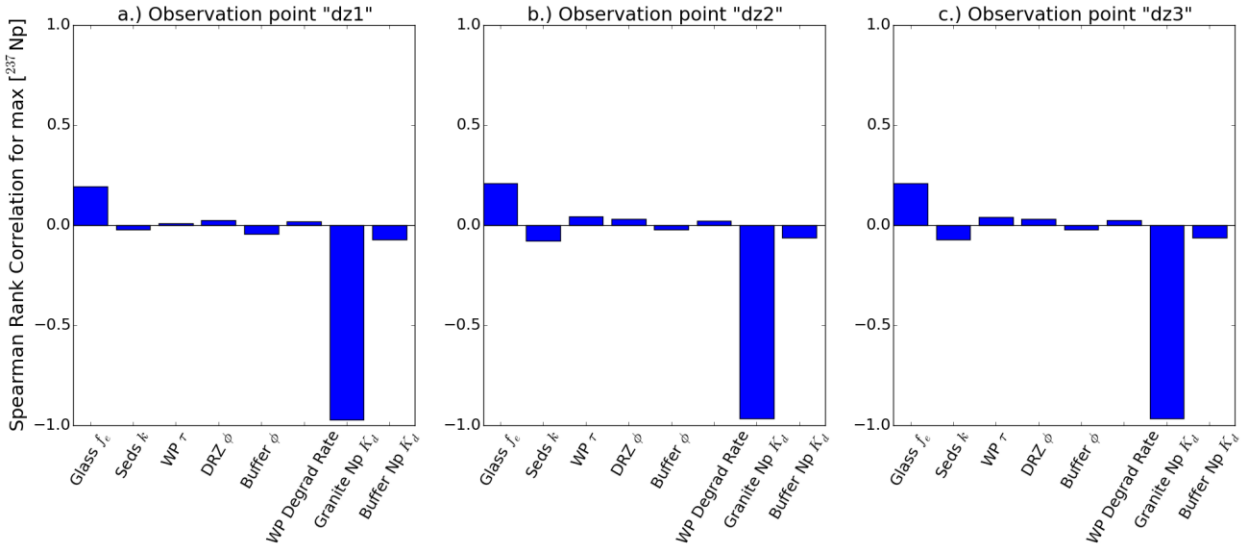

Figure 3-34. Spearman's rank correlation coefficients for maximum concentration of ^{237}Np at deformation zone observation points.

Scatter plots provide another means of explaining the relationship between uncertainty in the output (here, the maximum concentration of either ^{129}I or ^{237}Np) and uncertainty in sampled input parameters. Below are shown two examples that may be compared to the SRCCs in Figure 3-32. Figure 3-35 may be compared to Figure 3-32b, whose SRCCs indicate a strong negative correlation between maximum ^{237}Np concentration and neptunium K_d in the natural system for the "glacial2" observation point. This is confirmed by the left plot in Figure 3-35. Also, the ^{237}Np SRCC for sediment permeability at the "glacial2" observation point is effectively zero, which is confirmed by the lack of any visual trend in the right plot of Figure 3-35. From the SRCCs in Figure 3-32c, it would be expected that scatterplots would show visual trends

between maximum ^{237}Np concentration and both sampled neptunium K_d in the natural system (negative trend) and sampled sediment permeability (positive trend), at the "glacial3" observation point. This is confirmed by the trends shown in Figure 3-36. However, the trends are only present for about 60% of the 50 realizations. This is because there is no ^{237}Np breakthrough at the "glacial3" observation point for the other 40% of the realizations, as confirmed by Figure 3-29c, which indicates that not all of the realizations have ^{237}Np breakthrough at "glacial3" during the one-million-year simulation period.

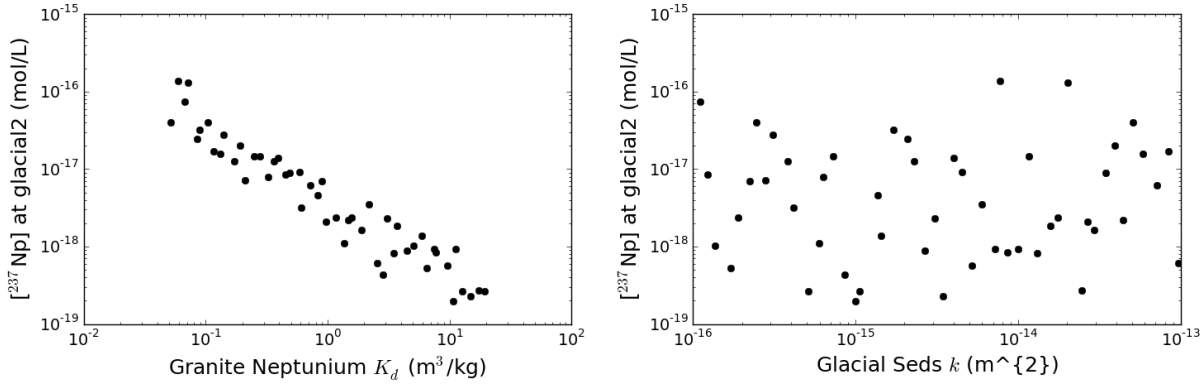

Figure 3-35. Maximum concentration of ^{237}Np versus sampled parameter values at "glacial2."

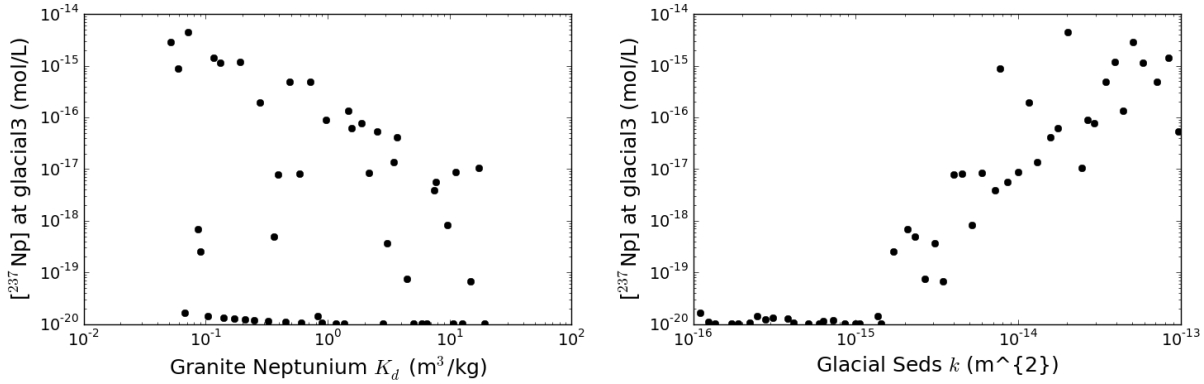

Figure 3-36. Maximum concentration of ^{237}Np versus sampled parameter values at "glacial3."

3.5 Granite Reference Case Conclusions and Recommendations

Comparison of breakthrough curves among fifteen fracture realizations and fifty simulations that sampled on other input parameters indicates that the uncertainty in magnitude and timing of predicted concentrations at any given location in the model domain is larger due to fracture distribution than to other sampled parameters. Maximum concentrations of ^{129}I and ^{237}Np are sensitive to properties of the engineered and natural barriers, including waste form dissolution rates in the engineered barrier, and sorption coefficients and permeability of flow pathways in the natural barrier. Fractured media also present new challenges in uncertainty and sensitivity analysis, which might be addressed through introduction of a performance metric other than concentration (or dose) at a specific point location—for example, a metric that averages concentrations over a series of aquifer points or a set of withdrawal wells that draw down many outcropping fractures. This latter point is discussed in more detail below.

The current representation of the fractured host rock is biased toward greater connectivity than is likely to exist in a sparsely fractured rock suitable for nuclear waste disposal. A large fracture density was necessary for this initial iteration of the crystalline reference case in order to test the model's ability to represent flow and transport in a fractured host rock, and to test the representation of a discrete fracture network with a continuous porous medium of varying permeability (Sec. 3.2.2.1). Having established the capability of simulating flow and transport in a fractured system, work in the future can (1) address the influence of deterministic features ("deformation zones"—see Perry 2016) on flow and transport pathways; (2) determine the probability of a percolating network existing at various length scales, given a realistic description of fractured crystalline rock; and (3) examine in more detail the effects of hydrodynamic dispersion and numerical diffusion/dispersion. If a crystalline rock disposal site is selected, site-specific understanding of deterministic features and of the probability of a percolating network existing at the scales of interest will be necessary.

Important related issues uncovered by this year's work on a granite reference case, both with respect to a DWR and a CSNF repository (Mariner et al. 2016), are as follows:

- Isolation. This is one of three primary safety functions generally acknowledged and often used for the safety case for most international programs (Sevougian and MacKinnon 2014). [The other two are containment and retardation (delayed/limited releases).]
- Quantitative safety metrics used to establish conformance to regulations.
- Uncertainty and heterogeneity, and their effect on safety confidence.

Regarding isolation, the current iteration of the generic crystalline reference case illustrates the importance of this safety function because some fracture maps indicate nearly instantaneous communication between the repository and the surface environment (e.g., see Fig. 3-20). This points to several possibilities for future reference-case work:

(1) as mentioned above, reduce conservatism in fracture connectivity;

(2) include a 200- to 300-meter sedimentary overburden (both directly over the repository site and downgradient, e.g., RWM 2016, Figure 8);

(3) site the generic repository in a location where the groundwater table is sufficiently deep, even during glacial maximums, i.e., where a deep unsaturated zone would allow upward radionuclide transport only via the slow process of molecular diffusion; or

(4) some combination of a deep unsaturated zone directly over the repository site and a sedimentary overburden some distance downgradient. This latter was the case for Yucca Mountain (DOE 2008). [In the current reference case, the rock overlying the repository site is saturated to the surface.]

Consider the second two bulleted issues together. Heterogeneity, and concomitant aleatory uncertainty, associated with a fracture network seem to be large enough to create a system for which a safety metric is not straightforward, at least for the present reference case with outcropping fractures where the fracture maps are widely varied from realization to realization. In this regard both the characteristics of the biosphere, i.e., how the dose receptor will be exposed, and the likely regulatory criteria must be considered. It must be assumed that regulations will be written in terms of a peak dose metric. But, at this generic stage, how should a peak dose metric be represented or evaluated in the PA conceptual model?

First is a modified reference case with a sedimentary overburden (Cases 2 and 4 above). Here, a single pumping well can be envisioned in the permeable sediments some distance downgradient from the land withdrawal boundary (e.g., DOE 2008). This is reasonably straightforward to model, as has been done previously for the argillite and bedded-salt generic reference cases (Sevougian et al. 2014; Mariner et al. 2015).

Second is a granite outcrop repository, with or without a deep unsaturated zone (Case 1 or 3 above). Here one can envision a grid of perhaps 25 monitor wells some distance downgradient from the land withdrawal zone. Each well in the grid is fixed in location but will intersect different fractures, depending on the fracture-map realization. The exact metric in this case is likely the peak concentration (or dose) in the well with the largest radionuclide concentration in each realization—probably a different well in each realization. Averaged over a set of say 50 to 100 fracture maps, this should tend toward a stable mean.

A final consideration from the present-year simulations of a granite repository is the durability of the waste package. A stainless steel waste package has been used in the current granite reference case, with a median lifetime (time to first throughgoing penetration) of about 45,000 years. Other repository concepts in crystalline host rock use oxygen-free copper overpacks (Matteo et al. 2016) with longer predicted lifetimes (SKB 2011). This may be an important modification to future simulations of the generic crystalline reference case.

4. BEDDED SALT REPOSITORY REFERENCE CASE

The bedded salt reference case for deep geologic disposal of defense-related HLW and SNF is developed from (1) the reference case for a commercial SNF/HLW repository in bedded salt, described in Sevougian et al. (2012) and Vaughn et al. (2013); (2) the repository design proposed in Carter et al. (2012) for a defense-only repository; and (3) elements of the engineered and natural barriers described in previous PAs of CSNF disposal in bedded salt (Mariner et al. 2015; Sevougian et al. 2014; Sevougian et al. 2013; Freeze et al. 2013a, Clayton et al. 2011)—the characterization of which drew heavily upon parameter values developed for WIPP PAs. The salt reference case assumes the same inventory assumed for the crystalline reference case (Section 3.1.2), i.e., disposal of cooler (≤ 1 kW/canister at the time of disposal) DOE-managed, research- and defense-related HLW and SNF in a low-temperature DWR in the year 2038.

The conceptual model includes a mined repository approximately half a kilometer below the surface in a thick bedded salt host rock in a geologically stable sedimentary basin. Characteristics of the bedded salt host rock that contribute to or impact post-closure safety include (Freeze et al. 2013b):

- The ability of salt to creep, which is expected heal fractures, reconsolidate crushed salt backfill, and encapsulate waste, contributing to waste containment;
- The geologic stability of deep salt beds, which have been isolated from surface processes for hundreds of millions of years, and can be expected to isolate the repository for the duration of the regulatory period;
- The low permeability and porosity of the host rock, which limits exposure of waste to water, thereby limiting and delaying radionuclide releases;
- The reducing chemical environment, which limits radionuclide solubility, limiting and delaying radionuclide releases.
- The potential presence of anhydrite interbeds, which are more brittle and of higher permeability than halite, providing potential pathways for radionuclide release.

The remainder of this section includes a description of the engineered (Section 4.1) and natural (Section 4.2) barriers followed by a quantitative post-closure performance assessment (PA) (Sections 4.3 and 4.4).

4.1 Waste and Engineered Barriers

Specific post-closure basis information related to the wastes and engineered barriers includes:

- Characteristics of the repository (Section 4.1.1),
- Inventory characterization (Section 4.1.2),
- Waste form characterization (Section 4.1.3),
- Waste package characterization (Section 4.1.4), and
- Characteristics of the engineered barriers (Section 4.1.5).

4.1.1 Characteristics of the Repository

This first iteration of the reference case considers disposal of the entire inventory of existing and projected glass HLW from Savannah River and Hanford and of DSNF with a heat output at the time of disposal (2038) of ≤ 1kW/canister. The reference case repository consists of 16 panels of 10 parallel waste disposal rooms, arranged symmetrically with 8 panels on either side of a central hallway. Rooms are 185 m in length with 155 m for waste emplacement, and 15 m at each end reserved for sealing with run-of-mine crushed salt. This design is based on Case 4 in Carter et al. (2012, Figure 4-6), a generic repository design that accommodates all defense-related HLW and DSNF excluding Naval SNF. Case 4 (Carter et al. 2012) is one panel larger than the current reference case due to a slightly larger inventory (which includes calcine waste) and the assumption of larger waste package spacing for hotter waste packages. As in Carter et al. (2012), repository access and ventilation is via vertical shafts at one end of the repository, and canisters of HLW and DSNF are emplaced transverse to the length of the room on the room floor. Shafts and halls are completely sealed and/or backfilled. Emplacement rooms in the generic reference case described here are assumed to be completely backfilled with run-of-mine crushed salt, although the original engineering designs call only for sufficient height of crushed salt in the emplacement portion of disposal rooms to provide shielding (Carter et al. 2012; Matteo et al. 2016).

Table 4-1 lists repository and waste package dimensions as derived from various sources under "Reference Value," and dimensions used in PA simulations under "Simulated Value"—simulated values reflect the adjustments needed to facilitate gridding and simulation in a half-symmetry domain (see Section 4.3.2.1).

Table 4-1. Dimensions and counts for the DWR bedded salt reference case.

Parameters	Reference Value	Simulated Value
HLW Waste Package (WP)		
WP length (m)	4.5[a]	4.44
WP outer diameter (m)	0.61[a]	0.56 (on a side)[g]
Number of Hanford WPs	11800[b]	11800
Number of Savannah River WPs	7824[b]	7824
DSNF Waste Package (WP)		
WP length (m)	4.6[c]	4.44
WP outer diameter (m)	0.61[c]	0.56 (on a side)[g]
Number of DSNF WPs (< 50 W bin)	1163[b]	1164
Number of DSNF WPs (50-100 W bin)	234[b]	234
Number of DSNF WPs (100-200 W bin)	940[b]	940
Number of DSNF WPs (200-300 W bin)	12[b]	12
Number of DSNF WPs (300-500 W bin)	41[b]	42
Number of DSNF WPs (500-1000 W bin)	88[b]	88
Number of DSNF WPs (1000-1500 W bin)	4[b]	4
Disposal Rooms		
Room height (m)	3.05[d]	3.33
Room width (m)	6.10[d]	6.67
Room center-to-center spacing (m)	36.58[d]	36.67

Parameters	Reference Value	Simulated Value
Room seal length (m)	15.24[d]	15
Room length, including seals (m)	182.9[d]	185
Number of WPs per room	166[d]	140
WP center-to-center spacing (m)	0.91[d]	1.11
Number of rooms per panel	10[d]	10
Repository		
Number of HLW panels	14[d]	14
Number of DSNF panels	3[d]	2
Access hall height (m)	6.10[d]	5
Access hall width (m)	9.14[d]	10
Number of shafts	5[d]	4
Shaft diameter (m)	7.38[d]	5 (on a side)[g]
Repository length (m)[e]	NA[d]	1925
Repository width (m)[f]	NA[d]	753
Repository Depth (m)	655[d]	601

[a] Hanford glass HLW canister (DOE 2008, Table 1.5.1-16).
[b] On the basis of canister counts reported in Wilson (2016) and Carter et al. (2013).
[c] Large, long standardized canister (DOE 2008, Figure 1.5.1-9).
[d] Carter et al. (2012, Section 4.2, Case 4). Dimensions are converted from feet. Overall repository dimensions are not explicitly calculated.
[e] Equivalent to the length of the long hall extending from the shafts to the furthest disposal panel.
[f] Equivalent to the length of the short halls connecting pairs of disposal panels.
[g] PFLOTRAN simulations represent waste packages as rectangular cuboids instead of right circular cylinders, in order to simplify the gridding.

4.1.2 Inventory

The reference case inventory is identical to that assumed in the crystalline reference case (Section 3.1.2). It includes 11800 canisters of Hanford glass HLW, 7824 canisters of Savannah River glass HLW (Carter et al. 2013), and 2482 canisters of DSNF with a heat output of less than 1500 W (on the basis of 2010 wattages) divided into seven bins (Wilson 2016). Bulk and average per canister radionuclide inventories for each waste type (Hanford HLW, Savannah River HLW, and 7 bins of DSNF) are given in Table 3-2 and Table 3-3, respectively. The heat of decay per waste package is plotted in Figure 4-1; time zero is the year 2038. Per waste package wattages for the Hanford and Savannah River HLW are less than in the crystalline reference case, because the crystalline reference case assumed five glass logs per waste package, while the salt reference case assumes one glass log per waste package.

4.1.3 Waste Forms

Glass HLW and DSNF waste forms are identical to those described in the crystalline reference case (Section 3.1.3). As in the crystalline reference case, at the time of waste package breach, glass HLW is assumed to begin dissolving according to a temperature-dependent rate law (Eq. 3-1). DSNF is assumed to degrade instantaneously upon exposure to water (i.e., at the time of waste package breach), as appropriate for metallic fuels.

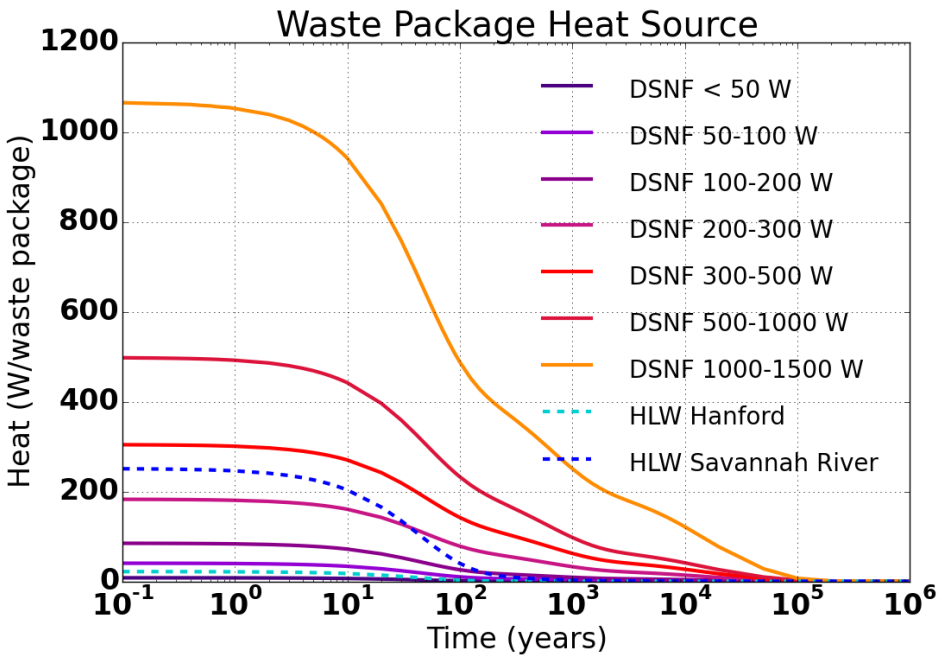

Figure 4-1. Heat of decay versus time per waste package for the glass HLW and DSNF bins included in bedded salt PA simulations. [Time zero is the year 2038.]

4.1.4 Waste Packages

Waste packages in a salt repository may comprise simply the canisters in which the waste is stored (i.e., the HLW canisters, MCOs, and standardized canisters considered part of the waste form and described in Section 3.1.4) as assumed in Carter et al. (2012) and as assumed for glass HLW in Matteo et al. (2016). Alternatively, thick carbon steel overpacks may be used in order to ensure waste package integrity during operations (as for DSNF in Matteo et al. 2016) and/or through peak repository temperatures (Sevougian et al. 2012).

In PA simulations, each waste package is a single region containing a radionuclide source term (due to waste form dissolution/degradation) and a heat source term (see Sections 4.3.2.4 and 4.3.2.5). The radionuclide source term is activated when a waste package is breached. This iteration of the salt reference case takes credit for a 7.5 cm thick carbon steel overpack, which is assumed to degrade via general corrosion. See Section 4.3.2.5 for a description of the implementation in PA.

Waste package material properties are set equal to those used in the crystalline reference case (Section 3.1.4), except for porosity (0.3), which is smaller in the salt case due to the likelihood that salt creep will crush waste packages.

4.1.5 Crushed Salt Backfill (Rooms, Halls)

The salt reference case assumes that disposal rooms and access halls are filled with run-of-mine-crushed salt backfill. As summarized in Sevougian et al. (2012; 2013), crushed salt backfill is expected to have an initial porosity of approximately 0.35 (Rothfuchs et al. 2003), and correspondingly, permeability higher than and thermal conductivity lower than that of intact salt. Over time, it will consolidate to a state approaching that of intact salt (Hansen and Leigh 2011,

Section 2.4.1.7), a process expected to be mostly complete within approximately 200 years (Clayton et al. 2012).

Following the example of Sevougian et al. (2013), in order to assign properties to the consolidated backfill, it is assumed that the backfill will evolve similarly to a crushed-salt shaft seal. Porosity and permeability values can be drawn from the WIPP parameter database (Fox 2008), which lists two distributions for the porosity and permeability of the shaft seal component in the host rock ("the lower portion of the simplified shaft seal"), one distribution for the first 200 years after emplacement and one for 200-10,000 years after emplacement. The permeability is higher during the initial period, prior to consolidation. The reference case uses the values for the initial 200-year period, because shaft seal consolidation is enhanced at WIPP with the addition of 1 wt. % water (Hansen et al. 2012, Section 4.1.1), which might not be used in run-of-mine backfill.

Backfill is assigned a porosity of 0.113 (Fox 2008, Table 19) and a permeability of 10^{-18} m^2 (Fox 2008, Table 4). Probabilistic simulations sample on porosity using a uniform uncertain distribution over the range 0.01 to 0.20.

4.1.6 Shaft Seals

Shafts will be sealed to prevent migration of water and radionuclides. Seals may be similar to those proposed for WIPP, consisting of clay, asphalt, concrete, and crushed salt components (James and Stein 2002). Concrete, clay, and asphalt components are expected to provide an immediate barrier to fluid flow, while the crushed salt component is expected to provide a permanent barrier to flow after consolidation (DOE 2009, Section PA-2.1.3).

The reference case assumes shaft seal properties identical to those assumed for the crushed salt backfill (previous section).

4.2 Geosphere/Natural Barriers

Specific post-closure basis information related to the geosphere and natural barriers include:

- Characteristics of the natural barriers (e.g., location, geologic setting) (Section 4.2.1),
- Host rock characterization (Section 4.2.2),
- Disturbed rock zone (DRZ) characterization (Section 4.2.3), and
- Characterization of additional geologic units (Sections 4.2.4 through 4.2.7).

4.2.1 Natural Barrier Characteristics

Bedded salt formations, often hundreds of meters thick, form in nearshore and shallow-marine environments during cycles of marine transgression and regression. In addition to beds of very low permeability and low porosity halite (the target for waste isolation), they may contain beds rich in other evaporite minerals (anhydrite, polyhalite), and carbonate and clastic (shale, sandstone) interbeds (Perry et al. 2014, Section 4.2.1). The present concept for a mined repository in a bedded salt formation places the repository in a stratum of relatively pure halite (> 50%) at least 76 m thick. Depth to top of the formation is between 305 m and 1067 m below land surface (Sevougian et al. 2012, Section 3.2.3), sufficiently deep to isolate the salt formation from surface processes, and shallow enough to make mining a repository technically feasible. Regionally, the topographic slope is ≤ 1°, providing little driving force for deep fluid flow. The reference repository site occurs in a geologically stable sedimentary basin with low probabilities of seismicity and igneous activity. The bedded salt formation is expected to have a lateral extent of tens of thousands of square kilometers (Perry et al. 2014; Sevougian et al. 2012), more than sufficient for the establishment of a controlled area "no more than 5 kilometers in any direction from the outer boundary" of the repository as specified in 40 CFR 191.12 and 10 CFR 60.2 (Sevougian et al. 2012). The probability of human intrusion is reduced by siting the repository sufficient distance from known geologic resources (other than the salt itself) such as extensive fresh water aquifers, ore deposits, fossil fuels, or high geothermal heat flux (which offers the potential for geothermal development).

Large areas fitting the depth criteria occur in the Michigan and Appalachian Basins, the Permian Basin, and the Paradox Basin, as shown in Figure 4-2. Small areas of other basins fit the criteria as well. Salt formations in the Michigan, Appalachian, Permian, and Paradox Basins range in age from Silurian (444 to 419 Ma) to Permian (299 to 252 Ma) (Sevougian et al. 2012, Section 3.2.3.1). Measured heat flow in these locations is generally between 35 and 65 mW/m^2 (Blackwell et al. 2011), though it may be locally higher or lower. At repository depth, the host rock is saturated with brine (see Section 4.2.2.1). The driving force for regional flow at depth is assumed to be on the order of 0.001 m/m, as observed in deep sedimentary basins (e.g., Downey and Dinwiddie 1988).

The generic stratigraphic section which comprises the natural barrier for the purpose of PA simulations consists of beds of halite and anhydrite with overlying mudstone and siltstone, and a fractured dolomite aquifer (Figure 4-3), which is assumed to provide a potential pathway for radionuclide release. Properties of each material, including the undisturbed host rock (halite) and the disturbed rock zone (DRZ) created by mining, are described in the following sections.

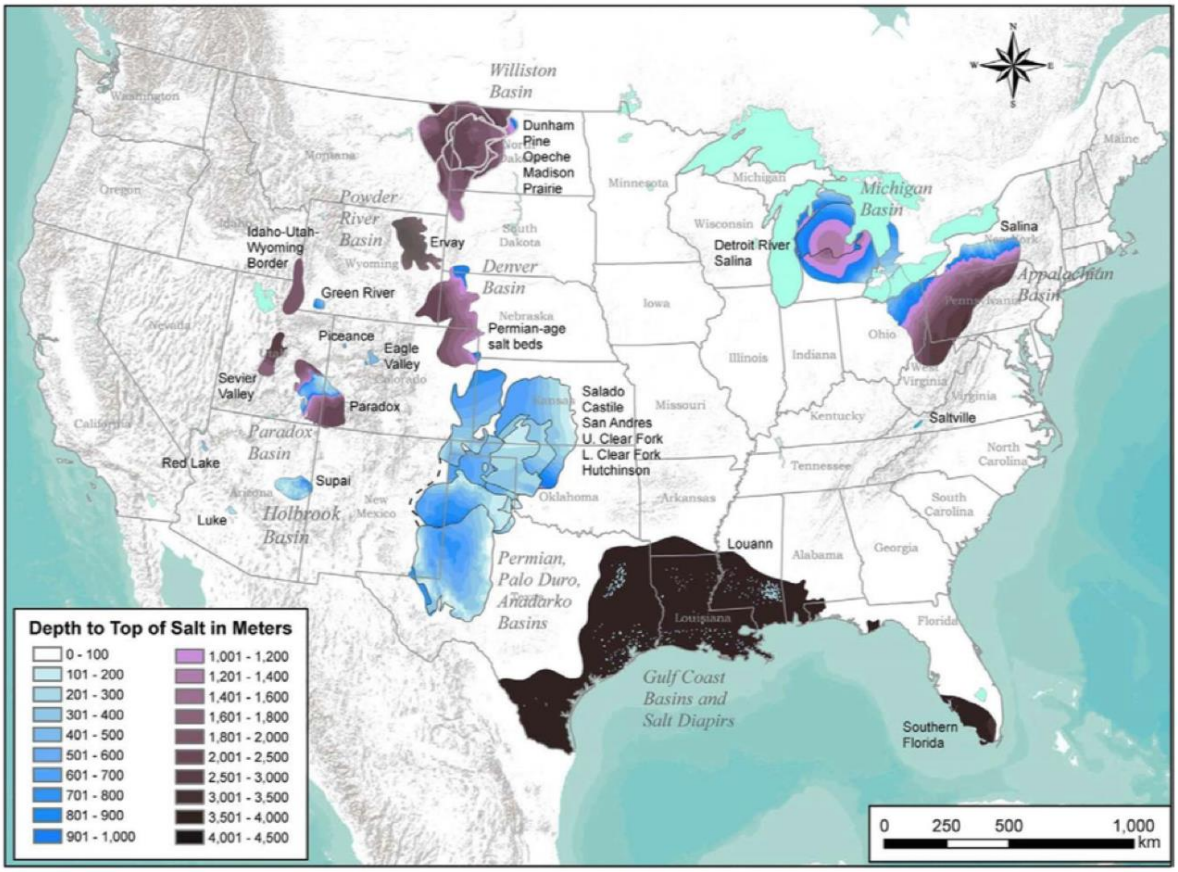

Figure 4-2. Distribution and depth to top of salt formations in major sedimentary basins of the US. Salt formations are labeled by name or by common reference and listed in stratigraphic order where more than one salt formation is present in a basin. [Figure from Perry et al. (2014).]

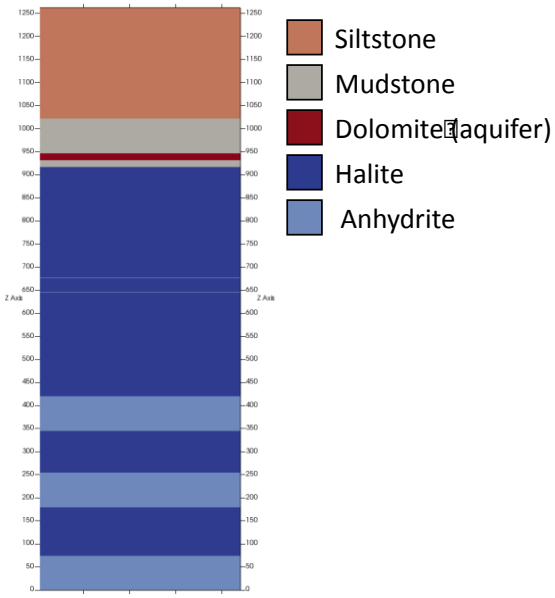

Figure 4-3. Generic stratigraphic column for salt reference case. The repository horizon is centered between the two thin beds of anhydrite at z = 661 m.

4.2.2 Halite Host Rock

The depth to the top of the halite is 345 m, and the thickness of relatively pure halite is 497 m (defining the base of the relatively pure halite as the top of the uppermost thick anhydrite bed). Within this thickness, two 1-m thick interbeds of anhydrite sandwich a 30-m thick repository horizon. Halite is represented using permeability and porosity drawn from the WIPP parameter database. The WIPP database gives a cumulative distribution for halite porosity with a minimum of 0.001, median of 0.01, and maximum of 0.0519 (Fox 2008; Freeze et al. 2013c; Sevougian et al. 2013; 2014; Mariner et al. 2015). The deterministic simulation uses the mean value of 0.0182. Probabilistic simulations simplify the cumulative distribution to uniform, and sample on halite porosity over the range 0.001 to 0.0519. Log halite permeability (m^2) is assumed to vary over a uniform distribution of –24 to –21 (Fox 2008; Freeze et al. 2013c; Sevougian et al. 2013; 2014; Mariner et al. 2015). Reference case simulations set the log of halite permeability equal to the mean of this range: –22.5 (permeability = 3.16×10^{-23} m^2).

4.2.2.1 Chemical Environment

Pore fluid chemistry will influence waste package degradation rate, waste form dissolution rate, and solubility and transport (diffusion and sorption) of dissolved radionuclides. Pore fluid chemistry is site-dependent, and may vary locally depending on composition and proximity of interbeds and impurities within the halite. Representative brine compositions from several salt formations are given in Table 4-2 (Sevougian et al. 2012, Table 3-2). Solubility is discussed in the following section. The reference case assumes no sorption in the halite and does not account for the effects of pore water composition on radionuclide diffusion rates. Waste package degradation and waste form dissolution are discussed in Section 4.3.2.5.

Table 4-2. Representative brine compositions for the salt reference case (Sevougian et al. 2012).

Description	Concentration (mg/l)							pH	SG
	Na^+	K^+	Mg^{2+}	Ca^{2+}	SO_4^{2-}	Cl^-	C		
1. ONWI Composite Permian Brine (Molecke 1983)	123000	39	134	1560	3197	191380	30	7.05	NR
2. WIPP Generic Brine A (Molecke 1983)	42000	30000	35000	600	35000	190000	700	6.5	NR
3. WIPP Generic Brine B (Molecke 1983)	115000	15	10	900	3500	175000	700	6.5	NR
4[a]. WIPP GWB Salado (DOE 2009, App. SOTERM)	81150	18260	24790	560	17000	207750	NR	NR	1.2
5[a]. WIPP ERDA-6 Castile (DOE 2009, App. SOTERM)	111960	3790	460	480	16330	170170	980	6.17	1.22
6. MCC Brine (Molecke 1983)	35400	25300	29600	NR	NR	164000	NR	6.5	NR
7. German Quinare Brine Q (Molecke 1983)	6500	29000	85000	NR	13000	270000	NR	NR	NR
8. Michigan Basin Devonian Brine (Wilson and Long 1993)	12400-103000	440-19300	3540-14600	7390-107000	0-1130	120000-251000	NR	3.5-6.2	1.136-1.295
9. Paradox Formation Brine-Moab Region (DOE 2007)	9800-25966	23400-41957	21000-47789	34000-65800	80-1800	29800-259106	NR	4.8-6.0	NR
10[b]. Paradox Basin Mississippian Formation (Garrett 2004; Mayhew and Heylmun 1966)	132000-168000	NR	324-9000	288-14400	2160-8800	183600-264000	NR	4.6-6.7	NR
11[b]. Paradox Basin Paradox Formation (Garrett 2004; Mayhew and Heylmun 1966)	26640-119880	25680-63000	5160-39480	6036-51240	306-5268	145080-260640	NR	4.9-6.2	NR

a. Brines 4 and 5 are now considered more representative of WIPP conditions in recent performance assessment calculations than Brines 2 and 3 (DOE 2009, App. SOTERM, Table SOTERM-2, http://www.wipp.energy.gov/library/CRA/2009_CRA/CRA/Appendix_SOTERM/Appendix_SOTERM.htm .

b. Converted from ppm assuming an average brine density of 1.2 g/cc.

4.2.2.2 Solubility

PA simulations apply element solubility limits calculated for a concentrated, reducing brine (Clayton et al. 2011; Wang and Lee 2010) to the entire model domain. The original authors (Wang and Lee 2010) described solubility limits in terms of triangular distributions (Table 4-3). The current iteration of the reference case uses the mode of each of these distributions.

Assuming that no fractionation of isotopes occurs between the liquid and solid phases, the solubility limit of a given isotope (e.g., ^{238}Pu, ^{239}Pu, ^{240}Pu, or ^{242}Pu) in the transport domain of a cell can be calculated by multiplying the element solubility limit by the isotope's element mole fraction in the transport domain (e.g., $^{238}Pu/Pu_{TOTAL}$) (Mariner et al. 2016, Section 3.2.4).

Table 4-3. Element solubility calculated at T = 25°C in concentrated brine (Wang and Lee 2010 as cited in Clayton et al. 2011).

Element	Distribution Type	Dissolved Concentration (mol kg^{-1})		
		Min	Mode	Max
Am	Triangular	1.85×10^{-7}	5.85×10^{-7}	1.85×10^{-6}
Np	Triangular	4.79×10^{-10}	1.51×10^{-9}	4.79×10^{-9}
Pu	Triangular	1.40×10^{-6}	4.62×10^{-6}	1.53×10^{-5}
Sn	Triangular	9.87×10^{-9}	2.66×10^{-8}	7.15×10^{-8}
Tc	Log-triangular	4.56×10^{-10}	1.33×10^{-8}	3.91×10^{-7}
Th	Triangular	2.00×10^{-3}	4.00×10^{-3}	7.97×10^{-3}
U	Triangular	4.89×10^{-8}	1.12×10^{-7}	2.57×10^{-7}
Cs, I	N/A	Unlimited[a]		

[a] Assumed by Clayton et al. (2011).

4.2.3 Disturbed Rock Zone (DRZ)

The DRZ is defined as the portion of the host rock adjacent to the engineered barrier system that experiences durable (but not necessarily permanent) changes due to the presence of the repository (Freeze et al. 2013b). The DRZ is expected to have elevated permeability and porosity with respect to the properties of the host rock matrix due to the changes in stress induced by mining. Within the repository, the lateral extent of the DRZ is assumed to be equal to half the width of a room (or hall). Vertically, the DRZ extends to the thin (1-m-thick) anhydrite interbeds above and below the repository (a total thickness of 30 m). PA simulations include a 5-m-thick DRZ surrounding each 5-m-wide shaft. Within the halite, DRZ permeability and porosity are based on values in the WIPP parameter database: 0.0129 for porosity and 1.12×10^{-16} m^2 for permeability, which is the mean of a log uniform distribution with a range of $10^{-19.4}$ to $10^{-12.5}$ m^2 (Fox 2008; Freeze et al. 2013c; Sevougian et al. 2013; 2014; Mariner et al. 2015). The shaft DRZ is continuous from the repository to the top of the model. Where it crosses overlying units, its permeability is set one order of magnitude higher than that of the adjacent unit. Probabilistic simulations sample on DRZ porosity within the halite using a uniform distribution between 0.001 and 0.01.

4.2.4 Anhydrite

Anhydrite beds and interbeds are more permeable than the surrounding halite. Near the repository, they may become fractured as a result of the excavation, and therefore serve as potential pathways for radionuclide transport. The reference case assumes 1-m-thick anhydrite interbeds located immediately above and below the repository DRZ. Thicker anhydrite beds are located at depth. On the basis of parameters used to characterize WIPP, anhydrite porosity is assumed to be 0.011. Log permeability (m^2) in the deterministic simulation is assumed to be −18.9 (permeability = 1.26×10^{-19} m^2), which is the mean of a Student-t distribution with a range of −21.0 to −17.1 (Fox 2008; Freeze et al. 2013c; Sevougian et al. 2013; 2014; Mariner et al. 2015). Probabilistic simulations sample on anhydrite permeability using a log uniform distribution over the range 10^{-21} to 10^{-17} m^2.

The reference case models radionuclide sorption in anhydrite strata using linear distribution coefficients (K_ds) compiled in Clayton et al. (2011) (Table 4-4). Probabilistic simulations sample on neptunium K_ds using a log uniform distribution over the range 1 to 10 mL/g.

Table 4-4. Anhydrite K_ds (compiled in Clayton et al. 2011)

Element	Distribution	Kd (mL/g)	
		Min	Max
Am	uniform	25	100
Cm	log uniform	5	500
Cs	uniform	1	20
I	constant	0	0
Np	uniform	1	10
Pu	uniform	70	100
Tc	uniform	0	2
Th	uniform	100	1000
U	uniform	0.2	1

4.2.5 Mudstone

A 105-m-thick unit of mudstone interrupted by a 15-m-thick dolomite aquifer overlies the halite. A lithostratigraphic unit overlying a thick halite formation might typically be composed of a large fraction of anhydrite—as at the WIPP site, where the Rustler Formation comprised of a basal mudstone and thick anhydrite beds interrupted by carbonate aquifers overlies the Salado halite (DOE 2014b). The reference case assigns a porosity of 0.20 and a permeability of 10^{-17} m^2 to the mudstone. Mudstone sorption coefficients are assumed to be the same as those of the anhydrite.

4.2.6 Fractured Dolomite Aquifer

A 15-m-thick aquifer, modeled as fractured dolomite, is separated from the halite by a 15-m thickness of mudstone. Aquifer properties are based on those of the Culebra dolomite, which occupies a similar stratigraphic position above the Salado halite at the WIPP site (DOE 2014b). In deterministic simulations, aquifer porosity and permeability are derived from those of the Culebra (0.15 and 10^{-13} m^2, respectively; Fox 2008; Freeze et al. 2013c; Sevougian et al. 2013; 2014; Mariner et al. 2015). In probabilistic simulations, aquifer permeability is sampled (using a log uniform distribution) over the upper end of likely values for dolomite formations (log permeability (m^2) from −14.0 to −12.0; Freeze and Cherry 1979; Mariner et al. 2015).

The reference case models sorption in the aquifer using radionuclide K_ds compiled in Clayton et al. (2011) for a carbonate aquifer (Table 4-5), with the exception of iodine, which is modeled as non-sorbing.

Table 4-5. Carbonate K_ds compiled in Clayton et al. (2011).

Element	Distribution	Kd (mL/g)		
		Min	Max	Mode
Am	uniform	20	400	
Cm	log uniform	100	1.00E+05	
Cs	triangular	40	3000	500
I	uniform	0.01	100	
Np	log uniform	1	200	
Pu	log uniform	20	1.00E+04	
Tc	triangular	0	100	50
Th	log uniform	7.00E+02	1.00E+04	
U	uniform	0.03	20	

4.2.7 Siltstone

A 240-m-thick siltstone lies at the top of the model domain. The reference case assumes a porosity of 0.20 and a permeability of 10^{-15} m^2. Siltstone sorption coefficients are assumed to be the same as those of the dolomite aquifer.

4.3 Post-Closure Performance Assessment

4.3.1 Conceptual Model

The conceptual framework for this preliminary generic post-closure PA focuses on the components of the engineered barrier (Section 4.1) and the natural barrier (Section 4.2) in the undisturbed scenario. Key characteristics of and processes occurring in each of the components of the engineered and natural barriers are summarized in Table 4-6. Because the PA does not consider the biosphere, the performance metric is maximum radionuclide concentration rather than dose. Concentrations are monitored at three points within the aquifer, including at a location 5 km downgradient of the repository.

Table 4-6. Conceptual representation of the engineered and natural barriers in PA.

Region	Component	Key characteristics	Key processes included in PA
Engineered Barrier	HLW (source term)	Glass waste form	Radionuclide decay, waste form dissolution
	DSNF (source term)	Metallic fuel waste form	Radionuclide decay, instantaneous dissolution
	Waste Package (control on source terms)	Carbon steel	Degradation and breach
	Waste Package (region of domain)	Package plus contents	Radionuclide advection, diffusion, and decay
	Crushed Salt Backfill	Enhance permeability and porosity compared to intact halite	Radionuclide advection, diffusion, decay
Natural Barrier	Halite	Low permeability and porosity	Radionuclide advection, diffusion, decay
	DRZ	Enhanced permeability and porosity compared to intact halite	Radionuclide advection, diffusion, decay
	Anhydrite	Higher permeability than halite, potential pathway for release	Radionuclide advection, diffusion, sorption, decay
	Mudstone	Moderately low permeability	Radionuclide advection, diffusion, sorption, decay
	Aquifer	Fractured dolomite	Radionuclide advection, diffusion, sorption, decay
	Siltstone	Moderately high permeability	Radionuclide advection, diffusion, sorption, decay

Simulations assume (1) a mined repository at 600 m depth in relatively pure halite; (2) a 15-m-thick aquifer overlying the halite; (3) a head gradient of –0.0013 m/m from west to east (as in previous salt, clay, and crystalline reference cases; Mariner et al. 2015; Mariner et al. 2016; Section 3.3.1 this report); (4) a regional heat flux of 60 mW/m^2 and a mean annual surface temperature of 10 °C; and (5) a saturated domain.

4.3.2 Numerical Implementation

PA simulations, comprising one deterministic simulations and a suite of 50 probabilistic simulations for uncertainty and sensitivity analyses, were implemented within the Generic Disposal System Analysis framework (Mariner et al. 2015; Mariner et al. 2016), which is briefly described in Section 3.3.2 of this report.

4.3.2.1 Model Domain and Discretization

The model domain (Figure 4-4) is 7440 m in length (x), 1005 m in width (y), and 1262 m in height (z). Most of the domain is discretized into cells 15 m on a side. The repository and adjacent cells are discretized into cells 1.67 m (5/3 m) on a side. Within the repository, waste emplacement regions are discretized into cells 0.56 m (5/9 m) on a side. A narrow transitional zone of cells 5 m on a side exists between the repository cells and the remainder of the domain. The domain contains 5,811,350 cells; of these, approximately half are the smaller cells in and around the repository.

The model domain is a half-symmetry domain, in which half of a repository (8 panels and 2 shafts) lies at the south edge ($y = 0$) of the domain adjacent to a reflection boundary (no fluid or heat flux). The presence of the reflection boundary means that simulations are effectively of a whole repository (16 panels and 4 shafts) in a domain twice as wide (in y) as explicitly gridded. Figure 4-5 shows an x-y slice through the repository at the level of the waste packages; the base of the figure ($y = 0$) is the symmetry plane.

From west to east (left to right), the first 7 panels contain Hanford HLW (5540 waste packages) followed by Savannah River HLW (3781 waste packages). The last panel contains DSNF emplaced in the order (from left (W) to right (E) and front (S) to back (N)): 582 < 50 W waste packages, 117 50-100 W waste packages, 470 100-200 W waste packages, six 200-300 W waste packages, 21 300-500 W waste packages, 44 500-1000 W waste packages, and two 1000-1500 W waste packages. When reflected, the entire inventory listed in Table 3-2 is included.

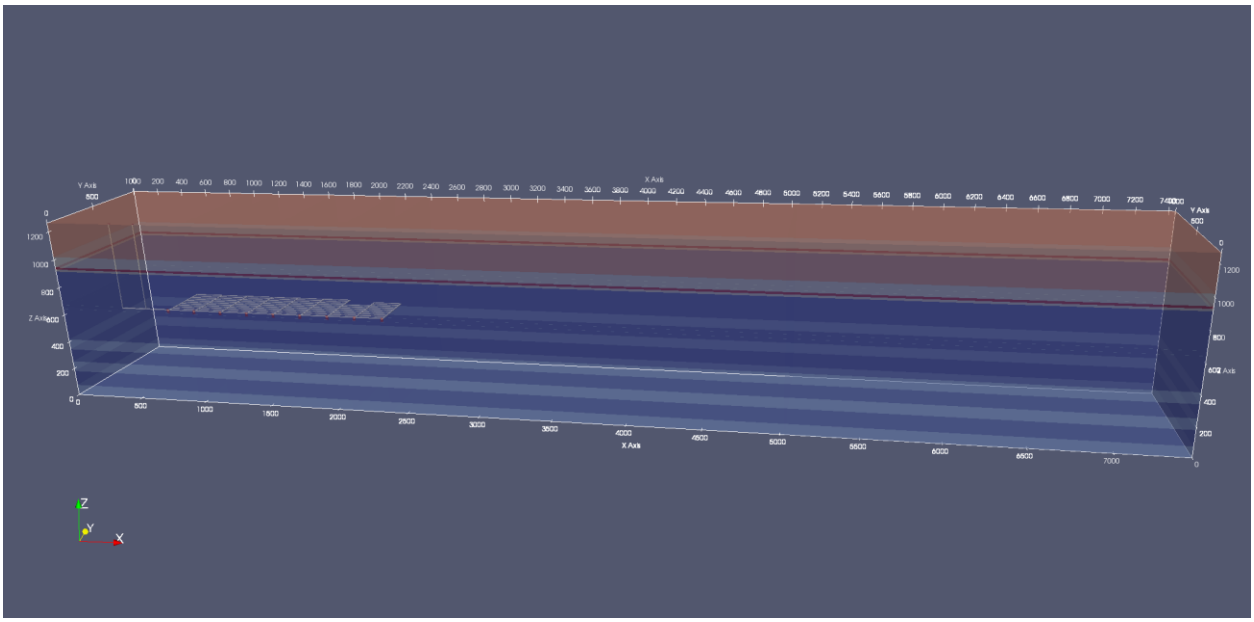

Figure 4-4. Transparent view of the model domain colored by material (as in Figure 4-3). The 3-dimensional structure inside the half-symmetry domain is the repository, including 8 disposal panels and 2 shafts.

a.

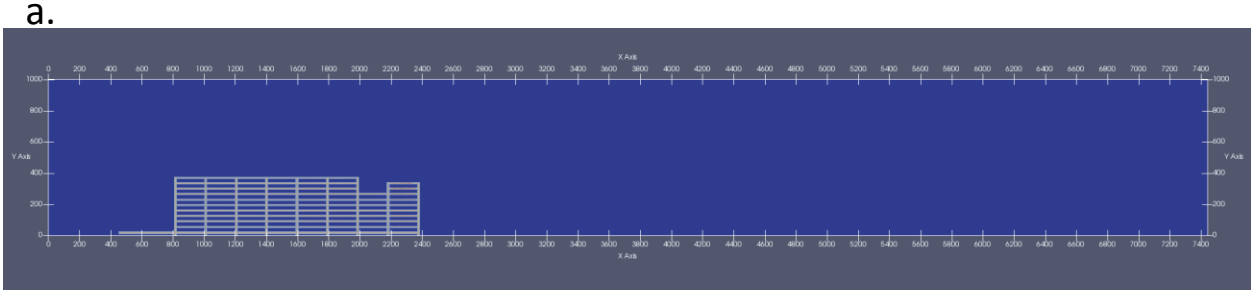

b.

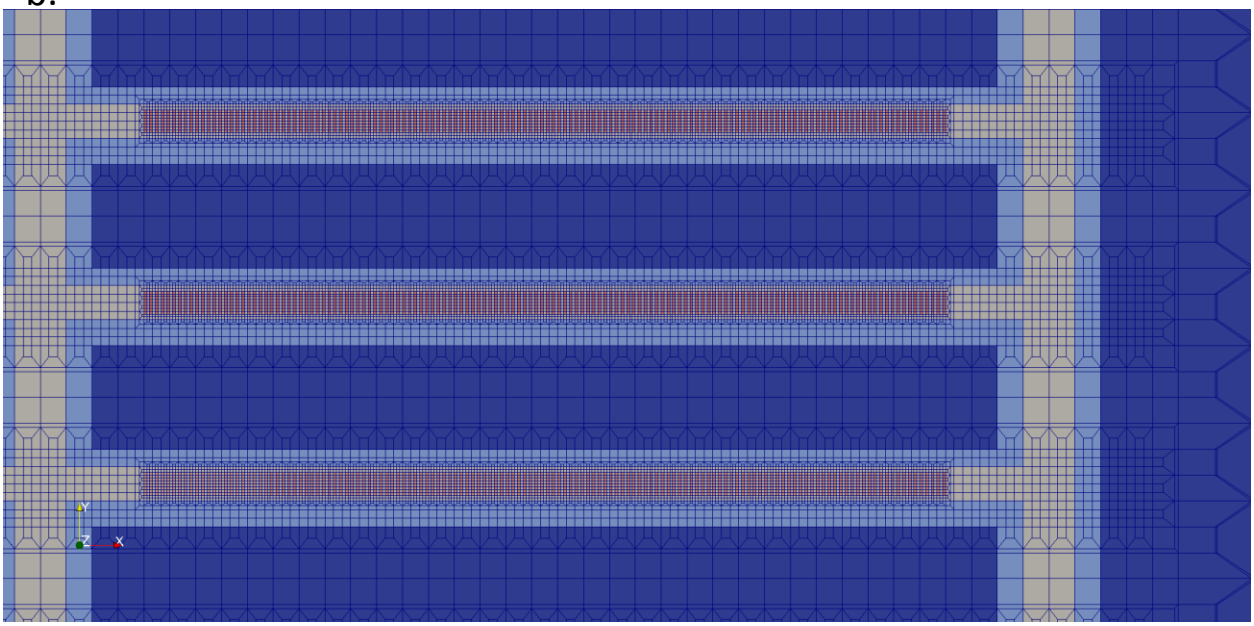

Figure 4-5. a.) *X-Y* slice of model domain (a reflection boundary lies at $y = 0$), and b.) close-up of three DSNF disposal rooms showing details of the discretization. Smallest cells are 5/9 m on a side; largest (at far right) transition to 15 m on a side. [Dark blue: undisturbed halite; light blue: DRZ; gray: backfill; red: waste packages.]

4.3.2.2 Initial Conditions

Initial conditions specified are pressure, temperature, and radionuclide concentrations. Initial pressures and temperatures throughout the model domain are calculated by applying a liquid flux of 0 m/s and an energy flux of 60 mW/m^2 to the base of the domain and holding temperature (10°C) and pressure (approximately atmospheric) constant at the top of the domain, and allowing the simulation to run to 10^6 years. Pressure at the top of the domain decreases from west (left) to east (right) with a head gradient of –0.0013 (m/m). This technique results in initial conditions that represent a geothermal temperature gradient and hydrostatic pressure gradient in the vertical direction, and a horizontal pressure gradient that drives flow from west to east. Simulations include ^{129}I and ^{237}Np as well as ^{241}Am (the parent of ^{237}Np) and ^{243}Am (which contributes to the total elemental solubility of Am). Initial concentrations of all radionuclides in all cells are 10^{-20} mol/L.

4.3.2.3 Boundary Conditions

Boundary conditions must be set for the six faces of the model domain. At all faces except the south face (y = 0), initial pressures and temperatures are held constant. At the south face, pressure and temperature gradients are set to zero, which prevents fluid and heat fluxes across this boundary. Radionuclide concentrations are held such that any fluid entering the model domain contains 10^{-20} mol/L of each radionuclide, while fluid exiting the model domain is allowed to carry with it ambient concentrations. Diffusive flux across boundaries is disallowed by specifying a zero concentration gradient.

4.3.2.4 Waste Package Heat Sources

Each waste package is modeled as a transient heat source. The energy (watts per waste package) entering the model domain is updated periodically according to values in a lookup table. The initial value for each waste type is that in the year 2038 (plotted in Figure 4-1). Between times specified in the lookup table, the energy input is linearly interpolated.

4.3.2.5 Waste Package Breach and Radionuclide Source Term

The waste package degradation model implemented in the salt reference case is essentially the same as that implemented in the crystalline reference case (Section 3.3.2.5), except for the choice of parameters. In the salt reference case, the canister material constant is set to zero, eliminating the dependence of waste package degradation rate on temperature (see Eq. 3-4). Deterministic simulations assign a base canister degradation rate for each waste package by sampling on a truncated log normal distribution with a mean of $10^{-3.4}$/yr, a standard deviation of 0.5 (log units), and an upper truncation of −3.0 (log units). Probabilistic simulations sample on the mean degradation rate using a log triangular distribution over the range $10^{-4.7}$/yr to $10^{-3.4}$/yr, with a mode of $10^{-3.6}$/yr. These values are derived from rates of carbon steel degradation at 90ºC measured in a variety of brine compositions and saturations (BSC 2004), assuming a waste package wall thickness of 7.5 cm (Sevougian et al. 2012).

As in the crystalline reference case (Section 3.3.2.5), simulations assume that exposure to water occurs (dissolution begins) at the time of waste package breach. DSNF waste forms are assumed to dissolve instantaneously: following the breach, the radionuclide inventory (updated to the current time) is released into the DSNF waste package region. Rate-controlled congruent dissolution of the HLW waste forms is modeled as in the crystalline case. In the deterministic simulations all HLW waste forms are assigned the same exposure factor, f_e = 4. Probabilistic simulations sample on f_e using a triangular distribution with a minimum, a mode of 4, and a maximum of 17 (Strachan 2004).

4.3.2.6 Material Properties

Material properties are discussed in Sections 4.1 and 4.2; values used in PA simulations are summarized in Table 4-7 (deterministic parameter values) and Table 4-8 (sampled parameter ranges). Additional information regarding the calculation of tortuosity and effective diffusion coefficient is given in Appendix B. Longitudinal and transverse dispersivities are set to zero in the PA simulations—see Appendix B.

Table 4-7. Parameter values used in deterministic simulation for the bedded salt DWR reference case (modified from Mariner et al. 2015).

Model Region	Permeability (m^2)	*Porosity,* ϕ	*Tortuosity,*[a] τ	Effective Diffusion Coefficient[b], D_e (m^2/s)	Saturated Thermal Conductivity[c] (W/m/K)	Heat Capacity[d] (J/kg/K)	Grain Density[e] (kg/m^3)
Waste Package	1×10^{-16}	0.30	1	6.9×10^{-10}	16.7	466	5000
Backfill	1×10^{-18}	0.113	0.48[1]	1.24×10^{-10}	2.5	927	2170
DRZ	1.12×10^{-16}	0.0129	0.23[1]	6.82×10^{-12}	4.9	927	2170
Halite	3.16×10^{-3}	0.0182	0.01	4.19×10^{-13}	4.9	927	2170
Anhydrite	1.26×10^{-19}	0.011	0.22[1]	5.57×10^{-12}	4.9	927	2960
Mudstone	1×10^{-17}	0.20	0.20	9.2×10^{-11}	1.7	830	2700
Dolomite	1×10^{-13}	0.15	0.15	5.18×10^{-11}	4.0	830	2820
Siltstone	1×10^{-15}	0.20	0.20	9.2×10^{-11}	2.0	830	2700

[a] $\tau = \phi^{1/3}$ as in Mariner et al. (2015)—see Appendix B, Eq. B-20 with $s = 1$.
[b] Effective diffusion coefficient, $D_e = D_w \phi \tau s$, where the free water diffusion coefficient (D_w) = 2.3×10^{-9} m^2/s (Cook and Herczeg 2000).
[c] Hardin et al. 2012, Tables D-1, D-2, and D-5 (based on Clayton and Gable 2009, Fluor 1985, and Fluor 1986).
[d] Hardin et al. 2012, Table D-3 (based on Clayton and Gable 2009, Fluor 1985, and Fluor 1986).
[e] Crain's Petrophysical Handbook and PetroWiki (online).

Table 4-8. Sampled parameters and their distributions for the bedded salt DWR reference case.

Parameter	Range	Units	Distribution
Glass exposure factor (f_e)	4 – 17 (mode = 4)		triangular
Mean Waste Package Degradation Rate	$10^{-4.7} – 10^{-3.4}$ (mode = $10^{-3.6}$)	yr^{-1}	log triangular
Waste Package τ	0.01 - 1.0		log uniform
Backfill ϕ	0.01 - 0.2		uniform
DRZ ϕ	0.001 - 0.1		uniform
Halite ϕ	0.001 – 0.0519		uniform
Np K_d anhydrite	0.001 – 0.01	m^3kg^{-1}	log uniform
Np K_d dolomite	0.001 – 0.2	m^3kg^{-1}	log uniform

4.4 Simulation Results

Deterministic and probabilistic results are discussed in terms of concentrations of the long-lived radionuclides ^{129}I ($t_{1/2} = 1.57\times10^{7}$ yr) and ^{237}Np ($t_{1/2} = 2.14\times10^{6}$ yr). ^{129}I is assumed to have unlimited solubility and to be non-sorbing; it thus behaves nearly conservatively. ^{237}Np is solubility-limited and sorbing. Temperature fields, flux vectors, and waste package breach times for the deterministic simulation are also presented.

4.4.1 Deterministic Results

4.4.1.1 Temperature and Fluid Flow Fields

Temperature and fluid flow fields at various times for the deterministic simulation are shown in Figure 4-6 through Figure 4-7. Peak repository temperatures occur between 5 and 20 years. At ten years, temperature increases associated with the Savannah River HLW and the warmer DSNF bins are apparent, and temperature perturbations are driving flow in some parts of the repository in the direction opposite to the regional flow field (Figure 4-7). The repository remains warmer than background at 100 years (Figure 4-8), and fluid flow contrary to the regional gradient is still occurring. By 1,000 years repository temperatures have returned to near background, and fluid flux through the repository is in the direction of the regional flow field (Figure 4-9).

4.4.1.2 Radionuclide Releases

Radionuclide releases depend not only on fluid fluxes, but also on timing of waste package breach. Sightly more than 10% of the waste packages have breached 1000 years into the simulation, and all waste packages have breached by 25,000 years, as shown in Figure 4-10. Waste packages breach after the temperature in most of the repository has returned to near ambient temperature (Figure 4-11).

The spatial distribution of the nearly conservative ^{129}I at times between 2000 years (shortly after waste packages begin to breach) to 10^{6} years is shown in Figure 4-12 and Figure 4-13. The spatial distribution of ^{237}Np, which both precipitates and sorbs, is shown in Figure 4-14. The 10^{-12} mol/L contours of ^{129}I and ^{237}Np do not reach the overlying aquifer in the course of the simulation.

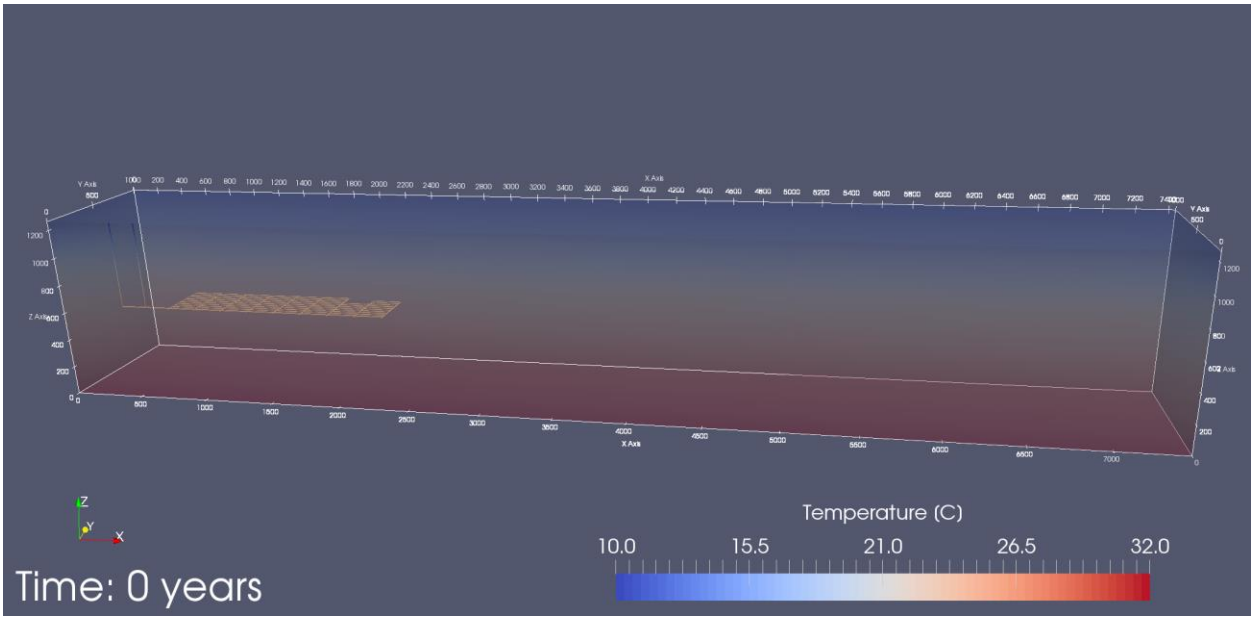

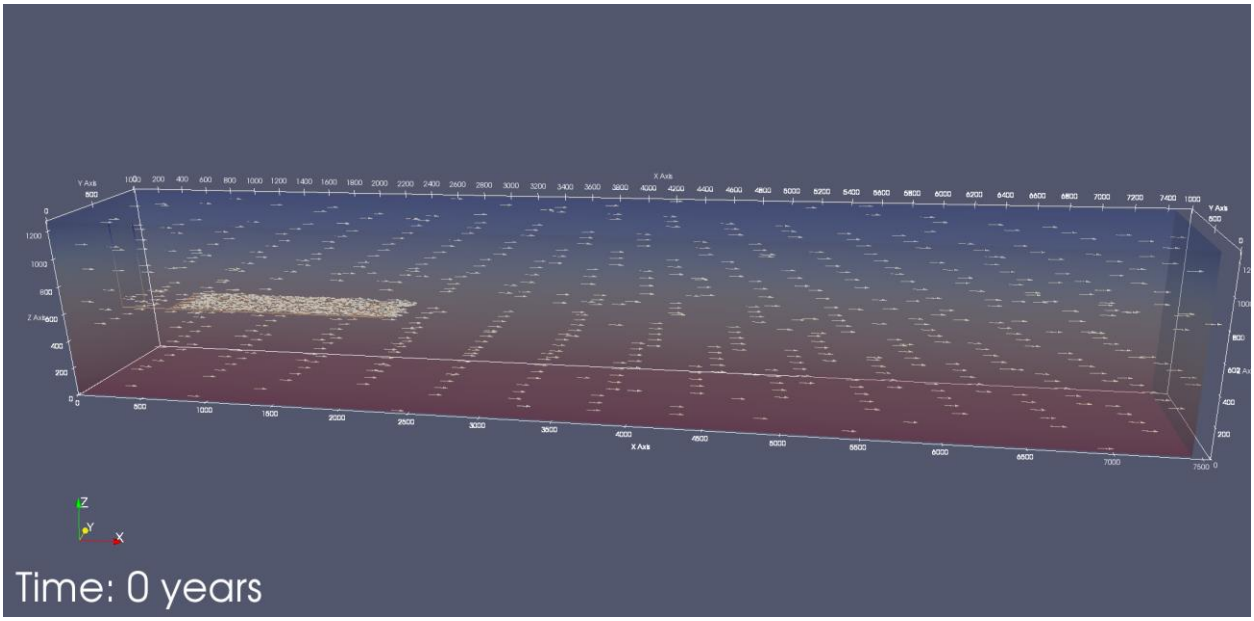

Figure 4-6. Background geothermal temperature gradient at 0 years (top). The repository is plotted as a 3-D object inside the transparent model domain. Both repository and domain are colored by temperature. Notice that the maximum temperature on the color scale of 32°C in this figure is less than the maximum of 90°C in the figures that follow. Fluid flux at 0 years (bottom); arrows indicate direction of flow.

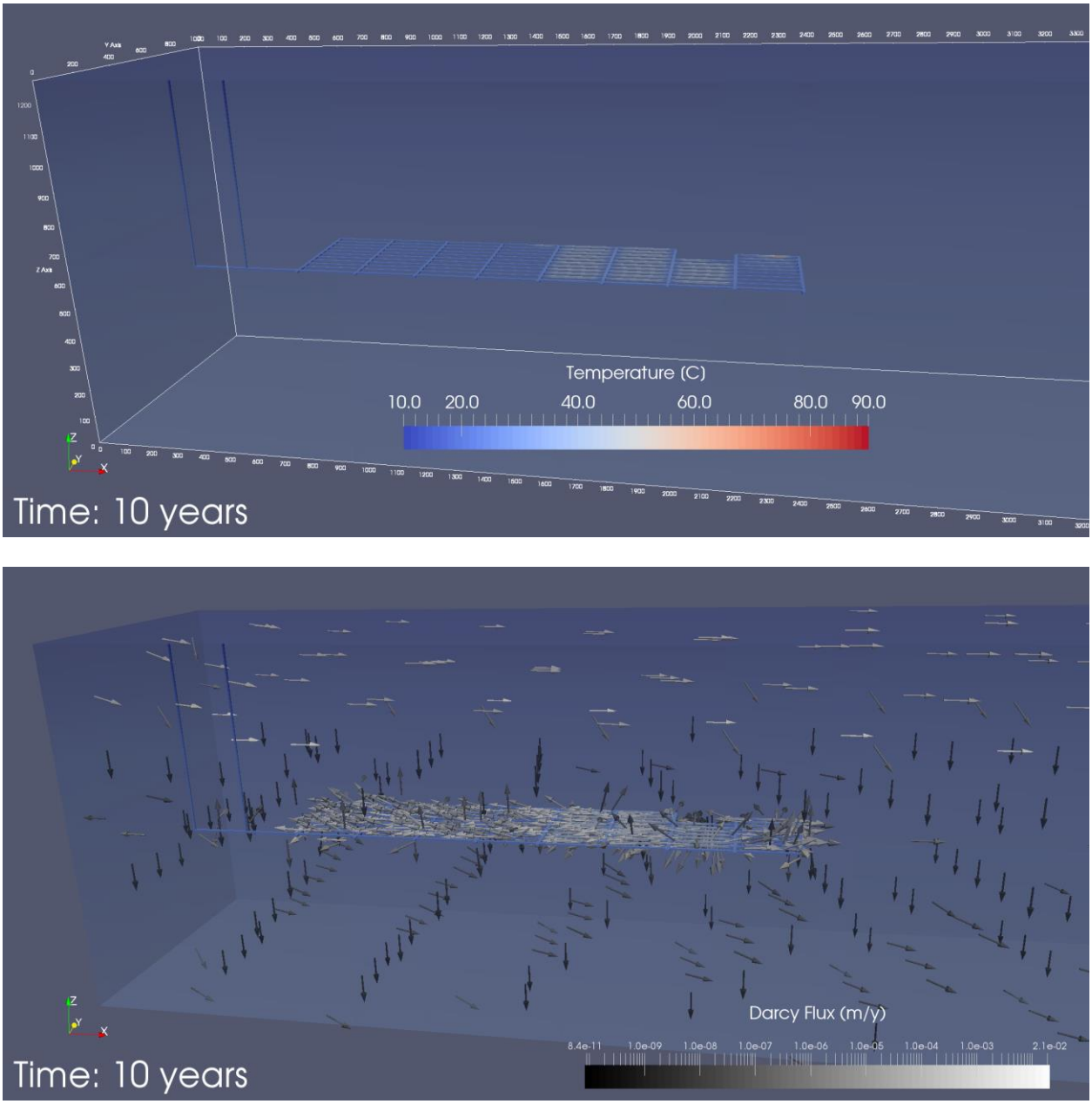

Figure 4-7. Repository temperature field at 10 years in the deterministic simulation. Plotted and colored as in Figure 4-6 except for difference in scale. Flux vectors at 10 years (bottom). Vectors are plotted for a subset of cells in the domain and colored by flux magnitude.

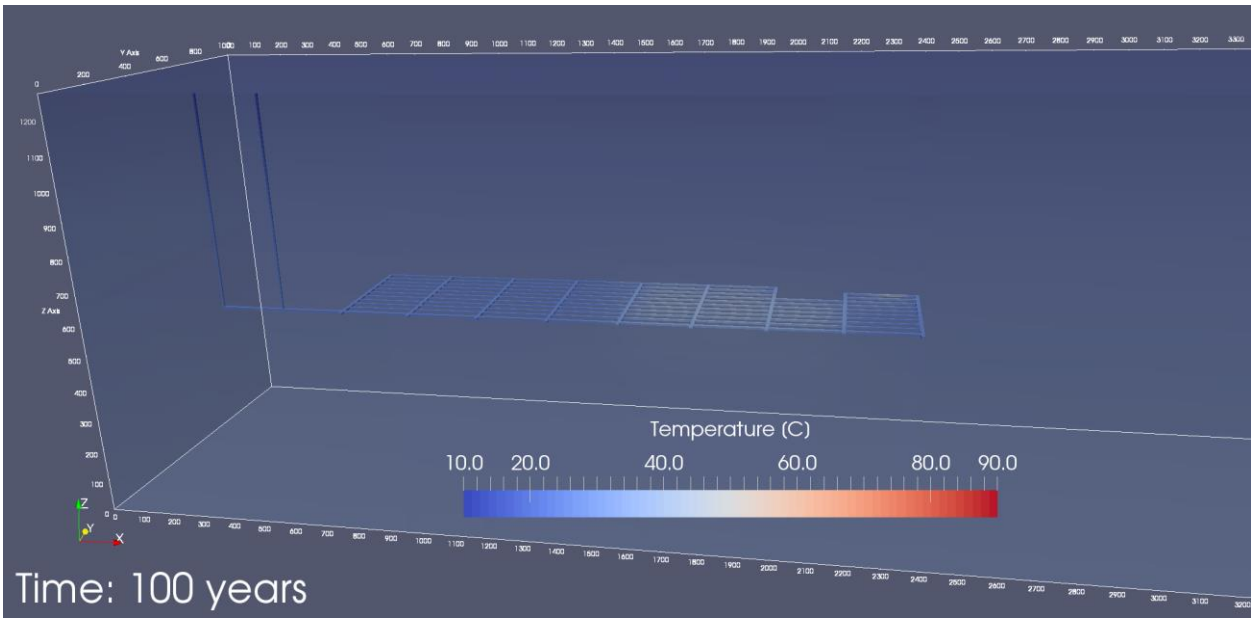

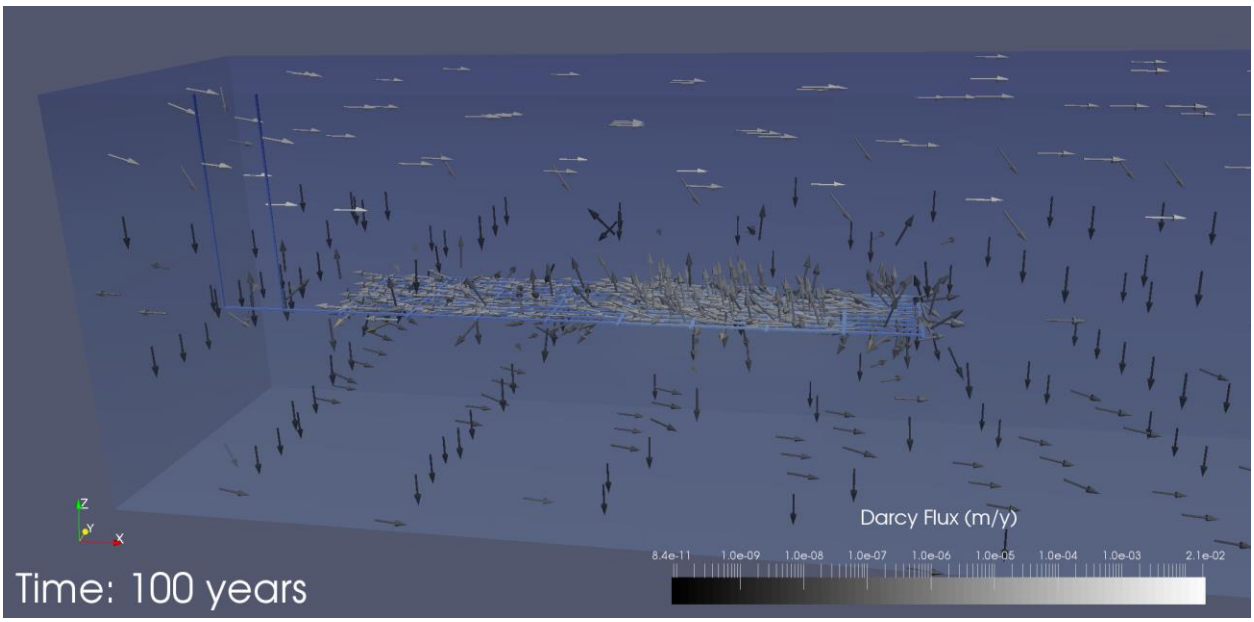

Figure 4-8. Repository temperature field (top) and Darcy flux vectors (bottom) at 100 years in the deterministic simulation. Plotted and colored as in Figure 4-7.

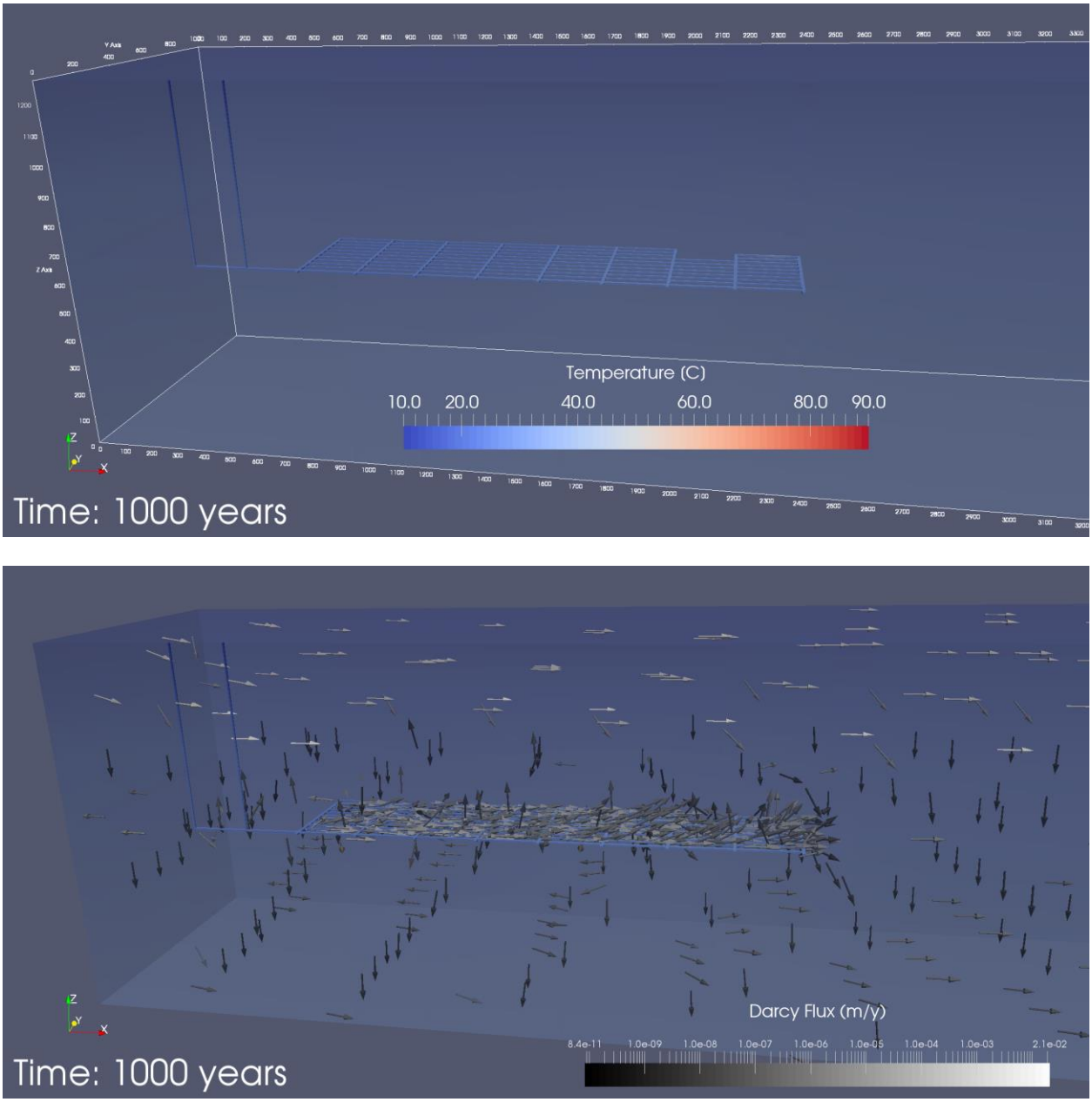

Figure 4-9. Repository temperature field (top) and Darcy flux vectors (bottom) at 1000 years in the deterministic simulation. Plotted and colored as in Figure 4-8.

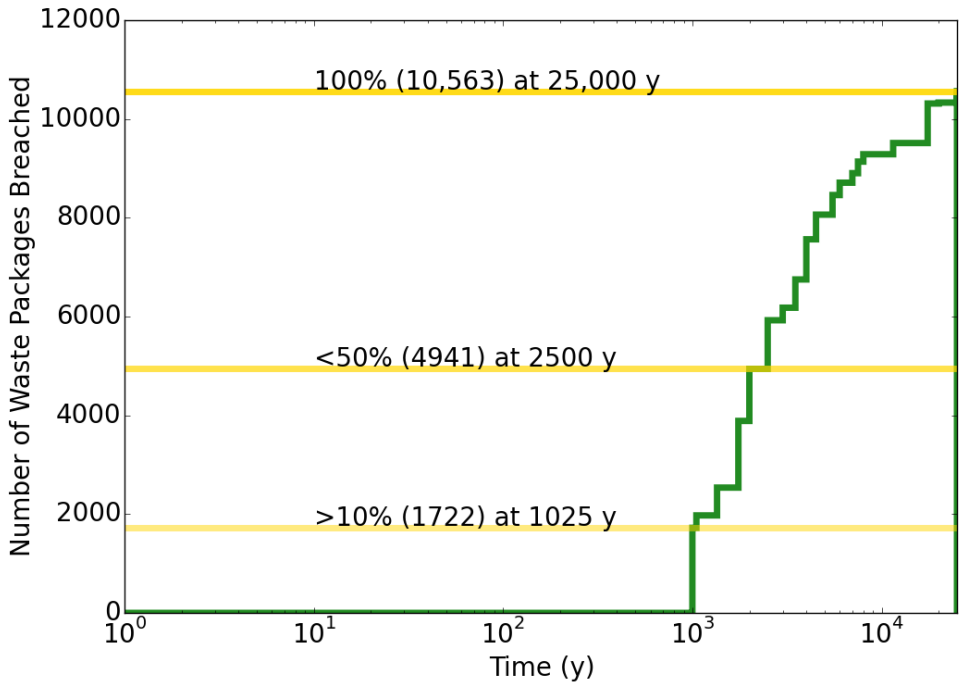

Figure 4-10. Cumulative number of waste packages breached versus time in the generic bedded salt repository simulation.

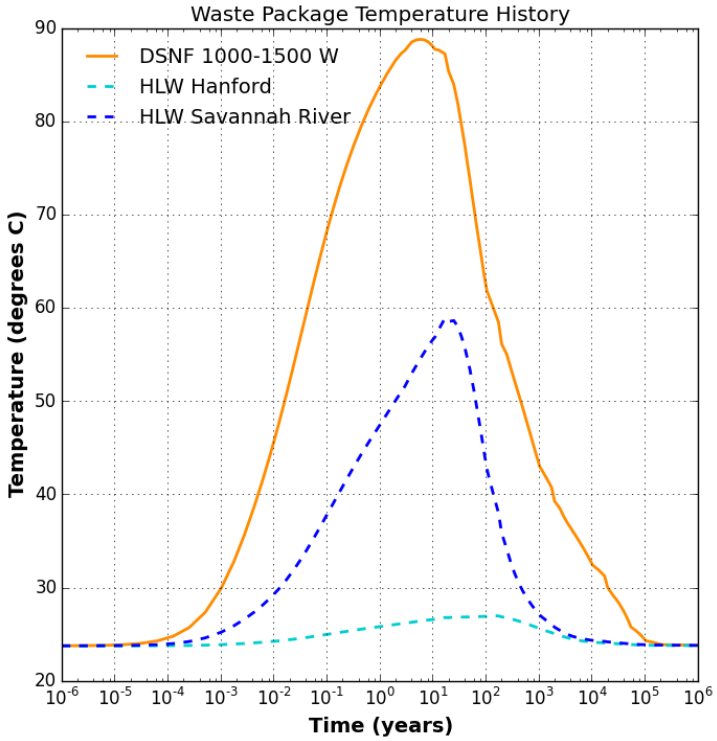

Figure 4-11. Waste package temperature histories for representative Hanford HLW (light blue), Savannah River HLW (dark blue), and the hottest DSNF bin (orange) in the generic bedded salt repository simulation.

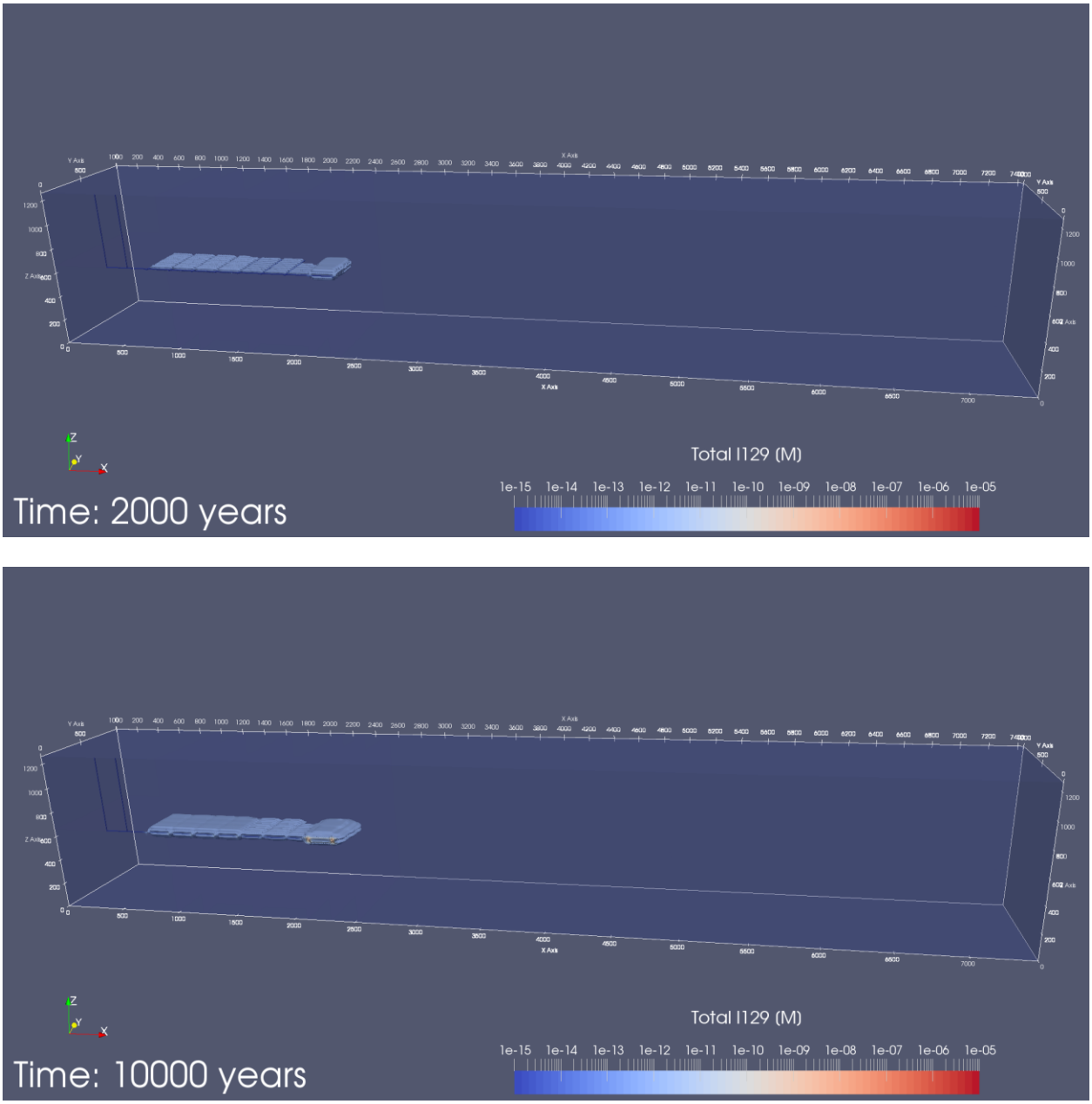

Figure 4-12. ^{129}I concentration at 2000 years (top) and 10,000 years (bottom) in the deterministic simulation.

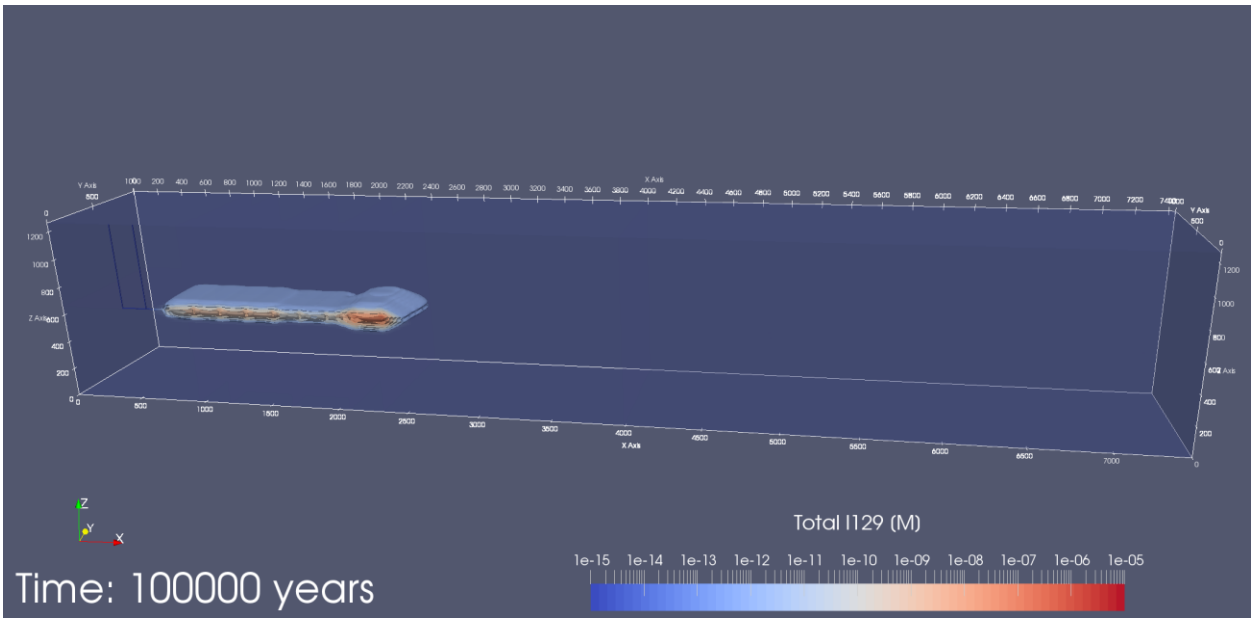

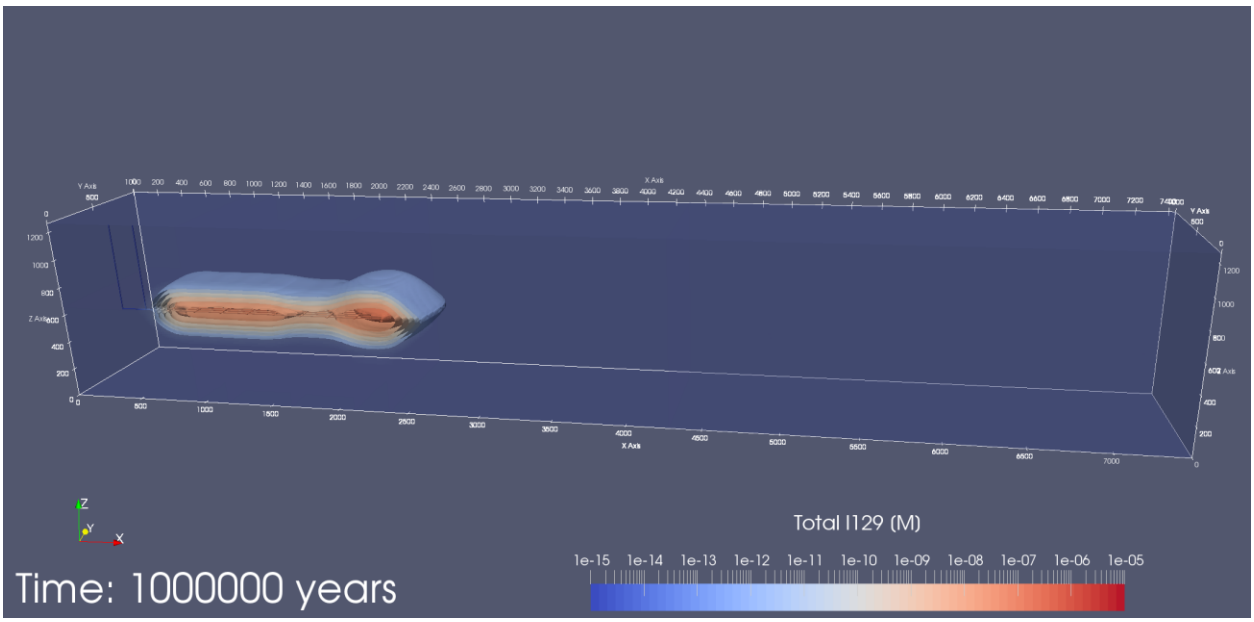

Figure 4-13. ^{129}I concentration at 100,000 years (top) and 10^6 years (bottom) in the deterministic simulation. [Note: Concentration contours in the far-field ^{129}I plume are not displayed below 10^{-12} mol/L in order to show more definition to the plume movement.]

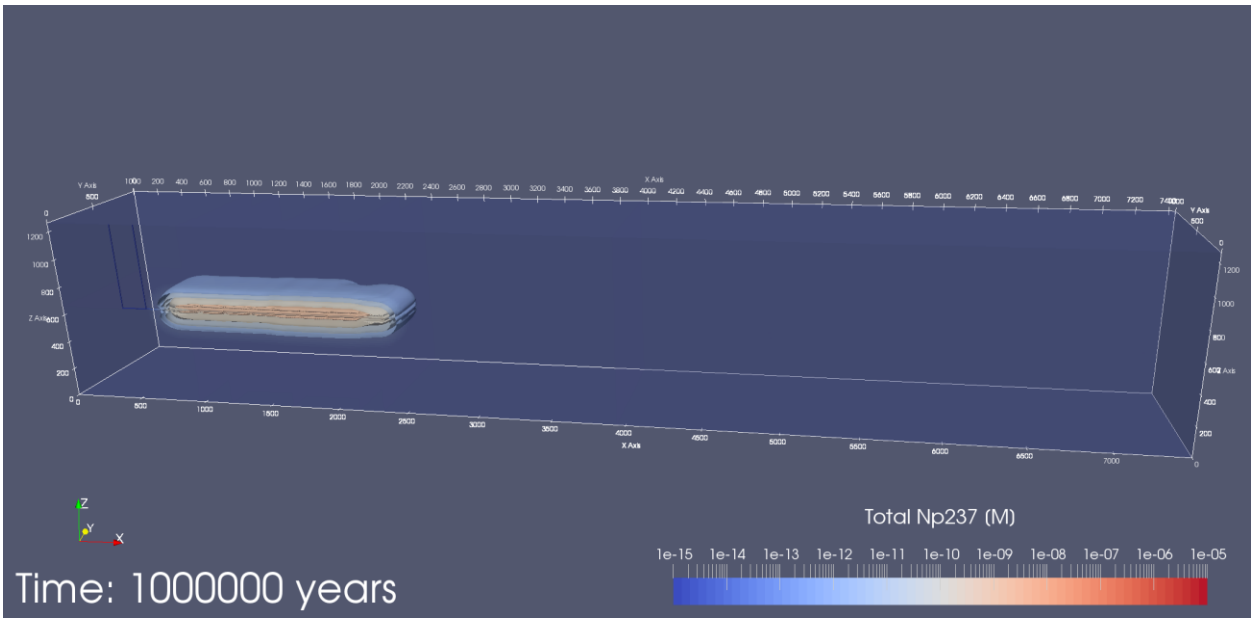

Figure 4-14. ^{137}Np concentration at 10^6 years in the deterministic simulation. Concentration is contoured and colored on the same scale as in previous figures of ^{129}I.

4.4.2 Probabilistic Simulations

A suite of 50 probabilistic simulations was run using the parameter distributions listed in Table 4-7. Breakthrough curves for ^{129}I at three observation points in the aquifer ("aqu1", "aqu2", and "aqu3") (Figure 4-15) are compared in Figure 4-16. Concentration in some simulations barely exceeds 10^{-16} mol/L at "aqu1" and does not exceed 10^{-16} mol/L at either "aqu2" or "aqu3" in any simulations. ^{237}Np concentration never increases above background concentration at any of the aquifer observation points, and is not plotted.

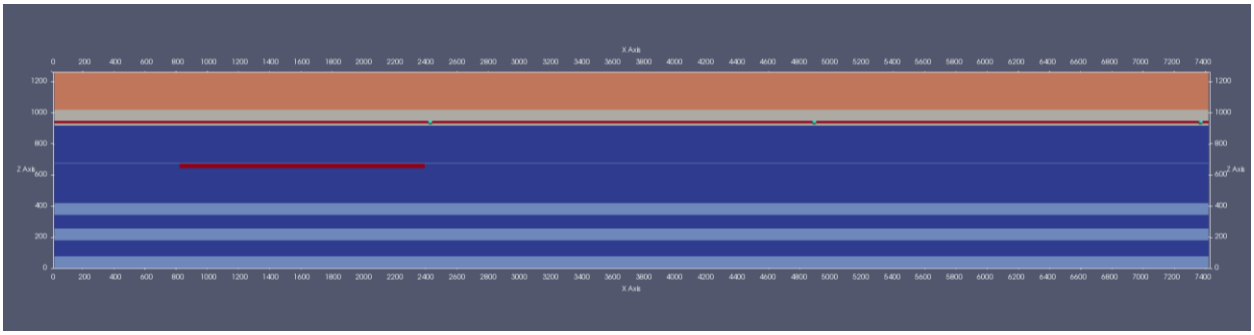

Figure 4-15. *X*-*Z* cross section at *Y* = 202.5 m showing the locations of observation points (teal spheres) used in uncertainty and sensitivity analysis. From left to right: "aqu1," "aqu2," and "aqu3."

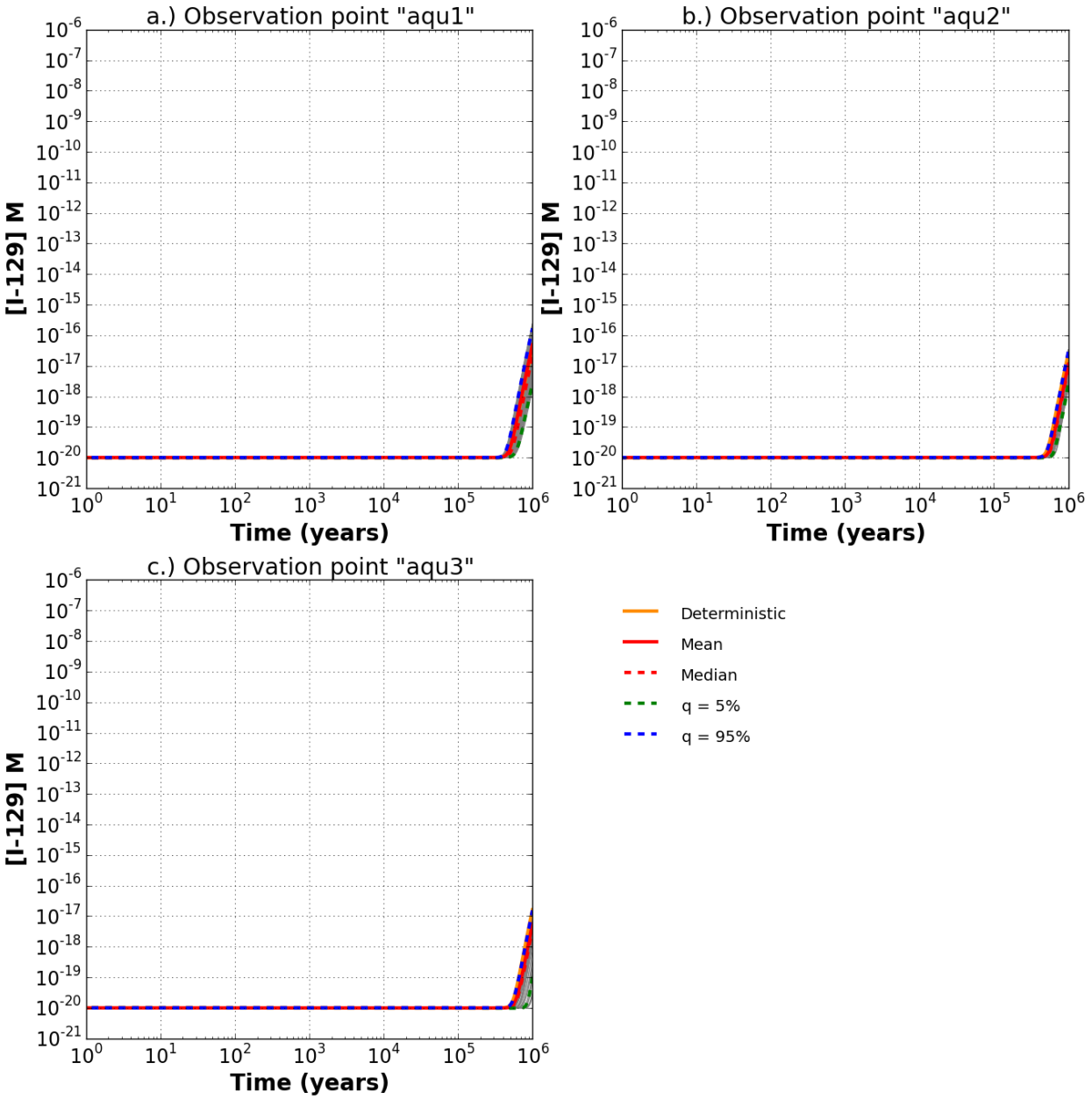

Figure 4-16. Predicted concentration of ^{129}I versus time for 50 probabilistic simulations. The orange line is the deterministic simulation.

Spearman's rank correlation coefficients (Eq. 3-8) were calculated in order to assess the sensitivity of maximum concentration of ^{129}I to sampled parameters (Figure 4-17). Maximum concentration of ^{129}I at the aquifer observation points exhibits a negative correlation with aquifer permeability at observation points "aqu1" and "aqu2," and a positive correlation at observation point "aqu3." Maximum concentration is positively correlated with halite porosity and negatively correlated with DRZ porosity at all three observation points.

Scatter plots provide another means of explaining the relationship between uncertainty in the output (here, the maximum concentration of either ^{129}I or ^{237}Np) and uncertainty in sampled input parameters. Figure 4-18 show scatter plots of maximum ^{129}I concentration versus sampled

values of the input parameters (Table 4-7) at "aqu1" observation point. The relationship between ^{129}I concentration and aquifer permeability (k), clearly visible in Figure 4-17, is also clearly shown by the trend in the corresponding scatter plot in Figure 4-18. No other clear trends are observable in Figure 4-18.

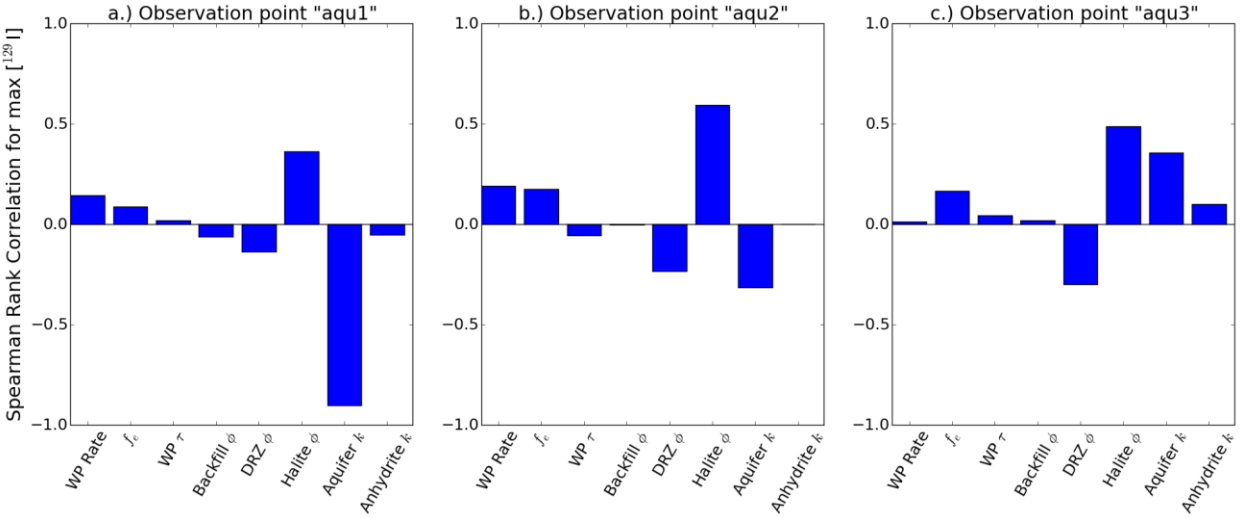

Figure 4-17. Spearman's rank correlation coefficients for maximum concentration of ^{129}I at aquifer observation points.

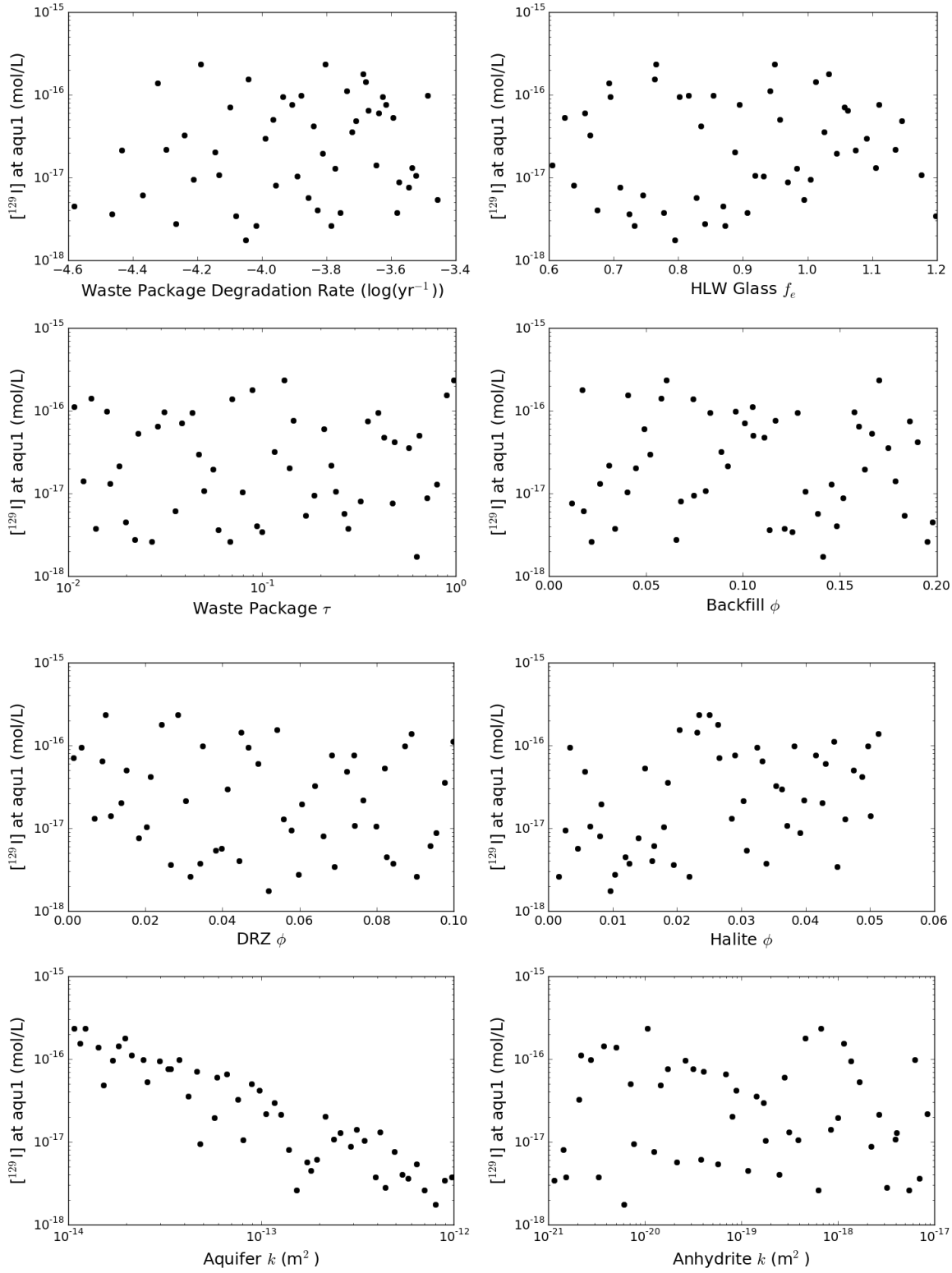

Figure 4-18. Maximum concentration of ^{129}I as a function of sampled input parameters at "aqu1" observation point.

4.5 Salt Reference Case Conclusions and Recommendations

The bedded salt reference case and simulation results are not dissimilar to earlier R&D for a commercial SNF repository in bedded salt (Sevougian et al. 2014), except the heat load is far lower for a Defense Waste Repository. Also, in the results presented here, a different emplacement concept is used than the previous commercial SNF repository. The DWR concept is on-floor emplacement of single waste canisters, which has operational advantages related to the much lower heat output of defense-related waste. The PA simulations show that because of the impermeable nature of the bedded salt host rock, radionuclide transport for this concept is greatly reduced compared to a generic crystalline concept discussed in Section 3, i.e., isolation from the surface is assured in bedded salt at all but extremely low radionuclide concentrations arising from the slow process of molecular diffusion.

Future simulations may examine different emplacement concepts and repository layouts, as well as the potential time-dependent effects on DRZ properties caused by salt creep. This latter investigation will help determine whether mechanical and coupled mechanical processes need to be explicitly represented in total system simulations.

5. CONCLUSIONS AND RECOMMENDATIONS

This deliverable is a status update on R&D progress during FY 2016 related to safety analysis (and safety case) activities for a generic Defense Waste Repository (DWR) for the permanent disposal of a portion of the HLW and SNF derived from national defense and R&D activities of the DOE, including:

- development of generic reference cases (i.e., knowledge or technical bases for "generic" or "non-site-specific" deep geologic repositories) for two primary host rocks under consideration for a DWR: crystalline (granite) and bedded salt;
- features, events, and processes (FEPs) analyses/screening to support the performance assessment and its underlying technical bases;
- performance evaluation of alternative engineered concepts for the layout of a repository and the design of an engineered barrier system (EBS), corresponding to the given host rock; and
- post-closure safety assessment of the repository system under consideration.

Using the known inventory for defense-related SNF, as well as for defense-related HLW stored at the Savannah River and Hanford sites, the Generic Disposal System Analysis (GDSA) modeling and software framework (Mariner et al. 2016) has been applied to examine the potential performance of a DWR in either crystalline host rock or bedded salt host rock. A variety of single-realization (i.e., deterministic) and multi-realization (probabilistic) 3-D flow and transport simulations for the generic granite and bedded salt repositories are presented, over a post-closure performance period of one million years. Sensitivity analyses examine the effect of key uncertain parameters on repository performance, including the effects of fracture distribution, waste package degradation rate, buffer and disturbed rock zone (DRZ) properties, and sorption parameters. Two types of emplacement concepts are examined, including single-canister vertical-borehole emplacement for the hotter DSNF waste (KBS-3V concept) and multi-canister horizontal emplacement for DHLW (similar to Yucca Mountain co-disposal waste packages).

Important issues uncovered by this year's work on a granite reference case are related to the uncertainty and heterogeneity associated with the spatial distribution and connectivity of fracture networks. These issues include:

1) Degree of isolation. Isolation is one of three primary safety functions generally acknowledged and often used for the Safety Case for most international programs. Direct connectivity of large fractures with the surface (outcrops) may pose challenges for repository performance depending on the degree of *in situ* fracture/feature connectivity, as well as the degree of liquid saturation in the fracture network. Two possible modifications to the generic crystalline reference case are suggested in this regard: either a sedimentary overburden or a deep unsaturated zone.

2) Quantitative safety metrics used to establish conformance to regulations. For outcropping saturated fractures, concentration or dose at a single location may not be a stable measure of performance. A suggested improvement is to use an array of monitor wells for the case of saturated fractures outcropping at the surface.

These results also point to a greater reliance on engineered barrier performance for a DWR in fractured crystalline host rock, indicating that future modifications to the granite reference case may include a longer-lived waste package overpack composed of oxygen-free copper, rather than the current generic design of a stainless steel overpack. Also, the influence of hydrodynamic dispersion and numerical diffusion/dispersion in fractured media warrant further study.

The bedded salt reference case and simulation results are not dissimilar to earlier R&D for a commercial SNF repository in bedded salt, except the heat load is far lower for a Defense Waste Repository. Also, in the results presented here, a different emplacement concept is used than the previous commercial SNF repository. The DWR concept is on-floor emplacement of single waste canisters, which has operational advantages related to the much lower heat output of defense-related waste. The PA simulations show that because of the impermeable nature of the bedded salt host rock, radionuclide transport for this concept is greatly reduced compared to a generic crystalline concept, i.e., isolation from the surface is assured in bedded salt at all but extremely low radionuclide concentrations arising from the slow process of molecular diffusion.

6. REFERENCES

Adams, B.M., M.S. Ebeida, M.S. Eldred, J.D. Jakeman, K.A. Maupin, J.A. Monschke, L.P. Swiler, J.A. Stephens, D.M. Vigil, T.M. Wildey, W.J. Bohnhoff, K.R. Dalbey, J.P. Eddy, R.W. Hooper, K.T. Hu, P.D. Hough, E.M. Ridgway, A. Rushdi 2016a. *Dakota, a Multilevel Parallel Object-Oriented Framework for Design Optimization, Parameter Estimation, Uncertainty Quantification, and Sensitivity Analysis: Version 6.4 User's Manual.* SAND2014-4633, July 2014, Updated May 9, 2016. Sandia National Laboratories, Albuquerque, NM. (http://dakota.sandia.gov/)

Adams, B.M., M.S. Ebeida, M.S. Eldred, J.D. Jakeman, K.A. Maupin, J.A. Monschke, L.P. Swiler, J.A. Stephens, D.M. Vigil, T.M. Wildey, W.J. Bohnhoff, K.R. Dalbey, J.P. Eddy, R.W. Hooper, K.T. Hu, P.D. Hough, E.M. Ridgway, A. Rushdi 2016b. *Dakota, a Multilevel Parallel Object-Oriented Framework for Design Optimization, Parameter Estimation, Uncertainty Quantification, and Sensitivity Analysis: Version 6.4 Theory Manual.* SAND2014-4253, July 2014, Updated May 9, 2016. Sandia National Laboratories, Albuquerque, NM. (http://dakota.sandia.gov/)

Arya A., T. A. Hewett, R. G. Larson, and L. W. Lake 1988. "Dispersion and Reservoir Heterogeneity," *SPE Reservoir Engineering*, **3**(1), February 1988, pp. 139-148, Society of Petroleum Engineers, SPE-14364-PA, http://dx.doi.org/10.2118/14364-PA

Balay S., J. Brown, K. Buschelman, V. Eijkhout, W.D. Gropp, D. Kaushik, M.G. Knepley, L. Curfman McInnes, B.F. Smith and H. Zhang 2013. *PETSc Users Manual*, ANL-95/11 – Revision 3.4, Argonne National Laboratory, Argonne IL.

Barton, K. E., D. G. Howell, J. F. Vigil, J. C. Reed, and J. O. Wheeler (Cartographer). (2003). *The North America Tapestry of Time and Terrain*. Retrieved from http://pubs.usgs.gov/imap/i2781/ October 25, 2016.

Baston, G. M. N., J. A. Berry, K. A. Bond, M. Brownsword, and C. M. Linklater 1991. "Studies of the Effects of Organic Materials on the Sorption of Uranium(IV) and Thorium(IV) on London Clay and Caithness Flagstones." U. Nirex. *JAEA Sorption Database System, Version 3*. Japan Atomic Energy Agency. Retrieved Sept. 2010 from http://migrationdb.jaea.go.jp/english.html.

Baston, G. M. N., J. A. Berry, M. Brownsword, T. G. Heath, D. J. Ilett, R. McCrohon, C. J. Tweed, and M. Yui 1999. "The sorption of polonium, actinium and protactinium onto geological materials." *Scientific Basis for Nuclear Waste Management Xxii*. D. J. Wronkiewicz and J. H. Lee (eds.). Materials Research Society, Warrendale. 556:1107-1114.

Bear, J. 1972. *Dynamics of Fluids in Porous Media*, American Elsevier Publishing, Inc., New York, NY.

Bear, J. and A. Cheng 2010. *Modeling Groundwater Flow and Contaminant Transport*, Springer, ISBN 978-1-4020-6681-8, DOI 10.1007/.978-1-4020-6682-5.

Bear, J., C. F. Tsang, and G. de Marsily 1993. *Flow and Contaminant Transport in Fractured Rock*, Academic Press, Inc., San Diego, CA 92101, ISBN 0-12-083980-6.

Beeckman, J.W. 1990. "Mathematical description of heterogeneous materials," *Chem. Eng. Sci*. 45:2603–2610. doi:10.1016/0009-2509(90)80148-8.

Bird, R. B., W. E. Stewart, and E. N. Lightfoot 1960. *Transport Phenomena*, John Wiley & Sons, Inc., New York, 780 pp.

Blacker, T., S. J. Owen, M. L. Staten, R. W. Quador, B. Hanks, B. Clark, R. J. Meyers, C. Ernst, K. Merkley, R. Morris, C. McBride, C. Stimpson, M. Plooster, and S. Showman 2016. *CUBIT Geometry and Mesh Generation Toolkit 15.2 User Documentation*. Sandia National Laboratories, Albuquerque, NM.

Blackwell, D. D., M. C. Richards, Z. S. Frone, J. F. Batir, M. A. Williams, A. A. Ruzo, and R. K. Dingwall 2011. "SMU Geothermal Laboratory Heat Flow Map of the Conterminous United States,

2011," Supported by Google.org. Available at http://www.smu.edu/geothermal Retrieved October 25, 2016.

Boudreau, B. P. 1996. "The diffusive tortuosity of fine-grained unlithified sediments." *Geochimica Et Cosmochimica Acta, 60*(16), 3139-3142. doi: 10.1016/0016-7037(96)00158-5

Bour, O. and P. Davy 1997. "Connectivity of random fault networks following a power law fault length distribution," *Water Resources Research, 33*(7), 1567-1583. doi: 10.1029/96wr00433

BRC (Blue Ribbon Commission on America's Nuclear Future). 2012. *Blue Ribbon Commission on America's Nuclear Future: Report to the Secretary of Energy.* January 2012.

BSC (Bechtel-SAIC Co.) 2004. *Aqueous Corrosion Rates for Waste Package Materials*. ANL-DSD-MD-000001 Rev. 1. Prepared for the U.S. Dept. of Energy, Office of Civilian Radioactive Waste Management, Las Vegas, Nevada.

Burnett, R. D. and E. O. Frind 1987. "Simulation of contaminant transport in three dimensions: 2. Dimensionality effects," *Water Resources Research, 23*(4), pp. 695-705.

Carman, P.C. 1937. "Fluid Flow Through Granular Beds," *Trans. Inst. Chem. Eng*. 15:150–166.

Carter, J. T., Rodwell, P. O, Robinson, B., Kehrman, B. 2012. *Defense Waste Salt Repository Study*, FCRD-UFD-2012-000113, May 5, 2012.

Carter, J. T., A. J. Luptak, J. Gastelum, C. Stockman, and A. Miller 2013. *Fuel Cycle Potential Waste Inventory for Disposition*. FCRD-USED-2010-000031 Rev 6. Savannah River National Laboratory, Aiken, SC.

Cho, W.-J., J.-S. Kim, C. Lee, and H.-J. Choi 2013. "Gas permeability in the excavation damaged zone at KURT". *Engineering Geology, 164*, 222-229. doi: 10.1016/j.enggeo.2013.07.010

Choi, H. J. and J. Choi 2008. "Double-layered buffer to enhance the thermal performance in a high-level radioactive waste disposal system". *Nuclear Engineering and Design, 238*(10), 2815-2820. doi: 10.1016/j.nucengdes.2008.04.017

Clayton, D.J., and C.W. Gable 2009. *3-D Thermal Analyses of High-Level Waste Emplaced in a Generic Salt Repository*. AFCI-WAST-PMO-MI-DV-2009 000002. February, 2009.

Clayton, D., G. Freeze, T. Hadgu, E. Hardin, J. Lee, J. Prouty, R. Rogers, W.M. Nutt, J. Birkholzer, H.H. Liu, L. Zheng, and S. Chu 2011. *Generic Disposal System Modeling – Fiscal Year 2011 Progress Report.* FCRD-USED-2011-000184, SAND2011-5828P. U.S. Department of Energy, Office of Nuclear Energy, Used Fuel Disposition Campaign, Washington, DC.

Clayton, D.J., J.G. Arguello Jr., E.L. Hardin, F.D. Hansen, and J.E. Bean 2012. "Thermal-Mechanical Modeling of a Generic High-Level Waste Salt Repository." In: SALTVII, 7th Conference on the Mechanical Behavior of Salt, Paris, France. April 16-19, 2012. (www.saltmech7.com), SAND2012-2741C.

Cook, P. and A.L. Herczeg 2000. *Environmental Tracers in Subsurface Hydrology*, Kluwer Academic Publishers, Norwell, MA.

Croff, A. G. 1983. "ORIGEN2: A Versatile Computer Code for Calculating the Nuclide Compositions and Characteristics of Nuclear Materials". *Nuclear Technology, 62*(3), 335-352. doi: dx.doi.org/10.13182/NT83-1

Delgado, J.M.P.Q. 2006. "A simple experimental technique to measure tortuosity in packed beds," *Can. J. Chem. Eng*. 84:651–655. doi:10.1002/cjce.5450840603.

De Marsily, G., *Quantitative Hydrogeology – Groundwater Hydrology for Engineers*, Academic Press, Inc., Orlando, FL, 1986.

DOE (U.S. Department of Energy) 2007. *Fall 2006 Assessment of Matheson Wetlands Hydrogeology and Ground Water Chemistry*, DOE-EM/GJ1441-2007, DOE Office of Environmental Management, Grand Junction, CO, March 2007, Doc. No. X0200300.

DOE (U.S. Department of Energy) 2008. *Yucca Mountain Repository License Application Safety Analysis Report.* DOE/RW-0573, Revision 1. U.S. Department of Energy, Washington, DC. (http://www.nrc.gov/waste/hlw-disposal/yucca-lic-app/yucca-lic-app-safety-report.html#1)

DOE (U.S. Department of Energy) 2009. *Waste Isolation Pilot Plant Compliance Recertification Application.* DOE 2009-24-34. March 2009.

DOE (U.S. Department of Energy) 2010. *Program and Project Management for the Acquisition of Capital Assets*, DOE O 413.3B, 11-29-2010, U.S. Department of Energy, Washington, D.C. 20585, available at https://www.directives.doe.gov/directives-documents/400-series/0413.3-BOrder-b

DOE (U.S. Department of Energy) 2011. *Technology Readiness Assessment Guide*, DOE G 413.3-4A, 9-15-2011, U.S. Department of Energy, Washington, D.C. 20585, www.directives.doe.gov

DOE (U.S. Department of Energy) 2012. Used Fuel Disposition Campaign Disposal Research and *Development Roadmap.* FCR&D-USED-2011-000065, REV 1, U.S. DOE Office of Nuclear Energy, Used Fuel Disposition, Washington, D.C., September 2012.

DOE (U.S. Department of Energy) 2014a. *Assessment of Disposal Options for DOE-Managed High-Level Radioactive Waste and Spent Nuclear Fuel*, October 2014.

DOE (U.S. Department of Energy) 2014b. Compliance Recertification Application 2014 for the Waste Isolation Pilot Plant: Appendix HYDRO-2014 Hydrological Investigations, DOE/WIPP-14–3503. Carlsbad, NM: US Department of Energy, Carlsbad Field Office. Available at http://www.wipp.energy.gov/library/cra/CRA-2014.html

DOE (U.S. Department of Energy) 2015. *Report on Separate Disposal of Defense High-Level Radioactive Waste*, March 2015.

Downey, J. S. and G. A. Dinwiddie 1988. *The Regional Aquifer System Underlying the Northern Great Plains in Parts of Montana, North Dakota, South Dakota, and Wyoming - Summary*. Professional Paper 1402-A. United States Geological Survey, Washington, D. C.

Fluor (Fluor Technology Inc.) 1985. *Waste Package/Repository Impact Study: Final Report*. Battelle Memorial Institute, Office of Nuclear Waste Isolation, Columbus, OH. BMI/ONWI/C-312. September, 1985.

Fluor (Fluor Technology Inc.) 1986. Site Characterization Plan Conceptual Design Report for a High-Level Nuclear Waste Repository in Salt, Vertical Emplacement Mode. U.S. Department of Energy, Office of Civilian Radioactive Waste Management, Salt Repository Office. September, 1986.

Follin, S., L. Hartley, I. Rhen, P. Jackson, S. Joyce, D. Roberts, and B. Swift 2014. "A methodology to constrain the parameters of a hydrogeological discrete fracture network model for sparsely fractured crystalline rock, exemplified by data from the proposed high-level nuclear waste repository site at Forsmark, Sweden," *Hydrogeology Journal, 22*(2), 313-331. doi: 10.1007/s10040-013-1080-2

Fox B. 2008. *Parameter Summary Report for CRA-2009, Revision 0*, WIPP:1.2.5:PA:QA-L:547488, Sandia National Laboratories, Carlsbad, NM.

Freeze, R.A. and J.A. Cherry 1979. *Groundwater*, Prentice-Hall, Englewood Cliffs, NJ.

Freeze, G., S.D. Sevougian, and M. Gross 2013a. *Safety Framework for Disposal of Heat-Generating Waste in Salt: Features, Events, and Processes (FEPs) Classification.* FCRD-UFD-2013-000191. SAND2013-5220P. Sandia National Laboratories, Albuquerque, NM.

Freeze, G., M. Voegele, P. Vaughn, J. Prouty, W.M. Nutt, E. Hardin, and S.D. Sevougian 2013b. *Generic Deep Geologic Disposal Safety Case*. FCRD-UFD-2012-000146 Rev. 1, SAND2013-0974P, August 2013, Sandia National Laboratories, Albuquerque, NM.

Freeze, G., P. Gardner, P. Vaughn, S.D. Sevougian, P. Mariner, V. Mousseau, and G. Hammond 2013c. *Enhancements to Generic Disposal System Modeling Capabilities.* FCRD-UFD-2014-000062. SAND2013-10532P. Sandia National Laboratories, Albuquerque, NM.

Freeze, G., S. D. Sevougian, C. Leigh, M. Gross, J. Wolf, J. Mönig, and D. Buhmann 2014. "A New Approach for Feature, Event, and Process (FEP) Analysis of UNF/HLW Disposal – 14314," in *Proceedings of the WM2014 Conference*, March 2 – 6, 2014, Phoenix, Arizona USA.

Garrett D. E. 2004. *Handbook of Lithium and Natural Calcium Chloride: Their Deposits, Processing, Uses and Properties*, Elsevier Academic Press, London, UK.

Gascoyne, M., C. C. Davison, J. D. Ross, and R. Pearson 1987. "Saline groundwaters and brines in plutons in the Canadian Shield." *Saline Water and Gases in Crystalline Rocks*. P. Fritz and S. K. Frape (eds.). Geological Association of Canada, Waterloo, Ontario. Special Paper 33:53-68.

Ghanbarian, B., Hunt, A.G., Ewing, R.P., Sahimi, M. 2013. "Tortuosity in Porous Media: A Critical Review," *Soil Science Society Of America Journal*, 2013 Sep-Oct, Vol.77(5), pp.1461-1477.

Halamickova, P., R. J. Detwiler, D. P. Bentz, and E. J. Garboczi 1995. "Water Permeability and Chloride-Ion Diffusion in Portland-Cement Mortars – Relationship to Sand Content and Critical Pore Diameter". *Cement and Concrete Research, 25*(4), 790-802. doi: 10.1016/0008-8846(95)00069-o

Hammond, G.E., P.C. Lichtner and M.L. Rockhold 2011. "Stochastic Simulation of Uranium Migration at the Hanford 300 Area", *Journal of Contaminant Hydrology*, v120-121, pp. 115-128, doi:10.1016/j.jconhyd.2010.04.005.

Hammond, G.E., P.C. Lichtner and R.T. Mills 2014. "Evaluating the Performance of Parallel Subsurface Simulators: An Illustrative Example with PFLORAN", *Water Resources Research*, 50, doi:10.1002/2012WR013483.

Hansen, F. D. and C .D. Leigh 2011. *Salt Disposal of Heat-Generating Nuclear Waste*, SAND2011-0161, Sandia National Laboratories, Albuquerque, New Mexico.

Hansen F. D., S. J. Bauer, S. T. Broome, and G. D. Callahan 2012. *Coupled Thermal-Hydrological-Mechanical Processes in Salt: Hot Granular Salt Consolidation, Constitutive Model and Micromechanics*, FCRD-USED-2012-000422, U.S. Department of Energy, Office of Nuclear Energy, Office of Used Nuclear Fuel Disposition, Washington, D.C. SAND2012-9893P, Albuquerque, NM: Sandia National Laboratories. November 15, 2012.

Hardin, E., T. Hadgu, D. Clayton, R. Howard, H. Greenberg, J. Blink, M. Sharma, M. Sutton, J. Carter, M. Dupont, and P. Rodwell 2012. *Repository Reference Disposal Concepts and Thermal Load Management Analysis.* FCRD-UFD-2012-000219 Rev. 2. U.S. Department of Energy, Office of Used Nuclear Fuel Disposition, Washington, DC.

Hedin, A. 2008. "Semi-analytic stereological analysis of waste package/fracture intersections in a granitic rock nuclear waste repository". *Mathematical Geosciences, 40*(6), 619-637. doi: 10.1007/s11004-008-9175-3

Helton, J.C., J.D. Johnson, C.J. Sallaberry, and C.B. Storlie 2006. "Survey of sampling-based methods for uncertainty and sensitivity analysis," *Reliability Engineering and System Safety*, **91**(2006), 1175-1209.

Huenges, E., J. Erzinger, J. Kuck, B. Engeser, and W. Kessels 1997. "The permeable crust: Geohydraulic properties down to 9101 m depth". *Journal of Geophysical Research-Solid Earth, 102*(B8), 18255-18265. doi: 10.1029/96jb03442

Hyman, J. D., S. L. Painter, H. Viswanathan, N. Makedonska, and S. Karra 2015a. "Influence of injection mode on transport properties in kilometer-scale three-dimensional discrete fracture networks". *Water Resources Research, 51*(9), 7289-7308. doi: 10.1002/2015wr017151

Hyman, J. D., S. Karra, N. Makedonska, C. W. Gable, S. L. Painter, and H. S. Viswanathan 2015b. "DFNWORKS: A discrete fracture network framework for modeling subsurface flow and transport". *Computers & Geosciences, 84*, 10-19. doi: 10.1016/j.cageo.2015.08.001

Ikeda, T., and T. Amaya 1998. "Model Development of Chemical Evolution in Repository Vol.II Acquisition of Nuclide Migration Data in Near-Field." *JAEA Sorption Database System, Version 3*. Japan Atomic Energy Agency. Retrieved Sept. 2010 from http://migrationdb.jaea.go.jp/english.html.

Iversen, N., and B.B. Jorgensen 1993. "Diffusion coefficients of sulfate and methane in marine sediments: Influence of porosity," *Geochim. Cosmochim. Acta* 57:571–578. doi:10.1016/0016-7037(93)90368-7.

James S. and J. Stein 2002. *Analysis Plan for the Development of a Simplified Shaft Seal Model for the WIPP Performance Assessment*, AP-094 Rev. 0, December 11, 2002, Sandia National Laboratories, Carlsbad NM.

Jobmann, M. and G. Buntebarth 2009. "Influence of graphite and quartz addition on the thermo-physical properties of bentonite for sealing heat-generating radioactive waste". *Applied Clay Science, 44*(3-4), 206-210. doi: 10.1016/j.clay.2009.01.016

Jové Colón, C. F., P. F. Weck, D. H. Sassani, L. Zheng, J. Rutqvist, C. I. Steefel, K. Kim, S. Nakagawa, J. Houseworth, J. Birkholzer, F. A. Caporuscio, M. Cheshire, M. S. Rearick, M. K. McCarney, M. Zavarin, A. Benedicto, A. B. Kersting, M. Sutton, J. Jerden, K. E. Frey, J. M. Copple, and W. Ebert 2014. *Evaluation of Used Fuel Disposition in Clay-Bearing Rock*, FCRD-UFD-2014-000056, SAND2014-18303 R, August 29, 2014, Sandia National Laboratories, Albuquerque, NM.

Joyce, S., L. Hartley, D. Applegate, J. Hoek, and P. Jackson 2014. "Multi-scale groundwater flow modeling during temperate climate conditions for the safety assessment of the proposed high-level nuclear waste repository site at Forsmark, Sweden". *Hydrogeology Journal, 22*(6), 1233-1249. doi: 10.1007/s10040-014-1165-6

Kienzler, B., M. Altmaier, C. Bube, and V. Metz 2012. *Radionuclide Source Term for HLW Glass, Spent Nuclear Fuel, and Compacted Hulls and End Pieces (CSD-C Waste)*, KIT Scientific Publishing, Report-Nr. KIT-SR 7624, Karlsruher Institut für Technologie (KIT), Straße am Forum 2, D-76131 Karlsruhe, www.ksp.kit.edu

Kitamura, A., T. Tomura, and T. Shibutani 2002. "Sorption Behavior of Neptunium onto Smectite under Reducing Conditions in Carbonate Media," *JAEA Sorption Database System, Version 3*. Japan Atomic Energy Agency. Retrieved Sept. 2010 from http://migrationdb.jaea.go.jp/english.html.

Li, Y. H. and S. Gregory 1974. "Diffusion of Ions in Sea-Water and in Deep-Sea Sediments," *Geochimica Et Cosmochimica Acta*, *38*(5), 703-714.

Lichtner, P.C. and G.E. Hammond. 2012. "Using High Performance Computing to Understand Roles of Labile and Nonlabile U(VI) on Hanford 300 Area Plume Longevity", *Vadose Zone Journal*, v11, n2, doi:10.2136/vzj2011.0097.

Lichtner, P. C., Kelkar, S., and B. Robinson 2002. "New form of dispersion tensor for axisymmetric porous media with implementation in particle tracking," *Water Resources Research, 38*(9), pp. 21-1 to 21-16, doi: 10.1029/2000WR000100.

Lichtner, P. C., G. E. Hammond, C. Lu, S. Karra, G. Bisht, B. Andre, R. Mills, and J. Kumar 2015. *PFLOTRAN User Manual: A Massively Parallel Reactive Flow and Transport Model for Describing Surface and Subsurface Processes*, http://www.pflotran.org/docs/user_manual.pdf, January 20, 2015

Liu, J. F., Y. Song, F. Skoczylas, and J. Liu 2016. "Gas migration through water-saturated bentonite-sand mixtures, COx argillite, and their interfaces". *Canadian Geotechnical Journal, 53*(1), 60-71. doi: 10.1139/cgj-2014-0412.

Mayhew, E. J., and E. B. Heylmun 1966. "Complex Salts and Brines of the Paradox Basin," *Second Symposium On Salt, Vol. 1*, May 3-5, 1965, Cleveland, OH, Rau, JL (ed.), pp. 221-235. Northern Ohio Geological Society, Cleveland, Ohio.

Mariner, P., J. H. Lee, E. Hardin, F. D. Hansen, G. Freeze, A. S. Lord, B. Goldstein, and R. H. Price 2011. *Granite Disposal of U.S. High-Level Radioactive Waste*. SAND2011-6203. Sandia National Laboratories, Albuquerque, NM.

Mariner, P. E., W. P. Gardner, G. E. Hammond, S. D. Sevougian, and E. R. Stein 2015. *Application of Generic Disposal System Models*. SAND2015-10037 R; FCRD-UFD-2015-000126. Sandia National Laboratories, Albuquerque, NM.

Mariner, P. E., E. R. Stein, J. M. Frederick, S. D. Sevougian, G. E. Hammond, and D. G. Fascitelli, 2016. *Advances in Geologic Disposal System Modeling and Application to Crystalline Rock*, FCRD-UFD-2016-000440, SAND2016-96107R. Sandia National Laboratories, Albuquerque, NM, September 22, 2016.

Martino, J. B. and N. A. Chandler 2004. "Excavation-induced damage studies at the Underground Research Laboratory". *International Journal of Rock Mechanics and Mining Sciences, 41*(8), 1413-1426. doi: 10.1016/j.ijmms.2004.09.010

Matteo, E., E. Hardin, T. Hadgu, H. Park, M. Rigali, and C. F. Jove-Colon 2016. *Status of Progress Made Toward Preliminary Design Concepts for the Inventory in Select Media for DOE-Managed HLW/SNF*. SAND2016-9823 R; FCRD-UFD-2016-000081. Sandia National Laboratories, Albuquerque, NM.

Millington, R. J. 1959. "Gas Diffusion in Porous Media", *Science*, Vol. 130, pp. 100-102.

Molecke, M.A. 1983. *A Comparison of Brines Relevant to Nuclear Waste Experimentation.* SAND83-0516. Albuquerque, NM: Sandia National Laboratories. May 1983.

Mucciardi, A. N., T. C. Johnson, and J. Saunier 1979. "Statistical Investigation of the Mechanics Controlling Radionuclide Sorption." B. N. Laboratory. *JAEA Sorption Database System, Version 3*. Japan Atomic Energy Agency. Retrieved Sept. 2010 from http://migrationdb.jaea.go.jp/english.html.

NWPA (Nuclear Waste Policy Act) 1987. Public Law 97-425; 96 Stat. 2201, as amended by P.L. 100-203. December 22, 1987.

Oda, C., T. Ikeda, and M. Shibata 1999. "Experimental Studies for Sorption Behavior of Tin on Bentonite and Rocks and Diffusion Behavior of Tin in Compacted Bentonite." *JAEA Sorption Database System, Version 3*. Japan Atomic Energy Agency. Retrieved Sept. 2010 from http://migrationdb.jaea.go.jp/english.html.

Oelkers, E. H. (1996). Properties of Rocks and Fluids for Mass Transport Calculations. In P. C. Lichtner, C. I. Steefel, & E. H. Oelkers (Eds.), *Reactive Transport in Porous Media* (pp. 131-191). Washington, D. C.: Mineralogical Society of America.

Perkins, T. K. and O. C. Johnston 1963. "A Review of Diffusion and Dispersion in Porous Media," *Society of Petroleum Engineers Journal*, **3**(1), March 1963, SPE-480-PA, http://dx.doi.org/10.2118/480-PA

Perry, F. V., R. E. Kelley, P. F. Dobson, and J. E. Houseworth 2014. *Regional Geology: A GIS Database for Alternative Host Rocks and Potential Siting Guidelines*. LA-UR-14-20368, FCRD-UFD-2014-000068. Los Alamos National Laboratory, Los Alamos, NM.

Perry, F. V., R. E. Kelley, and D. M. Milazzo 2016. *Regional Geologic Evaluations for Disposal of HLW and SNF: Archean Crystalline Rocks of the North-Central United States*. FCRD-UFD-2016-000634; LA-

UR-16-27845. Los Alamos National Laboratory, Los Alamos, NM.

Pettersson, S. and B. Lonnerberg. (2008). *Final Repository for Spent Nuclear Fuel in Granite - The KBS-3V Concept in Sweden and Finland*. Paper presented at the International Conference Underground Disposal Unit Design &Emplacement Processes for a Deep Geologic Repository, Prague.

Posiva 2010. *Models and Data Report 2010*. POSIVA 2010-01. Posiva Oy, Olkiluoto, Finland.

Rancon, D., and J. Rochon 1979. "Retention of long-lived radionuclides in different neutral materials." B. International Atomic Energy Agency. *JAEA Sorption Database System, Version 3*. Japan Atomic Energy Agency. Retrieved Sept. 2010 from http://migrationdb.jaea.go.jp/english.html.

Rothfuchs, T., K. Wieckzorek, B. Bazargan and S. Olivella 2003. "Results of the BAMBUS II Project – Experimental and Modelling Results concerning Salt Backfill Compaction and EDZ Evolution in a Spent Fuel Repository in Rock Salt Formations." *Eurosafe Forum*. Paris, November 25-26, 2003. www.eurosafe-forum.org

RWM (Radioactive Waste Management LTD) 2016. *Geological Disposal: Generic Post-Closure Safety Assessment*, DSSC/321/01, in preparation, Harwell Oxford, Didcot OX11 0RH, www.nda.gov.uk

Sassani, D. C., J.-H. Jang, P. Mariner, L. Price, R. P. Rechard, M. Rigali, R. Rogers, E. R. Stein, W. Walkow, and P. F. Weck 2016. *The On-line Waste Library (OWL): Usage and Inventory Status Report*. SAND2016-9485 R; FCRD-UFD-2016-000080. Sandia National Laboratories, Albuquerque, NM.

Schild, M., S. Siegesmund, A. Vollbrecht, and M. Mazurek 2001. "Characterization of granite matrix porosity and pore-space geometry by in situ and laboratory methods". *Geophysical Journal International, 146*(1), 111-125. doi: 10.1046/j.0956-540x.2001.01427.x

Sevougian, S. D. 2016. "Application of the Technology Readiness Assessment (TRA) Process to Deep Geologic Repository Systems," presented at the 2nd DAEF Conference on Key Topics in Deep Geological Disposal, Cologne, Germany, September 27-28, 2016, SAND2016-9353C, Sandia National Laboratories, Albuquerque, NM.

Sevougian, S. D. and R. J. MacKinnon 2014. "A Decision Methodology for Prioritizing R&D Supporting Geologic Disposal of SNF/HLW in Salt – 14030," in *Proceedings of the WM2014 Conference*, March 2 – 6, 2014, Phoenix, Arizona USA.

Sevougian, S.D., G.A. Freeze, M.B. Gross, J. Lee, C.D. Leigh, P. Mariner, R.J. MacKinnon, and P. Vaughn 2012. *TSPA Model Development and Sensitivity Analysis of Processes Affecting Performance of a Salt Repository for Disposal of Heat-Generating Nuclear Waste*. FCRD-UFD-2012-000320 Rev. 0, U.S. Department of Energy, Office of Used Nuclear Fuel Disposition, Washington, DC.

Sevougian, S.D., G.A. Freeze, P. Vaughn, P. Mariner, and W.P. Gardner 2013. *Update to the Salt R&D Reference Case*. FCRD-UFD-2013-000368, SAND2013-8255P. Sandia National Laboratories, Albuquerque, NM.

Sevougian, S. D., G.A. Freeze, W.P. Gardner, G. E. Hammond, and P. Mariner 2014. *Performance Assessment Modeling and Sensitivity Analyses of Generic Disposal System Concepts*. FCRD-UFD-2014-000320, SAND2014-17658. Sandia National Laboratories, Albuquerque, NM, September 12, 2014.

Sevougian, S. D., G. Freeze, M. Gross, J. Wolf, J. Mönig, and D. Buhmann 2015. "Generic Salt FEPs Catalogue – Volume II," Rev. 0, June 29, 2015, Carlsbad, NM: Sandia National Laboratories, Waste Isolation Pilot Plant (WIPP) Records Center, Sandia Level Three Milestone: No. INT-15-01.

Sevougian, S. D., G. Freeze, M. Gross, K. Kuhlman, C. Leigh, J. Wolf, D. Buhmann, and J. Mönig 2016. "Joint US-German FEPs Catalog," presented at the 7th US/German Workshop on Salt Repository Research, Design, and Operation, Washington, DC, September 7-9, 2016, SAND2016-8441C, Sandia National Laboratories, Albuquerque, NM.

Shelton, S. M. 1934. "Thermal conductivity of some irons and steels over the temperature range 100 to 500 C". *Bureau of Standards Journal of Research, 12*(4/6), 441-450.

SKB (Svensk Kärnbränslehantering AB) 2004. *SR-Can Data and uncertainty assessment: Migration parameters for the bentonite buffer in the KBS-3 concept*. Svensk Karnbranslehantering AB, Stockholm, Sweden.

SKB (Svensk Kärnbränslehantering AB) 2006a. *Data report for the safety assessment of SR-Can*. TR-06-18. Swedish Nuclear Fuel and Waste Management Co., Stockholm, Sweden.

SKB (Svensk Kärnbränslehantering AB) 2006b. *Fuel and canister process report for the safety assessment SR-Can*. TR-06-22. Swedish Nuclear Fuel and Waste Management Co., Stockholm, Sweden.

SKB (Svensk Kärnbränslehantering AB) 2007. *Geology Forsmark*. R-07-45 Swedish Nuclear Fuel and Waste Management Co., Stockholm, Sweden.

SKB (Svensk Kärnbränslehantering AB) 2008. *Bedrock hydrogeology Forsmark*. R-08-45. Swedish Nuclear Fuel and Waste Management Co., Stockholm, Sweden.

SKB (Svensk Kärnbränslehantering AB) 2010. *Data Report for the Safety Assessment SR-Site*. Technical Report TR-10-52. Swedish Nuclear Fuel and Waste Management Co., Stockholm, Sweden.

SKB (Svensk Kärnbränslehantering AB) 2011. *Long-term safety for the final repository for spent nuclear fuel at Forsmark: Main report of the SR-Site project* (3 volumes). TR-11-01. Swedish Nuclear Fuel and Waste Management Co., Stockholm, Sweden. (www.skb.se/publications)

SNL (Sandia National Laboratories) 2008: *Features, Events, and Processes for the Total System Performance Assessment: Methods*. ANL-WIS-MD-000026 REV 00, Sandia National Laboratories, Las Vegas, Nevada.

SNL (Sandia National Laboratories) 2014. *Evaluation of Options for Permanent Geologic Disposal of Spent Nuclear Fuel and High-Level Radioactive Waste*. SAND2014-0187P; FCRD-UFD-2013-000371, Rev. 1. Sandia National Laboratories, Albuquerque, NM.

Soler, J. M., J. Landa, V. Havlova, Y. Tachi, T. Ebina, P. Sardini, M. Siitari-Kauppi, J. Eikenberg, and A. J. Martin 2015. "Comparative modeling of an in situ diffusion experiment in granite at the Grimsel Test Site". *Journal of Contaminant Hydrology, 179*, 89-101. doi: 10.1016/j.jconhyd.2015.06.002

Stauffer, D. and A. Aharony 1994. *Introduction to Percolation Theory* (2 ed.). Boca Raton, FL: CRC Press.

Strachan, D. 2004. *Defense HLW Glass Degradation Model*. ANL-EBS-MD-000016 Rev 2. Bechtel SAIC Company, LLC, Las Vegas, NV.

Tachi, Y., and T. Shibutani 1999. "Sorption and Diffusion Behavior of Radium on Bentonite and Rocks." *JAEA Sorption Database System, Version 3*. Japan Atomic Energy Agency. Retrieved Sept. 2010 from http://migrationdb.jaea.go.jp/english.html.

Tachi, Y., T. Shibutani, Y. Nishikawa, and T. Shinozaki 1999a. "Sorption Behavior of Selenium on Bentonite and Granodiorite under Reducing Conditions." *JAEA Sorption Database System, Version 3*. Japan Atomic Energy Agency. Retrieved Sept. 2010 from http://migrationdb.jaea.go.jp/english.html.

Tachi, Y., T. Shibutani, H. Sato, and M. Shibata 1999b. "Sorption and Diffusion Behavior of Palladium in Bentonite, Granodiorite and Tuff." *JAEA Sorption Database System, Version 3*. Japan Atomic Energy Agency. Retrieved Sept. 2010 from http://migrationdb.jaea.go.jp/english.html.

Tsai, D.S., and W. Strieder 1986. "Effective conductivities of random fiber beds," *Chem. Eng. Commun*. 40:207–218. doi:10.1080/00986448608911698.

Twiss, R. J. and E. M. Moores 1992. *Structural Geology*. New York: W. H. Freeman and Company.

Ulrich, H. J., and C. Degueldre 1993. "The sorption of Pb-210, Bi-210 and Po-210 on montmorillonite - A study with emphasis on reversibility aspects and on the effect of the radioactive decay of adsorbed nuclides." *Radiochimica Acta*. 62(1-2):81-90.

Vaughn, P., S. D. Sevougian, E. L. Hardin, P. Mariner, and M. B. Gross 2013. "Reference Case For Generic Disposal of HLW and SNF in Salt," in *Proceedings of the 2013 International High-Level Radioactive Waste Management Conference*, Albuquerque, NM, April 28 – May 2, 2013, American Nuclear Society, La Grange Park, IL. (www.ans.org)

Vosteen, H. D. and R. Schellschmidt 2003. "Influence of temperature on thermal conductivity, thermal capacity and thermal diffusivity for different types of rock". *Physics and Chemistry of the Earth, 28*(9-11), 499-509. doi: 10.1016/s1474-7065(03)00069-x

Wang, Y. and J. H. Lee 2010. *Generic Disposal System Environment Modeling - Fiscal Year 2010 Progress Report*. SAND2010-8202P. Sandia National Laboratories, Albuquerque, NM.

Wang, Y., E. Matteo, Rutqvist, J. Davis, L. Zheng, V. Vilarrasa, J. Houseworth, J. Birkholzer, T. Dittrich, C. W. Gable, S. Karra, N. Makedonska, S. Chu, D. Harp, S. L. Painter, P. Reimus, F. Perry, P. Zhao, J. Begg, M. Zavarin, S. J. Tumey, Z. Dai, A. B. Kersting, J. Jerden, K. Frey, J. M. Copple, W. Ebert 2014. *Used Fuel Disposal in Crystalline Rocks: Status and FY14 Progress*, FCRD-UFD-2014-000060, SAND2014-17992R, Sandia National Laboratories, Albuquerque, New Mexico, September 2014.

Wang, M., Y. F. Chen, S. Zhou, R. Hu, and C. B. Zhou 2015. "A homogenization-based model for the effective thermal conductivity of bentonite-sand-based buffer material". *International Communications in Heat and Mass Transfer, 68*, 43-49. doi: 10.1016/j.icheatmasstransfer.2015.08.007

Weissberg, H.L. 1963. "Effective diffusion coefficient in porous media," *J. Appl. Phys*., 34:2636–2639. doi:10.1063/1.1729783.

Wilson, J. 2016. *Decay Heat of Selected DOE Defense Waste Materials*, FCRD-UFD-2016-000636, SRNL-RP-2016-00249, Savannah River National Laboratory, Aiken, SC.

Wilson, T. P. and D. T. Long 1993. "Geochemistry and isotope chemistry of Michigan Basin brines: Devonian formations," *Applied Geochemistry,* Vol. 8, pp. 81-100.

Zhou, Q. L., H. H. Liu, F. J. Molz, Y. Q. Zhang, and G. S. Bodvarsson 2007. "Field-scale effective matrix diffusion coefficient for fractured rock: Results from literature survey". *Journal of Contaminant Hydrology, 93*(1-4), 161-187. doi: 10.1016/j.jconhyd.2007.02.002

APPENDIX A: PRELIMINARY FEP SCREENING RECOMMENDATIONS FOR A DEEP GEOLOGIC REPOSITORY FOR DSNF AND DHLW AT A GENERIC SITE IN CRYSTALLINE ROCK

Table A-1 is a list of features, events, and processes (FEPs) relevant to a repository for DOE-managed spent nuclear fuel (DSNF) and DOE-managed high-level waste (DHLW) in a generic crystalline rock site. The FEP list in Table A-1 is based on the FEP list, FEP processes, and FEP numbering scheme developed by a collaborative effort between the United States and German repository programs (Sevougian et al. 2015; Sevougian et al. 2016). This collaborative effort began with development of a FEP list for a generic site in bedded or domal rock salt (halite), which was then generalized to be applicable to other geologies (such as crystalline rock). The resulting US-German master FEP list forms the basis for Table A-1.

In this appendix, and in the US program in general, a FEP screening decision refers to inclusion in, or exclusion from, the PA model and its quantitative dose/risk results. Based upon the generic crystalline reference case described in Section 3, the preliminary FEP screening recommendations in Table A-1 use the following assumptions and considerations regarding potential behavior of the engineered and natural barriers.

1. Conceptually, the host rock is comprised of two components: the fracture network and the rock matrix. The fractures are the preferential release pathway(s) because the crystalline rock matrix (i.e., the intact, unfractured rock) is assumed to have low permeability relative to the fracture system (Section 3.3.2; Table 3-10).
2. The major engineered barriers are the waste package corrosion barrier and a compacted bentonite buffer/backfill surrounding the waste package:
    a. Waste packages are emplaced in a saturated, reducing environment at the repository horizon. The waste package consists of a stainless steel overpack enclosing one or more stainless steel canisters (see Sections 3.1.3 and 3.1.4). Barrier longevity for waste packages loaded with DSNF and DHLW is assumed to be as shown in Figure 3-17, which assigns a base canister degradation rate for each waste package by sampling on a truncated log normal distribution with a mean of $10^{-4.5}$/yr, a standard deviation of 0.5 (log units), and an upper truncation of –3.5 (log units), as described in Section 3.3.2.5.
    b. A compacted bentonite buffer/backfill provides a low permeability, sorbing medium adjacent to each waste package. This low permeability, sorbing medium will prevent or delay releases of radionuclides into the fracture network surrounding the repository while the buffer/backfill is intact and in a uniform state (i.e., without cracks or channels).
3. The peak temperature of the thermal pulse will be less than 100°C for representative DSNF and DHLW waste forms in crystalline rock. Figure 3-8 shows two waste package temperature histories for each of the two primary EBS design concepts under consideration: vertical borehole emplacement of a waste package with a single canister of DSNF and horizontal emplacement of a much larger waste package containing five canisters of DHLW. For each of the two designs, Figure 3-8 shows two temperature extremes for each type of

waste: a relatively cool DSNF (100-200 W) and the hottest DSNF (1000-1500 W), and the coolest DHLW (Hanford glass) and hottest DHLW (Savannah River glass). The peak temperature for the Savannah River DHLW is less than 90°C at about 20 years after emplacement. The peak temperature for the hottest DSNF is slightly more than 80°C at about 5 years after emplacement. The peak temperature for Hanford DHLW is about 30°C, occurring at about 300 years after emplacement. The ambient temperature in the underground is 24°C for these calculations. Figure 3-8 also shows that the duration of the thermal pulses from both DHLW waste forms is about 1,000-2,000 years. The duration of the thermal pulse for the hot DSNF is about 50,000 years, although its increase in temperature above ambient is less than 20°C after about 1,000 years.

The thermal responses for the high decay heat DSNF and the Savannah River DHLW in Figure 3-8 are assumed to provide an upper bound on peak temperature during the post-closure thermal pulse, for the purpose of FEP screening analyses. Thus, for FEP screening purposes, the peak temperature during the thermal pulse is assumed to be less than 100°C in a defense waste repository with an ambient temperature of 24°C. This assumption means that complete dry-out of any buffer/backfill material surrounding the waste packages will not occur.

The longevity of the waste package and the duration of an associated thermal pulse are important factors in FEP screening. If the waste packages are predicted to remain intact as a flow barrier during the thermal pulse, then thermal coupling to repository processes will generally not be significant. In other words, thermal-mechanical (TM), thermal-hydrological (TH), thermal-chemical (TC), or thermal-transport (TT) coupling will likely not be significant if either the waste package barrier or the buffer/backfill barrier remains intact during the thermal pulse. There is one important caveat to this statement: the thermal pulse must be small enough not to cause permanent, irreversible changes or damage to the barriers (particularly the clay buffer). Given the information and assumptions in Items (1) through (3) above, this condition is likely to be satisfied and may result in many FEPs for coupled processes being excluded from the long-term performance assessment (PA) for a License Application, although they all require some type of preliminary PA analysis to ensure that this is true. (This type of FEP screening or exclusion analysis may imply that the process is represented as a look-up table in the full PA model for the purposes of screening, rather than as a detailed process model.)

Not all coupled FEPs would be excluded by the foregoing reasoning. The thermal pulse is expected to heat the pore water in and around the repository, generating a Darcy flux of groundwater away from the repository (Figures 3-10 to 3-12). Only 40 waste packages are predicted to fail during the first 1,380 years after repository closure, but these 40 packages define the initial source term. Coupled thermal processes that may affect radionuclide transport arising from releases from these 40 initial package failures are *not expected* to be excluded from PA, unless the compacted bentonite buffer/backfill can be shown with certainty to remain intact. An important consideration here is that a peak repository temperature less than 100°C (Figure 3-8) may reduce the incidence of cracking associated with partial dry-out of the buffer/backfill, thereby reducing or preventing releases of radionuclides through the buffer/backfill during the first 1,000 years after emplacement.

Based on the foregoing arguments, the longevity of the engineered barriers versus the magnitude and duration of the thermal pulse will clearly be important considerations in developing screening arguments or sensitivity analyses for individual coupled FEPs. Many coupled FEPs have therefore been identified as requiring Evaluation in Table A-1.

The preliminary screening decisions are documented in Table A-1. Because some FEPs are fairly broad in scope, a finer discretization of the FEP into more detailed or specific processes is generally necessary to facilitate screening. These processes appear in the third column of Table A-1—labeled as (A), (B), (C), etc.—and are the discretization level at which screening analyses and decisions are made. The first three columns of Table A-1 identify the Matrix FEP Number, the FEP Description, and the Associated Processes for each FEP. The fourth column of Table A-1 identifies a Preliminary Screening Recommendation for the individual processes in each FEP (many FEPs have multiple processes) and provides an explanation of the basis for the recommendation, when appropriate. Biosphere (BP) FEPs were not examined in this preliminary screening analysis because they are all considered to be either Site-Specific or "regulation specific."

The following categories are used for the screening recommendations in Table A-1:

- **Included**. A process that is almost certain to be screened in to the PA model for crystalline rock. Examples of FEPs with Included processes are FEP WP.00.TT.01, Transport of Dissolved Radionuclides in the Liquid Phase in Waste Packages, and FEP BB.01.TH.01, Pressure-Driven Darcy Flow Through Fractures and Porous Media in the Buffer.
- **Likely Included**. A process that is expected to be screened in but, on further analysis, might possibly be excluded. As an example, infiltration and drainage for FEP WP.00.TH.03, Gravity- and Density-Dominated Flow in the Waste Package, are likely included because these processes could be important for defining the hydrologic state in the waste package.
- **Excluded**. A process that is almost certain to be screened out of the PA model for crystalline rock. An example of an Excluded process for crystalline rock is creep closure of waste emplacement rooms, e.g., FEP WP.00.TM.01.
- **Likely Excluded**. A process that is expected to be screened out but, on further analysis, might be included. An example is FEP WF.00.TM.01, Dynamic Response of Fuel Rods and Cladding. The cladding is likely to be excluded as a barrier to releases because of the complexity of defining the initial damage to the cladding when it is removed from a reactor.
- **Site-Specific**. A FEP or process that requires detailed information for a specific site. An example is FEP WP.00.HE.01, Human Intrusion, which requires knowledge of the potential for mining and resource extraction activities at a specific site in order to develop a detailed screening argument.
- **Design-Specific**. A FEP or process that requires detailed information for a specific repository design. Examples would be FEP WP.00.TC.08, Electrochemical Effects in Waste Packages, or FEP WP.00.TC.09, Chemical Interactions Between Co-located Waste Forms. A screening decision requires knowledge of waste package design and waste form materials to formulate a detailed screening argument.
- **Evaluate**. All other FEPs are candidates for reasoned arguments or sensitivity studies to determine their disposition with respect to the PA model for crystalline rock. Some of these studies will involve coupled processes, with the results providing guidance on which phenomena must be included in the PA model. For

example, many processes related to FEP WP.00.TH.08, Thermal-Hydrological Effects on Exterior Surface of the Waste Packages, will require Evaluation because the thermal pulse may result in significant evaporation/condensation near the waste package, and the thermal conductivity of various materials are temperature dependent.

The foregoing FEP categories are not mutually exclusive, and multiple categories have sometimes been identified for an individual FEP. As an example, the magnitude and timing of seismic events is very **Site-Specific**. On the other hand, the damage from seismic ground motion when waste packages are surrounded by backfill may be excluded if backfill restricts the kinematic motion of a waste package and other EBS components during a seismic event. In this situation, the seismic-related FEPs have been identified as both **Site-Specific** and **Evaluate**.

For excluded FEPs, several standard exclusion criteria are possible (SNL 2008, Section 6.2):

- **Low Probability** – FEPs that are estimated to have a frequency of occurrence less than a specified threshold, usually defined by regulation, may be excluded. For example, in the US, 10 CFR 63 specifies a probability threshold of "less one chance in 10,000 of occurring within 10,000 years of disposal (less than one chance in 100,000,000 per year)". In other words, per 10 CFR 63, FEPs that have a frequency of occurrence of less than 10^{-8} per year can be excluded (screened out) from the performance assessment calculations on the basis of low probability.
- **Low Consequence** – FEPs that are not expected to materially affect performance may be excluded. For example, in the US, 10 CFR 63 states the specific FEPs "must be evaluated in detail if the magnitude and time of the resulting radiological exposures … or radionuclide releases to the accessible environment … would be significantly changed by their omission." In other words, if it can be shown that FEP has no significant adverse effect on radiological exposure, or radionuclide release, or on an intermediate-performance measure that can be linked to radiological exposure or radionuclide release, that FEP can be excluded (screened out) from the performance assessment on the basis of low consequence. [Most of the screening recommendations given in Table A-1 use this criterion.]
- **Design** – Some FEPs may be inconsistent with, or not relevant to, the repository system site and/or design. These FEPs may be excluded from the PA model "by design."
- **Regulation** – Some FEPs may inconsistent with, or explicitly excluded by, the regulations. The regulatory requirements that are most commonly relevant to FEP screening include the characteristics, concepts, and definitions pertaining to the reference biosphere, geologic setting, and the dose receptor.

FEP screening may include assessing both the likelihood of the FEP occurring and the potential consequences of the FEP were it to occur, because both aspects enter into the evaluation of radiological exposure and/or radionuclide releases. For example, even if the basis for screening cannot rely solely on the low-probability criterion (e.g., it is not possible to provide a sufficiently detailed quantification of the probability to justify its exclusion, given the current state of knowledge of data and models and the uncertainty associated with the FEP), the FEP may be excluded due to the combined effect of low likelihood and low consequence. These types of

evaluations represent a risk-informed approach that examines the joint outcome of the probability and the consequence of such FEPs.

The FEP numbering scheme for the FEPs listed in Table A-1 is based on a new alphanumeric designation (Sevougian et al. 2015). The new eight character alphanumeric FEP identifiers have the form FF.CC.PE.nn. The first group of characters (FF) indicates the Feature, as follows (see Figure 2-4):

- WF = Waste Form
- WP = Waste Package
- BB = Buffer/Backfill
- MW = Mine Workings
- SP = Seals/Plugs
- HR = Host Rock
- OU = Other Geologic Units
- BP = Biosphere
- RS = Repository System

The second group of characters (CC) indicates the Component, if applicable (if not, these two characters equal 00). As an example, under Seals/Plugs (SP) the following identifiers would apply:

- SP.00 = FEPs related to all Seals and Plugs (i.e., not component specific)
- SP.01 = FEPs related only to Drift/Tunnel Seals
- SP.02 = FEPs related only to Shaft Seals
- SP.03 = FEPs related only to Borehole Plugs

The third group of characters (PE) indicates the Process/Event category, as follows:

- CP = Characteristics
- TM = Mechanical and Thermal-Mechanical Processes
- TH = Hydrologic and Thermal-Hydrologic Processes
- TC = Chemical and Thermal-Chemical Processes
- TB = Biological and Thermal-Biological Processes
- TT = Transport and Thermal-Transport Processes
- TL = Thermal
- RA = Radiological
- LG = Long-Term Geologic
- CL = Climatic

- HP = Human Activities (Processes, long timescale)
- OP = Other (Processes)
- NC = Nuclear Criticality
- EF = Early Failure
- SM = Seismic
- IG = Igneous
- HE = Human Activities (Events, short timescale)
- OE = Other (Events)

The final group of characters (nn) is simply a sequential tracking number for FEPs in a specific FEP matrix cell (e.g., .01, .02, etc.), necessary to create a unique identifier for every FEP. As an example, a FEP describing hydrologic processes in the Disturbed Rock Zone could have a FEP identifier such as HR.01.TH.01. Further examples are:

- BB.00.TM.01 Mechanical Effects on Buffer/Backfill
- BB.00.TM.02 Thermal-Mechanical Effects on Buffer/Backfill
- SP.02.CP.01 Shaft Seal Characteristics
- SP.02.TC.01 Chemical Interaction of Groundwater with Shaft Seals

These new FEP designators better indicate where a FEP is mapped in the FEP matrix classification scheme, and the Feature (FF) and Process/Event (PE) characters within the FEP identifiers are more descriptive than strictly numeric identifiers. However, each individual FEP can also be mapped to a traditional NEA-based FEP number if it is desired to maintain traceability to a prior FEP list or to the NEA classification scheme.

It should be noted that Characteristic FEPs (CP) describe the properties of the features or components that need to be evaluated. Characteristics are not typical FEPs (i.e., they cannot be screened in or out), instead they contain characteristic information (and changes to that information) that influences the screening of the other FEPs. For example, the initial radionuclide inventory is considered a characteristic of the waste form, and material properties are considered characteristics of the geosphere features. Finally, more detailed information defining specific features/components (rows in the FEP matrix) and processes/events (columns in the FEP matrix) may be found in Sevougian et al. (2015).

Table A-1. Preliminary FEP screening recommendations for a deep geologic repository for DSNF and DHLW at a generic site in crystalline host rock.

Matrix FEP Number	Description	Associated Processes	Preliminary Screening Recommendations
WF.00.CP.01	Waste Characteristics	- Waste form types - Flow and transport properties (flow type [i.e., porous medium vs. thin film], porosity, permeability, tortuosity, dispersion coefficients, types of colloids and concentrations, other colloidal properties, surface complexation and K_d's) - Properties of any flammable or pyrophoric materials - Spatial heterogeneity of waste forms (waste package scale, emplacement drift/room/repository scale)	
WF.00.TM.01	Dynamic Response of Fuel Rods and Cladding	- (A) Swelling of fuel pellets and corrosion products - (B) Unzipping of cladding - (C) Bending, buckling, or rupture of fuel rods from rock block impacts - (D) Bending or buckling of fuel rods from contact with internal support structures or end caps	(A), (B), (C), and (D) are **Likely Excluded.** Extensive data/analysis may be required to define the initial state of cladding and the probability and effects of clad failure from (A) through (D). If PA does not take credit for cladding as a long-term hydrologic barrier, (A) through (D) will be Excluded.
WF.00.TM.02	Dynamic Loading on Waste Form From Closure of Entries or From Buffer-Backfill Compaction/ Expansion	- (A) Creep closure of the excavation causes deformation, buckling, or cracking of the waste form - (B) Buffer-backfill compaction / expansion causes deformation, buckling or cracking of the waste form - (C) Mechanical stresses generated by Interaction of co-located waste forms	(A) is **Excluded** because creep closure is not expected to occur in crystalline rock. (B) is **Likely Included** because the response of the bentonite buffer is an important consideration in the transient mechanical loading on the waste form and waste package. (C) requires **Evaluation**.
WF.00.TM.03	Dynamic Loading on Waste Form from Rockfall or Drift Collapse	- (A) Rock block impacts cause cracking of vitrified waste forms - (B) Rubble loading deforms the waste forms - (C) Mechanical stresses generated by Interaction of co-located waste forms	(A) requires **Evaluation.** (B) requires **Evaluation.** (C) requires **Evaluation**.
WF.00.TM.04	Pressure Loading on Waste Form from Gas Generation	- (A) Elastic-plastic response of the waste form from internal pressurization due to gas generation - (B) Effects of pyrophoricity or flammable gas from DSNF or DHLW on internal gas pressure	(A) is **Included** for the response to mechanical loading from internal pressurization. (B) requires **Evaluation** for DSNF and spent uranium fuels (B) is **Likely Excluded** for other spent fuels and waste forms
WF.00.TM.05	Thermal-Mechanical Effects in the Waste Form	- (A) Thermally-induced expansion / stress / cracking - (B) Thermally-induced changes in backstress on the waste form - (C) Drift collapse alters thermal environment in the drift and inside the waste package	(A) requires **Evaluation** (B) requires **Evaluation** (C) is **Likely Excluded** because the presence of rubble may not significantly alter the thermal environment when the peak thermal pulse is expected to be less than 100°C.

Matrix FEP Number	Description	Associated Processes	Preliminary Screening Recommendations
WF.00.TH.01	Pressure-Driven Darcy Flow Through Fractures and Porous Media in the Waste Forms	- (A) Pressure-driven flow of liquid (wetting) phase - (B) Pressure-driven flow of gas (non-wetting) phase - (C) Flow of any additional phases (e.g., hydrocarbons) - (D) Pressure-driven flow between fractures and matrix (local non-equilibrium)	(A), (B), (C), and (D) are **Included** because pressure-driven Darcy flow is an important hydrological process in a discrete fracture network.
WF.00.TH.02	Capillarity-Dominated Darcy Flow in the Waste Forms	- (A) Wicking and imbibition (i.e., infiltration without gravity) - (B) Vapor barrier (i.e., reduction in relative liquid permeability at low saturation) - (C) Immiscible phase interaction and displacement - (D) Trapping, discontinuous blobs, or viscous fingering in non-wetting phase	(A), (B), (C), and (D) require **Evaluation**.
WF.00.TH.03	Gravity- and Density-Dominated Flow in the Waste Forms	- (A) Free convection due to density variation (from temperature or salinity effects) - (B) Infiltration and drainage	(A) requires **Evaluation**. (B) is **Likely Included** because these processes may determine the boundary conditions for the flow model.
WF.00.TH.04	Adsorption-Dominated Flow in the Waste Forms (Water held by electrostatic, van der Waals, or hydration forces)	- (A) Thin film flow below residual saturation (i.e., near liquid dry-out) - (B) Hygroscopy (equilibration of solid phase with humidity) - (C) Immobile water in nano-pores or in small-aperture fractures	(A), (B), and (C) require **Evaluation.**
WF.00.TH.05	Diffusion or Dispersion in Miscible Phases in the Waste Forms	- (A) Diffusion of vapor in air phase - (B) Diffusion of dissolved gas in liquid phase	(A) and (B) require **Evaluation.**
WF.00.TH.06	Non-Darcy Flow Through Fractures and Porous Media in the Waste Forms	- (A) High Reynolds number fluid flow in large-aperture fractures - (B) Erosion or sedimentation (i.e., non-chemical plugging) of fractures and flow paths - (C) Threshold gradient flow in low-permeability matrix	(A), (B), and (C) require **Evaluation.**
WF.00.TH.07	Thermal-Hydrological Effects on Flow in Waste Forms	- (A) Convection and conduction of energy via liquid phase - (B) Convection of energy via vapor (i.e., heat pipe) - (C) Fluid density and viscosity changes due to temperature (e.g., thermal expansion of brine) - (D) Phase changes (i.e., condensation, boiling) leading to dry-out or resaturation - (E) Release of water from hydrated minerals during heating - (F) Decrepitation, creation (during reconsolidation), and migration of fluid inclusions - (G) Effects of pyrophoricity	(A) is **Likely Included** because the thermal pulse drives fluid out of the repository. (B), (C), (E), (F), and (G) require **Evaluation**. Coupled thermal-hydrological processes will be most important during the thermal pulse and require Evaluation. (D) is **Likely Excluded** because peak thermal pulse is expected to be less than 100°C.
WF.00.TC.01	Thermal-Chemical Gas Generation in Waste Forms	- (A) Generation of H_2 from corrosion of metals or fuels - (B) Gas generation from pyrophoricity W-1. (C) Generation of flammable gases	(A) is **Included** (B) requires **Evaluation** for DSNF and spent uranium fuels (B) is **Likely Excluded** for other spent fuels and waste forms (C) requires **Evaluation**.

Matrix FEP Number	Description	Associated Processes	Preliminary Screening Recommendations
WF.00.TC.02	Thermal-Chemical Degradation of Organic Materials in Waste	- (A) Degradation of plastic or synthetic rubber compounds without microbial activity	(A) is **Likely Excluded** because the inventory of DSNF and DHLW is not expected to have significant amounts of plastic or synthetic rubber compounds.
WF.00.TB.01	Microbial Activity in Waste Forms	- (A) Effects on corrosion - (B) Formation of complexants (humates, fulvates, organic waste) - (C) Formation of microbial colloids - (D) Formation of biofilms - (E) Biodegradation - (F) Biomass production - (G) Bioaccumulation - (H) CO_2, CH_4, and H_2S generation from microbial degradation - (I) Nitrification - (J) Sulfurization - (K) Methanogenesis	(A) through (K) are **Likely Excluded** because the inventory of DSNF and DHLW is not expected to have significant amounts of organic carbon in the waste.
WF.00.TB.02	Thermal Effects on Microbial Activity in Waste Forms	- (A) Thermal effects on microbial activity	(A) is **Likely Excluded** because the inventory of DSNF and DHLW is not expected to have significant amounts of organic carbon in the waste.
WF.00.TT.01	Transport of Dissolved Radionuclides in the Liquid Phase in Waste Forms	- (A) Advection - (B) Dispersion - (C) Diffusion - (D) Matrix Diffusion - (E) Intra-aqueous complexation - (F) Isotopic dilution - (G) Dilution by mixing with formation waters - (H) Solubility of radionuclides and other species	(A), (B), (C), (D), and (H) are **Included** because they are basic transport processes. (E), (F), and (G) require **Evaluation**.
WF.00.TT.02	Interaction of Dissolved Radionuclides with Stationary Phases in Waste Forms	- (A) Reversible/irreversible physical sorption - (B) Surface complexation - (C) Ion exchange - (D) Precipitation / dissolution, including limited dissolution due to inclusion in secondary phases and enhanced dissolution due to alpha recoil	(A), (B), (C), and (D) are **Included** because they are basic sorption or chemical processes.
WF.00.TT.03	Interaction of Dissolved Radionuclides with Other Mobile Phases (Colloids, Gas Phase) in Waste Forms	- (A) Reversible/irreversible physical sorption - (B) Interactions with organic complexants - (C) Ion exchange - (D) Precipitation / dissolution - (E) Partitioning	(A), (B), (C), (D), and (E) are **Included** because they are basic sorption or chemical processes.
WF.00.TT.04	Coupled Process Effects on Transport of Dissolved Radionuclides in Waste Forms	- (A) Thermal diffusion (Soret effect) - (B) Thermal osmosis - (C) Thermal conduction or convection within the waste form and waste package - (D) Other thermal effects, such as other Onsager relationships	(A), (B), (C), and (D) require **Evaluation**.
WF.00.TT.05	Transport of Radionuclides in the Gas Phase in Waste Forms	- (A) Advection - (B) Diffusion W-2.	(A) and (B) require **Evaluation** for gas phase transport.

Matrix FEP Number	Description	Associated Processes	Preliminary Screening Recommendations
WF.00.TT.06	Formation of Colloids in Waste Forms	- (A) Intrinsic colloids - (B) Pseudo-colloids (host rock fragments, waste form fragments, corrosion products, microbes) - (C) Sorption of radionuclides to colloids	(A), (B), and (C) are **Included** because they are important for transport processes via colloids.
WF.00.TT.07	Transport of Radionuclides on Colloids in Waste Forms	- (A) Advection - (B) Dispersion - (C) Diffusion - (D) Matrix Diffusion - (E) Stability/flocculation (mechanical stability, chemical stability) - (F) Filtration (physical, electrostatic) - (G) Dilution by mixing with formation waters	(A) through (D) are **Included** because they are basic processes for transport via colloids. (E), (F), and (G) require **Evaluation** for the local geochemical environment and types of colloids.
WF.00.TT.08	Interaction of Colloids with Other Phases in Waste Forms	- (A) Reversible/irreversible physical sorption onto stationary phases - (B) Sorption at air-water interfaces	(A) and (B) require **Evaluation** for the local chemical environment and types of colloids
WF.00.TL.01	Heat Generation in Waste Forms - DSNF - Vitrified DHLW - Other (non-glass) DHLW - Metal parts from reprocessing	- (A) Heat generation from radionuclide decay W-3. W-4.	(A) is **Included**.
WF.00.TL.02	Exothermic Reactions in Waste Forms	- (A) Hydration of concrete - (B) Oxidation of DSNF	(A) and (B) require **Evaluation** for relevant exothermic reactions.
WF.00.RA.01	Radioactive Decay and Ingrowth	- (A) Decay chains - (B) Decay products - (C) Neutron activation	(A), (B), and (C) are **Included**.
WF.00.RA.02	Radiolysis in Waste Forms	- (A) He generation from waste form alpha decay - (B) H_2 generation from radiolysis - (C) Altered water chemistry	(A), (B), and (C) require **Evaluation**.
WF.00.RA.03	Radiation Damage to Waste Form	- (A) Enhanced waste form degradation	(A) requires **Evaluation**.
WF.00.CL.01	Climatic Effects on Waste Forms	- (A) Variations in precipitation and temperature - (B) Melt water	(A) and (B) are **Likely Excluded** because climatic effects may not be significant inside the waste packages.
WF.00.SM.01	Dynamic Loading on Waste Form from a Seismic Event	- (A) Thermal-mechanical response of the waste form to ground motion, rockfall, drift collapse, or fault displacement causes deformation or damage. - (B) Bending or buckling of fuel rods or cracking of vitrified waste forms due to ground motion, rockfall, drift collapse, or fault displacement.	(A) and (B) require **Evaluation** because the frequency, magnitude, and consequences of seismic events are **Site-Specific.** .
WF.00.IG.01	Igneous Activity Impacts Waste Forms	- (A) Chemical interaction with magmatic volatiles - (B) Transport of radionuclides in magma, pyro clasts, vents	(A) and (B) require **Evaluation**. The frequency, type, magnitude and consequences of igneous events are **Site-Specific.**
WF.00.IG.02	Dynamic Loading on Waste Form from an Igneous Event	- (A) An igneous intrusion causes thermal-mechanical deformation and damage to the waste form.	(A) is **Site-Specific** and requires **Evaluation.**

Matrix FEP Number	Description	Associated Processes	Preliminary Screening Recommendations
WF.01.CP.01	DSNF and Cladding Properties	- Geometry - Radionuclide inventory - Non-radionuclide inventory - Materials and properties (initial condition, enrichment/burnup, damage) - Fluids, colloids, and their properties (initial saturation, initial water chemistry (pH, ionic strength, p_{CO2}) initial water composition (radionuclides and dissolved species), initial void chemistry (air/gas), initial colloidal concentrations) - Flow and transport properties (flow type [i.e., porous medium vs. thin film], porosity, permeability, tortuosity, dispersion coefficients, surface complexation, and K_d's) - Instant release fraction	
WF.01.TM.01	Thermal-Mechanical DSNF Cladding Degradation and Failure	- (A) Initial damage - (B) Stress corrosion cracking - (C) Unzipping - (D) Creep - (E) Internal pressure - (F) Mechanical impact	(A) through (F) are **Likely Excluded.** Extensive data/analysis may be required to define the initial state of cladding and to define the probability and effects of clad failure from (A) through (F). If PA does not take credit for cladding as a long-term hydrologic barrier, (A) through (F) will be Excluded.
WF.01.TC.01	Evolution of the Water Chemistry in DSNF and Cladding	- (A) Speciation - (B) Oxidation/reduction processes, reaction kinetics - (C) Dissolution, reaction kinetics - (D) Precipitation, inclusion in secondary phase, reaction kinetics - (E) Formation and filtration of colloids - (F) Effect of sorption - (G) Solubility of radionuclides and other species - (H) Thermal-chemical interactions with waste form / WP components, including chemical effects on fluid density - (I) Thermal-chemical interaction with corrosion products, including effects on fluid density - (J) Thermal-chemical Interaction with intruding fluids, including effects on fluid density - (K) Chemical interaction with gas phase - (L) Osmotic stress and osmotic binding	(A), (B), (C), (D), (E), (F), and (G) are **Likely Included** because they are basic chemistry processes. (H) through (L) require **Evaluation**.
WF.01.TC.02	UO_2 Degradation	- (A) Thermal-chemical alteration processes - (B) Oxidation/reduction processes, reaction kinetics, interaction with metals - (C) Dissolution / leaching, including limited dissolution due to inclusion in secondary phases and enhanced dissolution due to alpha recoil - (D) Thermal cracking - (E) Thermally-enhanced corrosion - (F) Radiolysis and altered water chemistry	(A), (B), (C), (D), (E), and (F) require **Evaluation**.

Matrix FEP Number	Description	Associated Processes	Preliminary Screening Recommendations
WF.01.TC.03	Na-Bonded Fuel Degradation	- (A) Thermal-chemical alteration processes - (B) Oxidation/reduction processes, reaction kinetics, interaction with metals - (C) Dissolution / leaching, including enhanced dissolution from alpha recoil and limited dissolution due to inclusion in secondary phases - (D) Thermal cracking - (E) Thermally-enhanced corrosion - (F) Radiolysis and altered water chemistry	(A), (B), (C), (D), (E), and (F) require **Evaluation**.
WF.01.TC.04	Graphite-Bonded Fuel Degradation	- (A) Thermal-chemical alteration processes - (B) Oxidation/reduction processes, reaction kinetics, interaction with metals - (C) Dissolution / leaching, including enhanced dissolution due to alpha recoil and limited dissolution due to inclusion in secondary phases - (D) Thermal cracking - (E) Thermally-enhanced corrosion - (F) Radiolysis and altered water chemistry	(A), (B), (C), (D), (E), and (F) require **Evaluation**.
WF.01.TC.05	Thermal-Chemical DSNF Cladding Degradation and Failure	- (A) Thermal-chemical alteration processes - (B) Oxidation/reduction processes, reaction kinetics, interaction with metals - (C) Dissolution / leaching, including enhanced dissolution due to alpha recoil - (D) Thermal cracking - (E) General Corrosion - (F) Microbially-influenced corrosion - (G) Localized corrosion and/or stress-corrosion cracking - (H) Enhanced corrosion (silica, fluoride) - (I) Hydride cracking - (J) Radiolysis and altered water chemistry	(A) through (H) **Likely Excluded.** Extensive data/analysis may be required to define the initial state of cladding and the probability and effects of clad failure from (A) through (J). If PA does not take credit for cladding as a long-term barrier, (A) through (J) will be excluded.
WF.02.CP.01	Vitrified DHLW Properties	- Geometry - Radionuclide inventory - Non-radionuclide inventory - Materials and properties (initial condition, damage, corrosion products) - Fluids, colloids, and their properties (initial saturation, initial water chemistry (pH, ionic strength, p_{CO2}) initial water composition (radionuclides and dissolved species), initial void chemistry (air/gas), initial colloidal concentrations) - Flow and transport properties (flow type [i.e., porous medium vs. thin film], porosity, permeability, tortuosity, dispersion coefficients, surface complexation, and K_d's)	

Matrix FEP Number	Description	Associated Processes	Preliminary Screening Recommendations
WF.02.TC.01	Evolution of the Water Chemistry in Vitrified DHLW	- (A) Speciation - (B) Oxidation/reduction processes, reaction kinetics - (C) Dissolution, reaction kinetics - (D) Precipitation, inclusion in secondary phase, reaction kinetics - (E) Formation and filtration of colloids - (F) Effect of sorption - (G) Solubility of radionuclides and other species - (H) Thermal-chemical interactions with waste form / WP components, including chemical effects on fluid density - (I) Thermal-chemical interaction with corrosion products, including effects on fluid density - (J) Thermal-chemical Interaction with intruding fluids, including effects on fluid density - (K) Interaction with gas phase - (L) Osmotic stress and osmotic binding	(A) through (L) require **Evaluation**.
WF.02.TC.02	Glass Degradation	- (A) Thermal-chemical alteration processes and recrystallization - (B) Oxidation/reduction processes, reaction kinetics, interaction with metals - (C) Dissolution / leaching, including enhanced dissolution due to alpha recoil and limited dissolution due to inclusion in secondary phases - (D) Thermal cracking - (E) Thermally-enhanced corrosion - (F) Radiolysis and altered water chemistry	(A), (B), (C), (D), (E), and (F) require **Evaluation**.
WF.03.CP.01	Other (Non-Glass) DHLW Properties	- Geometry - Radionuclide inventory - Non-radionuclide inventory - Materials and properties (initial condition, damage, corrosion products) - Fluids, colloids, and their properties (initial saturation, initial water chemistry (pH, ionic strength, p_{CO2}) initial water composition (radionuclides and dissolved species), initial void chemistry (air/gas), initial colloidal concentrations) - Flow and transport properties (flow type [i.e., porous medium vs. thin film], porosity, permeability, tortuosity, dispersion coefficients, surface complexation, and K_d's)	

Matrix FEP Number	Description	Associated Processes	Preliminary Screening Recommendations
WF.03.TC.01	Evolution of the Water Chemistry in Other (Non-Glass) DHLW Forms	- (A) Speciation - (B) Oxidation/reduction processes, reaction kinetics - (C) Dissolution, reaction kinetics - (D) Precipitation, inclusion in secondary phase, reaction kinetics - (E) Formation and filtration of colloids - (F) Effect of sorption - (G) Solubility of radionuclides and other species - (H) Thermal-chemical interactions with waste form / WP components, including chemical effects on fluid density - (I) Thermal-chemical interaction with corrosion products, including effects on fluid density - (J) Thermal-chemical Interaction with intruding fluids, including effects on fluid density - (K) Interaction with gas phase - (L) Osmotic stress and osmotic binding	(A) through (L) require **Evaluation**.
WF.03.TC.02	Degradation of Other (Non-Glass) DHLW	- (A) Thermal-chemical alteration processes and recrystallization - (B) Oxidation/reduction processes, reaction kinetics, interaction with metals - (C) Dissolution / leaching, including enhanced dissolution due to alpha recoil and limited dissolution due to inclusion in secondary phases - (D) Thermal cracking - (E) Thermally-enhanced corrosion - (F) Radiolysis and altered water chemistry	(A), (B), (C), (D), (E), and (F) require **Evaluation**.
WF.04.CP.01	Metal Parts from Reprocessing Properties	- Geometry - Radionuclide inventory - Non-radionuclide inventory - Materials and properties (initial condition, damage, corrosion products) - Fluids, colloids, and their properties (initial saturation, initial water chemistry (pH, ionic strength, p_{CO2}) initial water composition (radionuclides and dissolved species), initial void chemistry (air/gas), initial colloidal concentrations) - Flow and transport properties (flow type [i.e., porous medium vs. thin film], porosity, permeability, tortuosity, dispersion coefficients, surface complexation, and K_d's)	

Matrix FEP Number	Description	Associated Processes	Preliminary Screening Recommendations
WF.04.TC.01	Evolution of the Water Chemistry in Metals Parts from Reprocessing	- (A) Speciation - (B) Oxidation/reduction processes, reaction kinetics - (C) Dissolution, reaction kinetics - (D) Precipitation, inclusion in secondary phase, reaction kinetics - (E) Formation and filtration of colloids - (F) Effect of sorption - (G) Solubility of radionuclides and other species - (H) Thermal-chemical interactions with waste form / WP components, including chemical effects on fluid density - (I) Thermal-chemical interaction with corrosion products, including effects on fluid density - (J) Thermal-chemical Interaction with intruding fluids, including effects on fluid density - (K) Interaction with gas phase - (L) Osmotic stress and osmotic binding	(A) through (L) require **Evaluation**.
WF.04.TC.02	Degradation of Metals Parts from Reprocessing	- (A) Thermal-chemical alteration processes - (B) Oxidation/reduction processes, reaction kinetics, interaction with metals - (C) Dissolution / leaching - (D) Thermal cracking - (E) Thermally-enhanced corrosion - (F) Radiolysis and altered water chemistry	(A), (B), (C), (D), (E), and (F) require **Evaluation**.
WP.00.CP.01	Waste Package Characteristics	- Waste package types - Spatial heterogeneity of waste packages (emplacement drift/room scale, repository scale) - Co-located waste forms	
WP.00.TM.01	Dynamic Loading on Waste Package From Closure of Entries or From Buffer-Backfill Compaction/ Expansion	- (A) Creep closure of the entries causes deformation, buckling, or cracking of the waste package - (B) Buffer-backfill compaction / expansion near the package causes deformation, buckling or rupture of the waste package - (C) Creep closure or buffer-backfill compaction / expansion causes deformation or failure of the internal support structures in the waste package - (D) Swelling of corrosion products	(A) is **Excluded** because creep closure is not expected to occur in crystalline rock. (B), (C), and (D) are **Included** for compaction / expansion of the buffer-backfill because the response of the buffer is an important consideration in the transient mechanical loading on the waste form and waste package. (C) is **Excluded** for creep closure because it is not expected to occur in crystalline rock.

Matrix FEP Number	Description	Associated Processes	Preliminary Screening Recommendations
WP.00.TM.02	Dynamic Loading on Waste Package from Rockfall or Drift Collapse	- (A) Rock block impacts cause bending, buckling, or rupture of the inner / outer corrosion barriers - (B) Rock block impacts damage the internal support structures in the waste package - (C) Deformation of the waste package from rubble loading - (D) The presence of rubble from rockfall may limit the damage to the waste package from future events. - (E) The presence of buffer or backfill material around the waste package may mitigate the loads from rock block impacts or from drift collapse	(A), (B), (C), (D), and (E) require **Evaluation** for the specific discrete fracture network in the host rock and for the specific design of the repository.
WP.00.TM.03	Pressure Loading on the Waste Package from Gas Generation	- (A) Elastic-plastic response of the waste package to internal pressurization due to gas generation - (B) Elastic-plastic response of the waste package to external pressurization caused by entry closure - (C) Effects of pyrophoricity or flammable gas from DSNF or DHLW on internal gas pressure	(A) is **Included** for the response to mechanical loading from internal pressurization. (B) is **Likely Excluded** because entry closure will not be significant in crystalline rock. (C) requires **Evaluation** for DSNF and spent uranium fuels (C) is **Likely Excluded** for other spent fuels and waste forms
WP.00.TM.04	Thermal-Mechanical Effects in the Waste Package	- (A) Thermally-induced expansion / stress / cracking - (B) Thermal acceleration of buffer / backfill compaction / expansion changes backstress on the waste package - (C) Drift collapse alters thermal environment in the drift and around the waste package - (D) Thermal sensitization / phase changes - (E) Waste package movement / lifting / sinking	(A) requires **Evaluation** (B) requires **Evaluation** (C) is **Likely Excluded** because the peak thermal pulse is expected to be less than 100°C. (D) is **Likely Excluded** because the peak thermal pulse is expected to be less than 100°C. (E) requires **Evaluation**.
WP.00.TH.01	Pressure-Driven Darcy Flow Through Fractures and Porous Media in the Waste Packages	- (A) Pressure-driven flow of liquid (wetting) phase - (B) Pressure-driven flow of gas (non-wetting) phase - (C) Flow of any additional phases (e.g., hydrocarbons) - (D) Pressure-driven flow between fractures and matrix (local non-equilibrium	(A), (B), (C), and (D) are **Included** because pressure-driven Darcy flow is an important hydrological process.
WP.00.TH.02	Capillarity-Dominated Darcy Flow in the Waste Packages	- (A) Wicking and imbibition (i.e., infiltration without gravity) - (B) Vapor barrier (i.e., reduction in relative liquid permeability at low saturation) - (C) Immiscible phase interaction and displacement - (D) Trapping, discontinuous blobs, or viscous fingering in non-wetting phase	(A), (B), (C), and (D) require **Evaluation**.

Matrix FEP Number	Description	Associated Processes	Preliminary Screening Recommendations
WP.00.TH.03	Gravity- and Density-Dominated Flow in the Waste Packages	- (A) Free convection due to density variation (from temperature or salinity effects) - (B) Infiltration and drainage - (C) Dripping and ponding	(A) requires **Evaluation**. (B) is **Likely Included** because these processes determine the boundary conditions for the flow model. (C) requires **Evaluation**.
WP.00.TH.04	Adsorption-Dominated Flow in the Waste Packages (Water held by electrostatic, van der Waals, or hydration forces)	- (A) Thin film flow below residual saturation (i.e., near liquid dry-out) - (B) Hygroscopy (equilibration of solid phase with humidity) - (C) Immobile water in nano-pores or in small-aperture fractures	(A), (B), and (C) require **Evaluation.**
WP.00.TH.05	Diffusion or Dispersion in Miscible Phases in the Waste Packages	- (A) Diffusion of vapor in air phase - (B) Diffusion of dissolved gas in liquid phase	(A) and (B) require **Evaluation.**
WP.00.TH.06	Non-Darcy Flow Through Fractures and Porous Media in the Waste Packages	- (A) High Reynolds number fluid flow in large-aperture fractures - (B) Erosion or sedimentation (i.e., non-chemical plugging) of fractures and flow paths - (C) Threshold gradient flow in low-permeability matrix	(A), (B), and (C) require **Evaluation.**
WP.00.TH.07	Thermal-Hydrological Effects on Flow in the Waste Packages	- (A) Convection and conduction of energy via liquid phase - (B) Convection of energy via vapor (i.e., heat pipe) - (C) Fluid density and viscosity changes due to temperature (e.g., thermal expansion of brine) - (D) Phase changes (i.e., condensation, boiling) leading to dry-out or resaturation - (E) Release of water from hydrated minerals during heating - (F) Decrepitation, creation (during reconsolidation), and migration of fluid inclusions - (G) Effects of pyrophoricity or flammable gas from DSNF or DHLW	(A) is **Likely Included** because the thermal pulse drives fluid out of the repository. (B), (C), (E), (F), and (G) require **Evaluation**. Coupled thermal-hydrological processes will be most important during the thermal pulse and require Evaluation. (D) is **Likely Excluded** because the peak thermal pulse is expected to be less than 100°C.
WP.00.TH.08	Thermal-Hydrological Effects on Exterior Surface of the Waste Packages	- (A) Dripping onto surface of waste packages - (B) Ponding on waste packages - (C) Thin-film flow near dry-out on surface of waste packages - (D) Hygroscopy (equilibration of waste package surface with humidity) - (E) Non-Darcy (i.e., high Reynolds number) open-channel fluid flow on surface of waste package - (F) Phase changes (i.e., condensation or boiling) on surface of waste package	(A), (B), (C), (D), and (E) require **Evaluation**. (F) is **Likely Excluded** because the peak thermal pulse is expected to be less than 100°C.
WP.00.TC.01	Gas Generation Inside Waste Packages	- (A) H_2 generation from corrosion of the inner waste package walls and internal supports - (B) Gas generation from pyrophoricity - (C) Generation of flammable gases	(A) is **Included** (B) requires **Evaluation** for DSNF and spent uranium fuels (B) is **Likely Excluded** for other spent fuels and waste forms (C) requires **Evaluation**.
WP.00.TC.02	Gas Generation Outside Waste Packages	- (A) Anoxic corrosion of metal - (B) Aerobic corrosion of metal - (C) Thermal-chemical degradation of organic material - (D) Generation of flammable gases	(A) and (B) are **Included.** (C) is **Likely Excluded** because the repository is not expected to have significant amounts of organic carbon. (D) requires **Evaluation.**

Matrix FEP Number	Description	Associated Processes	Preliminary Screening Recommendations
WP.00.TC.03	General Corrosion of Waste Packages	- (A) Dry-air oxidation - (B) Humid-air corrosion - (C) Aqueous phase corrosion - (D) Passive film formation and stability	(A), (B), and (C) are **Included** because they are basic corrosion processes. (D) requires **Evaluation**.
WP.00.TC.04	Stress Corrosion Cracking (SCC) of Waste Packages	- (A) Crack initiation, growth and propagation - (B) Stress distribution around cracks	(A) and (B) require **Evaluation**.
WP.00.TC.05	Localized Corrosion of Waste Packages	- (A) Pitting - (B) Crevice corrosion - (C) Salt deliquescence	(A) and (B) are **Likely Included**. (C) requires **Evaluation**.
WP.00.TC.06	Hydride Cracking of Waste Packages	- (A) Hydrogen diffusion through metal matrix - (B) Crack initiation and growth in metal hydride phases - (C) Hydrogen embrittlement	(A), (B), and (C) require **Evaluation**.
WP.00.TC.07	Internal Corrosion of Waste Packages Prior to Breach	- (A) Corrosion prior to breach	(A) is Design-Specific and requires **Evaluation**.
WP.00.TC.08	Electrochemical Effects in Waste Packages	- (A) Enhanced metal corrosion	(A) is Design Specific and requires **Evaluation**.
WP.00.TC.09	Chemical Interactions Between Co-Located Waste	- (A) Interaction of corrosion products, groundwater species, complexants, and actinides from multiple waste forms in the same waste package	(A) is **Design-Specific** and requires **Evaluation**.
WP.00.TC.10	Evolution of the Water Chemistry in Waste Packages	- (A) Speciation - (B) Oxidation/reduction processes, reaction kinetics - (C) Dissolution, reaction kinetics - (D) Precipitation, inclusion in secondary phase, reaction kinetics - (E) Formation and filtration of colloids - (F) Effect of sorption - (G) Solubility of radionuclides and other species - (H) Thermal-chemical interactions with waste forms / WP components, including chemical effects on fluid density - (I) Thermal-chemical interaction with corrosion products, including effects on fluid density - (J) Thermal-chemical Interaction with intruding fluids, including effects on fluid density - (K) Interaction with gas phase - (L) Osmotic stress and osmotic binding	(A), (B), (C), (D), (E), (F), and (G) are **Likely Included** because they are basic chemistry processes. (H) through (L) require **Evaluation**.
WP.00.TB.01	Microbial Activity in Waste Packages	- (A) Microbial effects on corrosion - (B) Formation of complexants W-5. (humates, fulvates, organic waste) - (C) Formation of microbial colloids - (D) Formation of biofilms - (E) Biodegradation - (F) Biomass production - (G) Bioaccumulation - (H) CO_2, CH_4, H_2O and H_2S generation from microbial degradation - (I) Nitrification - (J) Sulfurization - (K) Methanogenesis	(A) through (K) are **Likely Excluded** because the inventory of DSNF and DHLW is not expected to have significant amounts of organic carbon.

Matrix FEP Number	Description	Associated Processes	Preliminary Screening Recommendations
WP.00.TB.02	Thermal Effects on Microbial Activity in Waste Packages	-(A) Thermal effects on microbial activity	(A) is **Likely Excluded** because the inventory of DSNF and DHLW is not expected to have significant amounts of organic carbon.
WP.00.TB.03	Thermal-Microbial Activity on External Surfaces of the Waste Packages	-(A) Microbial-enhanced corrosion on the surface of the waste packages -(B) Formation and biodegradation of colloids, biomass, and biofilms on the surface of the waste packages	(A) and (B) are **Likely Excluded** because the waste emplacement areas are not expected to have significant amounts of organic carbon
WP.00.TT.01	Transport of Dissolved Radionuclides in the Liquid Phase in Waste Packages	-(A) Advection -(B) Dispersion -(C) Diffusion -(D) Matrix Diffusion -(E) Intra-aqueous complexation -(F) Isotopic dilution -(G) Dilution by mixing with formation waters -(H) Solubility of radionuclides and other species	(A), (B), (C), (D), and (H) are **Included** because they are basic transport processes. (E), (F), and (G) require **Evaluation**.
WP.00.TT.02	Interaction of Dissolved Radionuclides with Stationary Phases in Waste Packages	-(A) Reversible/irreversible physical sorption -(B) Surface complexation -(C) Ion exchange -(D) Precipitation / dissolution, including limited dissolution due to inclusion in secondary phases and enhanced dissolution due to alpha recoil	(A), (B), (C), and (D) are **Included** because they are basic sorption or chemical processes.
WP.00.TT.03	Interaction of Dissolved Radionuclides with Other Mobile Phases (Colloids, Gas Phase) in Waste Packages	-(A) Reversible/irreversible physical sorption -(B) Interactions with organic complexants -(C) Ion exchange -(D) Precipitation / dissolution -(E) Partitioning	(A), (B), (C), (D), and (E) are **Included** because they are basic sorption or chemical processes.
WP.00.TT.04	Coupled Process Effects on Transport of Dissolved Radionuclides in Waste Packages	-(A) Thermal diffusion (Soret effect) -(B) Thermal osmosis -(C) Thermal conduction or convection to adjacent components (buffer/backfill/host rock) -(D) Other thermal effects, such as other Onsager relationships	(A), (B), (C), and (D) require **Evaluation**.
WP.00.TT.05	Transport of Radionuclides in the Gas Phase in Waste Packages	-(A) Advection -(B) Diffusion W-6.	(A) and (B) require **Evaluation** for gas phase transport.
WP.00.TT.06	Formation of Colloids in Waste Packages	-(A) Intrinsic colloids -(B) Pseudo-colloids (host rock fragments, waste form fragments, corrosion products, microbes) -(C) Sorption of radionuclides to colloids	(A), (B), and (C) are **Included** because they are basic sorption or chemical processes.
WP.00.TT.07	Transport of Radionuclides on Colloids in Waste Packages	-(A) Advection -(B) Dispersion -(C) Diffusion -(D) Matrix Diffusion -(E) Stability/flocculation (mechanical stability, chemical stability) -(F) Filtration (physical, electrostatic) -(G) Dilution by mixing with formation waters	(A) through (D) are **Included** because they are basic processes for transport via colloids. (E), (F), and (G) require **Evaluation** for the local geochemical environment and types of colloids.
WP.00.TT.08	Interaction of Colloids with Other Phases in Waste Packages	-(A) Reversible/irreversible physical sorption onto stationary phases -(B) Sorption at air-water interfaces	(A) and (B) require **Evaluation** for the local chemical environment and types of colloids

Matrix FEP Number	Description	Associated Processes	Preliminary Screening Recommendations
WP.00.TT.09	Interaction of Dissolved Radionuclides with Stationary Phases on the Exterior Surface of the Waste Package	- (A) Reversible/irreversible physical sorption with waste package surface - (B) Surface complexation on waste package surface - (C) Ion exchange on waste package surface - (D) Precipitation and dissolution on waste package surface	(A), (B), (C), and (D) require **Evaluation**.
WP.00.TL.01	Exothermic Reactions in Waste Packages	- (A) Hydration of concrete - (B) Reactions with waste package internals	(A) and (B) are **Design-Specific** and require **Evaluation**.
WP.00.TL.02	Heat Transfer in Waste Packages	- (A) Conduction - (B) Convection - (C) Radiation	(A) is **Included**. (B) requires **Likely Included**. (C) requires **Evaluation**.
WP.00.RA.01	Radiolysis in Waste Packages	- (A) Helium generation from alpha decay in the waste form - (B) H_2 generation from radiolysis - (C) Altered water chemistry	(A), (B), and (C) require **Evaluation**.
WP.00.RA.02	Radiation Damage to Waste Package	- (A) Enhanced waste package degradation	(A) requires **Evaluation**.
WP.00.RA.03	Radiological Mutation of Microbes	- (A) Radiation-induced mutation of microbes within a waste package	(A) is **Likely Excluded** because of the lack of organic carbon in DSNF or DHLW.
WP.00.CL.01	Climatic Effects on Waste Packages	- (A) Variations in precipitation and temperature - (B) Melt water	(A) and (B) are **Likely Excluded** because climatic effects may not be significant inside the waste packages.
WP.00.NC.01	Criticality In-Package	- (A) Formation of critical configuration	(A) requires **Evaluation**.
WP.00.EF.01	Early Failure of Waste Packages	- (A) Manufacturing defects - (B) Improper sealing - (C) Error in emplacement	(A), (B), and (C) are **Design-Specific** and require **Evaluation**.
WP.00.SM.01	Dynamic Loading on Waste Package from a Seismic Event	- (A) Thermal-mechanical response of the waste package to ground motion, rockfall, drift collapse, or fault displacement. - (B) Bending, cracking, or rupture of the inner / outer corrosion barriers during a seismic event - (C) Deformation, bending, or cracking of the internal support structures in the waste package during a seismic event	(A), (B), and (C) require **Evaluation** because the frequency, type, magnitude and consequences of igneous events are **Site-Specific**.
WP.00.IG.01	Igneous Activity Impacts Waste Packages	- (A) Chemical interaction with magmatic volatiles - (B) Transport of radionuclides in magma, pyro clasts, vents	(A) and (B) require **Evaluation** because the frequency, type, magnitude and consequences of igneous events are **Site-Specific**.
WP.00.IG.02	Dynamic Loading on Waste Package from an Igneous Event	- (A) An igneous intrusion causes thermal-mechanical deformation, bending, or cracking of the waste package and its inner support structures.	(A) is **Site-Specific** and requires **Evaluation**.
WP.00.HE.01	Human Intrusion (Deliberate or Inadvertent) - Effects on Waste Packages	- (A) Drilling (resource exploration, …) - (B) Mining / tunneling - (C) Nonintrusive site investigation (airborne, surface-based, …)	(A) and (B) are **Site-Specific** and require **Evaluation**. (C) is **Excluded** because it is a nonintrusive process.

Matrix FEP Number	Description	Associated Processes	Preliminary Screening Recommendations
WP.01.CP.01	Waste Package for DSNF Design and Properties	- Geometry - Flow pathways - Materials and properties (initial condition / damage / corrosion products) (porosity, tortuosity, diffusion coefficients, sorption/surface complexation properties, chemical potential) - Fluids, colloids, and their properties (initial saturation, initial water chemistry (pH, ionic strength, p_{CO2}) initial water composition (radionuclides and dissolved species), initial void chemistry (air/gas), initial colloidal concentrations) - Flow and transport properties (flow type [i.e., porous medium vs. thin film], porosity, permeability, tortuosity, dispersion coefficients, surface complexation, and K_d's)	
WP.02.CP.01	Waste Package for Vitrified DHLW Design and Properties	- Geometry - Materials and properties (initial condition / damage / corrosion products) - Fluids, colloids, and their properties (initial saturation, , initial water chemistry (pH, ionic strength, p_{CO2}) initial water composition (radionuclides and dissolved species), initial void chemistry (air/gas), initial colloidal concentrations) - Flow and transport properties (flow type [i.e., porous medium vs. thin film], porosity, permeability, tortuosity, dispersion coefficients, surface complexation, and K_d's)	
WP.03.CP.01	Waste Package for Other DHLW Design and Properties	- Geometry - Materials and properties (initial condition / damage / corrosion products) - Fluids, colloids, and their properties (initial saturation, , initial water chemistry (pH, ionic strength, p_{CO2}) initial water composition (radionuclides and dissolved species), initial void chemistry (air/gas), initial colloidal concentrations) - Flow and transport properties (flow type [i.e., porous medium vs. thin film], porosity, permeability, tortuosity, dispersion coefficients, surface complexation, and K_d's)	

Matrix FEP Number	Description	Associated Processes	Preliminary Screening Recommendations
WP.04.CP.01	Waste Package for Metal Parts from Reprocessing Design and Properties	- Geometry - Materials and properties (initial condition / damage / corrosion products) - Fluids, colloids, and their properties (initial saturation, , initial water chemistry (pH, ionic strength, p_{CO2}) initial water composition (radionuclides and dissolved species), initial void chemistry (air/gas), initial colloidal concentrations) - Flow and transport properties (flow type [i.e., porous medium vs. thin film], porosity, permeability, tortuosity, dispersion coefficients, surface complexation, and K_d's)	
BB.00.TL.01	Exothermic Reactions in Buffer/Backfill	- (A) Hydration of concrete	(A) is **Design-Specific** and requires **Evaluation**.
BB.00.TL.02	Effects of Buffer/Backfill on Thermal Environment	- (A) Thermal blanket - (B) Condensation - (C) Heat transfer via conduction, convection, or radiation	(A) is **Likely Excluded** because the presence of rubble may not significantly alter the thermal environment when the peak thermal pulse is expected to be less than 100°C. (B) requires **Evaluation**. (C) is **Included** for conduction, **Likely Included** for convection, and requires **Evaluation** for radiation
BB.00.RA.01	Radiolysis in Buffer/Backfill	- (A) He generation from alpha decay in buffer/backfill - (B) H_2 generation from radiolysis - (C) Altered water chemistry	(A), (B), and (C) require **Evaluation**.
BB.00.RA.02	Radiation Damage to Buffer/Backfill	- (A) Enhanced buffer degradation - (B) Enhanced backfill degradation	(A) and (B) require **Evaluation**.
BB.00.RA.03	Radiological Mutation of Microbes	- (A) Radiation-induced mutation of microbes in buffer/backfill materials	(A) is **Likely Excluded** because of the lack of organic carbon in DSNF or DHLW.
BB.00.CL.01	Climatic Effects on Buffer and Backfill	- (A) Variations in precipitation and temperature - (B) Buffer/backfill erosion arising from glaciation	(A) and (B) are **Likely Excluded** because climatic effects may not be significant in the buffer-backfill.
BB.00.NC.01	Criticality in Buffer/Backfill	- (A) Formation of critical configuration	(A) requires **Evaluation**.
BB.00.EF.01	Early Failure of Buffer/Backfill	- (A) Error in emplacement - (B) Inadequate construction	(A) and (B) are **Design-Specific** and require **Evaluation.**
BB.00.HE.01	Human Intrusion (Deliberate or Inadvertent) - Effects on Buffer/Backfill	- (A) Drilling (resource exploration, …) - (B) Mining / tunneling - (C) Nonintrusive site investigation (airborne, surface-based, …)	(A) and (B) require **Evaluation** because they are **Site-Specific**. (C) is **Excluded** because it is a nonintrusive process.
BB.01.CP.01	Buffer Design and Properties	- Geometry - Materials and properties - Fluids, colloids, and their properties - Flow and transport properties (flow type [i.e., porous medium vs. thin film], porosity, permeability, tortuosity, dispersion coefficients, surface complexation, and K_d's)	(A) and (B) require **Evaluation** because they are **Site-Specific**. (C) is **Excluded** because it is a nonintrusive process.

Matrix FEP Number	Description	Associated Processes	Preliminary Screening Recommendations
BB.01.TM.01	Dynamic Loading on Buffer From Closure of Boreholes or Entries	- (A) Creep closure of the emplacement borehole causes compaction / expansion of the buffer - (B) Creep closure of the entries causes compaction / expansion of buffer - (C) Compaction or reconsolidation of buffer alters backstress on waste package - (D) Non-thermally-induced volume changes (e.g., swelling, cracking, corrosion products) - (E) Mechanical changes from erosion / dissolution	(A) and (B) are **Excluded** because creep closure is not expected to occur in crystalline rock. (C) and (D) are **Likely Included** because volume changes, including compaction or reconsolidation, are important processes for determining backstress on the waste package. (E) requires **Evaluation**.
BB.01.TM.02	Dynamic Loading on Buffer from Rockfall or Drift Collapse	- (A) Rock block impacts cause compaction / expansion of buffer - (B) Rubble loading causes compaction / expansion of buffer - (C) The presence of rubble from rockfall may limit the damage to the buffer from future events.	(A), (B), and (C) require **Evaluation** for the discrete fracture network at a candidate site.
BB.01.TM.03	Thermal-Mechanical Effects in Buffer	- (A) Thermally-induced changes to the rates of compaction / expansion in the buffer - (B) Dry-out of the buffer may cause cracking and change mechanical properties of the buffer material - (C) Thermally-induced volume changes (expansion / stress / cracking) - (D) Buffer settlement or compaction / expansion alters temperatures in the buffer near the waste package - (E) Thermal alteration or thermally-accelerated backstress from buffer	(A) requires **Evaluation.** (B) is **Likely Excluded** because the peak thermal pulse is less than 100°C. (C) requires **Evaluation**. (D) is **Likely Excluded** because the peak thermal pulse is less than 100°C. (E) is **Likely Included.**
BB.01.TH.01	Pressure-Driven Darcy Flow Through Fractures and Porous Media in the Buffer	- (A) Pressure-driven flow of liquid (wetting) phase - (B) Pressure-driven flow of gas (non-wetting) phase - (C) Flow of any additional phases (e.g., hydrocarbons) - (D) Pressure-driven flow between fractures and matrix (local non-equilibrium	(A), (B), (C), and (D) are **Included** because pressure-driven Darcy flow is an important hydrological process.
BB.01.TH.02	Capillarity-Dominated Darcy Flow in the Buffer	- (A) Wicking and imbibition (i.e., infiltration without gravity) - (B) Vapor barrier (i.e., reduction in relative liquid permeability at low saturation) - (C) Immiscible phase interaction and displacement - (D) Trapping, discontinuous blobs, or viscous fingering in non-wetting phase	(A) and (B) are **Included** because the bentonite backfill is a key hydrological barrier. (C) and (D) require **Evaluation**.
BB.01.TH.03	Gravity- and Density-Dominated Flow in the Buffer	- (A) Free convection due to density variation (from temperature or salinity effects) - (B) Infiltration and drainage	(A) requires **Evaluation**. (B) is **Likely Included** because these processes determine the hydrologic condition in the bentonite buffer.
BB.01.TH.04	Adsorption-Dominated Flow in the Buffer (Water held by electrostatic, van der Waals, or hydration forces)	- (A) Thin film flow below residual saturation (i.e., near liquid dry-out) - (B) Hygroscopy (equilibration of solid phase with humidity) - (C) Immobile water in nano-pores or in small-aperture fractures	(A), (B), and (C) require **Evaluation.**

Matrix FEP Number	Description	Associated Processes	Preliminary Screening Recommendations
BB.01.TH.05	Diffusion or Dispersion in Miscible Phases in the Buffer	- (A) Diffusion of vapor in air phase - (B) Diffusion of dissolved gas in liquid phase	(A) and (B) require **Evaluation.**
BB.01.TH.06	Non-Darcy Flow Through Fractures and Porous Media in the Buffer	- (A) High Reynolds number fluid flow in large-aperture fractures - (B) Erosion or sedimentation (i.e., non-chemical plugging) of fractures and flow paths - (C) Threshold gradient flow in low-permeability matrix	(A), (B), and (C) require **Evaluation.**
BB.01.TH.07	Thermal-Hydrological Effects on Flow in the Buffer	- (A) Convection and conduction of energy via liquid phase - (B) Convection of energy via vapor (i.e., heat pipe) - (C) Fluid density and viscosity changes due to temperature (e.g., thermal expansion of brine) - (D) Phase changes (i.e., condensation, boiling) leading to dry-out or resaturation - (E) Release of water from hydrated minerals during heating - (F) Decrepitation, creation (during reconsolidation), and migration of fluid inclusions	(A) is **Likely Included** because the thermal pulse drives fluid out of the repository. (B), (C), (E), (F), and (G) require **Evaluation**. Coupled thermal-hydrological processes will be most important during the thermal pulse and require Evaluation. (D) is **Likely Excluded** because peak thermal pulse is expected to be less than 100°C.
BB.01.TC.01	Evolution of the Water Chemistry in Buffer	- (A) Speciation - (B) Oxidation/reduction processes, reaction kinetics - (C) Dissolution, reaction kinetics - (D) Precipitation, inclusion in secondary phase, reaction kinetics - (E) Formation and filtration of colloids - (F) Effect of sorption - (G) Solubility of radionuclides and other species - (H) Thermal-chemical interactions with waste forms / WP components, including chemical effects on fluid density - (I) Thermal-chemical interaction with corrosion products, including effects on fluid density - (J) Thermal-chemical Interaction with intruding fluids and the host rock, including effects on fluid density - (K) Interaction with gas phase - (L) Osmotic stress and osmotic binding	(A), (B), (C), (D), (E), (F), and (G) are **Likely Included** because they are basic chemistry processes. (H) through (L) require **Evaluation**.
BB.01.TC.02	Thermal-Chemical Degradation of Buffer	- (A) Thermal-chemical alteration processes - (B) Oxidation/reduction processes, reaction kinetics, interaction with metals - (C) Dissolution / leaching - (D) Thermal expansion/cracking - (E) Thermally-enhanced corrosion - (F) Radiolysis and altered water chemistry	(A), (B), (C), (D), (E), and (F) require **Evaluation**.

Matrix FEP Number	Description	Associated Processes	Preliminary Screening Recommendations
BB.01.TB.01	Microbial Activity in Buffer	- (A) Microbial effects on corrosion - (B) Formation of complexants (humates, fulvates, organics) - (C) Formation of microbial colloids - (D) Formation of biofilms - (E) Biodegradation - (F) Biomass production - (G) Bioaccumulation - (H) CO_2, CH_4, H_2O and H_2S generation from microbial degradation - (I) Nitrification - (J) Sulfurization - (K) Methanogenesis	(A) through (K) are **Likely Excluded** because the bentonite buffer is not expected to support long-term microbial activity.
BB.01.TB.02	Thermal Effects on Microbial Activity in Buffer	- (A) Thermal effects on microbial activity	(A) is **Likely Excluded** because the bentonite buffer is not expected to support microbial activity.
BB.01.TT.01	Transport of Dissolved Radionuclides in the Liquid Phase in Buffer	- (A) Advection - (B) Dispersion - (C) Diffusion - (D) Matrix Diffusion - (E) Intra-aqueous complexation - (F) Isotopic dilution - (G) Dilution by mixing with formation waters - (H) Solubility of radionuclides and other species	(A), (B), (C), (D), and (H) are **Included** because they are basic transport processes. (E), (F), and (G) require **Evaluation**.
BB.01.TT.02	Interaction of Dissolved Radionuclides with Stationary Phases in Buffer	- (A) Reversible/irreversible physical sorption - (B) Surface complexation - (C) Ion exchange - (D) Precipitation / dissolution, including limited dissolution due to inclusion in secondary phases and enhanced dissolution due to alpha recoil	(A), (B), (C), and (D) are **Included** because they are basic sorption or chemical processes.
BB.01.TT.03	Interaction of Dissolved Radionuclides with Other Mobile Phases (Colloids, Gas Phase) in Buffer	- (A) Reversible/irreversible physical sorption - (B) Interactions with organic complexants - (C) Ion exchange - (D) Precipitation / dissolution - (E) Partitioning	(A), (B), (C), (D), and (E) are **Included** because they are basic sorption or chemical processes.
BB.01.TT.04	Coupled Process Effects on Transport of Dissolved Radionuclides in Buffer	- (A) Thermal diffusion (Soret effect) - (B) Thermal osmosis - (C) Thermal conduction to adjacent components and the host rock - (D) Other thermal effects, such as other Onsager relationships	(A), (B), (C), and (D) require **Evaluation**.
BB.01.TT.05	Transport of Radionuclides in the Gas Phase in Buffer	- (A) Advection - (B) Diffusion	(A) and (B) require further **Evaluation** for gas phase transport.
BB.01.TT.06	Formation of Colloids in Buffer	- (A) Intrinsic colloids - (B) Pseudo-colloids (host rock fragments, waste form fragments, corrosion products, microbes) - (C) Sorption of radionuclides to colloids	(A), (B), and (C) are **Included** because they are important for transport via colloids.

Matrix FEP Number	Description	Associated Processes	Preliminary Screening Recommendations
BB.01.TT.07	Transport of Radionuclides on Colloids in Buffer	- (A) Advection - (B) Dispersion - (C) Diffusion - (D) Matrix Diffusion - (E) Stability/flocculation (mechanical stability, chemical stability) - (F) Filtration (physical, electrostatic) - (G) Dilution by mixing with formation waters	(A), (B), (C), and (D) are **Included** because they are basic processes for transport via colloids. (E), (F), and (G) require **Evaluation** for the local geochemical environment and the types of colloids.
BB.01.TT.08	Interaction of Colloids with Other Phases in Buffer	- (A) Reversible/irreversible physical sorption onto stationary phases - (B) Sorption at air-water interfaces	(A) and (B) require **Evaluation**.
BB.01.SM.01	Dynamic Loading on Buffer from a Seismic Event	- (A) Mechanical damage to buffer from ground motion, rockfall, drift collapse, or fault displacement	(A) requires **Evaluation** because the frequency, magnitude, and consequences of seismic events are **Site-Specific**
BB.01.IG.01	Igneous Activity Impacts Buffer	- (A) Chemical interaction with magmatic volatiles - (B) Transport of radionuclides in magma, pyro clasts, vents	(A) and (B) require **Evaluation** because the frequency, type, magnitude and consequences of igneous events are **Site-Specific**.
BB.01.IG.02	Dynamic Loading on Buffer from an Igneous Event	- (A) An igneous intrusion causes thermal-mechanical deformation of the buffer	(A) is **Site-Specific** and requires **Evaluation**.
BB.02.CP.01	Backfill Design and Properties	- Geometry - Materials and properties - Fluids, colloids, and their properties - Flow and transport properties (flow type [i.e., porous medium vs. thin film], porosity, permeability, tortuosity, dispersion coefficients, surface complexation, and K_d's)	
BB.02.TM.01	Dynamic Loading on Backfill From Closure of Boreholes or Entries	- (A) Creep closure of the entries causes compaction / expansion of backfill - (B) Compaction or reconsolidation of backfill alters backstress on entry walls or on waste package - (C) Non-thermally-induced volume changes (e.g., swelling, cracking, corrosion products) - (D) Mechanical changes from erosion / dissolution	(A) is **Excluded** because creep closure is not expected to occur in crystalline rock. (B) is **Likely Included** because compaction or reconsolidation, are important processes for determining backstress on the waste package. (C) and (D) require **Evaluation**.
BB.02.TM.02	Dynamic Loading on Backfill from Rockfall or Drift Collapse	- (A) Rock block impacts cause compaction / expansion of backfill - (B) Rubble loading causes compaction / expansion of backfill -	(A) and (B) require **Evaluation** for the discrete fracture network at a candidate site.
BB.02.TM.03	Thermal-Mechanical Effects in Backfill	- (A) Thermally-induced changes to the rates of compaction / expansion in the backfill - (B) Dry-out of the backfill may change mechanical properties - (C) Thermally-induced volume changes (expansion / stress / cracking) - (D) Backfill settlement or compaction / expansion alters temperatures in the entries - (E) Thermal alteration or thermally-accelerated backstress from backfill	(A), (C), (D), and (E) require **Evaluation**. (B) is **Likely Excluded** because the peak thermal pulse is less than 100°C.

Matrix FEP Number	Description	Associated Processes	Preliminary Screening Recommendations
BB.02.TH.01	Pressure-Driven Darcy Flow Through Fractures and Porous Media in the Backfill	- (A) Pressure-driven flow of liquid (wetting) phase - (B) Pressure-driven flow of gas (non-wetting) phase - (C) Flow of any additional phases (e.g., hydrocarbons) - (D) Pressure-driven flow between fractures and matrix (local non-equilibrium	(A), (B), (C), and (D) are **Included** because pressure-driven Darcy flow is an important hydrological process.
BB.02.TH.02	Capillarity-Dominated Darcy Flow in the Backfill	- (A) Wicking and imbibition (i.e., infiltration without gravity) - (B) Vapor barrier (i.e., reduction in relative liquid permeability at low saturation) - (C) Immiscible phase interaction and displacement - (D) Trapping, discontinuous blobs, or viscous fingering in non-wetting phase	(A) is **Included** because it is a key process for determining the hydrologic conditions in the backfill. (B), (C), and (D) require **Evaluation**.
BB.02.TH.03	Gravity- and Density-Dominated Flow in the Backfill	- (A) Free convection due to density variation (from temperature or salinity effects) - (B) Infiltration and drainage - (C) Dripping through or ponding at the bottom of the backfill	(A) and (C) require **Evaluation**. (B) is **Likely Included** because these processes are important for determining the hydrologic conditions in the backfill.
BB.02.TH.04	Adsorption-Dominated Flow in the Backfill (Water held by electrostatic, van der Waals, or hydration forces)	- (A) Thin film flow below residual saturation (i.e., near liquid dry-out) - (B) Hygroscopy (equilibration of solid phase with humidity) - (C) Immobile water in nano-pores or in small-aperture fractures	(A), (B), and (C) require **Evaluation.**
BB.02.TH.05	Diffusion or Dispersion in Miscible Phases in the Backfill	- (A) Diffusion of vapor in air phase - (B) Diffusion of dissolved gas in liquid phase	(A) and (B) require **Evaluation.**
BB.02.TH.06	Non-Darcy Flow Through Fractures and Porous Media in the Backfill	- (A) High Reynolds number fluid flow in large-aperture fractures - (B) Erosion or sedimentation (i.e., non-chemical plugging) of fractures and flow paths - (C) Threshold gradient flow in low-permeability matrix	(A), (B), and (C) require **Evaluation.**
BB.02.TH.07	Thermal-Hydrological Effects on Flow in Backfill	- (A) Convection and conduction of energy via liquid phase - (B) Convection of energy via vapor (i.e., heat pipe) - (C) Fluid density and viscosity changes due to temperature (e.g., thermal expansion of brine) - (D) Phase changes (i.e., condensation, boiling) leading to dry-out or resaturation - (E) Release of water from hydrated minerals during heating - (F) Decrepitation, creation (during reconsolidation), and migration of fluid inclusions	(A) is **Likely Included** because the thermal pulse drives fluid out of the repository. (B), (C), (E), and (F) require **Evaluation**. (D) is **Likely Excluded** because peak thermal pulse is expected to be less than 100°C.

Matrix FEP Number	Description	Associated Processes	Preliminary Screening Recommendations
BB.02.TC.01	Evolution of the Water Chemistry in Backfill	- (A) Speciation - (B) Oxidation/reduction processes, reaction kinetics - (C) Dissolution, reaction kinetics, - (D) Precipitation, inclusion in secondary phase, reaction kinetics - (E) Formation and filtration of colloids - (F) Effect of sorption - (G) Solubility of radionuclides and other species - (H) Thermal-chemical interactions with waste forms /EBS WP components / MW components, including chemical effects on fluid density - (I) Thermal-chemical interaction with corrosion products, including effects on fluid density - (J) Thermal-chemical Interaction with intruding fluids, including effects on fluid density components, and with the host rock - (K) Interaction with gas phase - (L) Osmotic stress and osmotic binding	(A), (B), (C), (D), (E), (F), and (G) are **Likely Included** because they are basic chemistry processes. (H) through (L) require **Evaluation**.
BB.02.TC.02	Thermal-Chemical Degradation of Backfill	- (A) Thermal-chemical alteration processes - (B) Oxidation/reduction processes, reaction kinetics, interaction with metals - (C) Dissolution / leaching - (D) Thermal expansion/cracking - (E) Thermally-enhanced corrosion - (F) Radiolysis and altered water chemistry	(A), (B), (C), (D), (E), and (F) require **Evaluation**.
BB.02.TB.01	Microbial Activity in Backfill	- (A) Microbial effects on corrosion - (B) Formation of complexants - (C) Formation of microbial colloids - (D) Formation of biofilms - (E) Biodegradation - (F) Biomass production - (G) Bioaccumulation - (H) CO_2, CH_4, H_2O and H_2S generation from microbial degradation - (I) Nitrification - (J) Sulfurization - (K) Methanogenesis	(A) through (K) are **Likely Excluded** because the backfill is not expected to support long-term microbial activity.
BB.02.TB.02	Thermal Effects on Microbial Activity in Backfill	- (A) Thermal effects on microbial activity	(A) is **Likely Excluded** because the backfill is not expected to support long-term microbial activity.
BB.02.TT.01	Transport of Dissolved Radionuclides in the Liquid Phase in Backfill	- (A) Advection - (B) Dispersion - (C) Diffusion - (D) Matrix Diffusion - (E) Intra-aqueous complexation - (F) Isotopic dilution - (G) Dilution by mixing with formation waters - (H) Solubility of radionuclides and other species	(A), (B), (C), (D), and (H) are **Included** because they are basic transport processes. (E), (F), and (G) require **Evaluation**.

Matrix FEP Number	Description	Associated Processes	Preliminary Screening Recommendations
BB.02.TT.02	Interaction of Dissolved Radionuclides with Stationary Phases in Backfill	-(A) Reversible/irreversible physical sorption -(B) Surface complexation -(C) Ion exchange -(D) Precipitation / dissolution, including limited dissolution due to inclusion in secondary phases and enhanced dissolution due to alpha recoil	(A), (B), (C), and (D) are **Included** because they are basic sorption or chemical processes.
BB.02.TT.03	Interaction of Dissolved Radionuclides with Other Mobile Phases (Colloids, Gas Phase) in Backfill	-(A) Reversible/irreversible physical sorption -(B) Interactions with organic complexants -(C) Ion exchange -(D) Precipitation / dissolution -(E) Partitioning	(A), (B), (C), (D), and (E) are **Included** because they are basic sorption or chemical processes.
BB.02.TT.04	Coupled Process Effects on Transport of Dissolved Radionuclides in Backfill	-(A) Thermal diffusion (Soret effect) -(B) Thermal osmosis -(C) Thermal conduction or convection to adjacent components and the host rock -(D) Other thermal effects, such as other Onsager relationships	(A), (B), (C), and (D) require **Evaluation**.
BB.02.TT.05	Transport of Radionuclides in the Gas Phase in Backfill	-(A) Advection -(B) Diffusion	(A) and (B) require **Evaluation** for gas phase transport.
BB.02.TT.06	Formation of Colloids in Backfill	-(A) Intrinsic colloids -(B) Pseudo-colloids (host rock fragments, waste form fragments, corrosion products, microbes) -(C) Sorption of radionuclides to colloids	(A), (B), and (C) are **Included** because these processes are important for transport via colloids.
BB.02.TT.07	Transport of Radionuclides on Colloids in Backfill	-(A) Advection -(B) Dispersion -(C) Diffusion -(D) Matrix Diffusion -(E) Stability/flocculation (mechanical stability, chemical stability) -(F) Filtration (physical, electrostatic) -(G) Dilution by mixing with formation waters	(A), (B), (C), and (D) are **Included** because they are important for transport via colloids. (E), (F), and (G) require **Evaluation** for the local geochemical environment and types of colloids.
BB.02.TT.08	Interaction of Colloids with Other Phases in Backfill	-(A) Reversible/irreversible physical sorption onto stationary phases -(B) Sorption at air-water interfaces	(A) and (B) require **Evaluation.**
BB.02.SM.01	Dynamic Loading on Backfill from a Seismic Event	-(A) Mechanical damage to backfill from ground motion, rockfall, drift collapse, or fault displacement	(A) requires **Evaluation** because the frequency, magnitude, and consequences of seismic events are **Site-Specific**
BB.02.IG.01	Igneous Activity Impacts Backfill	-(A) Chemical interaction with magmatic volatiles -(B) Transport of radionuclides in magma, pyro clasts, vents	(A) and (B) require **Evaluation** because the frequency, type, magnitude and consequences of igneous events are **Site-Specific**.
BB.02.IG.02	Dynamic Loading on Backfill from an Igneous Event	-(A) An igneous intrusion causes thermal-mechanical deformation of the backfill	(A) is **Site-Specific** and requires **Evaluation**.
MW.00.CP.01	Design of Mine Workings	-Geometry -Components -Materials and properties (initial condition / damage / corrosion products) -Flow and transport properties (flow type [i.e., porous medium vs. thin film], porosity, permeability, tortuosity, dispersion coefficients, surface complexation, and K_d's)	

Matrix FEP Number	Description	Associated Processes	Preliminary Screening Recommendations
MW.00.TM.01	Dynamic Loading on Mine Workings from Closure of Entries	- (A) Creep closure of the entries causes deformation and failure of the drift/tunnel/room supports, the liners, or the open excavations - (B) Floor heave or spalling from the walls and back causes deformation and failure of the mine workings. - (C) Non-thermally-induced volume changes (e.g., swelling, cracking, corrosion products) - (D) Changes in mechanical loads from erosion or dissolution	(A) is **Excluded** because creep closure is not expected to occur in crystalline rock. (B) requires **Evaluation** for the discrete fracture network.at a candidate site. (C) and (D) require **Evaluation**.
MW.00.TM.02	Dynamic Loading on Mine Workings from Rockfall or Drift Collapse	- (A) Rock block impacts cause bending, buckling, or rupture of the drift/tunnel/room supports or liners - (B) Rubble loading causes deformation of the mine workings	(A) and (B) require **Evaluation** for the discrete fracture network at a candidate site.
MW.00.TM.03	Pressure Loading on the Mine Workings from Gas Generation	- (A) Elastic-plastic response of the mine workings to pressurization caused by gas generation, gas explosion, or entry closure W-7.	(A) is **Likely Excluded** for entry closure because it will not be significant in crystalline rock. (A) is **Likely Included** for gas generation from corrosion of metal components. (A) requires **Evaluation** for gas explosions.
MW.00.TM.04	Thermal-Mechanical Effects on or from Mine Workings	- (A) Thermally-accelerated convergence / rockfall / drift collapse / floor buckling - (B) Thermally-induced volume changes(expansion/stress/cracking) - (C) Thermal blanket from drift collapse or backfill consolidation	(A) requires **Evaluation** for the discrete fracture network at a candidate site**.** (B) requires **Evaluation**. (C) is **Likely Excluded** because the presence of rubble may not significantly alter the thermal environment when the peak thermal pulse is expected to be less than 100°C.
MW.00.TH.01	Pressure-Driven Darcy Flow Through the Mine Workings	- (A) Pressure-driven flow of liquid (wetting) phase - (B) Pressure-driven flow of gas (non-wetting) phase - (C) Flow of any additional phases (e.g., hydrocarbons)	(A), (B), and (C) are **Included** because pressure-driven Darcy flow is an important hydrological process.
MW.00.TH.02	Capillarity-Dominated Darcy Flow Through the Mine Workings	- (A) Wicking and imbibition (i.e., infiltration without gravity) - (B) Vapor barrier (i.e., reduction in relative liquid permeability at low saturation) - (C) Immiscible phase interaction and displacement - (D) Trapping or discontinuous blobs in non-wetting phase	(A) is **Included** because it is a key process for determining the hydrologic conditions in the mine workings. (B), (C), and (D) require **Evaluation**.
MW.00.TH.03	Gravity- and Density-Dominated Flow Through the Mine Workings	- (A) Free convection due to density variation (from temperature or salinity effects) - (B) Infiltration and drainage - (C) Dripping	(A) and (C) require **Evaluation**. (B) is **Likely Included** because these processes are important for determining the hydrologic conditions in the mine workings.
MW.00.TH.04	Adsorption-Dominated Flow Through the Mine Workings (Water held by electrostatic, van der Waals, or hydration forces)	- (A) Thin film flow below residual saturation (i.e., near liquid dry-out) - (B) Hygroscopy (equilibration of solid phase with humidity) - (C) Immobile water in nano-pores or in small-aperture fractures	(A), (B), and (C) require **Evaluation.**
MW.00.TH.05	Diffusion or Dispersion in Miscible Phases Through the Drift/Tunnel/Room Supports	- (A) Diffusion of vapor in air phase - (B) Diffusion of dissolved gas in liquid phase	(A) and (B) require **Evaluation.**

Matrix FEP Number	Description	Associated Processes	Preliminary Screening Recommendations
MW.00.TH.06	Non-Darcy Flow Through the Drift/Tunnel/Room Supports	- (A) High Reynolds number fluid flow in large-aperture fractures - (B) Erosion or sedimentation (i.e., non-chemical plugging) of fractures and flow paths - (C) Threshold gradient flow in low-permeability matrix	(A), (B), and (C) require **Evaluation.**
MW.00.TH.07	Thermal-Hydrological Effects on Flow in the Drift/Tunnel/Room Supports	- (A) Convection and conduction of energy via liquid phase - (B) Convection of energy via vapor (i.e., heat pipe) - (C) Fluid density and viscosity changes due to temperature (e.g., thermal expansion of brine) - (D) Phase changes (i.e., condensation, boiling) leading to dry-out or resaturation - (E) Release of water from hydrated minerals during heating	(A) is **Likely Included** because the thermal pulse drives fluid out of the repository. (B), (C), and (E) require **Evaluation**. (D) is **Likely Excluded** because peak thermal pulse is expected to be less than 100°C.
MW.00.TC.01	Evolution of Water Chemistry in Mine Workings (no drift collapse)	- (A) Speciation - (B) Oxidation/reduction processes, reaction kinetics - (C) Dissolution, reaction kinetics - (D) Precipitation, inclusion in secondary phase, reaction kinetics - (E) Formation and filtration of colloids - (F) Effect of sorption - (G) Solubility of radionuclides and other species - (H) Thermal-chemical interactions with other WP / MW components, including chemical effects on fluid density - (I) Thermal-chemical interaction with corrosion products, including effects on fluid density - (J) Thermal-chemical Interaction with intruding fluids, host rock, and backfill, including effects on fluid density - (K) Interaction with gas phase - (L) Osmotic stress and osmotic binding	(A), (B), (C), (D), (E), (F), and (G) are **Likely Included** because they are important chemical processes. (H) through (L) require **Evaluation**.
MW.00.TC.02	Evolution of Water Chemistry in Mine Workings After Drift Collapse	- (A) Evolution of water chemistry in mine workings due to altered seepage and altered rock contact with MW components after drift collapse - (B) Thermal-chemical reactions from waste-to-host rock contact, including effects on fluid density - (C) Thermal-chemical reactions from MW component-to-host rock contact, including effects on fluid density - (D) Chemical effects on fluid density	(A) is **Likely Included** because it defines the chemical evolution of groundwaters in the mine workings. (B), (C), and (D) require **Evaluation.**
MW.00.TC.03	Electrochemical Effects in Mine Workings	- (A) Thermally-enhanced metal corrosion	(A) is **Design-Specific** and requires **Evaluation.**

Matrix FEP Number	Description	Associated Processes	Preliminary Screening Recommendations
MW.00.TC.04	Thermal-Chemical Degradation of Mine Workings	-(A) Thermal-chemical alteration processes -(B) Oxidation/reduction processes, reaction kinetics, interaction with metals -(C) Dissolution / leaching -(D) Cracking induced by thermal-chemical alteration -(E) Enhanced corrosion -(F) Radiolysis and altered water chemistry	(A), (B), (C), (D), (E), and (F) require **Evaluation**.
MW.00.TB.01	Microbial Activity in Mine Workings	-(A) Microbial effects on corrosion -(B) Formation of complexants -(C) Formation of microbial colloids -(D) Formation of biofilms -(E) Biodegradation -(F) Biomass production -(G) Bioaccumulation -(H) CO_2, CH_4, H_2O and H_2S generation from microbial degradation -(I) Nitrification -(J) Sulfurization -(K) Methanogenesis	(A) through (K) are **Likely Excluded** because the waste does not contain significant amounts of organic carbon that could support long-term microbial activity in the mine workings.
MW.00.TB.02	Thermal Effects on Microbial Activity in Mine Workings	-(A) Thermal effects on microbial activity	(A) is **Likely Excluded** because the waste does not contain significant amounts of organic carbon that could support long-term microbial activity in the mine workings.
MW.00.TT.01	Transport of Dissolved Radionuclides in the Liquid Phase in Mine Workings	-(A) Advection -(B) Dispersion -(C) Diffusion -(D) Matrix Diffusion -(E) Intra-aqueous complexation -(F) Isotopic dilution -(G) Dilution by mixing with formation waters -(H) Solubility of radionuclides and other species	(A), (B), (C), (D), and (H) are **Included** because they are basic transport processes. (E), (F), and (G) require **Evaluation**.
MW.00.TT.02	Interaction of Dissolved Radionuclides with Stationary Phases in Mine Workings	-(A) Reversible/irreversible physical sorption -(B) Surface complexation -(C) Ion exchange -(D) Precipitation / dissolution, including limited dissolution due to inclusion in secondary phases and enhanced dissolution due to alpha recoil	(A), (B), (C), and (D) are **Included** because they are basic sorption or chemical processes.
MW.00.TT.03	Interaction of Dissolved Radionuclides with Other Mobile Phases (Colloids, Gas Phase) in Mine Workings	-(A) Reversible/irreversible physical sorption -(B) Interactions with organic complexants -(C) Ion exchange -(D) Precipitation / dissolution -(E) Partitioning	(A), (B), (C), (D), and (E) are **Included** because they are basic sorption or chemical processes.
MW.00.TT.04	Coupled Process Effects on Transport of Dissolved Radionuclides in Mine Workings	-(A) Thermal diffusion (Soret effect) -(B) Thermal osmosis -(C) Thermal conduction or convection to adjacent components and the host rock -(D) Other thermal effects, such as other Onsager relationships	(A), (B), (C), and (D) require **Evaluation.**
MW.00.TT.05	Transport of Radionuclides in the Gas Phase in Mine Workings	-(A) Advection -(B) Diffusion W-8.	(A) and (B) require **Evaluation** for gas phase transport.

Matrix FEP Number	Description	Associated Processes	Preliminary Screening Recommendations
MW.00.TT.06	Formation of Colloids in Mine Workings	- (A) Intrinsic colloids - (B) Pseudo-colloids (host rock fragments, waste form fragments, corrosion products, microbes) - (C) Sorption of radionuclides to colloids	(A), (B), and (C) are **Included** because these processes are important for transport via colloids.
MW.00.TT.07	Transport of Radionuclides on Colloids in Mine Workings	- (A) Advection - (B) Dispersion - (C) Diffusion - (D) Matrix Diffusion - (E) Stability/flocculation (mechanical stability, chemical stability) - (F) Filtration (physical, electrostatic) - (G) Dilution by mixing with formation waters	(A), (B), (C), and (D) are **Included** because they are important for transport via colloids. (E), (F), and (G) require **Evaluation** for the local geochemical environment and types of colloids.
MW.00.TT.08	Interaction of Colloids with Other Phases in Mine Workings	- (A) Reversible/irreversible physical sorption onto stationary phases - (B) Sorption at air-water interfaces	(A) and (B) require **Evaluation**.
MW.00.TL.01	Exothermic Reactions in Mine Workings	- (A) Hydration of concrete W-9.	(A) is **Design-Specific** and requires **Evaluation.**
MW.00.TL.02	Effects of Drift Collapse on Thermal Environment in Mine Workings	- (A) Thermal blanket - (B) Condensation - (C) Changes in influx may affect temperature and relative humidity - (D) Conduction - (E) Convection - (F) Radiation	(A) is **Likely Excluded** because the presence of rubble may not significantly alter the thermal environment when the peak thermal pulse is expected to be less than 100°C. (B) and (C) require **Evaluation**. (D) is **Included**. (E) requires **Likely Included**. (F) requires **Evaluation**.
MW.00.RA.01	Radiolysis in Mine Workings	- (A) He generation from alpha decay in the mined workings - (B) H_2 generation from radiolysis - (C) Altered water chemistry	(A), (B), and (C) require **Evaluation**.
MW.00.RA.02	Radiation Damage to Mine Workings	- (A) Enhanced degradation of MW components (liner/rock reinforcement materials, and waste support structures	(A) is **Design-Specific** and requires **Evaluation**.
MW.00.RA.03	Radiological Mutation of Microbes in Mine Workings	- (A) Radiation-induced mutation of microbes within mined workings	(A) is **Likely Excluded** because of the lack of organic carbon in DSNF or DHLW.
MW.00.CL.01	Climatic Effects on Mine Workings	- (A) Variations in precipitation and temperature - (B) Melt water	(A) and (B) are **Likely Excluded** because climatic effects may not be significant in the Mine Workings.
MW.00.NC.01	Criticality in Mine Workings	- (A) Formation of critical configuration	(A) requires **Evaluation**.
MW.00.EF.01	Early Failure of Mine Workings	- (A) Inadequate construction	(A) is **Design-Specific** and requires **Evaluation.**
MW.00.SM.01	Dynamic Loading on Mine Workings from a Seismic Event	- (A) Mechanical damage to drift/tunnel/room supports or liners from ground motion, rockfall, drift collapse, fault displacement	(A) requires **Evaluation** for a candidate site. The frequency, magnitude, and consequences of seismic events are **Site-Specific.**
MW.00.IG.01	Igneous Activity Impacts Mine Workings	- (A) Chemical interaction with magmatic volatiles - (B) Transport of radionuclides in magma, pyro clasts, vents	(A) and (B) require **Evaluation** for a candidate site. The frequency, type, magnitude and consequences of igneous events are **Site-Specific.**

Matrix FEP Number	Description	Associated Processes	Preliminary Screening Recommendations
MW.00.IG.02	Dynamic Loading on Mine Workings from an Igneous Event	- (A) An igneous intrusion causes thermal-mechanical deformation of the drift/tunnel/room supports or the liners	(A) is **Site-Specific** and requires **Evaluation.**
MW.00.HE.01	Human Intrusion (Deliberate or Inadvertent) - Effects on Mine Workings	- (A) Drilling (resource exploration, …) - (B) Mining / tunneling - (C) Nonintrusive site investigation (airborne, surface-based, …)	(A) and (B) are **Site-Specific** and require **Evaluation**. (C) is **Excluded** because it is a nonintrusive process.
SP.00.CP.01	Design and Properties of Seals and Plugs	- Geometry - Materials and properties (initial condition / damage / corrosion products) - Fluids, colloids, and their properties - Flow and transport properties (flow type [i.e., porous medium vs. thin film], porosity, permeability, tortuosity, dispersion coefficients, surface complexation, and K_d's)	
SP.00.TM.01	Dynamic Loading on Seals/Plugs from Closure of Entries, Shafts, and Boreholes	- (A) Creep closure of the entries, shafts, or boreholes causes deformation and failure of the drift/room seals, shaft seals, or borehole plugs - (B) Non-thermally-induced volume changes (e.g., swelling, cracking, corrosion products) - (C) Changes in mechanical loads from erosion or dissolution at the surface of a seal/plug - (D) Backstress on the host rock from seals and plugs	(A) is **Excluded** because creep closure is not expected to occur in crystalline rock (B), (C), and (D) require **Evaluation**.
SP.00.TM.02	Dynamic Loading on Seals/Plugs from Rockfall or Drift Collapse	- (A) Rock block impacts cause failure of drift/tunnel seals - (B) Rubble loading causes deformation of the drift/tunnel seals	(A) and (B) require **Evaluation** for the local geologic conditions near the seals/plugs.
SP.00.TM.03	Thermal-Mechanical Effects on or from Seals and Plugs	- (A) Heat of hydration of concrete or other exothermic reaction in seal-plug changes thermal environment - (B) Thermally-enhanced backstress from closure of entries, shafts or boreholes cracks or fails drift/tunnel seals, shaft seals or borehole plugs - (C) Thermally-enhanced compaction / expansion of backfill as a long-term seal or plug material - (D) Thermally-induced volume changes(expansion/stress/cracking)	(A) is **Design-Specific** and requires **Evaluation**. (B), (C), and (D) require **Evaluation**.
SP.00.TH.01	Pressure-Driven Darcy Flow Through Fractures and Porous Media in Seals and Plugs	- (A) Pressure-driven flow of liquid (wetting) phase - (B) Pressure-driven flow of gas (non-wetting) phase - (C) Flow of any additional phases (e.g., hydrocarbons) - (D) Pressure-driven flow between fractures and matrix (local non-equilibrium)	(A), (B), (C), and (D) are **Included** because pressure-driven Darcy flow is an important hydrological process.
SP.00.TH.02	Capillarity-Dominated Darcy Flow In Seals and Plugs	- (A) Wicking and imbibition (i.e., infiltration without gravity) - (B) Vapor barrier (i.e., reduction in relative liquid permeability at low saturation) - (C) Immiscible phase interaction and displacement - (D) Trapping, discontinuous blobs, or viscous fingering in non-wetting phase	(A), (B), (C), and (D) require **Evaluation**.

Matrix FEP Number	Description	Associated Processes	Preliminary Screening Recommendations
SP.00.TH.03	Gravity- and Density-Dominated Flow In Seals and Plugs	- (A) Free convection due to density variation (from temperature or salinity effects) - (B) Infiltration and drainage	(A) requires **Evaluation**. (B) is **Likely Included** because these processes determine the hydrologic condition in the shafts and boreholes.
SP.00.TH.04	Adsorption-Dominated Flow In Seals and Plugs (Water held by electrostatic, van der Waals, or hydration forces)	- (A) Thin film flow below residual saturation (i.e., near liquid dry-out) - (B) Hygroscopy (equilibration of solid phase with humidity) - (C) Immobile water in nano-pores or small-aperture fractures	(A), (B), and (C) require **Evaluation.**
SP.00.TH.05	Diffusion or Dispersion in Miscible Phases In Seals and Plugs	- (A) Diffusion of vapor in air phase - (B) Diffusion of dissolved gas in liquid phase	(A) and (B) require **Evaluation.**
SP.00.TH.06	Non-Darcy Flow Through Fractures and Porous Media In Seals and Plugs	- (A) High Reynolds number fluid flow in large-aperture fractures - (B) Erosion or sedimentation (i.e., non-chemical plugging) of fractures and flow paths - (C) Threshold gradient flow in low-permeability matrix	(A), (B), and (C) require **Evaluation.**
SP.00.TH.07	Thermal-Hydrological Effects on Flow in Seals and Plugs	- (A) Convection and conduction of energy via liquid phase - (B) Convection of energy via vapor (i.e., heat pipe) - (C) Fluid density and viscosity changes due to temperature (e.g., thermal expansion of brine) - (D) Phase changes (i.e., condensation, boiling) leading to dry-out or resaturation - (E) Release of water from hydrated minerals during heating - (F) Decrepitation, creation (during reconsolidation), and migration of fluid inclusions	(A) is **Likely Included** because the thermal pulse drives fluid out of the repository. (B), (C), (E), and (F) require **Evaluation**. (D) is **Likely Excluded** because peak thermal pulse is expected to be less than 100°C.
SP.00.TB.01	Microbial Activity in Seals and Plugs	- (A) Microbial effects on corrosion - (B) Formation of complexants - (C) Formation of microbial colloids - (D) Formation of biofilms - (E) Biodegradation - (F) Biomass production - (G) Bioaccumulation - (H) CO_2, CH_4, H_2O and H_2S generation from microbial degradation - (I) Nitrification - (J) Sulfurization - (K) Methanogenesis	(A) through (K) are **Likely Excluded** because the seals or plugs are not expected to support long-term microbial activity.
SP.00.TB.02	Thermal Effects on Microbial Activity in Seals and Plugs	- (A) Thermal effects on microbial activity	(A) is **Likely Excluded** because the seals or plugs are not expected to support microbial activity.
SP.00.TT.01	Transport of Dissolved Radionuclides in the Liquid Phase in Seals and Plugs	- (A) Advection - (B) Dispersion - (C) Diffusion - (D) Matrix Diffusion - (E) Intra-aqueous complexation - (F) Isotopic dilution - (G) Dilution by mixing with formation waters - (H) Solubility of radionuclides and other species	(A), (B), (C), (D), and (H) are **Included** because they are basic transport processes. (E), (F), and (G) require **Evaluation**.

Matrix FEP Number	Description	Associated Processes	Preliminary Screening Recommendations
SP.00.TT.02	Interaction of Dissolved Radionuclides with Stationary Phases (Rock Matrix, Fracture Surfaces) in Seals and Plugs	-(A) Reversible/irreversible physical sorption -(B) Surface complexation -(C) Ion exchange -(D) Precipitation / dissolution, including limited dissolution due to inclusion in secondary phases and enhanced dissolution due to alpha recoil	(A), (B), (C), and (D) are **Included** because they are basic sorption or chemical processes.
SP.00.TT.03	Interaction of Dissolved Radionuclides with Other Mobile Phases (Colloids, Gas Phase) in Seals and Plugs	-(A) Reversible/irreversible physical sorption -(B) Interactions with organic complexants -(C) Ion exchange -(D) Precipitation / dissolution -(E) Partitioning	(A), (B), (C), (D), and (E) are **Included** because they are basic sorption or chemical processes.
SP.00.TT.04	Coupled Process Effects on Transport of Dissolved Radionuclides in Seals and Plugs	-(A) Thermal diffusion (Soret effect) -(B) Thermal osmosis W-10. (C) Thermal conduction or convection to the host rock -(D) Other thermal effects, such as other Onsager relationships	(A), (B), (C), and (D) require **Evaluation**.
SP.00.TT.05	Transport of Radionuclides in the Gas Phase in Seals and Plugs	-(A) Advection -(B) Diffusion W-11.	(A) and (B) require **Evaluation** for gas phase transport.
SP.00.TT.06	Formation of Colloids in Seals and Plugs	-(A) Intrinsic colloids -(B) Pseudo-colloids (host rock fragments, waste form fragments, corrosion products, microbes) -(C) Sorption of radionuclides to colloids	(A), (B), and (C) are **Included** because these processes are important for transport via colloids.
SP.00.TT.07	Transport of Radionuclides on Colloids in Seals and Plugs	-(A) Advection -(B) Dispersion -(C) Diffusion -(D) Matrix Diffusion -(E) Stability/flocculation (mechanical stability, chemical stability) -(F) Filtration (physical, electrostatic) -(G) Dilution by mixing with formation waters	(A), (B), (C), and (D) are **Included** because they are important for transport via colloids. (E), (F), and (G) require **Evaluation** for the local geochemical environment and types of colloids.
SP.00.TT.08	Interaction of Colloids with Other Phases (Rock Matrix, Fracture Surfaces) in Seals and Plugs	-(A) Reversible/irreversible physical sorption onto stationary phases -(B) Sorption at air-water interfaces	(A) and (B) require **Evaluation**.
SP.00.TL.01	Exothermic Reactions in Seals and Plugs	-(A) Hydration of concrete	(A) is **Design-Specific** and requires **Evaluation**.
SP.00.RA.01	Radiolysis in Seals and Plugs	-(A) He generation from alpha decay in seals or plugs -(B) H_2 generation from radiolysis -(C) Altered water chemistry	(A), (B), and (C) require **Evaluation**.
SP.00.RA.02	Radiation Damage to Seals and Plugs	-(A) Enhanced degradation of seals and plugs	(A) requires **Evaluation**.
SP.00.NC.01	Criticality in Seals/Plugs	-(A) Formation of critical configuration	(A) requires **Evaluation**.
SP.00.EF.01	Early Failure of Seals/Plugs	-(A) Error in emplacement -(B) Inadequate construction	(A) and (B) are **Design-Specific** and require **Evaluation.**
SP.00.SM.01	Dynamic Loading on Seals/Plugs from a Seismic Event	-(A) Mechanical damage to seals/plugs from ground motion, rockfall, drift collapse, and fault displacement	(A) requires **Evaluation** for a candidate site. The frequency, magnitude, and consequences of seismic events are **Site-Specific.**

Matrix FEP Number	Description	Associated Processes	Preliminary Screening Recommendations
SP.00.IG.01	Igneous Activity Impacts Seals/Plugs	- (A) Chemical interaction with magmatic volatiles - (B) Transport of radionuclides in magma, pyroclasts, vents	(A) and (B) require **Evaluation** for a candidate site. The frequency, type, magnitude and consequences of igneous events are **Site-Specific.**
SP.00.IG.02	Dynamic Loading on Seals/Plugs from an Igneous Event	- (A) An igneous intrusion causes thermal-mechanical deformation and failure of the seals/plugs	(A) is Site-Specific and requires **Evaluation.**
SP.00.HE.01	Human Intrusion (Deliberate or Inadvertent) - Effects on Seals/Plugs	- (A) Drilling (resource exploration, …) - (B) Mining / tunneling - (C) Nonintrusive site investigation (airborne, surface-based, …)	(A) and (B) require **Evaluation** because they are **Site-Specific**. (C) is **Excluded** because it is a nonintrusive process.
SP.01.CP.01	Emplacement Drift/Room Seal Design and Properties	- Geometry - Materials and properties (initial condition / damage / corrosion products) - Fluids, colloids, and their properties - Flow and transport properties (flow type [i.e., porous medium vs. thin film], porosity, permeability, tortuosity, dispersion coefficients, surface complexation, and K_d's)	
SP.01.TC.01	Evolution of Water Chemistry in Drift/Room Seals	- (A) Speciation - (B) Oxidation/reduction processes, reaction kinetics - (C) Dissolution, reaction kinetics - (D) Precipitation, inclusion in secondary phase, reaction kinetics - (E) Formation and filtration of colloids - (F) Effect of sorption - (G) Solubility of radionuclides and other species - (H) Thermal-chemical interactions with WP/MW/BB/seal components, including chemical effects on fluid density - (I) Thermal-chemical interaction with corrosion products, including effects on fluid density - (J) Thermal-chemical Interaction with intruding fluids, including effects on fluid density - (K) Interaction with gas phase - (L) Osmotic stress and osmotic binding	(A), (B), (C), (D), (E), (F), and (G) are **Likely Included** because they are basic chemistry processes. (H) through (L) require **Evaluation**.
SP.01.TC.02	Thermal-Chemical Degradation of Emplacement Drift/Room Seals	- (A) Thermal-chemical alteration processes - (B) Oxidation/reduction processes, reaction kinetics, interaction with metals - (C) Dissolution / leaching - (D) Cracking induced by thermal-chemical alteration - (E) Enhanced corrosion - (F) Radiolysis and altered water chemistry	(A), (B), (C), (D), (E), and (F) require **Evaluation**
SP.01.CL.01	Climatic Effects on Emplacement Drift/Room Seals	- (A) Variations in precipitation and temperature - (B) Melt water - (C) Seal erosion arising from glaciation	(A), (B), and (C) are **Likely Excluded** because climatic effects may not be significant for the emplacement drift/room seals.

Matrix FEP Number	Description	Associated Processes	Preliminary Screening Recommendations
SP.02.CP.01	Shaft Seal Design and Properties	- Geometry - Materials and properties (initial condition / damage / corrosion products) - Fluids, colloids, and their properties - Flow and transport properties (flow type [i.e., porous medium vs. thin film], porosity, permeability, tortuosity, dispersion coefficients, surface complexation, and K_d's)	
SP.02.TC.01	Evolution of Water Chemistry in Shaft Seals	- (A) Speciation - (B) Oxidation/reduction processes, reaction kinetics - (C) Dissolution, reaction kinetics - (D) Precipitation, inclusion in secondary phase, reaction kinetics - (E) Formation and filtration of colloids - (F) Effect of sorption - (G) Solubility of radionuclides and other species - (H) Thermal-chemical interactions with other WP/BB/MW/seal components, including chemical effects on fluid density - (I) Thermal-chemical interaction with corrosion products, including effects on fluid density - (J) Thermal-chemical Interaction with intruding fluids, including effects on fluid density - (K) Interaction with gas phase - (L) Osmotic stress and osmotic binding	(A), (B), (C), (D), (E), (F), and (G) are **Likely Included** because they are basic chemistry processes. (H) through (L) require **Evaluation**.
SP.02.TC.02	Thermal-Chemical Degradation of Shaft Seals	- (A) Thermal-chemical alteration processes - (B) Oxidation/reduction processes, reaction kinetics, interaction with metals - (C) Dissolution / leaching - (D) Cracking induced by thermal-chemical alteration - (E) Enhanced corrosion - (F) Radiolysis and altered water chemistry	(A), (B), (C), (D), (E), and (F) require **Evaluation**
SP.02.CL.01	Periglacial Effects on Shaft Seals	- (A) Variations in precipitation and temperature - (B) Permafrost - (C) Seasonal freeze/thaw	(A), (B), and (C) require **Evaluation** for the shaft seals.
SP.02.CL.02	Glacial and Ice Sheet Effects on Shaft Seals	- (A) Glaciation - (B) Glacial erosion, glacial valleys - (C) Isostatic depression - (D) Melt water - (E) Shaft seal erosion arising from glaciation	(A), (B), (C), (D), and (E) require **Evaluation** for the shaft seals.
SP.03.CP.01	Borehole Plugs Design and Properties	- Geometry - Materials and properties (initial condition / damage / corrosion products) - Fluids, colloids, and their properties - Flow and transport properties (flow type [i.e., porous medium vs. thin film], porosity, permeability, tortuosity, dispersion coefficients, surface complexation, and K_d's)	

Matrix FEP Number	Description	Associated Processes	Preliminary Screening Recommendations
SP.03.TC.01	Evolution of Water Chemistry in Borehole Plugs	- (A) Speciation - (B) Oxidation/reduction processes, reaction kinetics - (C) Dissolution, reaction kinetics - (D) Precipitation, inclusion in secondary phase, reaction kinetics - (E) Formation and filtration of colloids - (F) Effect of sorption - (G) Solubility of radionuclides and other species - (H) Thermal-chemical interactions with other WP/BB/MW/seal components, including chemical effects on fluid density - (I) Thermal-chemical interaction with corrosion products, including effects on fluid density - (J) Thermal-chemical Interaction with intruding fluids, including effects on fluid density - (K) Interaction with gas phase - (L) Osmotic stress and osmotic binding	(A), (B), (C), (D), (E), (F), and (G) are **Likely Included** because they are basic chemistry processes. (H) through (L) require **Evaluation**.
SP.03.TC.02	Thermal-Chemical Degradation of Borehole Plugs	- (A) Thermal-chemical alteration processes - (B) Oxidation/reduction processes, reaction kinetics, interaction with metals - (C) Dissolution / leaching - (D) Cracking induced by thermal-chemical alteration - (E) Enhanced corrosion - (F) Radiolysis and altered water chemistry	(A), (B), (C), (D), (E), and (F) require **Evaluation**
SP.03.CL.01	Climatic Effects on Plugged Boreholes	- (A) Variations in precipitation and temperature - (B) Permafrost - (C) Seasonal freeze/thaw - (D) Glaciation - (E) Glacial erosion, glacial valleys - (F) Isostatic depression - (G) Melt water - (H) Borehole plug erosion arising from glaciation	(A), (B), (C), (D), (E), (F), (G), and (H) require **Evaluation** for the borehole plugs.
HR.00.CP.01	Stratigraphic and Groundwater Properties of Host Rock	- Stratigraphy / component rock units and their properties - Regional features (e.g., fractures, faults, discontinuities, contacts) - Rock properties - Fluid properties - Groundwater chemistry - Presence or organic complexants (humates, fulvates, carbonates, …) in groundwater	
HR.00.TH.01	Effects of Recharge on Host Rock	- (A) Pressure-driven flow of liquid (wetting) phase - (B) Pressure-driven flow of gas (non-wetting) phase - (C) Flow of any additional phases (e.g., hydrocarbons) - (D) Pressure-driven flow between fractures and matrix (local non-equilibrium)	(A), (B), (C), and (D) are **Included** because pressure-driven Darcy flow is an important hydrological process.

Matrix FEP Number	Description	Associated Processes	Preliminary Screening Recommendations
HR.00.TC.01	Thermal-Chemical Gas Generation in Host Rock	- (A) Degassing (clathrates, deep gases) - (B) Thermal-chemical degradation of organic materials	(A) requires **Evaluation** for the **Site-Specific** rocks at a candidate site. (B) is **Likely Excluded** because the host rock is not expected to contain significant amounts of organic materials.
HR.00.TB.01	Microbial Activity in Host Rock	- (A) Microbial effects on corrosion - (B) Presence of complexants - (humates, fulvates, carbonates) - (C) Formation of microbial colloids - (D) Formation of biofilms - (E) Biodegradation - (F) Biomass production - (G) Bioaccumulation - (H) CO_2, CH_4, H_2O and H_2S generation from microbial degradation - (I) Nitrification - (J) Sulfurization - (K) Methanogenesis	(A) through (K) are **Likely Excluded** because the host rock is not expected to support long-term microbial activity.
HR.00.TB.02	Thermal Effects on Microbial Activity in Host Rock	- (A) Thermal effects on microbial activity	(A) is **Likely Excluded** because the host rock is not expected to support microbial activity.
HR.00.LG.01	Tectonic Activity (Large Scale) in Host Rock	- (A) Uplift - (B) Folding	(A) and (B) are **Site-Specific** and require **Evaluation.**
HR.00.LG.02	Subsidence in Host Rock	- (A) Potential for subsidence to impact the integrity and performance of the repository	(A) is **Design-Specific** and **Site Specific** and requires **Evaluation**.
HR.00.LG.03	Metamorphism in Host Rock	- (A) Structural changes due to natural heating and/or pressure	(A) is **Site Specific** and requires **Evaluation**.
HR.00.LG.04	Diagenesis in Host Rock	- (A) Mineral alteration due to natural processes	(A) is **Site Specific** and requires **Evaluation**.
HR.00.LG.05	Diapirism in Host Rock	- (A) Plastic flow of rocks under lithostatic loading - (B) Creep of salt / evaporates - (C) Clay phase transformations	(A) is **Site Specific** and requires **Evaluation**. (B) is **Excluded** for a crystalline rock site. (C) is **Site Specific** and requires **Evaluation**.
HR.00.LG.06	Large-Scale Dissolution in Host Rock	- (A) Changes to host rock due to dissolution over geologic time scales	(A) is **Site Specific** and requires **Evaluation**.
HR.00.CL.01	Periglacial Effects on Host Rock	- (A) Variations in precipitation and temperature - (B) Permafrost - (C) Seasonal freeze/thaw	(A), (B), and (C) require **Evaluation**.
HR.00.CL.02	Glacial and Ice Sheet Effects on Host Rock	- (A) Glaciation - (B) Glacial erosion and valleys - (C) Isostatic depression - (D) Melt water	(A), (B), (C), and (D) require **Evaluation**.
HR.00.NC.01	Criticality in Far-Field	- (A) Formation of critical configuration	(A) requires **Evaluation**.
HR.00.SM.01	Seismic Activity Impacts Geosphere - Host Rock	- (A) Altered flow pathways and properties after a seismic event - (B) Altered stress regimes (faults, fractures) after a seismic event	(A) and (B) require **Evaluation** for a candidate site because the frequency and magnitude of seismic events is **Site-Specific**.
HR.00.IG.01	Igneous Activity Impacts Geosphere - Host Rock	- (A) Altered flow pathways and properties - (B) Altered stress regimes (faults, fractures) - (C) Igneous intrusions - (D) Altered thermal and chemical conditions	(A), (B), (C), and (D) require **Evaluation** for a candidate site because the frequency and magnitude of igneous events is **Site-Specific**.

Matrix FEP Number	Description	Associated Processes	Preliminary Screening Recommendations
HR.00.HE.01	Human Intrusion (Deliberate or Inadvertent) - Effects on Host Rock	-(A) Drilling (resource exploration, …) -(B) Mining / tunneling -(C) Nonintrusive site investigation (airborne, surface-based, …)	(A) and (B) require **Evaluation** because they are **Site-Specific**. (C) is **Excluded** because it is a nonintrusive process.
HR.01.CP.01	Stratigraphy and Properties of the DRZ	-Stratigraphic units (thickness, lateral extent, heterogeneities) -Rock properties -Fluid properties -Fractures and fault properties	
HR.01.TM.01	Dynamic Loading on the DRZ from Closure of Entries	-(A) Creep closure of the entries causes opening/closing of fractures or healing of fractures in the DRZ -(B) Backstress from waste, backfill, or drift/tunnel seals accelerates healing of fractures in the DRZ -(C) Floor heave or spalling from the walls and back changes the geometry or depth of the DRZ. -(D) Non-thermally-induced volume changes (e.g., closure of fractures) in the DRZ -(E) Change in mechanical loads on the DRZ from erosion or dissolution near the Mine Workings	(A) is **Excluded** because creep closure is not expected to occur in crystalline rock. (B) is **Likely Included** because backstress increases the mechanical loads on the DRZ. (C), (D), and (E) require **Evaluation** because these effects may alter the mechanical loads on the DRZ.
HR.01.TM.02	Dynamic Loading on the DRZ from Rockfall or Drift Collapse	-(A) Ejection of rock blocks or roof beam separation alters the geometry or depth of the DRZ -(B) Drift collapse alters the state, geometry or depth of the DRZ	(A) and (B) require **Evaluation** for the discrete fracture network at a candidate site.
HR.01.TM.03	Pressure Loading on the DRZ	-(A) Pressurization caused by gas generation, gas explosion, or entry closure alters the state or depth of the DRZ	(A) is **Likely Included** for gas generation from corrosion of metal components. (A) requires **Evaluation** for gas explosions. (A) is **Likely Excluded** for entry closure because it will not be significant in crystalline rock.
HR.01.TM.04	Thermal-Mechanical Effects on the Evolution of the DRZ	-(A) Thermally-enhanced convergence / rockfall / drift collapse /floor buckling / backfill consolidation alters the DRZ -(B) Thermally-induced volume changes(expansion/stress/cracking)	(A) and (B) require **Evaluation.** Note that coupled thermal-mechanical response is most important during the thermal pulse and may not be significant for long-term performance of the DRZ.
HR.01.TH.01	Pressure-Driven Darcy Flow Through Fractures and Porous Media in the DRZ	-(A) Pressure-driven flow of liquid (wetting) phase -(B) Pressure-driven flow of gas (non-wetting) phase -(C) Flow of any additional phases (e.g., hydrocarbons) -(D) Pressure-driven flow between fractures and matrix (local non-equilibrium)	(A), (B), (C), and (D) are **Included** because pressure-driven Darcy flow is an important hydrological process.
HR.01.TH.02	Capillarity-Dominated Darcy Flow In the DRZ	-(A) Wicking and imbibition (i.e., infiltration without gravity) -(B) Vapor barrier (i.e., reduction in relative liquid permeability at low saturation) -(C) Immiscible phase interaction and displacement -(D) Trapping, discontinuous blobs, or viscous fingering in non-wetting phase	(A) is **Included** because it determines, in part, the hydrologic conditions in the DRZ. (B), (C), and (D) require **Evaluation**.

Matrix FEP Number	Description	Associated Processes	Preliminary Screening Recommendations
HR.01.TH.03	Gravity- and Density-Dominated Flow In the DRZ	- (A) Free convection due to density variation (from temperature or salinity effects) - (B) Infiltration and drainage - (C) Dripping or ponding	(A) and (C) require **Evaluation**. (B) is **Likely Included** because these processes are important for determining the hydrologic conditions in the DRZ.
HR.01.TH.04	Adsorption-Dominated Flow In the DRZ (Water held by electrostatic, van der Waals, or hydration forces)	- (A) Thin film flow below residual saturation (i.e., near liquid dry-out) - (B) Hygroscopy (equilibration of solid phase with humidity) - (C) Immobile water in nano-pores or small-aperture fractures	(A), (B), and (C) require **Evaluation.**
HR.01.TH.05	Diffusion or Dispersion in Miscible Phases In the DRZ	- (A) Diffusion of vapor in air phase - (B) Diffusion of dissolved gas in liquid phase	(A) and (B) require **Evaluation.**
HR.01.TH.06	Non-Darcy Flow Through Fractures and Porous Media In the DRZ	- (A) High Reynolds number fluid flow in large-aperture fractures - (B) Erosion or sedimentation (i.e., non-chemical plugging) of fractures and flow paths - (C) Threshold gradient flow in low-permeability matrix	(A), (B), and (C) require **Evaluation.**
HR.01.TH.07	Thermal-Hydrological Effects on Flow in the DRZ	- (A) Convection and conduction of energy via liquid phase - (B) Convection of energy via vapor (i.e., heat pipe) - (C) Fluid density and viscosity changes due to temperature (e.g., thermal expansion of brine) - (D) Phase changes (i.e., condensation, boiling) leading to dry-out or resaturation - (E) Release of water from hydrated minerals during heating - (F) Decrepitation, creation (during reconsolidation), and migration of fluid inclusions	(A), (B), (C), (E), and (F) require **Evaluation**. (D) is **Likely Excluded** because peak thermal pulse is expected to be less than 100°C.
HR.01.TC.01	Evolution of Groundwater Chemistry in the DRZ	- (A) Speciation - (B) Oxidation/reduction processes, reaction kinetics - (C) Dissolution, reaction kinetics - (D) Precipitation, inclusion in secondary phase, reaction kinetics - (E) Formation and filtration of colloids - (F) Effect of sorption - (G) Solubility of radionuclides and other species - (H) Thermal-chemical interactions with repository components, including chemical effects on fluid density - (J) Thermal-chemical Interaction with intruding fluids, including chemical effects on fluid density - (K) Interaction with gas phase	(A), (B), (C), (D), (E), (F), and (G) are **Likely Included** because they are basic chemistry processes. (H) through (K) require **Evaluation**.
HR.01.TC.02	Thermal-Chemical Evolution of the DRZ	- (A) Thermal-chemical alteration processes for fractures, faults, rock matrix - (B) Thermal-chemical alteration of minerals / volume changes / cracking - (C) Thermal-chemical alteration of solubility, mineral precipitation / dissolution / leaching - (D) Oxidation/reduction processes, reaction kinetics, interaction with metals in Mine Workings	(A), (B), (C), and (D) require **Evaluation**

Matrix FEP Number	Description	Associated Processes	Preliminary Screening Recommendations
HR.01.TT.01	Transport of Dissolved Radionuclides in the Liquid Phase in the DRZ	-(A) Advection -(B) Dispersion -(C) Diffusion -(D) Matrix Diffusion -(E) Intra-aqueous complexation -(F) Isotopic dilution -(G) Dilution by mixing with formation waters -(H) Solubility of radionuclides and other species	(A), (B), (C), (D), and (H) are **Included** because they are basic transport processes. (E), (F), and (G) require **Evaluation**.
HR.01.TT.02	Interaction of Dissolved Radionuclides with Stationary Phases (Rock Matrix, Fracture Surfaces) in the DRZ	-(A) Reversible/irreversible physical sorption -(B) Surface complexation -(C) Ion exchange -(D) Precipitation / dissolution, including limited dissolution due to inclusion in secondary phases and enhanced dissolution due to alpha recoil	(A), (B), (C), and (D) are **Included** because they are basic sorption or chemical processes.
HR.01.TT.03	Interaction of Dissolved Radionuclides with Other Mobile Phases (Colloids, Gas Phase) in the DRZ	-(A) Reversible/irreversible physical sorption -(B) Interactions with organic complexants -(C) Ion exchange -(D) Precipitation / dissolution -(E) Partitioning	(A), (B), (C), (D), and (E) are **Included** because they are basic sorption or chemical processes.
HR.01.TT.04	Coupled Process Effects on Transport of Dissolved Radionuclides in the DRZ	-(A) Thermal diffusion (Soret effect) -(B) Thermal osmosis -(C) Thermal conduction or convection -(D) Other thermal effects, such as other Onsager relationships	(A), (B), (C), and (D) require **Evaluation**.
HR.01.TT.05	Transport of Radionuclides in the Gas Phase in the DRZ	-(A) Advection -(B) Diffusion W-12.	(A) and (B) require **Evaluation** for gas phase transport.
HR.01.TT.06	Formation of Colloids in the DRZ	-(A) Intrinsic colloids -(B) Pseudo-colloids (host rock fragments, waste form fragments, corrosion products, microbes) -(C) Sorption of radionuclides to colloids	(A), (B), and (C) are **Included** because these processes are important for transport via colloids.
HR.01.TT.07	Transport of Radionuclides on Colloids in the DRZ	-(A) Advection -(B) Dispersion -(C) Diffusion -(D) Matrix Diffusion -(E) Stability/flocculation (mechanical stability, chemical stability) -(F) Filtration (physical, electrostatic) -(G) Dilution by mixing with formation waters	(A), (B), (C), and (D) are **Included** because they are important for transport via colloids. (E), (F), and (G) require **Evaluation** for the local geochemical environment and types of colloids.
HR.01.TT.08	Interaction of Colloids with Other Phases (Rock Matrix, Fracture Surfaces) in the DRZ	-(A) Reversible/irreversible physical sorption onto stationary phases -(B) Sorption at air-water interfaces	(A) and (B) require **Evaluation**.
HR.01.SM.01	Dynamic Loading on the DRZ from a Seismic Event	-(A) Mechanical changes to the DRZ from ground motion, rockfall, drift collapse, or fault displacement	(A) requires **Evaluation** for a candidate site. The frequency, magnitude, and consequences of seismic events are **Site-Specific.**
HR.01.IG.01	Igneous Activity Impacts the DRZ	-(A) Chemical interaction with magmatic volatiles -(B) Transport of radionuclides in magma, pyro clasts, vents	(A) and (B) require **Evaluation** for a candidate site. The frequency, type, magnitude and consequences of igneous events are **Site-Specific.**

Matrix FEP Number	Description	Associated Processes	Preliminary Screening Recommendations
HR.01.IG.02	Dynamic Loading on the DRZ from an Igneous Event	- (A) An igneous intrusion causes thermal-mechanical deformation of the DRZ	(A) is **Site-Specific** and requires **Evaluation.**
HR.02.CP.01	Stratigraphy and Properties of Emplacement Unit(s)	- Stratigraphic units (thickness, lateral extent, heterogeneities) - Rock properties - Fluid properties - Fractures and fault properties	
HR.02.TM.01	Dynamic Loading on the Emplacement Unit(s) from Closure of Entries	- (A) Creep closure of the entries causes deformation and failure of the emplacement unit(s) - (B) Floor heave or spalling from the walls and back changes the mechanical state in the emplacement unit(s). - (C) Non-thermally-induced volume changes (e.g., swelling, cracking, corrosion products).	(A) is **Likely Excluded** because creep closure is not expected to occur in crystalline rock (B) requires **Evaluation** because floor heave or spalling may alter the mechanical state in the emplacement units. (C) requires **Evaluation**.
HR.02.TM.02	Dynamic Loading on the Emplacement Unit(s) from Rockfall or Drift Collapse	- (A) Ejection of rock blocks or roof beam separation alters the mechanical state of the emplacement unit(s) - (B) Drift collapse or formation of a rock chimney alters the mechanical state of the emplacement unit(s)	(A) and (B) require **Evaluation** for the discrete fracture network at a candidate site.
HR.02.TM.03	Pressure Loading on the Emplacement Unit(s)	- (A) Pressurization caused by gas generation, gas explosion, or entry convergence alters the mechanical state of the emplacement unit(s)	(A) is **Likely Included** for gas generation from corrosion of metal components. (A) requires **Evaluation** for gas explosions. (A) is **Likely Excluded** for entry closure because it will not be significant in crystalline rock.
HR.02.TM.04	Thermal-Mechanical Effects in the Emplacement Unit(s)	- (A) Thermally-accelerated convergence / rockfall / drift collapse / floor buckling in the emplacement unit(s) - (B) Subsidence - (C) Thermally-induced volume changes(expansion/stress/cracking)	(A) and (C) require **Evaluation.** Note that coupled thermal-mechanical response is most important during the thermal pulse and may not be significant for long-term performance of the emplacement units. (B) is **Design-Specific** and **Site-Specific** and requires **Evaluation**.
HR.02.TH.01	Pressure-Driven Darcy Flow Through Fractures and Porous Media in Emplacement Unit(s)	- (A) Pressure-driven flow of liquid (wetting) phase - (B) Pressure-driven flow of gas (non-wetting) phase - (C) Flow of any additional phases (e.g., hydrocarbons) - (D) Pressure-driven flow between fractures and matrix (local non-equilibrium)	(A), (B), (C), and (D) are **Included** because pressure-driven Darcy flow is an important hydrological process.
HR.02.TH.02	Capillarity-Dominated Darcy Flow In Emplacement Unit(s)	- (A) Wicking and imbibition (i.e., infiltration without gravity) - (B) Vapor barrier (i.e., reduction in relative liquid permeability at low saturation) - (C) Immiscible phase interaction and displacement - (D) Trapping, discontinuous blobs, or viscous fingering in non-wetting phase	(A) is **Included** because it determines, in part, the hydrologic conditions in the DRZ. (B), (C), and (D) require **Evaluation**.

Matrix FEP Number	Description	Associated Processes	Preliminary Screening Recommendations
HR.02.TH.03	Gravity- and Density-Dominated Flow In Emplacement Unit(s)	- (A) Free convection due to density variation (from temperature or salinity effects) - (B) Infiltration and drainage	(A) requires **Evaluation**. (B) is **Likely Included** because these processes are important for determining the hydrologic conditions in the emplacement units.
HR.02.TH.04	Adsorption-Dominated Flow In Emplacement Unit(s) (Water held by electrostatic, van der Waals, or hydration forces)	- (A) Thin film flow below residual saturation (i.e., near liquid dry-out) - (B) Hygroscopy (equilibration of solid phase with humidity) - (C) Immobile water in nano-pores or small-aperture fractures	(A), (B), and (C) require **Evaluation.**
HR.02.TH.05	Diffusion or Dispersion in Miscible Phases In Emplacement Unit(s)	- (A) Diffusion of vapor in air phase - (B) Diffusion of dissolved gas in liquid phase	(A) and (B) require **Evaluation.**
HR.02.TH.06	Non-Darcy Flow Through Fractures and Porous Media In Emplacement Unit(s)	- (A) High Reynolds number fluid flow in large-aperture fractures - (B) Erosion or sedimentation (i.e., non-chemical plugging) of fractures and flow paths - (C) Threshold gradient flow in low-permeability matrix	(A), (B), and (C) require **Evaluation.**
HR.02.TH.07	Thermal-Hydrological Effects on Flow in Emplacement Unit(s)	- (A) Convection and conduction of energy via liquid phase - (B) Convection of energy via vapor (i.e., heat pipe) - (C) Fluid density and viscosity changes due to temperature (e.g., thermal expansion of brine) - (D) Phase changes (i.e., condensation, boiling) leading to dry-out or resaturation - (E) Release of water from hydrated minerals during heating - (F) Decrepitation, creation (during reconsolidation), and migration of fluid inclusions	(A) is **Likely Included** because the thermal pulse drives fluid out of the repository. (B), (C), (E), and (F) require **Evaluation**. (D) is **Likely Excluded** because the peak thermal pulse is expected to be less than 100°C.
HR.02.TC.01	Evolution of Groundwater Chemistry in Emplacement Unit(s)	- (A) Speciation - (B) Oxidation/reduction processes, reaction kinetics - (C) Dissolution, reaction kinetics - (D) Precipitation, inclusion in secondary phase, reaction kinetics - (E) Formation and filtration of colloids - (F) Effect of sorption - (G) Solubility of radionuclides and other species - (H) Thermal-chemical interactions with repository components, including chemical effects on fluid density - (I) Thermal-chemical interaction with corrosion products, including effects on fluid density - (J) Thermal-chemical Interaction with intruding fluids, including chemical effects on fluid density - (K) Interaction with gas phase	(A), (B), (C), (D), (E), (F), and (G) are **Likely Included** because they are basic chemistry processes. (H), (I), (J), and (K) require **Evaluation**.

Matrix FEP Number	Description	Associated Processes	Preliminary Screening Recommendations
HR.02.TC.02	Thermal-Chemical Evolution of Emplacement Unit(s)	- (A) Thermal-chemical alteration processes for fractures, faults, rock matrix - (B) Thermal-chemical alteration of minerals / volume changes / cracking - (C) Thermal-chemical alteration of solubility, mineral precipitation / dissolution / leaching - (D) Oxidation/reduction processes, reaction kinetics, interaction with metals in Mine Workings	(A), (B), (C), and (D) require **Evaluation**
HR.02.TT.01	Transport of Dissolved Radionuclides in the Liquid Phase in Emplacement Unit(s)	- (A) Advection - (B) Dispersion - (C) Diffusion - (D) Matrix Diffusion - (E) Intra-aqueous complexation - (F) Isotopic dilution - (G) Dilution by mixing with formation waters - (H) Solubility of radionuclides and other species	(A), (B), (C), (D), and (H) are **Included** because they are basic transport processes. (E), (F), and (G) require **Evaluation**.
HR.02.TT.02	Interaction of Dissolved Radionuclides with Stationary Phases (Rock Matrix, Fracture Surfaces) in Emplacement Unit(s)	- (A) Reversible/irreversible physical sorption - (B) Surface complexation - (C) Ion exchange - (D) Precipitation / dissolution, including limited dissolution due to inclusion in secondary phases and enhanced dissolution due to alpha recoil	(A), (B), (C), and (D) are **Included** because they are basic sorption or chemical processes.
HR.02.TT.03	Interaction of Dissolved Radionuclides with Other Mobile Phases (Colloids, Gas Phase) in Emplacement Unit(s)	- (A) Reversible/irreversible physical sorption - (B) Interactions with organic complexants - (C) Ion exchange - (D) Precipitation / dissolution - (E) Partitioning	(A), (B), (C), (D), and (E) are **Included** because they are basic sorption or chemical processes.
HR.02.TT.04	Coupled Process Effects on Transport of Dissolved Radionuclides in Emplacement Unit(s)	- (A) Thermal diffusion (Soret effect) - (B) Thermal osmosis - (C) Thermal conduction or convection - (D) Other thermal effects, such as other Onsager relationships	(A), (B), (C), and (D) require **Evaluation**.
HR.02.TT.05	Transport of Radionuclides in the Gas Phase in Emplacement Unit(s)	- (A) Advection - (B) Diffusion W-13.	(A) and (B) require **Evaluation** for gas phase transport.
HR.02.TT.06	Formation of Colloids in Emplacement Unit(s)	- (A) Intrinsic colloids - (B) Pseudo-colloids (host rock fragments, waste form fragments, corrosion products, microbes) - (C) Sorption of radionuclides to colloids	(A), (B), and (C) are **Included** because these processes are important for transport via colloids.
HR.02.TT.07	Transport of Radionuclides on Colloids in Emplacement Unit(s)	- (A) Advection - (B) Dispersion - (C) Diffusion - (D) Matrix Diffusion - (E) Stability/flocculation (mechanical stability, chemical stability) - (F) Filtration (physical, electrostatic) - (G) Dilution by mixing with formation waters	(A), (B), (C), and (D) are **Included** because they are important for transport via colloids. (E), (F), and (G) require **Evaluation** for the local geochemical environment and types of colloids.
HR.02.TT.08	Interaction of Colloids with Other Phases (Rock Matrix, Fracture Surfaces) in Emplacement Unit(s)	- (A) Reversible/irreversible physical sorption onto stationary phases - (B) Sorption at air-water interfaces	(A) and (B) require **Evaluation**.

Matrix FEP Number	Description	Associated Processes	Preliminary Screening Recommendations
HR.02.SM.01	Dynamic Loading on the Emplacement Unit(s) from a Seismic Event	- (A) Mechanical changes to the Emplacement Unit(s) from ground motion, rockfall, drift collapse, or fault displacement	(A) requires **Evaluation** for a candidate site. The frequency, magnitude, and consequences of seismic events are **Site-Specific.**
HR.02.IG.01	Igneous Activity Impacts the Emplacement Unit(s)	- (A) Chemical interaction with magmatic volatiles - (B) Transport of radionuclides in magma, pyro clasts, vents	(A) and (B) require **Evaluation** for a candidate site. The frequency, type, magnitude and consequences of igneous events are **Site-Specific.**
HR.02.IG.02	Dynamic Loading on the Emplacement Unit(s) from an Igneous Event	- (A) An igneous intrusion causes thermal-mechanical deformation of the Emplacement Unit(s)	(A) is **Site-Specific** and requires **Evaluation.**
HR.03.CP.01	Stratigraphy and Properties of Other Host Rock Units	- Stratigraphic units (thickness, lateral extent, heterogeneities) - Rock properties - Fluid properties - Fractures and fault properties	
HR.03.TM.01	Dynamic Loading on Other Host Rock Units from Closure of Entries	- (A) Creep closure of the entries causes deformation and failure of the interbeds and seams - (B) Floor heave or spalling from the walls and back changes the mechanical state in the interbeds and seams - (C) Non-thermally-induced volume changes (e.g., swelling, cracking, compression).	(A) is **Likely Excluded** because creep closure is not expected to occur in crystalline rock. (B) and (C) require **Evaluation** for the interbeds and seams at a candidate site.
HR.03.TM.02	Mechanical Loading on Other Host Rock Units from Rockfall or Drift Collapse	- (A) Ejection of rock blocks or roof beam separation alters the mechanical state of the interbeds and seams - (B) Drift collapse or formation of a rock chimney alters the mechanical state of the interbeds and seams	(A) and (B) require **Evaluation** for the discrete fracture network and interbeds and seams at a candidate site.
HR.03.TM.03	Pressure Loading on Other Host Rock Units	- (A) Pressurization caused by gas generation, gas explosion, or entry convergence alters the mechanical state of the interbeds and seams	(A) requires **Evaluation** for conditions in the interbeds and seams.
HR.03.TM.04	Thermal-Mechanical Effects in Other Host Rock Units	- (A) Thermally-accelerated convergence / rockfall / drift collapse / floor buckling alters the mechanical state in the interbeds and seams - (B) Subsidence - (C) Thermally-induced volume changes(expansion/stress/cracking)	(A) and (C) require **Evaluation.** Note that coupled thermal-mechanical response is most important during the thermal pulse and may not be significant for long-term performance of the other host rock units (B) is **Design-Specific** and **Site-Specific** and requires **Evaluation**.
HR.03.TH.01	Pressure-Driven Darcy Flow In Other Host Rock Units	- (A) Pressure-driven flow of liquid (wetting) phase - (B) Pressure-driven flow of gas (non-wetting) phase - (C) Flow of any additional phases (e.g., hydrocarbons) - (D) Pressure-driven flow between fractures and matrix (local non-equilibrium)	(A), (B), (C), and (D) are **Included** because pressure-driven Darcy flow is an important hydrological process.

Matrix FEP Number	Description	Associated Processes	Preliminary Screening Recommendations
HR.03.TH.02	Capillarity-Dominated Darcy Flow In Other Host Rock Units	- (A) Wicking and imbibition (i.e., infiltration without gravity) - (B) Vapor barrier (i.e., reduction in relative liquid permeability at low saturation) - (C) Immiscible phase interaction and displacement - (D) Trapping, discontinuous blobs, or viscous fingering in non-wetting phase	(A) is **Included** because it determines, im part, the hydrologic conditions in the interbeds and seams. (B), (C), and (D) require **Evaluation**.
HR.03.TH.03	Gravity- and Density-Dominated Flow In Other Host Rock Units	- (A) Free convection due to density variation (from temperature or salinity effects) - (B) Infiltration and drainage	(A) requires **Evaluation**. (B) is **Likely Included** because these processes are important for determining the hydrologic conditions in the interbeds and seams.
HR.03.TH.04	Adsorption-Dominated Flow In Other Host Rock Units (Water held by electrostatic, van der Waals, or hydration forces)	- (A) Thin film flow below residual saturation (i.e., near liquid dry-out) - (B) Hygroscopy (equilibration of solid phase with humidity) - (C) Immobile water in nano-pores or small-aperture fractures	(A), (B), and (C) require **Evaluation.**
HR.03.TH.05	Diffusion or Dispersion in Miscible Phases In Other Host Rock Units	- (A) Diffusion of vapor in air phase - (B) Diffusion of dissolved gas in liquid phase	(A) and (B) require **Evaluation.**
HR.03.TH.06	Non-Darcy Flow Through Fractures and Porous Media In Emplacement Unit(s)	- (A) High Reynolds number fluid flow in large-aperture fractures - (B) Erosion or sedimentation (i.e., non-chemical plugging) of fractures and flow paths - (C) Threshold gradient flow in low-permeability matrix	(A), (B), and (C) require **Evaluation.**
HR.03.TH.07	Thermal-Hydrological Effects on Flow in Other Host Rock Units	- (A) Convection and conduction of energy via liquid phase - (B) Convection of energy via vapor (i.e., heat pipe) - (C) Fluid density and viscosity changes due to temperature (e.g., thermal expansion of brine) - (D) Phase changes (i.e., condensation, boiling) leading to dry-out or resaturation - (E) Release of water from hydrated minerals during heating - (F) Decrepitation, creation (during reconsolidation), and migration of fluid inclusions	(A) is **Likely Included** because the thermal pulse drives fluid out of the repository. (B), (C), (E), and (F) require **Evaluation**. (D) is **Likely Excluded** because the peak thermal pulse is expected to be less than 100°C.

Matrix FEP Number	Description	Associated Processes	Preliminary Screening Recommendations
HR.03.TC.01	Evolution of Groundwater Chemistry in Other Host Rock Units	- (A) Speciation - (B) Oxidation/reduction processes, reaction kinetics - (C) Dissolution, reaction kinetics - (D) Precipitation, inclusion in secondary phase, reaction kinetics - (E) Formation and filtration of colloids - (F) Effect of sorption - (G) Solubility of radionuclides and other species - (H) Thermal-chemical interactions with repository components, including effects on fluid density - (I) Thermal-chemical interaction with corrosion products, including effects on fluid density - (J) Thermal-chemical Interaction with intruding fluids, including effects on fluid density - (K) Interaction with gas phase	(A), (B), (C), (D), (E), (F), and (G) are **Likely Included** because they are basic chemistry processes. (H) through (K) require **Evaluation**.
HR.03.TC.02	Thermal-Chemical Evolution of Other Host Rock Units	- (A) Thermal-chemical alteration processes for fractures, faults, rock matrix - (B) Thermal-chemical alteration of minerals / volume changes / cracking - (C) Thermal-chemical alteration of solubility, mineral precipitation / dissolution / leaching - (D) Oxidation/reduction processes, reaction kinetics	(A), (B), (C), and (D) require **Evaluation**
HR.03.TT.01	Transport of Dissolved Radionuclides in the Liquid Phase in Other Host Rock Units	- (A) Advection - (B) Dispersion - (C) Diffusion - (D) Matrix Diffusion - (E) Intra-aqueous complexation - (F) Isotopic dilution - (G) Dilution by mixing with formation waters - (H) Solubility of radionuclides and other species	(A), (B), (C), (D), and (H) are **Included** because they are basic transport processes. (E), (F), and (G) require **Evaluation**.
HR.03.TT.02	Interaction of Dissolved Radionuclides with Other Mobile Phases (Colloids, Gas Phase) in Other Host Rock Units	- (A) Reversible/irreversible physical sorption - (B) Surface complexation - (C) Ion exchange - (D) Precipitation / dissolution, including limited dissolution due to inclusion in secondary phases and enhanced dissolution due to alpha recoil - (E) Partitioning - (F) Enhanced transport of radionuclides associated with organic complexants	(A), (B), (C), (D), (E), and (F) are **Included** because they are basic sorption or chemical processes.
HR.03.TT.03	Interaction of Dissolved Radionuclides with Other Mobile Phases (Colloids, Gas Phase) in Other Host Rock Units	- (A) Reversible/irreversible physical sorption - (B) Interactions with organic complexants - (C) Ion exchange - (D) Precipitation / dissolution - (E) Partitioning	(A), (B), (C), (D), and (E) are **Included** because they are basic sorption or chemical processes.

Matrix FEP Number	Description	Associated Processes	Preliminary Screening Recommendations
HR.03.TT.04	Coupled Process Effects on Transport of Dissolved Radionuclides in Other Host Rock Units	- (A) Thermal diffusion (Soret effect) - (B) Thermal osmosis - (C) Thermal conduction or convection - (D) Other thermal effects, such as other Onsager relationships	(A), (B), (C), and (D) require **Evaluation**.
HR.03.TT.05	Transport of Radionuclides in the Gas Phase in Other Host Rock Units	- (A) Advection - (B) Diffusion W-14.	(A) and (B) require **Evaluation** for gas phase transport.
HR.03.TT.06	Formation of Colloids in Other Host Rock Units	- (A) Intrinsic colloids - (B) Pseudo-colloids (host rock fragments, waste form fragments, corrosion products, microbes) - (C) Sorption of radionuclides to colloids	(A), (B), and (C) are **Included** because these processes are important for transport via colloids.
HR.03.TT.07	Transport of Radionuclides on Colloids in Other Host Rock Units	- (A) Advection - (B) Dispersion - (C) Diffusion - (D) Matrix Diffusion - (E) Stability/flocculation (mechanical stability, chemical stability) - (F) Filtration (physical, electrostatic) - (G) Dilution by mixing with formation waters	(A), (B), (C), and (D) are **Included** because they are important for transport via colloids. (E), (F), and (G) require **Evaluation** for the local geochemical environment and types of colloids.
HR.03.TT.08	Interaction of Colloids with Other Phases (Rock Matrix, Fracture Surfaces) in Other Host Rock Units	- (A) Reversible/irreversible physical sorption onto stationary phases - (B) Sorption at air-water interfaces	(A) and (B) require **Evaluation**.
HR.03.SM.01	Dynamic Loading on the Other Host Rock Units from a Seismic Event	- (A) Mechanical changes to the interbeds or seams from ground motion, rockfall, drift collapse, or fault displacement	(A) requires **Evaluation** for a candidate site. The frequency, magnitude, and consequences of seismic events are **Site-Specific.**
HR.03.IG.01	Igneous Activity Impacts the Other Host Rock Units	- (A) Chemical interaction with magmatic volatiles - (B) Transport of radionuclides in magma, pyro clasts, vents	(A) and (B) require **Evaluation** for a candidate site. The frequency, type, magnitude and consequences of igneous events are **Site-Specific.**
HR.03.IG.02	Dynamic Loading on the Other Host Rock Units from an Igneous Event	- (A) An igneous intrusion causes thermal-mechanical deformation of the interbeds and seams	(A) is **Site-Specific** and requires **Evaluation.**
OU.00.CP.01	Stratigraphic and Groundwater Properties of Other Geologic Units	- Stratigraphy / component rock units - Regional features (e.g., fractures, faults, discontinuities, contacts) - Rock Properties - Fluid properties - Groundwater chemistry W-15. Presence of organic complexants (humates, fulvates, carbonates, …) in groundwater	
OU.00.TH.01	Effects of Recharge on Other Geologic Units	- (A) Pressure-driven flow of liquid (wetting) phase - (B) Pressure-driven flow of gas (non-wetting) phase - (C) Flow of any additional phases (e.g., hydrocarbons) - (D) Pressure-driven flow between fractures and matrix (local non-equilibrium)	(A), (B), (C), and (D) are **Included** because pressure-driven Darcy flow is an important hydrological process.
OU.00.TC.01	Thermal-Chemical Gas Generation in Other Geologic Units	- (A) Degassing (clathrates, deep gases) - (B) Thermal-chemical degradation of organic materials	(A) and (B) require **Evaluation** for the **Site-Specific** rocks at a candidate site.

Matrix FEP Number	Description	Associated Processes	Preliminary Screening Recommendations
OU.00.LG.01	Tectonic Activity (Large Scale) in Other Geologic Units	- (A) Uplift - (B) Folding	(A) and (B) are **Site-Specific** and require **Evaluation.**
OU.00.LG.02	Subsidence in Other Geologic Units	- (A) Potential for subsidence to impact the integrity and performance of other geologic units	(A) is **Site Specific** and requires **Evaluation**.
OU.00.LG.03	Metamorphism in Other Geologic Units	- (A) Structural changes due to natural heating and/or pressure	(A) is **Site Specific** and requires **Evaluation**.
OU.00.LG.04	Diagenesis in Other Geologic Units	- (A) Mineral alteration due to natural processes	(A) is **Site Specific** and requires **Evaluation**.
OU.00.LG.05	Diapirism in Other Geologic Units	- (A) Plastic flow of rocks under lithostatic loading - (B) Creep of salt / evaporates - (C) Clay phase transformations	(A) is **Site Specific** and requires **Evaluation**. (B) is **Excluded** for a crystalline rock site. (C) is **Site Specific** and requires **Evaluation**.
OU.00.LG.06	Large-Scale Dissolution in Other Geologic Units	- (A) Changes to other geologic units due to dissolution over geologic time scales	(A) is **Site Specific** and requires **Evaluation**.
OU.00.HP.01	Human Influences on Climate (Intentional and Accidental) - Effects on Geosphere	- (A) Variations in precipitation and temperature W-16.	(A) is **Site Specific** and requires **Evaluation**.
OU.00.NC.01	Criticality in Far-Field	- (A) Formation of critical configuration	(A) requires **Evaluation**.
OU.00.SM.01	Seismic Activity Impacts Geosphere - Other Geologic Units	- (A) Altered flow pathways and properties after a seismic event - (B) Altered stress regimes (faults, fractures) after a seismic event	(A) and (B) require **Evaluation** for a candidate site because the frequency and magnitude of seismic events is **Site-Specific**.
OU.00.IG.01	Igneous Activity Impacts Geosphere - Other Geologic Units	- (A) Altered flow pathways and properties - (B) Altered stress regimes (faults, fractures) - (C) Igneous intrusion - (D) Altered thermal and chemical condition	(A), (B), (C), and (D) require **Evaluation** for a candidate site because the frequency and magnitude of igneous events is **Site-Specific**.
OU.00.HE.01	Human Intrusion (Deliberate or Inadvertent) - Effects on Other Geologic Units	- (A) Drilling (resource exploration, …) - (B) Mining / tunneling - (C) Nonintrusive site investigation (airborne, surface-based, …)	(A) and (B) require **Evaluation** because they are **Site-Specific**. (C) is **Excluded** because it is a nonintrusive process.
OU.01.CP.01	Stratigraphic and Groundwater Properties of Overlying / Adjacent Units	- Stratigraphic units (thickness, lateral extent, heterogeneities) - Rock properties - Fluid properties - Fractures and fault properties - Groundwater chemistry - Presence or organic complexants (humates, fulvates, carbonates, …) in groundwater	
OU.01.TM.01	Dynamic Loading on the Overlying/Adjacent Unit(s) from Closure of Entries	- (A) Creep closure of the entries causes deformation and failure of the overlying/adjacent unit(s) - (B) Floor heave or spalling from the walls and back changes the mechanical state in the overlying/adjacent unit(s). - (C) Non-thermally-induced volume changes (e.g., swelling, cracking, corrosion products).	(A), (B), and (C) require **Evaluation** for the overlying/adjacent unit(s) at a candidate site.

Matrix FEP Number	Description	Associated Processes	Preliminary Screening Recommendations
OU.01.TM.02	Dynamic Loading on the Overlying/Adjacent Unit(s) from Rockfall or Drift Collapse	- (A) Ejection of rock blocks or roof beam separation alters the mechanical state of the overlying/adjacent unit(s) - (B) Drift collapse or formation of a rock chimney alters the mechanical state of the overlying/adjacent unit(s)	(A) and (B) require **Evaluation** for the overlying/adjacent unit(s) at a candidate site.
OU.01.TM.03	Pressure Loading on the Overlying/Adjacent Unit(s)	- (A) Pressurization caused by gas generation, gas explosion, or entry convergence alters the mechanical state of the overlying/adjacent unit(s)	(A) requires **Evaluation** for conditions in the overlying/adjacent units.
OU.01.TM.04	Thermal-Mechanical Effects in Overlying / Adjacent Units	- (A) Thermally-accelerated convergence / rockfall / drift collapse / floor buckling in the overlying/adjacent units - (B) Subsidence - (C) Thermally-induced volume changes(expansion/stress/cracking)	(A) and (C) require **Evaluation.** (B) is **Design-Specific** and **Site-Specific** and requires **Evaluation**.
OU.01.TH .01	Pressure-Driven Darcy Flow Through Fractures and Porous Media in Overlying / Adjacent Units	- (A) Pressure-driven flow of liquid (wetting) phase - (B) Pressure-driven flow of gas (non-wetting) phase - (C) Flow of any additional phases (e.g., hydrocarbons) - (D) Pressure-driven flow between fractures and matrix (local non-equilibrium)	(A), (B), (C), and (D) are **Included** because pressure-driven Darcy flow is an important hydrological process.
OU.01.TH.02	Capillarity-Dominated Darcy Flow In Overlying / Adjacent Units	- (A) Wicking and imbibition (i.e., infiltration without gravity) - (B) Vapor barrier (i.e., reduction in relative liquid permeability at low saturation) - (C) Immiscible phase interaction and displacement - (D) Trapping, discontinuous blobs, or viscous fingering in non-wetting phase	(A) is **Included** because it determines, in part, the hydrologic conditions in the overlying/adjacent units (B), (C), and (D) require **Evaluation**.
OU.01.TH.03	Gravity- and Density-Dominated Flow In Overlying / Adjacent Units	- (A) Free convection due to density variation (from temperature or salinity effects) - (B) Infiltration and drainage	(A) requires **Evaluation**. (B) is **Likely Included** because these processes are important for determining the hydrologic conditions in the overlying/adjacent units.
OU.01.TH.04	Adsorption-Dominated Flow In Overlying / Adjacent Units (Water held by electrostatic, van der Waals, or hydration forces)	- (A) Thin film flow below residual saturation (i.e., near liquid dry-out) - (B) Hygroscopy (equilibration of solid phase with humidity) - (C) Immobile water in nano-pores or small-aperture fractures	(A), (B), and (C) require **Evaluation.**
OU.01.TH.05	Diffusion or Dispersion in Miscible Phases In Overlying / Adjacent Units	- (A) Diffusion of vapor in air phase - (B) Diffusion of dissolved gas in liquid phase	(A) and (B) require **Evaluation.**
OU.01.TH.06	Non-Darcy Flow Through Fractures and Porous Media In Overlying / Adjacent Units	- (A) High Reynolds number fluid flow in large-aperture fractures - (B) Erosion or sedimentation (i.e., non-chemical plugging) of fractures and flow paths - (C) Threshold gradient flow in low-permeability matrix	(A), (B), and (C) require **Evaluation.**

Matrix FEP Number	Description	Associated Processes	Preliminary Screening Recommendations
OU.01.TH.07	Thermal-Hydrological Effects on Flow in Overlying / Adjacent Units	- (A) Convection and conduction of energy via liquid phase - (B) Convection of energy via vapor (i.e., heat pipe) - (C) Fluid density and viscosity changes due to temperature (e.g., thermal expansion of brine) - (D) Phase changes (i.e., condensation, boiling) leading to dry-out or resaturation - (E) Release of water from hydrated minerals during heating - (F) Decrepitation, creation (during reconsolidation), and migration of fluid inclusions	(A), (B), (C), and (D) are **Included** because they are important for transport via colloids. (E), (F), and (G) require **Evaluation** for the local geochemical environment and types of colloids.
OU.01.TH.08	Groundwater Discharge to Biosphere Boundary	- (A) Infiltration and drainage at the surface (water table, capillary rise, surface water) - (B) Pressure-driven flow of liquid (wetting) phase - (C) Pressure-driven flow of gas (non-wetting) phase - (D) Flow of any additional phases (e.g., hydrocarbons)	(A) is Site-Specific. (B), (C), and (D) require **Evaluation**.
OU.01.TH.09	Groundwater Discharge to Well	- (A) Human use (drinking water, bathing water, industrial) - (B) Agricultural use (irrigation, animal watering)	(A) and (B) are **Included** because these are the two major uses of well water with the potential to cause dose to humans.
OU.01.TC.01	Evolution of Groundwater Chemistry in Overlying / Adjacent Units	- (A) Speciation - (B) Oxidation/reduction processes, reaction kinetics - (C) Dissolution, reaction kinetics - (D) Precipitation, inclusion in secondary phase, reaction kinetics - (E) Formation and filtration of colloids - (F) Effect of sorption - (G) Solubility of radionuclides and other species - (H) Thermal-chemical interaction with recharge water, including effects on fluid density - (I) Thermal-chemical interaction with intruding fluids (saline or fresh water), including effects on fluid density - (J) Interaction with gas phase	(A), (B), (C), (D), (E), (F), and (G) are **Likely Included** because they are basic chemistry processes. (H) through (J) require **Evaluation**.
OU.01.TC.02	Thermal-Chemical Evolution of Overlying / Adjacent Units	- (A) Thermal-chemical alteration processes for fractures, faults, rock matrix - (B) Thermal-chemical alteration of minerals / volume changes / cracking - (C) Thermal-chemical alteration of solubility, mineral precipitation / dissolution / leaching - (D) Oxidation/reduction processes, reaction kinetics W-17.	(A), (B), (C), and (D) require **Evaluation**

Matrix FEP Number	Description	Associated Processes	Preliminary Screening Recommendations
OU.01.TB.01	Microbial Activity in Overlying / Adjacent Units	- (A) Microbial effects on corrosion - (B) Presence of complexants - (humates, fulvates, carbonates) - (C) Formation of microbial colloids - (D) Formation of biofilms - (E) Biodegradation - (F) Biomass production - (G) Bioaccumulation - (H) CO_2, CH_4, H_2O and H_2S generation from microbial degradation - (I) Nitrification - (J) Sulfurization - (K) Methanogenesis	(A) through (K) are **Likely Excluded** because the overlying/adjacent units are not expected to support long-term microbial activity.
OU.01.TB.02	Thermal Effects on Microbial Activity in Overlying / Adjacent Units	- (A) Thermal effects on microbial activity	(A) is **Likely Excluded** because the overlying/adjacent units are not expected to support long-term microbial activity.
OU.01.TT.01	Transport of Dissolved Radionuclides in the Liquid Phase in Overlying / Adjacent Units	- (A) Advection - (B) Dispersion - (C) Diffusion - (D) Matrix Diffusion - (E) Intra-aqueous complexation - (F) Isotopic dilution - (G) Dilution by mixing with formation waters - (H) Solubility of radionuclides and other species	(A), (B), (C), (D), and (H) are **Included** because they are basic transport processes. (E), (F), and (G) require **Evaluation**.
OU.01.TT.02	Interaction of Dissolved Radionuclides with Stationary Phases (Rock Matrix, Fracture Surfaces) in Overlying / Adjacent Units	- (A) Reversible/irreversible physical sorption - (B) Surface complexation - (C) Ion exchange - (D) Precipitation / dissolution, including limited dissolution due to inclusion in secondary phases and enhanced dissolution due to alpha recoil	(A), (B), (C), and (D) are **Included** because they are basic sorption or chemical processes.
OU.01.TT.03	Interaction of Dissolved Radionuclides with Other Mobile Phases (Colloids, Gas Phase) in Overlying / Adjacent Units	- (A) Reversible/irreversible physical sorption - (B) Interactions with organic complexants - (C) Ion exchange - (D) Precipitation / dissolution - (E) Partitioning	(A), (B), (C), (D), and (E) are **Included** because they are basic sorption or chemical processes.
OU.01.TT.04	Coupled Process Effects on Transport of Dissolved Radionuclides in Overlying / Adjacent Units	- (A) Thermal diffusion (Soret effect) - (B) Thermal osmosis - (C) Thermal conduction or convection - (D) Other thermal effects, such as other Onsager relationships	(A), (B), (C),and (D) require **Evaluation**.
OU.01.TT.05	Transport of Radionuclides in the Gas Phase in Overlying / Adjacent Units	- (A) Advection - (B) Diffusion W-18.	(A) and (B) require **Evaluation** for gas phase transport.
OU.01.TT.06	Formation of Colloids in Overlying / Adjacent Units	- (A) Intrinsic colloids - (B) Pseudo-colloids (host rock fragments, waste form fragments, corrosion products, microbes) - (C) Sorption of radionuclides to colloids	(A), (B), and (C) are **Included** because these processes are important for transport via colloids.

Matrix FEP Number	Description	Associated Processes	Preliminary Screening Recommendations
OU.01.TT.07	Transport of Radionuclides on Colloids in Overlying / Adjacent Units	- (A) Advection - (B) Dispersion - (C) Diffusion - (D) Matrix Diffusion - (E) Stability/flocculation (mechanical stability, chemical stability) - (F) Filtration (physical, electrostatic) - (G) Dilution by mixing with formation waters	(A), (B), (C), and (D) are **Included** because they are important for transport via colloids. (E), (F), and (G) require **Evaluation** for the local geochemical environment and types of colloids.
OU.01.TT.08	Interaction of Colloids with Other Phases (Rock Matrix, Fracture Surfaces) in Overlying / Adjacent Units	- (A) Reversible/irreversible physical sorption onto stationary phases - (B) Sorption at air-water interfaces	(A) and (B) require **Evaluation**.
OU.01.CL.01	Periglacial Effects on Overlying / Adjacent Units	- (A) Variations in precipitation and temperature - (B) Permafrost - (C) Seasonal freeze/thaw	(A), (B), and (C) require **Evaluation**.
OU.01.CL.02	Glacial and Ice Sheet Effects on Overlying / Adjacent Units	- (A) Glaciation - (B) Glacial erosion and valleys - (C) Isostatic depression - (D) Melt water	(A), (B), (C), and (D) require **Evaluation**.
OU.01.SM.01	Dynamic Loading on the Overlying/Adjacent Units from a Seismic Event	- (A) Mechanical changes to the overlying/adjacent units from ground motion, rockfall, drift collapse, or fault displacement	(A) requires **Evaluation** for a candidate site. The frequency, magnitude, and consequences of seismic events are **Site-Specific.**
OU.01.IG.01	Igneous Activity Impacts the Overlying/Adjacent Units	- (A) Chemical interaction with magmatic volatiles - (B) Transport of radionuclides in magma, pyro clasts, vents	(A) and (B) require **Evaluation** for a candidate site. The frequency, type, magnitude and consequences of igneous events are **Site-Specific.**
OU.01.IG.02	Dynamic Loading on the Overlying/Adjacent Units from an Igneous Event	- (A) An igneous intrusion causes thermal-mechanical deformation of the overlying/adjacent units	(A) is **Site-Specific** and requires **Evaluation.**
OU.02.CP.01	Stratigraphic and Groundwater Properties of Underlying Units	- Stratigraphic units (thickness, lateral extent, heterogeneities) - Rock properties - Fluid properties - Fractures and fault properties - Groundwater chemistry - Presence of organic complexants (humates, fulvates, carbonates, …) in groundwater	
OU.02.TM.01	Dynamic Loading on the Underlying Units from Closure of Entries	- (A) Creep closure of the entries causes deformation and failure of the underlying unit(s) - (B) Floor heave or spalling from the walls and back changes the mechanical state in the underlying unit(s). - (C) Non-thermally-induced volume changes (e.g., swelling, cracking, corrosion products).	(A), (B), and (C) require **Evaluation** for the underlying units at a candidate site.
OU.02.TM.02	Dynamic Loading on the Underlying Units from Rockfall or Drift Collapse	- (A) Ejection of rock blocks alters the mechanical state of the underlying units - (B) Drift collapse alters the mechanical state of the underlying units	(A) and (B) require **Evaluation** for the underlying units at a candidate site.
OU.02.TM.03	Pressure Loading on the Underlying Units	- (A) Pressurization caused by gas generation, gas explosion, or entry convergence alters the mechanical state of the underlying units	(A) requires **Evaluation** for conditions in the underlying units.

Matrix FEP Number	Description	Associated Processes	Preliminary Screening Recommendations
OU.02.TM.04	Thermal-Mechanical Effects in Underlying Units	-(A) Thermally-accelerated convergence / rockfall / drift collapse / floor buckling in the overlying/adjacent units -(B) Subsidence -(C) Thermally-induced volume changes(expansion/stress/cracking)	(A) and (C) require **Evaluation.** (B) is **Excluded** because subsidence is unlikely to affect underlying units.
OU.02.TH.01	Pressure-Driven Darcy Flow Through Fractures and Porous Media in Other Underlying Units	-(A) Pressure-driven flow of liquid (wetting) phase -(B) Pressure-driven flow of gas (non-wetting) phase -(C) Flow of any additional phases (e.g., hydrocarbons) -(D) Pressure-driven flow between fractures and matrix (local non-equilibrium)	(A), (B), (C), and (D) are **Included** because pressure-driven Darcy flow is an important hydrological process.
OU.02.TH.02	Capillarity-Dominated Darcy Flow In Underlying Units	-(A) Wicking and imbibition (i.e., infiltration without gravity) -(B) Vapor barrier (i.e., reduction in relative liquid permeability at low saturation) -(C) Immiscible phase interaction and displacement -(D) Trapping, discontinuous blobs, or viscous fingering in non-wetting phase	(A) is **Likely Included** because it determines, in part, the hydrologic conditions in the underlying units (B), (C), and (D) require **Evaluation**.
OU.02.TH.03	Gravity- and Density-Dominated Flow In Underlying Units	-(A) Free convection due to density variation (from temperature or salinity effects) -(B) Infiltration and drainage	(A) requires **Evaluation**. (B) is **Likely Included** because these processes are important for determining the hydrologic conditions in the underlying units.
OU.02.TH.04	Adsorption-Dominated Flow In Underlying Units (Water held by electrostatic, van der Waals, or hydration forces)	-(A) Thin film flow below residual saturation (i.e., near liquid dry-out) -(B) Hygroscopy (equilibration of solid phase with humidity) -(C) Immobile water in nano-pores or small-aperture fractures	(A), (B), and (C) require **Evaluation.**
OU.02.TH.05	Diffusion or Dispersion in Miscible Phases In Underlying Units	-(A) Diffusion of vapor in air phase -(B) Diffusion of dissolved gas in liquid phase	(A) and (B) require **Evaluation.**
OU.02.TH.06	Non-Darcy Flow Through Fractures and Porous Media In Underlying Units	-(A) High Reynolds number fluid flow in large-aperture fractures -(B) Erosion or sedimentation (i.e., non-chemical plugging) of fractures and flow paths -(C) Threshold gradient flow in low-permeability matrix	(A), (B), and (C) require **Evaluation.**
OU.02.TH.07	Thermal-Hydrological Effects on Flow in Underlying Units	-(A) Convection and conduction of energy via liquid phase -(B) Convection of energy via vapor (i.e., heat pipe) -(C) Fluid density and viscosity changes due to temperature (e.g., thermal expansion of brine) -(D) Phase changes (i.e., condensation, boiling) leading to dry-out or resaturation -(E) Release of water from hydrated minerals during heating -(F) Decrepitation, creation (during reconsolidation), and migration of fluid inclusions	(A) is **Likely Included** because the thermal pulse drives fluid out of the repository. (B), (C), (E), and (F) require **Evaluation**. (D) is **Likely Excluded** because the peak thermal pulse is expected to be less than 100°C.

Matrix FEP Number	Description	Associated Processes	Preliminary Screening Recommendations
OU.02.TC.01	Evolution of Groundwater Chemistry in Underlying Units	- (A) Speciation - (B) Oxidation/reduction processes, reaction kinetics - (C) Dissolution, reaction kinetics - (D) Precipitation, inclusion in secondary phase, reaction kinetics - (E) Formation and filtration of colloids - (F) Effect of sorption - (G) Solubility of radionuclides and other species - (H) Thermal-chemical interaction with upwelling deep waters, including effects on fluid density - (I) Interaction with gas phase	(A), (B), (C), (D), (E), (F), and (G) are **Likely Included** because they are basic chemistry processes. (H) and (I) require **Evaluation**.
OU.02.TC.02	Thermal-Chemical Evolution of Underlying Units	- (A) Thermal-chemical alteration processes for fractures, faults, rock matrix - (B) Thermal-chemical alteration of minerals / volume changes / cracking - (C) Thermal-chemical alteration of solubility, mineral precipitation / dissolution / leaching - (D) Oxidation/reduction processes, reaction kinetics W-19.	(A), (B), (C), and (D) require **Evaluation.**
OU.02.TB.01	Microbial Activity in Underlying and Adjacent Units	- (A) Microbial effects on corrosion - (B) Presence of complexants - (humates, fulvates, carbonates) - (C) Formation of microbial colloids - (D) Formation of biofilms - (E) Biodegradation - (F) Biomass production - (G) Bioaccumulation - (H) CO_2, CH_4, H_2O and H_2S generation from microbial degradation - (I) Nitrification - (J) Sulfurization - (K) Methanogenesis	(A) through (K) are **Likely Excluded** because the underlying units are not expected to support long-term microbial activity.
OU.02.TB.02	Thermal Effects on Microbial Activity in Underlying and Adjacent Units	- (A) Thermal effects on microbial activity	(A) is **Likely Excluded** because the underlying units are not expected to support long-term microbial activity.
OU.02.CL.01	Climatic Effects on Underlying Units	- (A) Variations in precipitation and temperature - (B) Permafrost - (C) Isostatic depression	(A), (B), and (C) require **Evaluation**.
OU.02.SM.01	Dynamic Loading on the Underlying Unit(s) from a Seismic Event	- (A) Mechanical changes to the underlying unit(s) from ground motion, rockfall, drift collapse, or fault displacement	(A) requires **Evaluation** for a candidate site. The frequency, magnitude, and consequences of seismic events are **Site-Specific.**
OU.02.IG.01	Igneous Activity Impacts the Underlying Unit(s)	- (A) Chemical interaction with magmatic volatiles - (B) Transport of radionuclides in magma, pyro clasts, vents	(A) and (B) require **Evaluation** for a candidate site. The frequency, type, magnitude and consequences of igneous events are **Site-Specific.**
OU.02.IG.02	Dynamic Loading on the Underlying Unit(s) from an Igneous Event	- (A) An igneous intrusion causes thermal-mechanical deformation of the underlying units	(A) is **Site-Specific** and requires **Evaluation.**
		-	

Matrix FEP Number	Description	Associated Processes	Preliminary Screening Recommendations
BP.00.TB.01	Microbial Activity in Biosphere	- (A) Effect on biosphere characteristics - (B) Effect on transport through biosphere	All biosphere FEPs are considered to be **Site-Specific**, and not further considered in this preliminary analysis.
BP.00.TL.01	Effects of Repository Heat on Biosphere	- (A) Thermal effects on biosphere	
BP.00.RA.02	Radionuclide Alteration in Biosphere	- (A) Altered physical and chemical properties - (B) Isotopic dilution	
BP.00.CL.01	Periglacial Effects on Biosphere	- (A) Variations in precipitation and temperature - (B) Permafrost - (C) Seasonal freeze/thaw	
BP.00.CL.02	Glacial and Ice Sheet Effects on Biosphere	- (A) Glaciation - (B) Glacial erosion and valleys - (C) Isostatic depression - (DC) Melt water	
BP.00.CL.03	Climate Change (Natural and Anthropogenic) - Effects on Biosphere	- (A) Long-term global effects (sea level, rain fall, …) - (B) Short-term regional and local effects - (C) Seasonal local effects (flooding, storms, …)	
BP.00.HP.01	Human Influences on Climate (Intentional and Accidental) - Effects on Biosphere	- (A) Variations in precipitation and temperature - (B) Global, regional, and/or local - (C) Greenhouse gases, ozone layer failure	
BP.00.OP.01	Radiation Doses	- (A) Exposure rates (ingestion, inhalation, external exposure) - (B) Dose conversion factors	
BP.00.SM.01	Seismic Activity Impacts Biosphere	- (A) Altered human behavior - (B) Altered surface characteristics - (C) Altered surface transport pathways - (D) Altered recharge	
BP.00.IG.01	Igneous Activity Impacts Biosphere	- (A) Altered human behavior - (B) Altered surface characteristics - (C) Altered surface transport pathways - (D) Altered recharge - (E) Ash fall and ash redistribution	
BP.01.CP.01	Biosphere Surface Characteristics	- (A) Climate - (B) Soils (physical and chemical attributes)	
BP.01.CP.02	Topography and Surface Morphology	- (A) Recharge and discharge areas - (B) Surface topography	
BP.01.CP.03	Surface Water Characteristics	- (A) Lakes, rivers, springs - (B) Dams, reservoirs, canals, pipelines - (C) Coastal and marine features - (D) Water management activities	
BP.01.TM.01	Erosion	- (A) Mechanical or chemical weathering - (B) Aeolian or fluvial erosion - (C) Denudation - (D) Subsidence - (E) Mass wasting (erosion)	
BP.01.TM.02	Deposition	- (A) Mechanical or chemical weathering - (B) Aeolian or fluvial or lacustrine deposition - (C) Mass wasting (landslides)	

Matrix FEP Number	Description	Associated Processes	Preliminary Screening Recommendations
BP.01.TH.01	Precipitation	- (A) Spatial and temporal distribution	
BP.01.TH.02	Surface Runoff and Evapotranspiration	- (A) Runoff, impoundments, flooding, increased recharge - (B) Evaporation - (C) Condensation - (D) Transpiration (root uptake)	
BP.01.TH.03	Infiltration and Recharge	- (A) Spatial and temporal distribution - (B) Future changes to hydraulic gradients - (C) Future changes to water table elevation	
BP.01.TC.01	Chemical Evolution of Soil and Surface Water	- (A) Altered recharge chemistry (natural) - (B) Altered recharge chemistry (anthropogenic – e.g., acid rain) - (C) Speciation - (D) Solubility of radionuclides and other species	
BP.01.TT.01	Transport of Radionuclides in Air (as gas, vapor, particulates, aerosols)	- (A) wind, - (B) Plowing - (C) Degassing, precipitation	
BP.01.TT.02	Transport of Radionuclides in Surface Water	- (A) River flow - (B) Spring discharge - (C) Irrigation - (D) Overland flow, aeration, sedimentation - (E) Dilution by mixing with surface waters (e.g., lake mixing)	
BP.01.TT.03	Transport of Radionuclides in or on Soil and Sediments	- (A) fluvial (runoff, river flow) - (B) Eolian (wind) - (C) Saltation - (D) Glaciation - (E) Bioturbation (animals)	
BP.01.TT.04	Radionuclide Accumulation in Soils	- (A) Leaching/evaporation from discharge (well, groundwater upwelling) - (B) Deposition from atmosphere or water (irrigation, runoff) - (C) Recycling of accumulated radionuclides from soils to groundwater	
BP.01.RA.01	Radionuclides in Biosphere Media	- (A) Soil - (B) Surface Water - (C) Air - (D) Plant Uptake - (E) Animal (Livestock, Fish) Uptake - (F) Bioaccumulation	
BP.01.RA.02	Radionuclides in Non-Food Products	- (A) Dwellings (location, building materials and sources, fuel sources) - (B) Household products (clothing and sources, furniture and sources, tobacco, pets) - (C) Biosphere media	
BP.01.HP.01	Land and Water Use	- (A) Agricultural (irrigation, plowing, fertilization, crop storage, greenhouses, hydroponics) - (B) Farms and Fisheries (feed, water, soil) - (C) Urban / Industrial (development, energy production, earthworks, population density) - (D) Natural / Wild (grasslands, forests, bush, surface water)	

Matrix FEP Number	Description	Associated Processes	Preliminary Screening Recommendations
BP.01.HP.02	Evolution of Land and Water Use	- (A) New practices (agricultural, farming, fisheries) - (B) Technological developments - (C) Social developments (new/expanded communities)	
BP.01.OP.01	Inhalation	- (A) Gases and vapors - (B) Suspended particulates (dust, smoke, pollen)	
BP.01.OP.02	External Exposure	- (A) Non-Food products - (B) Soil, surface water	
BP.02.CP.01	Biosphere Flora and Fauna Characteristics	- (A) Flora and fauna - (B) Microbes	
BP.02.TM.01	Animal Intrusion into Repository	- (A) Impact on surface sediments - (B) Burrowing into repository	
BP.03.CP.01	Human Characteristics	- (A) Physiology - (B) Metabolism - (C) Adults, children	
BP.03.CP.02	Human Evolution	- (A) Changing human characteristics - (B) Sensitization to radiation - (C) Changing lifestyle	
BP.03.CP.03	Human Lifestyle	- (A) Diet and fluid intake (food, water, tobacco/drugs, etc.) - (B) Dwellings - (C) Household activities - (D) Leisure activities	
BP.03.OP.01	Radiological Toxicity and Effects	- (A) Human health effects from radiation doses	
BP.03.OP.02	Non-Radiological Toxicity and Effects	- (A) Human health effects from non-radiological toxicity	
BP.04.RA.01	Radionuclides in Food Products	- (A) Diet and fluid sources (location, degree of contamination, dilution with uncontaminated sources) - (B) Foodstuff and fluid processing and preparation (water filtration, cooking techniques)	
BP.04.OP.01	Ingestion	- (A) Food products - (B) Soil, surface water	
		-	
RS.01.CP.01	Repository System Assessment	- (A) Timescales of concern - (B) Spatial domain of concern - (C) Model and data issues	(A), (B), (C) are **Included** because they are generally important for any PA.
RS.01.CP.02	Repository System Regulatory Basis	- (A) Regulatory requirements and exclusions - (B) Retrievability	(A) is necessarily **Included** (B) may be **Included** if the regulations require it.
RS.02.CP.01	Repository Design	- (A) Layout of access drifts and waste emplacement drifts/tunnels - (B) Waste package emplacement and areal heat loading - (C) Backfill around packages and in drifts/tunnels - (D) Drift/tunnel/panel closures and shaft seals	(A), (B), (C), and (D) are **Included** because they are generally important for any PA.

Matrix FEP Number	Description	Associated Processes	Preliminary Screening Recommendations
RS.02.CP.02	Deviations from Design and Inadequate Quality Control	- (A) Error in waste emplacement (waste forms, waste packages, waste package support materials) - (B) Error in BB/MW/SP component emplacement (backfill, seals, liner) - (C) Inadequate excavation / construction (planning, schedule, implementation) - (D) Aborted / incomplete closure of repository - (E) Material and/or component defects	(A), (B), and (E) are **Included** because they may be important for a PA. (C) and (D) are **Excluded**, since they would play no part in a PA analysis
RS.02.CP.03	Control of Repository Site	- (A) Active controls (controlled area) - (B) Retention of records - (C) Passive controls (markers)	(A), (B), and (C) are **Excluded**, since they would play no part in a PA analysis
RS.02.TM.01	Mechanical Effects from Preclosure Operations - In MW - In DRZ - In Host Rock	- (A) Creation of disturbed rock zone (DRZ) - (B) Stress relief - (C) Boring and blasting effects - (D) Rock reinforcement effects (drill holes) - (E) Accidents and unplanned events - (F) Enhanced flow pathways	(A) is **Included** because the DRZ is included in almost all PAs. (F) requires **Evaluation** and may be **Site-Specific** (B) through (E) are generally operational concerns and would usually be **Excluded** from a PA
RS.02.TH.01	Thermal-Hydrologic Effects from Preclosure Operations - In BB/MW - In DRZ - In Host Rock	- (A) Site flooding - (B) Preclosure ventilation - (C) Accidents and unplanned events	(A), (B), and (C) are **Excluded**, since they are operational concerns and would generally play no part in a PA analysis
RS.02.TH.02	Open Boreholes	- (A) Site investigation boreholes (open, improperly sealed) - (B) Preclosure and postclosure monitoring boreholes -	(C) and (D) are **Site-Specific** and require **Evaluation**
RS.02.TC.01	Chemical Effects from Preclosure Operations - In BB/MW - In DRZ - In Host Rock	- (A) Water contaminants (explosives residue, diesel, organics, etc.) - (B) Water chemistry different than host rock (e.g., oxiding) - (C) Undesirable materials left - (D) Accidents and unplanned events	(A) through (D) are generally operational concerns and controls should be put in place during operations to ensure that these are not important for post-closure, from which they would usually be **Excluded**
RS.03.HE.01	Explosions and Crashes from Human Activities	- (A) War - (B) Sabotage - (C) Testing - (D) Resource exploration / exploitation - (E) Aircraft	Usually **Excluded** because of low probability
RS.03.OE.01	Meteorite Impact	- (A) Cratering, host rock removal - (B) Exhumation of waste - (C) Alteration of flow pathways	Usually **Excluded** because of low probability
RS.03.OE.02	Extraterrestrial Events	- (A) Solar systems (supernova) - (B) Celestial activity (sun - solar flares, gamma-ray bursters; moon – earth tides) - (C) Alien life forms	Usually **Excluded** because of low probability
RS.03.OE.03	Earth Planetary Changes	- (A) Changes in earth's magnetic field - (B) Changes in earth's gravitational field (tides) - (C) Changes in ocean currents	Usually **Excluded** because of low probability

APPENDIX B:
DIFFUSION, TORTUOSITY, AND DISPERSION

A key purpose of this appendix is simply to summarize how diffusion, dispersion, and tortuosity are included in the solute mass balance equations in PFLOTRAN. For transport of a dilute solute (tracer) in a porous medium through advective and dispersive/diffusive processes, PFLOTRAN adopts the commonly used model for dispersion or "concentration spreading" processes, which includes a separate component for molecular diffusion (Brownian motion) and one for velocity dispersion arising from the heterogeneity of the pore space and associated local velocity gradients (see Eq. B-1). The latter effect is variously called *mechanical dispersion* (Bear 1972), *kinematic dispersion* (de Marsily 1986), or *advective dispersion* (Bear and Cheng 2010), and requires advective motion of the fluid phase (i.e., an imposed driving force for movement of the fluid phase, such as a pressure gradient). The former effect, molecular diffusion, occurs in the absence of bulk fluid movement. The sum of the two effects is usually difficult to separate experimentally and together they are called *hydrodynamic dispersion* (Bear 1972, Sec. 10.1) or simply dispersion (Lake 1989). The molecular diffusion component of hydrodynamic dispersion is generally only important at very low values of either the average pore (interstitial) velocity, v, or the Peclet number, N_{Pe} (Perkins and Johnston 1963, Fig. 6; Bear 1972, Figure 10.4.1; Lake 1989, Figure 5-16).

For molecular diffusion, the spreading force is a chemical concentration gradient described by Fick's first law of diffusion, while for mechanical (or advective) dispersion the primary spreading "force" is the pressure gradient acting upon fluid phase particles in a heterogeneous pore space giving rise to local gradients in pore fluid velocity. These local gradients and heterogeneities of the pore space cause a spreading of dissolved solutes that is often represented with an equation similar to Fick's law, wherein the dispersive solute flux is equal to a concentration gradient times an advective dispersion coefficient (e.g., de Marsily 1986, Section 10.1.1(c); Bear and Cheng 2010, Eq. 7.1.32). Thus, the advective dispersion coefficient is analagous to the molecular diffusion coefficient (de Marsily 1986, Sec. 10.1.1) because both can be included in the solute mass conservation (balance) equation in a similar way (Bear 1972, Eq. 10.5.45; Lake 1989, Eq. 5.5-1; deMarsily 1989, Eq. 10.1.4)—as a Fickian-type law (Bird et al. 1960).

The mass/mole balance equations in PFLOTRAN are on a bulk-volume (REV) basis, wherein the specific fluid-phase flux vector (Darcy velocity) for phase p, $\boldsymbol{q}_p$, is per unit area of the porous medium, i.e., "bulk area" (see Lichtner et al. 2015, Eq. 10-96; also, Lichtner et al. 2002, Eq. 1). Combining Eqs. 10-96 and 10-101 from Lichtner et al. (2015), and simplifying the chemical reaction source term on the right-hand-side of Eq. 10-96, gives the balance equation for primary solute species j in the aqueous phase:

$$\frac{\partial}{\partial t}(\varphi s C_j) + \boldsymbol{\nabla} \cdot \left(\boldsymbol{q}_a C_j - \varphi s \mathbf{D}_{\mathbf{h}}^{a} \cdot \boldsymbol{\nabla} C_j\right) = Q_j \tag{B-1}$$

where φ denotes the porosity, s is the aqueous phase saturation (fraction of porosity occupied by the aqueous phase), C_j denotes the molar concentration of solute species j [moles per aqueous phase volume], $\mathbf{D}_{\mathbf{h}}^{a}$ denotes the hydrodynamic dispersion tensor in the aqueous phase, and Q_j

denotes a source/sink term for C_j (which could include chemical reactions—a simplification of Eq. 10-96). A general expression for the specific discharge or Darcy velocity of the aqueous phase, $\boldsymbol{q}_a$, is given as (Lichtner et al. 2015, Eq. 10-102):

$$\boldsymbol{q}_a = \frac{k_{ra}\mathbf{k}}{\mu} \cdot (\boldsymbol{\nabla} p_a + \rho_a g \boldsymbol{\nabla} z) \tag{B-2}$$

where $\mathbf{k}$ is the intrinsic permeability tensor (second-order symmetric) [m^2]; k_{ra} is the relative permeability of the aqueous phase (a function of s); μ is dynamic fluid viscosity [kg/(s·m)] of the aqueous phase; p_a is the aqueous-phase fluid pressure [kg/(s^2·m)]; $\boldsymbol{\nabla} p_a$ is the fluid pressure gradient [kg/(s^2·m^2)]; ρ_a is the fluid phase density [kg/m^3]; and $\boldsymbol{\nabla} z$ is the vertical head gradient [m/m]. If it is desired to use a dual-continuum representation to represent solute transport in a fractured host rock, the source/sink term Q_j can used for mass transfer across the fracture-matrix interface, thereby including the effect of matrix diffusion (e.g., see Bear et al. 1993; Zhou et al. 2007, App. A).

Separating $\mathbf{D}_{\mathbf{h}}^{a}$ into its two components—the mechanical or advective dispersion tensor, $\mathbf{D}^{a}$, and the molecular diffusion tensor, $\mathbf{D}_{\mathbf{m}}^{a,j}$, for species j in the aqueous phase—gives the following:[2]

$$\frac{\partial}{\partial t}(\varphi s C_j) + \boldsymbol{\nabla} \cdot \left[\boldsymbol{q}_a C_j - \varphi s (\mathbf{D}^{a} + \mathbf{D}_{\mathbf{m}}^{a,j}) \cdot \boldsymbol{\nabla} C_j\right] = Q_j \tag{B-3}$$

Molecular diffusion, $\mathbf{D}_{\mathbf{m}}^{a,j}$, is represented as a tensor because of the heterogeneity of the porous medium, meaning that diffusing solute particles must travel along a tortuous pathway relative to the straight-line length of the medium in any direction. It can be written as

$$\mathbf{D}_{\mathbf{m}}^{a,j}(\varphi s) = D_m^{a,j} \mathbf{T}^{*}(\varphi s) \tag{B-4}$$

where $D_m^{a,j}$ is the molecular diffusion coefficient for the given solute species in the aqueous phase; and $\mathbf{T}^{*}(\varphi s)$ is a second-order (i.e., 3-by-3) tensor, called the tortuosity tensor (Bear and Cheng 2010, Eq. 7.1.23), which represents the geometric distribution of the aqueous phase in the pore space—which is why it is shown as a function of aqueous phase volume fraction, φs, i.e., it is a macroscopic parameter that accounts for the tortuous pathways followed by diffusing solute particles.

Combining Eq. B-4 with Eq. B-3 gives:

$$\frac{\partial}{\partial t}(\varphi s C_j) + \boldsymbol{\nabla} \cdot \left[\boldsymbol{q}_a C_j - \varphi s (\mathbf{D}^{a} + D_m^{a,j} \mathbf{T}^{*}) \cdot \boldsymbol{\nabla} C_j\right] = Q_j \tag{B-5}$$

Use of tortuosity in the PFLOTRAN simulations is discussed in more detail after the following discussion of $\mathbf{D}^{a}$.

[2] Bear and Cheng (2010, Eq. 7.2.20) provide a similar balance equation to Eq. 10-96 in Lichtner et al. (2015), which may be combined with their separate definitions of advective (mechanical) dispersion flux (their Eq. 7.1.32) and mass diffusion flux (their Eq. 7.1.23), to give an equation similar to Eq. B-3. Eq. B-3 is also effectively the same as Eq. 4.6.28 in Bear (1972), with the exception that Eq. B-3 is written on a bulk-volume concentration basis and Bear's equation is on a fluid-volume concentration basis; also Bear assumes an incompressible fluid, i.e, $\boldsymbol{\nabla} \cdot \boldsymbol{q}_a = 0$.

B.1 Advective (Mechanical) Dispersion

The second-order (3-by-3) advective dispersion tensor, $\mathbf{D}^a$, can be written as a product of a fundamental medium property called dispersivity, **a** (which is described by Bear and Cheng 2010, Sec. 7.1.6, to be a fourth-order tensor[3]), times a function of the average macroscopic pore velocity vector, $\boldsymbol{v}$. According to Bear and Cheng (2010), dispersivity "expresses the effect, on the flow, of the microscopic configuration of the interface between the considered fluid phase and all other phases within the REV." Based on symmetry considerations, Bear and Cheng note that of the 81 elements of the fourth-order dispersivity tensor, only 36 are independent. Nevertheless, this many independent parameters seem quite unwieldy from an experimental perspective. Thus, much of the literature reduces the representation of dispersivity to anywhere from two to six independent components by making assumptions about medium isotropy or symmetry (Bear and Cheng 2010, Sec. 7.1.6).

In an *isotropic* medium there are only two independent components of dispersivity, called the longitudinal dispersivity, α_L, and the transverse dispersivity, α_T. The general form of the dispersion tensor, $\mathbf{D}^a$, in this case has been given by Lichtner et al. (2002, Eq. 26); Lichtner et al. (2015, Eq. 10-103); and Bear and Cheng (2010, Eqs. 7.1.44 and 7.1.45):

$$\mathbf{D}^a = \alpha_T v \mathbf{I} + (\alpha_L - \alpha_T)\frac{\boldsymbol{vv}}{v} \tag{B-6}$$

where $\boldsymbol{v} = (v_x, v_y, v_z)$ is the average macroscopic pore velocity vector (interstitial or solute velocity), **I** is the unit dyadic or identity tensor, $\boldsymbol{vv}$ is a dyadic product of the pore velocity vector $\boldsymbol{v}$, and $v = \sqrt{\sum_i v_i^2} = |\boldsymbol{q}|/(\varphi s)$ = is the magnitude of the pore velocity $\boldsymbol{v}$.

If, the flow is uniform and oriented along one of the principal directions of $\mathbf{D}^a$ (e.g., $v_x = v$, $v_y = 0$, $v_z = 0$), the advective dispersion tensor, $\mathbf{D}^a$ can be simplified to the following (Bear and Cheng 2010, Eq. 7.1.47; deMarsily 1986, Sec. 10.1.1):[4]

$$\mathbf{D}^a = \begin{bmatrix} D_L & 0 & 0 \\ 0 & D_T & 0 \\ 0 & 0 & D_T \end{bmatrix} = \begin{bmatrix} \alpha_L & 0 & 0 \\ 0 & \alpha_T & 0 \\ 0 & 0 & \alpha_T \end{bmatrix} v \tag{B-7}$$

Bear and Cheng (2010, p. 360) note that α_L should be on the order of magnitude of the size of a typical pore and α_T should be about 8 to 24 times less than α_L. Longitudinal dispersivity α_L is in the direction of the flow, while transverse dispersivity α_T is perpendicular to flow (i.e.,

[3] Another common example of a fourth-order tensor is the elasticity or stiffness tensor, **E**, in solid mechanics. It represents a linear mapping between the second-order *strain* tensor, $\boldsymbol{\epsilon}$, and the second-order *stress* tensor, $\boldsymbol{\sigma}$, i.e., $\boldsymbol{\sigma} = \mathbf{E} \cdot \boldsymbol{\epsilon}$. In index notation, this is shown as $\sigma_{ij} = \sum_{k=1}^{3} \sum_{l=1}^{3} E_{ijkl}\epsilon_{kl}$, which is the generalized form of Hooke's law. Similarly, the dispersivity tensor, **a**, relates the dyadic product $\boldsymbol{vv}$ (see Eq. B-6) to the dispersion tensor $\mathbf{D}^a = \mathbf{a} \cdot (\boldsymbol{vv}/v)$—see Bear and Cheng (2010, Eq. 7.1.39).

[4] The right-hand side of Eq. B-7 is how the dispersion coefficient is expressed by most authors, in terms of dispersivity and *solute (pore) velocity*. DeMarsily (1986) chose to express it in his initial equations in terms of Darcy velocity rather than pore velocity, which can introduce some confusion. However, as he points out, the dispersivities stay the same regardless of how the balance equation is written.

concentration spreading is always greater in the direction of the flow than in the direction perpendicular to the flow).

Other relatively simple representations of $\mathbf{D}^a$ arise when the porous medium is *axisymmetric*, i.e, anisotropic in only two directions (or "transversely isotropic"—a medium with one axis of rotational symmetry, i.e., isotropic in the plane perpendicular to the symmetry axis). In this instance, there are generally three independent parameters in the dispersion tensor, often labeled as longitudinal dispersivity, α_L, horizontal transverse dispersivity, α_{TH}, and vertical transverse dispersivity, α_{TV}. In this axisymmetric case, the exact form of $\mathbf{D}^a$ in terms of dispersivity coefficients and components of the average pore velocity depends on how the flow is oriented relative to the axis of symmetry. Lichtner et al. (2002) show the many different examples in this case, including when flow is parallel to the axis of symmetry (i.e., in the *z* direction) or perpendicular to the axis of symmetry (e.g., in the *x* direction) or at some angle, $\emptyset$, in between. They also discuss how the typical Burnett and Frind (1987) representation of $\mathbf{D}^a$ (used in many computer codes—see Eq. 7.1.56 in Bear and Cheng) may not be appropriate, since it does not follow certain tensor transformation rules. A general representation of $\mathbf{D}^a$ in an axisymmetric medium, with fluid flow oriented in an arbitrary direction, is given by Eq. 47 (and Eq. 40) in Lichtner et al. (2002), which Bear and Chang (2010) have reduced to a much simpler form when flow is oriented horizontally (i.e., perpendicular to the axis of symmetry) (Bear and Cheng 2010, Eq. 7.1.55 or Eq. 7.1.62):

$$\mathbf{D}^a = \begin{bmatrix} \alpha_L & 0 & 0 \\ 0 & \alpha_{TH} & 0 \\ 0 & 0 & \alpha_{TV} \end{bmatrix} v \tag{B-8}$$

An important observation in the foregoing representation of advective dispersion, which has been reported on extensively (e.g., Arya et al. 1988; Lake 1989; Gelhar et al. 1992), is its scale dependence. In particular, measured values of dispersivity increase with the scale or length of the domain being investigated. At the field scale, the term "macrodispersion" has been used to describe the effect of large-scale permeability and porosity heterogeneity on solute transport over large distances (Bear and Cheng 2010, Sec. 7.1.8). A rule of thumb has been given that the longitudinal dispersivity is approximately equal to 1/10 of the length scale of interest; the horizontal transverse dispersivity is 1/10 of the longitudinal one; and the vertical transverse dispersivity is about 1 to 2 orders of magnitude less than the horizontal one (Bear and Cheng 2010, Sec. 7.1.8). A more quantitative expression for α_L, depending on the length scale (or travel distance), L_s, of interest is given by Neuman (1990) as:

$$\alpha_L = 0.017 {L_s}^{1.5}, \qquad L_s \leq 100\ m \tag{B-9}$$

$$\alpha_L = 0.32 {L_s}^{0.83}, \qquad L_s > 100\ m \tag{B-10}$$

However, as discussed above in Section 3.2.2.4, Gelhar et al. (1992) argue strongly against using a linear regression fit to their data (such as in Eqs. B-9 and B-10) because of the uncertain reliability of much of their reported data, especially those at larger length scales. Nevertheless, for illustration purposes, Figure B-1 is a reproduction of Gelhar et al.'s dispersivity data and the two Neuman least-square-fit lines, reproduced from Bear and Chang (2010). Additional detail on scale dependency and dispersivity is given in Section 3.2.2.4 of this report.

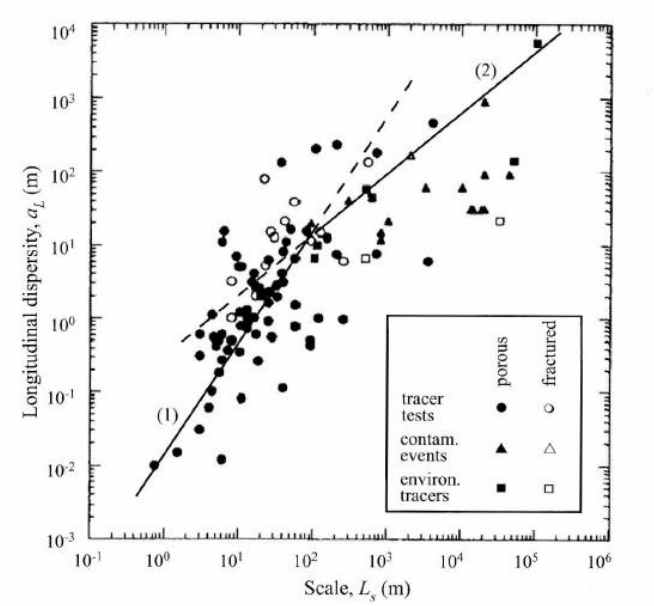

Figure B-1. Longitudinal dispersivity versus plume travel distance for various types of observations and media, with two least square fits to the data, as derived by Neuman (1990). [Reproduced from Bear and Cheng 2010, Fig. 7.1.5).]

B.2 Tortuosity and Diffusion

The tortuosity tensor, $\mathbf{T}^*$, as derived by Bear (1972, Sections 4.6.2 and 4.8.1) is a geometric quantity describing how any type of diffusive flux in a porous medium (mass flux, electrical current flux, heat flux, etc.) is "slowed down" by the sinuous pathway through the pore space.[5] According to Bear (1972, Sec. 4.8.1), $\mathbf{T}^*$ is a second-order, symmetric tensor, implying that it can be transformed to diagonal form, where the diagonal components of the transformed tensor are its eigenvalues, each of which is associated with one of the three principal directions or eigenvectors of the tensor. Representing these components or eigenvalues as τ_{xx}, τ_{yy}, and τ_{zz} gives (Bear 1972, Eq. 4.8.9):

$$\mathbf{T}^* = \begin{bmatrix} \tau_{xx} & 0 & 0 \\ 0 & \tau_{yy} & 0 \\ 0 & 0 & \tau_{zz} \end{bmatrix} \tag{B-11}$$

Because these three tortuosity components always have values < 1 (see discussion below), they have the effect in Eq. B-5 of "contracting" the ∇C_j vector, i.e., of reducing its magnitude. In other words, a macroscopic concentration gradient has less motive force in a medium with tortuous flow pathways than in one with straight flow pathways, i.e., molecular diffusion is reduced or slowed down. In this case the so-called *effective diffusion coefficient*, $D^j_{e,x}$, in the x direction (see Eq. B-5) is defined as (ignoring the superscript a):

[5] He calls it a "tensor of directions" (Bear 1972, Eq. 10.4.23) and describes how it tranforms the (x, y, z) components of any driving force, e.g., $\nabla C_j = \left(\frac{\partial C_j}{\partial x}, \frac{\partial C_j}{\partial y}, \frac{\partial C_j}{\partial z}\right)$, in the "straight-line" coordinate system to a reduced set of (x, y, z) components of that force in the same straight-line coordinate system, through a two-step transformation that first maps the (x, y, z) force components to the velocity streamlines in the pores and then maps those streamline projections of the force components back to the straight-line (x, y, z) coordinate system (Bear 1972, Sec. 4.8.1).

$$D_{e,x}^{j} = \varphi s D_{m,x}^{j} \tau_{xx} \tag{B-12}$$

There seems to be little discussion in the literature (based on this author's investigations) as to measuring different numerical values (or different functional representations) for τ_{xx}, τ_{yy}, and τ_{zz}; and, as mentioned by Bear (1972, Eq. 4.8.10), $\tau_{xx} = \tau_{yy} = \tau_{zz} = \tau$ in an isotropic medium. Thus, in the rest of this discussion (and in PFLOTRAN), the tortuosity tensor is represented as:

$$\mathbf{T}^{*} = \begin{bmatrix} \tau & 0 & 0 \\ 0 & \tau & 0 \\ 0 & 0 & \tau \end{bmatrix} \tag{B-13}$$

so that Eq. B-12 becomes:

$$D_{e}^{j} = \varphi s D_{m}^{j} \tau \tag{B-14}$$

Discussions of the geometric interpretation of tortuosity go back at least to Carman (1937), whose work is summarized by Bear (1972, Sec. 4.8.1). Carman used the phrase "correcting factor" for the geometric term (L_e/L), which is the ratio of the length, L_e, traveled by a fluid particle in a tortuous or winding channel in a porous medium (the pathline) to the straight-line length, L, of that medium. The inverse of the ratio squared, i.e., $(L/L_e)^2$, appears on the right hand side of Darcy's Law in Carman's Eq. 8. This quantity is obviously < 1, and is Bear's definition of the tortuosity, $\tau = (L/L_e)^2$, of a porous medium (Bear 1972, Eq. 4.8.21). Most of the porous-medium literature defines tortuousity as the inverse of Bear's definition (e.g., Ghanbarian et al. 2013, Eq. 3)[6]; however, as stated by Bear (1972, p. 111), it is, in fact, "only a matter of definition." De Marsily (1986) and Lichtner et al. (2015)—and therefore, PFLOTRAN—use Bear's definition that τ is a number less than 1, as represented in Eqs. B-5 and B-14 above.

The important thing with regard to tortuosity is how to experimentally measure it, and also how to express it in terms of the fundamental medium properties it depends upon, such as porosity and fluid-phase volume fraction. It has been commonly determined with electrical resistivity measurements (since it lowers the electrical current flux) by relating it to the porous-medium *formation factor*, *F*, which is defined as the ratio of the electrical resistivity of the bulk medium (rock + pore fluids), $\hat{R}_b$, to the electrical resistivity of the pore fluid alone, $\hat{R}_w$:

$$F = \frac{\hat{R}_b}{\hat{R}_w} \tag{B-15}$$

[6] Ghanbarian et al. (2013), who give a fairly comprehensive summary of the tortuosity literature, state that: "The concept of tortuosity is used to characterize the structure of porous media, to estimate their electrical and hydraulic conductivity, and to study the travel time and length for tracer dispersion, but different types of tortuosity—geometric, hydraulic, electrical, and diffusive—have been used essentially interchangeably in the literature…Given the variety of models that have been developed, and the sharp differences between some of them, no consensus has emerged unifying the models in a coherent way." Ghanbarian et al. also use the inverse of Bear's definition of tortuosity derived from electrical resistivity measurements (see Eq. B-16), i.e, they say that $\tau = \varphi F$ (rather than $1/\varphi F$) because they define τ as a factor >1, namely, as $\tau = (L_e/L)^2$.

As discussed by Bear (1972, Sec. 4.8.3), F has been related to tortuosity and porosity (in a fully saturated medium) with a number of empirical formulas, the most simple of which is:

$$F = \frac{1}{\varphi\tau} \tag{B-16}$$

A commonly used relationship between formation factor and porosity, derived empirically from resistivity measurements, is due to Archie (1942):

$$F = \varphi^{-m} \tag{B-17}$$

where m is often called the *cementation factor* (Bear 1972, Eq. 4.8.45), with a value approximately equal to 2 for a variety of rock types including unconsolidated sediment, consolidated sedimentary rock, and crystalline rock (Oelkers 1996). Combining Eqs. B-16 and B-17 gives (for a fully saturated medium) gives:

$$\tau_{Archie} = \varphi^{m-1} \tag{B-18}$$

Many other formulas for τ in a fully saturated medium have been compiled by Boudreau (1996, Table 1) and Ghanbarian et al. (2013, Tables 3 through 5 and accompanying text, which discuss hydraulic tortuosity, τ_h, electrical tortuosity, τ_e, and diffusive tortuosity, τ_d).[7] Ghanbarian et al. (2013, Fig. 8) have plotted a variety of formulas for diffusive tortuosity versus porosity:

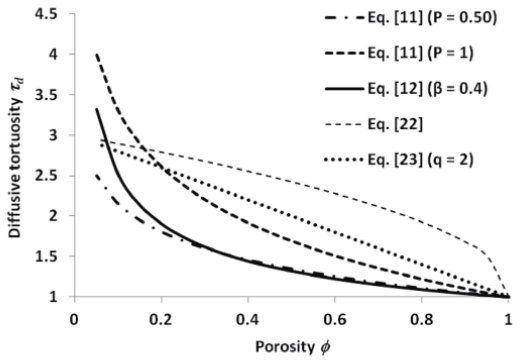

Fig. 8. Comparison of the prediction of diffusive tortuosity τ_d using the Weissberg (1963) model, Eq. [11], with constant $P = 0.50$; the Tsai and Strieder (1986) model, Eq. [11], with $P = 1$; the Delgado (2006) model, Eq. [12], with exponent $\beta = 0.40$; the Beeckman (1990) model, Eq. [22]; and the Iversen and Jorgensen (1993) model, Eq. [23], with soil texture related constant $q = 2$ in a saturated porous medium.

Figure B-2. Inverse of (diffusive) tortuosity (as used in Eqs. B-5 and B-14) versus fully saturated system porosity, φ. [Reproduced from Ghanbarian et al. (2013, Fig. 8).]

When the porous medium is partially saturated, the tortuosity must depend on the liquid saturation, as indicated in Eq. B-4, since the microscopic configuration of this phase geometrically constrains the solute pathlines through the medium. In this case, several relationships between tortuosity τ and water saturation s (or water content, θ) have been suggested. One such commonly used relationship is attributed to Millington (1959). Its appropriate form for use in Eq. B-14 comes from Eq. 7.1.26 in Bear and Cheng (2010):

[7] Again, the inverse of all the formulas in Boudreau (1996) and Ghanbarian et al. (2013) is what should be inserted into Eq. B-5 or Eq. B-14.

$$\tau_{Mill} = \frac{\theta^{\frac{7}{3}}}{\varphi^2} \tag{B-19}$$

or, replacing water content θ with φs:

$$\tau_{Mill} = \varphi^{\frac{1}{3}} s^{\frac{7}{3}} \tag{B-20}$$

For natural materials of sedimentary origin and engineered materials of similar nature (e.g., bentonite buffer), the post-closure PA simulations reported here apply Eq. B-18 assuming $m = 2$, resulting in $\tau = \varphi$. For other materials (waste package, DRZ, crystalline host rock), τ is chosen to achieve the appropriate value of the effective diffusion coefficient, D_e – see Table 3-10. In particular, τ is not always available or measured for a given situation. However, D_e is often measured in lab or field experiments, by fitting measured field tracer data (solute concentrations) to an advective-dispersion/diffusion equation. For example, at the small- or lab-scale, Soler et al. (2015) derive experimental values of D_e in crystalline rock based on a single-continuum model (similar to the conceptual model in Eq. B-5 but including the effect of linear adsorption, K_d). Such values are probably appropriate for rock-matrix grid cells used in the PFLOTRAN simulations—see Section 3.2.2.4 and Table 3-10. On the other hand, at the field scale of meters to kilometers, Zhou et al. (2007) use a dual continuum model (with the process of "matrix diffusion" between fracture and matrix continua) to determine values of an effective matrix diffusion coefficient, D_e^{MD}, that can be used for large-scale transport in a fractured host rock. However, its use here would also require that a fracture-matrix transfer term be included in Eq. B-5 as part of the source/sink term, Q_j. (See Section 3.2.2.4 for additional discussion.)